London South Bank University

EST 1892

ALGORITHMS FOR EFFICIENT, RESILIENT, AND ECONOMIC OPERATION OF PRE-EMPTIVELY REINFORCED RECONFIGURABLE DISTRIBUTION SUBSTATIONS

ROBERT ADAM BROWN

https://orcid.org/0000-0003-0375-3000

A thesis submitted in partial fulfilment of the

requirements of London South Bank University

for the degree of Doctor of Philosophy

June 2023

Abstract

Stochasticity of demand profiles at electricity distribution substations is increasing due to the proliferation of low carbon technologies; in particular mobile, bi-directional, or intermittent loads such as electric vehicles and heat pumps. The decarbonisation of heat and transport will cause a long-term increase in overall connected load, making substation reinforcement necessary, whilst planning of upgrade locations and capacities remains challenging. This project will investigate pre-emptive substation reinforcement with algorithmic topology control, to utilise the additional installed substation capacity only when required.

Distribution Substation Dynamic Reconfiguration (DSDR) proposes the installation of additional transformers in parallel with the existing transformer in each substation, removing the need to scrap and replace these. Telematics-controlled switches are installed on the high- and low-voltage side of each transformer in the substation, with local agent algorithms deployed to control in real-time when each parallel transformer is brought into or taken out of service. Substation reconfiguration is thus controlled to optimise for maximum operating efficiency. The threshold algorithm most recently trialled in medium voltage parallel transformer substations is implemented as a baseline, and a novel model-based reconfiguration algorithm is proposed, implemented, and evaluated in software and hardware.

This work led to a 1.34% improvement in algorithm performance on substation efficiency, over a yearly demand profile including residential and new electric vehicle load for the year 2050, equivalent to a potential saving of 2.68 TWh annually if deployed UK-wide. This approach unlocks several opportunities to operate existing substations in the smart, flexible, resilient, and efficient manner that will be required to reach the net zero target by 2050.

Acknowledgments

I would like to sincerely thank the following individuals and organisations, for providing support throughout my studies, and without whom I would not have been able to complete this project.

Professor Sandra Dudley of London South Bank University, for selflessly providing supervision, guidance, support, and kindness over the past few years. Akshat and Yash Kulkarni of OrxaGrid Ltd for providing industrial sponsorship for my studies. My father David for patiently encouraging and inspiring me to pursue an interest in engineering over the past three decades. The various funding bodies which supported projects on which I have worked over the past few years. And finally, Zayna and Alex, who bring sunshine and joy to everyone in our lab whenever they visit.

Publications

A paper on the topic of this thesis has been submitted and accepted for the IEEE Energy Conversion Congress and Exposition to be held in Nashville, Tennessee on October 29-November 2, 2023. A further two papers are currently in the review process.

Table of Contents

List of Figures

List of Tables

Abbreviations

ABC	Aerial Bundled Conductors
AC	Alternating Current
ADC	Analogue to Digital Converter
ADD	After Diversity Demand
BaU	Business as Usual
BE	Branch Exchange
BESS	Battery Energy Storage System
BTSM	Bench Top Scale Model
CCC	Current Carrying Capacity
CI	Customer Interruptions
CML	Customer Minutes Lost
CPOW	Continuous Point on Wave
CSA	Cross Sectional Area
CVR	Conservation Voltage Reduction
DC	Direct Current
DFES	Distribution Future Energy Scenarios
DG	Distributed Generation
DGA	Dissolved Gas Analysis
DNO	Distribution Network Operator
DNR	Distribution Network Reconfiguration
DP	Decimal Places
DR	Demand Response
DSDR	Distribution Substation Dynamic Reconfiguration
DSO	Distribution System Operator
DSR	Demand Side Response
DT	Digital Twin
DUT	Device Under Test
EMT	Electromagnetic Transient
ENWL	Electricity Northwest Ltd
ESS	Energy System Scenarios
EV	Electric Vehicle

EVCP	Electric Vehicle Charge Point
FES	Future Energy Scenarios
FR	Frequency Response
GSP	Grid Supply Point
HP	Heat Pump
HVDC	High Voltage Direct Current
ICE	Internal Combustion Engine
JSON	JavaScript Object Notation
KCL	Kirchhoff’s Current Law
KVL	Kirchhoff’s Voltage Law
kW	Kilowatt
LAN	Local Area Network
LCT	Low Carbon Technologies
LF	Load Factor
LP	Load Profile
LSOA	Lower Super Output Area
LV	Low Voltage
MD	Maximum Demand
MV	Medium Voltage
MW	Megawatt
NG	National Grid
NZ	Net Zero
OCT	Open Circuit Test
OOP	Object Oriented Programming
OSS	Open-Source Software
PCC	Point of Common Coupling
PHiL	Power Hardware in the Loop
PILC	Paper Insulated Lead Covered
PMU	Phasor Measurement Unit
PU	Per Unit
RMS	Root Mean Square
RMU	Ring Main Unit
SCADA	Supervisory Control and Data Acquisition

SCT	Short Circuit Test
SFRA	Sweep Frequency Response Analysis
SG	Smart Grid
SLD	Single Line Diagram
SOP	Soft Open Point
SSEG	Small Scale Embedded Generators
TCP	Transmission Control Protocol
TWh	Tera Watt Hours
TX	Transformer
UK	United Kingdom
V2G	Vehicle to Grid
VI	Virtual Instrument
VPN	Virtual Private Network
WEC	World Energy Council
WES	World Energy Scenarios
XLPE	Cross Linked Polyethylene
ZIP	Impedance, Current, Power (load model)

1 Introduction

The United Kingdom (UK) has set an ambitious target of becoming net zero by the year 2050; which means achieving balance in the CO_2 emitted to and absorbed from the atmosphere. To achieve this, it will ban the sale of internal combustion engine vehicles by 2035. As a result, thirty million electric vehicles are forecast to be registered within the forthcoming decade, most of these drawing power from the existing electricity distribution networks. Total existing domestic base load served by distribution substations will be at least matched by the addition of these electric vehicle loads, meaning transformers which were sized to be adequate until at least 2050 will now become overloaded by the mid 2030's.

Distribution Network Operators (DNOs) are the UK's utility licensees responsible for delivering electricity between the transmission system and end users. They own and operate assets including electrical lines and cables which connect different parts of the distribution system, and substations which contain switchgear and transformers to convert the electricity into a useful voltage level for consumers. Traditional methods (known as system reinforcement) relied upon by DNOs to serve increased loads involve either upgrading a substation after substantial new load has materialised, or doing so in response to confirmation that a new load will be connected, such as new homes construction. In either case, existing substations are currently upgraded by removing their existing transformer then replacing it with one of a larger capacity.

New electric vehicle load differs from the historical load increases experienced by these networks, because the load is mobile, and therefore difficult to predict to which substations it will be connected, and when drivers will choose to plug in their vehicles. To summarise, domestic power requirements will be doubled by the proliferation of electric vehicles, but there exists much uncertainty around when and where the new demand will overload the existing electricity distribution infrastructure at postcode level. Adopting existing methods of reinforcement, which were designed to facilitate a steadily growing load base and planned developments, will lead to wasteful scrapping of existing transformers with many years of service left; and increased no-load losses in substations which are pre-emptively reinforced but where significant electric vehicle load never materialises.

Meanwhile, waiting to upgrade substations until electric vehicle load at each location does materialise, given the lead times involved in such reinforcement, risks long periods of heavy overloads which could cause transformers to fail in service.

Low Carbon Technologies (LCT) with respect to electricity distribution networks are equipment such as Electric Vehicles (EV), Heat Pumps (HP), and solar photovoltaics, which will enable net zero by supporting consumer's lifestyles without emitting more CO2 than they offset. This work presents a new method for smart reinforcement of substations, to prepare for unpredictable LCT loads which will proliferate during the UK's transition to net zero. The proposal, DSDR, proposes the installation of additional transformers in parallel with the existing transformer in each substation, removing the need to scrap and replace it. Telematics-controlled switches are installed on the high- and low-voltage side of each transformer in the substation, and local agent algorithms are deployed to control in real - time when each parallel transformer is brought into or taken out of service.

This approach unlocks several opportunities to operate existing substations in the smart, flexible, resilient, and efficient manner that will be required to support net zero targets. However, care must be taken with the real-world installation of parallel distribution transformers into existing substations. From a technical perspective, in order that transformers share power equally when in parallel, their power rating and percentage impedance should be similar. From an operational perspective, adequate space will be required for an additional transformer; in ground mounted substations, although additional space would also be required to up-rate the existing transformer, the physical envelope of this may differ for parallel transformers therefore careful measurement and planning is necessary.

With pole-mounted substations there is no issue with space, as a parallel transformer can be installed onto an adjacent pole. Finally, with respect to cost, as distribution transformer cost increases with power rating, specifying a smaller additional transformer rather than replacing the existing with a larger transformer is cost-effective, but of course the cost of additional switchgear must be taken into account.

One or more of several objectives may be optimised by the agent algorithms, by reconfiguring the substation's topology in response to real-time events. Secondly, substations may be reinforced well in advance of load materialising, without risk of upgrading the wrong locations; if electric vehicle load materialises elsewhere, the parallel transformers may be moved to that location. Should a transformer fail in-service in a smart reinforced substation, due to the redundant architecture there should be no supply interruption experienced by customers, and much of the existing load could remain being served until repairs can be made.

None of these benefits are available under existing reinforcement practices. Regarding the optimisation objectives introduced above, these include maximising substation operating efficiency, managing the effects on transformer windings of phase-imbalanced loads, and providing fast frequency response through managing voltage levels (referred to as conservation voltage reduction).

In this work, the former objective – maximising substation operating efficiency - is thoroughly investigated through development, evaluation, and validation of suitable algorithms on a software-based digital twin and a hardware-based scale model.

1.1 Research Question

The research question addressed in this thesis is that of how existing electricity distribution substations can be pre-emptively and cost-effectively upgraded to unlock the Net Zero target by enabling electrification of transport, whilst managing efficiency, reliability, and maintainability.

1.2 Motivation

The motivation for this work is as transport and heat move away from fossil fuels and thus are rapidly electrified, last-mile electricity distribution networks are uniquely placed to either act as blockers or enablers of these technologies. In order to meet net zero targets, substations must become smartly operated in real-time to ensure the latter is the case in the UK.

1.3 Research Contributions

The research contributions of this work are as follows.

- A new concept for smart, flexible, efficient, and resilient reinforcement and operation of last-mile electricity distribution substations to enable connection of low carbon technologies.
- A digital twin model of distribution substation dynamic reconfiguration infrastructure for rapid development and evaluation of optimisation algorithms.
- A bench top scale model of a distribution substation dynamic reconfiguration location for validation of the optimisation algorithms before pilot trial in real networks.
- Development, evaluation, and validation of two algorithms for maximising substation operating efficiency under a mix of domestic base load and electric vehicle charging patterns.

1.4 Structure of Thesis

The structure of this thesis is as follows; chapter two reviews the history, background, and academic literature relating to electrical energy networks, system modelling, net zero, low carbon Technologies, electrification of heat and transport, energy scenarios, and optimisation of distribution networks. Chapter three presents the concept and implementation of a software-based digital twin model for distribution substation dynamic reconfiguration, on which optimisation algorithms can be developed and evaluated.

Chapter four introduces the bench top scale model developed to demonstrate real-world operation and applications of distribution substation dynamic reconfiguration. Chapter five plans the experiments to be performed for evaluation and validation, whilst chapter six describes the new optimisation algorithms developed. Chapter seven presents the results of the experiments performed, going on to discuss the findings.

Finally, chapter eight summarises the work carried out in this project, draws conclusions from the results obtained, and suggests future topics for extending this research.

2 Background and Literature Review

2.1 Introduction

This chapter presents a background and literature review to the newly proposed method of DSDR, a pre-emptive reinforcement and flexibility strategy for distribution final substations. The technique involves provisioning additional transformer(s) in parallel with a substation's existing transformer as the reinforcement method, and introducing DNO-side flexibility by switching individual transformers in and out of service. Applications include managing losses, voltage levels, harmonics propagation, and phase imbalances.

The system under study is a theoretical final distribution substation in the UK, which contains a single distribution transformer at risk of becoming overloaded as EV charging proliferates downstream to it in the coming years (the issue being addressed). The motivation for proposing a parallel transformer arrangement and DSDR control of the substation is to enable a managed rollout of reinforcement flexibly, so that the reinforcement process over a large population of substations can take place before the load materialises, whilst keeping substation technical losses as low as possible.

Reviewed topics in this chapter include electricity distribution, substation assets including transformers, smart grid technologies, and parallel transformer operational switching algorithms. Related UK innovation trials are also discussed, to understand how the proposed method could lead to pilot trials and business-as-usual deployment.

2.2 Electrical Energy Networks

Electrical energy networks are formed by a collection of nodes at which energy may leave or enter the system, connected by edges along which energy may travel. The structure of the network is known as its topology, and may be represented as a mathematical graph [1]. Such networks are used to transport electrical energy between generators which convert other energy types (fuels) into electrical energy, ultimately to consumers. Here, the electrical energy is converted into energy types useful at the point of utilisation, such as heat or motion. A representative diagram showing how the electricity generation, transmission and distribution systems work together is shown in Figure 1.

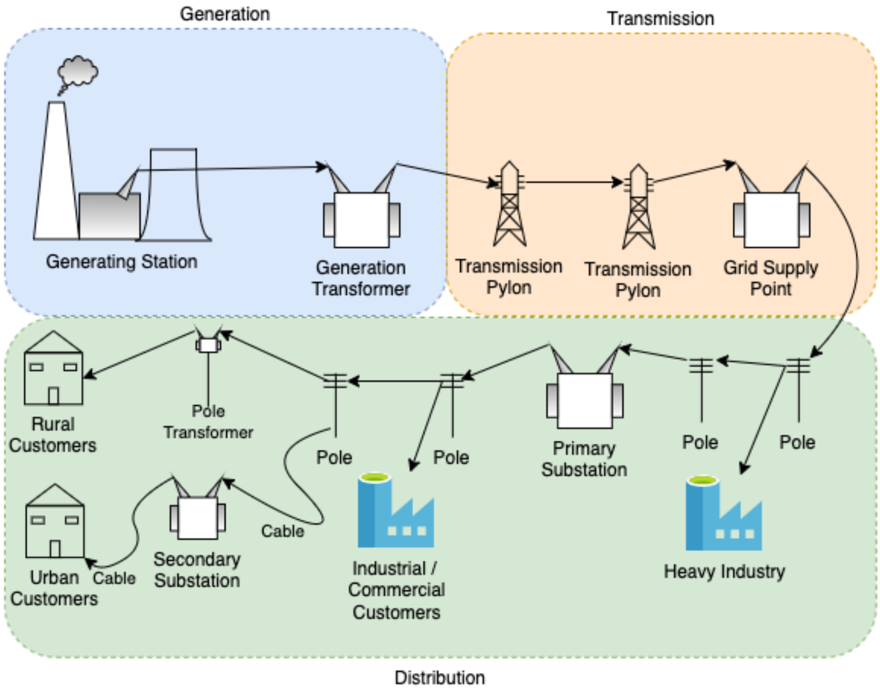

Figure 1 - Generation, transmission and distribution systems..

The above representation of the distribution system shows heavy industry customers connected at primary voltage levels, with general industrial and commercial customers connected at the lower MV levels, and domestic customers fed at LV via overhead lines in rural areas, and underground feeders in urban areas.

2.2.1 Generation

Electrical generation plants convert thermal or renewable energy sources into electrical energy which is then supplied to an electrical energy network; the principles of electrical generation were introduced by Michael Faraday in the early nineteenth century [2].

The earliest electrical generators provided power locally, for example to light a local area or power a single building. To achieve electricity networks spanning a larger distance than a few streets, central generation was introduced by Sebastian Ferranti [3]. This required electricity to be generated or transformed to a higher voltage at which it could be transported with minimal losses, and meant that larger, more economical generators could be operated outside of densely populated areas. Central electricity generation is still employed today, most often generated at 25 kV before being transformed to extra high voltage for long distance transmission. More recently, local electricity generation, known as 'Distributed Generation' (DG) has been connected to electricity distribution networks, much closer to consumers than to the central generating stations [4].

Most typically such local generation converts renewable energy sources such as solar and wind into electrical energy at distribution voltage levels using power electronic converters. An extension of this concept is utility scale renewable energy farms, which are located away from densely populated locations where energy is consumed, and typically connect to the electricity network at higher level distribution voltages such a 11 kV or 33 kV. Such solar farms and wind farms may include local storage, and also use power electronic converters which rely on conventional central generation to produce stable AC voltages to which they can inject power. [5]

2.2.1.1 Synchronous Generation

Contemporary central generating stations are most often of the thermal type, meaning that they convert stored energy such as fossil fuels or nuclear into heat, which is used to heat water into steam, operating a turbine which couples rotational mechanical power into an electrical generator. Such stations are able to operate as synchronous generators, meaning they spin synchronously with the AC frequency of the electricity network voltage and are thus locked to that frequency. When synchronous generators export power, they cause the frequency of the electricity network to increase. The spinning mass of synchronous generators produces inertia, which is resistance to the change in frequency caused by fluctuating loads. In addition, synchronous generators may be configured to automatically export additional power when the network frequency reduces below nominal, and to reduce their export when the frequency increases above nominal. [6]

2.2.1.2 Asynchronous Generation

Asynchronous generators, typically comprising induction machines or power electronics converters, are differentiated from synchronous generators as they do not contain parts which rotate at the same frequency as that of the network to which they are connected. Such generators typically cannot form electricity networks from a non-energised state (which is known as 'black start' [7]), and do not produce inertia. Instead, they follow the frequency formed by synchronous generators which must exist within the same network in order for asynchronous generators to operate. Distributed and renewable generators tend to be connected to electricity networks as asynchronous generators [8].

2.2.2 Transmission

Power transmission is the transport of electrical power over large geographical distances, aiming to connect sources of generation with load centres with minimal power loss. As all synchronous generators connected to a transmission system rotate at the same speed, a power system shares a common system frequency across all nodes. There exist small differences in phase angle between the distant nodes in a transmission system, affected by the magnitude and direction of power flowing through the node. [9]

2.2.2.1 Wide Area Operation

Electricity is transmitted at 400 kV and 275 kV over a system referred to as the super grid, before being transformed to 132 kV to supply regional Distribution Network Operators' (DNOs) systems at Grid Supply Points (GSP), where bulk energy transfer is metered for settlement purposes. The stability of the transmission system is primarily managed from second to second by monitoring and controlling the system fundamental frequency; additional generation is dispatched to increase or decrease the system frequency respectively, keeping it within 0.5 Hz of the nominal 50 Hz target. [6], [9], [10]

2.2.2.2 Reliability Indices

The principal purpose of distribution systems from a customer's perspective is to maintain voltages within a tolerance range around the nominal for each voltage level, to ensure that customer's equipment can operate correctly, and to deliver power reliably by minimising Customer Interruptions (CI) and Customer Minutes Lost (CML). DNOs are regulated based partially on their performance against these [11].

2.2.3 Distribution

Electricity distribution systems operate at lower voltages and over smaller geographical areas than transmission systems, delivering energy from GSPs to utilisation customers within a defined region. Energy enters these networks at 132 kV and is distributed in multiples of 11 kV, following the convention of Ferranti's original central distribution system serving central London from Deptford power station. Standard distribution voltage levels are 66 kV, 33 kV and 11 kV, at which some large customers are also supplied; these are referred to as Medium Voltage (MV).

Domestic customers are supplied at 230 V single phase, whilst small to medium commercial buildings are connected at 400 V three phase; these voltage levels are referred to as 'Low Voltage' (LV). [1], [3], [12], [13]

2.2.3.1 Network Topologies

Three feeder circuit topologies are used in distribution networks, primarily to manage voltage levels, thermal limits of cable and lines, and system resilience. Radial circuits [14], the most typical at LV, emanate from a distribution transformer, serving a number of customers before ending at a link box with a normally open point, i.e. with links removed for urban systems, or at an end pole for rural systems. Such radial circuits often taper, meaning that the conductor Cross Sectional Area (CSA) and therefore its Current Carrying Capacity (CCC) becomes reduced towards the remote end of the feeder. [15], [16]

Ring circuits [14], most commonly used at MV levels, connect multiple substations via Ring Main Unit (RMU) switches to a continuous ring, meaning that power can flow in either direction. The major advantage of ring circuits is that a fault in any cable section may be isolated by opening the two adjacent RMUs, with power thus either maintained or quickly restored to each substation.

Whilst radial feeder circuits may be protected using simple, low cost and low maintenance fuses, ring circuits require more coordinated protection consisting of circuit breakers and relays. [15], [16] Meshed topologies [14], which are often used at LV levels within cities, consist of multiple radial feeders connected together, these often being supplied by a set of substations . Upon a fault occurring in any individual feeder cable, power continues to flow to all customers via the healthy sections of the feeder, whilst the fault is expected to clear itself by causing local damage to the cable which can later be repaired. As with ring topologies, coordinated protection and monitoring is required on meshed LV networks to isolate any faults which do not clear themselves, and to prevent faulty substations from being back-fed when their MV protection has tripped. [15], [16]

2.2.3.2 Net-Zero Technologies

Small Scale Embedded Generators (SSEG) [17] are distribution system connected renewable energy generators, referred to as behind-the-meter [18] because they are typically within a consumers installation. Installation of such systems is often subsidised by government schemes in order to assist energy systems with meeting net-zero targets [19]. Benefits of such technology include the reduction of load seen by the distribution system and reduced imported energy bills for consumers. Technical challenges for the DSO in hosting SSEG's include over-voltages on feeders when high local generation is coincident with low base load [20].

Microgrids are sections of one or more consumer's installations, typically containing SSEGs, which are configured to work together, and not to shut down when disconnected from the distribution system as described above but instead to become self or mutually supporting in that event. Such operation is referred to as islanding, which is a topic of much recent research as well as innovation work by DSO's, but is yet to become widespread in real-world distribution systems [21].

Low Carbon Technologies (LCT) are those which cause or support significantly less carbon to be emitted than conventional technologies either through increased energy efficiency or alternative fuels or energy sources. Examples include electric vehicles, heat pumps and renewable SSEGs. LCTs support the path to net-zero, whilst often presenting significant operational challenges for electricity distribution networks.
Electrification of heat and transport marks a move away from fossil fuels in providing these services, whilst putting additional load on electrical energy systems [22].

2.2.4 Substations

Electricity substations are locations where voltage levels are transformed within transmission and distribution systems. These present both a major asset management challenge for DSO's, and a focus of attention for smart grid innovations which are scalable to many nodes [23]. The focal point of any substation is the electrical transformer, responsible for converting the system operating voltage – usually to a lower level, except for at power stations where the voltage levels are increased for transmission.

Within many substations will also be found busbars, solid conductive bars mounted to a wall or frame on insulating stand-offs. Low voltage busbars are often uninsulated, whilst high-voltage busbars are enclosed and often insulated with dielectric fluid. Busbars permit easy connection of substation equipment including monitoring and test equipment. Outgoing distribution feeders from a substation may emanate from the bus-bars via protective fuses, or from a dedicated feeder pillar which contains busbars, protective fuses and conductor terminals within a protective enclosure. [15]

Distribution substations are unattended for most of their operational life, and traditionally have contained minimal instrumentation. Typical monitoring devices within low-voltage substations include a maximum load indicator, which records the peak electrical current or power demand, and holds that value until the next maintenance visit upon which it is noted and the instrument reset. A similar instrument for recording the peak transformer oil temperature may also be fitted within a temperature pocket of the transformer tank. Contemporary distribution substations, those within urban areas, and those operating at medium voltage and above, are furnished with electronic instrumentation connected to a control centre via Supervisory Control and Data Acquisition (SCADA) systems. Typically, system voltage and load current will be recorded and transmitted at half-hourly intervals, whilst circuit breaker status is transmitted asynchronously as open or close events occur. [24] [25]

2.2.5 Transformers

Transformers contain a higher voltage and lower voltage winding per phase (and optional additional windings known as tertiaries), which are wound around and therefore magnetically coupled to a common iron core. These are contained within a grounded tank and power is conveyed through the tank by use of insulated bushings [26]. Transformers within transmission and distribution systems are filled with an insulating oil which also serves as a heat transfer medium to provide a cooling effect [27]. The principal installation methods are pad-mounted, where the transformer is placed on a pre-formed concrete base, and pole-mounted where the transformer is fixed atop a pair of wooden poles. The former is found within urban areas and at large load centres, whilst the latter is more typical of rural installations [15].

2.2.5.1 Critical Factors

Numerous factors surrounding distribution transformers are critical to the selection and operation of such equipment.

2.2.5.1.1 Faults and protection

As transformers can experience various fault mechanisms such as overheating of windings, oil leaks, and short circuits, it is necessary to consider protective equipment which can prevent a destructive event should such a fault develop. Two widely used and cost-effective protective devices are commonly installed alongside distribution transformers for this purpose. Firstly, a Buchholz relay de-energises the transformer should gas develop within the transformer oil system, such as might happen due to overheating or low oil level [28]. Secondly, a medium voltage circuit breaker de-energises the transformer should an overcurrent occur, for example during a short circuit [29].

2.2.5.1.2 Thermal Issues

Unlike other electrical distribution equipment such as lines, cables, busbars and switchgear, transformers contain tens to hundreds of metres of conductors within a constrained physical envelope. It is therefore critical to consider how the excess heat generated by resistive losses in the windings can be removed so as to prevent them overheating, which would damage the insulation.

2.2.5.1.3 Saturation and inrush currents

Transformer ferromagnetic cores can saturate when an excess of magnetic flux is induced within them, which leads to harmonic pollution of the input current and output voltage [30]. The two main causes of core saturation are overvoltage at the transformer primary, and the presence of DC voltage at any of the transformer terminals [31]. Additionally, when first energised, abnormally large currents known as inrush currents can be drawn by the transformer until the core's magnetic flux stabilises, which can cause tripping operation of protective devices [32]. Mitigation methods against high inrush currents include Point-on-Wave switching and DC pre-fluxing [33].

2.2.5.2 Transformer Modelling

Distribution transformers may be simulated electrically using equivalent circuit models, which are available in varying levels of fidelity, according to the phenomena being studied.

The π-equivalent circuit shown in Figure 2 [34] separately models, using discrete components, the primary and secondary winding resistances (R_1 and R'_2), core losses (R_{m1} and R_{m2}), magnetising reactances (L_{m1} and L_{m2}), and leakage reactance (L_s). This model is suitable for accurately modelling the inrush currents mentioned in section 2.2.5.1.3, at the expense of additional measurements and calculations to determine a transformer's equivalent circuit component parameters, and of running a simulation with suitably small timesteps to capture transient waveforms.

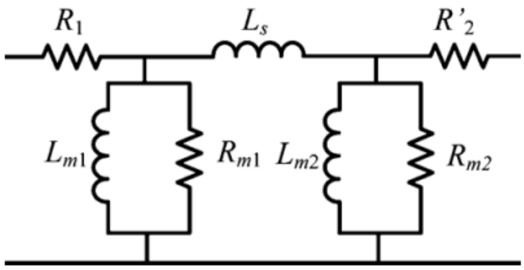

Figure 2 – The π-equivalent circuit model of a distribution transformer [34].

The T-equivalent model shown in Figure 3 [34] is a reduced fidelity model, which is most suited to capturing losses within the transformer under steady state operating conditions.

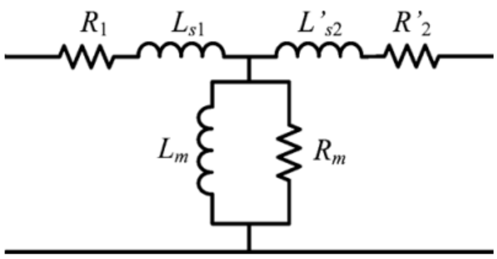

Figure 3 –The T-equivalent circuit model of a distribution transformr [34].

Here, the magnetising reactances are combined into a single lumped component, which simplifies the measurement of equivalent parameters on physical transformers. Digital simulations based on the T-equivalent model will be used within this thesis, as the focus is on algorithms for managing losses.

2.3 Electricity System Modelling

This section reviews the introduction, development and state-of-the-art in electricity system modelling, which began in the 1950's with physical scale models known as AC network analysers, which reduced the 'sheer labour of computation' required for hand calculation of AC circuit analysis [35].

Each analyser consisted of circuit elements contained in cubicle units, operating at a nominal 50 volts (V) and 50 milliamperes (mA). Frequency of operation was a nominal 50 Hz, to 'enable smaller components'. Both steady-state load studies and system stability studies were performed by interconnection of cubicles implementing generator, load, capacitor and transformer models using modelled lines to represent a section of the real-world or proposed system under investigation [36].

Measurements of voltage and current were then made at nodes of interest on the analyser, and the readings scaled up according to system operating levels. Figure 4 shows an AC network analyser [36], with the mimic panel to the left indicating the network diagram and node states, the cubicles to the right implementing passive and active circuit elements, and an oscilloscope in the foreground for measuring waveforms at any node in the system. Such systems were large and expensive, therefore attention soon turned to using digital computers for electricity system modelling, beginning in the 1960's [37].

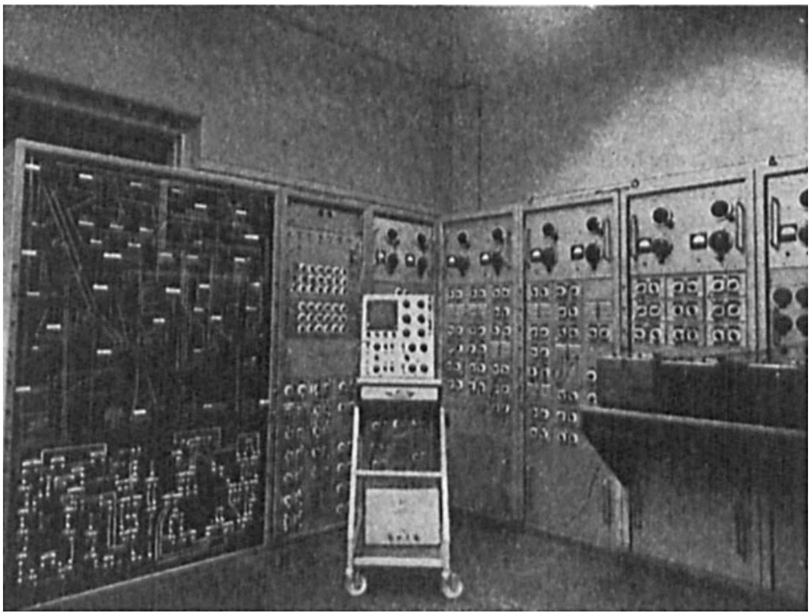

Figure 4 - Steady state and transient AC Network Analyser [36].

Early electricity system modelling using digital computers was suited to steady state load flow, 'economy loading', 'economic dispatch', and transmission losses studies, relying on punch cards for data input and output [37]. The proliferation of digital computers was aided by the discovery that they could be utilised in real time for 'digital control' of parts of the electricity system, a clear advantage over prior analogue systems, although AC network analysers continued to be used into the 1980's for transient studies [37].

Simulation of large AC systems required a reduction in model complexity in order to achieve reasonable convergence durations, therefore the 'DC Load Flow Model' was introduced into digital modelling systems [38]. This approach ignores reactive power flow and losses, with the aim of determining real power flows through each line, which is useful for managing thermal constraints due to line and transformer loading.

Since the 1990's, computer simulation tools have been available for modelling power system transients, negating the need for analogue analysers [39]. Such software is used for understanding effects on a network of switching operations and system faults, known as 'Electromagnetic Transients' (EMT) [39]. From the 2000's, EMT modelling has been extended into real-time simulations through 'Power Hardware in the Loop' (PHiL) systems [40]. PHiL combines an EMT software model in which each time step can be solved in real time, connected via an analogue interface and power amplifier to real power hardware, such as a photovoltaic inverter. This approach enables the transient behaviour of power system components such as protection relays, or consumer equipment such as power electronic converters and electric vehicles to be determined experimentally similar to AC network analysers, whilst the electricity network to which it is connected is entirely software defined. PHiL requires dedicated computer hardware, interfaces, amplifiers and real-time software, which are complex and therefore almost always proprietary. Figure 5 shows a PHiL block diagram, with a software-modelled electricity system in blue, analogue interfaces in purple, and power hardware in orange.

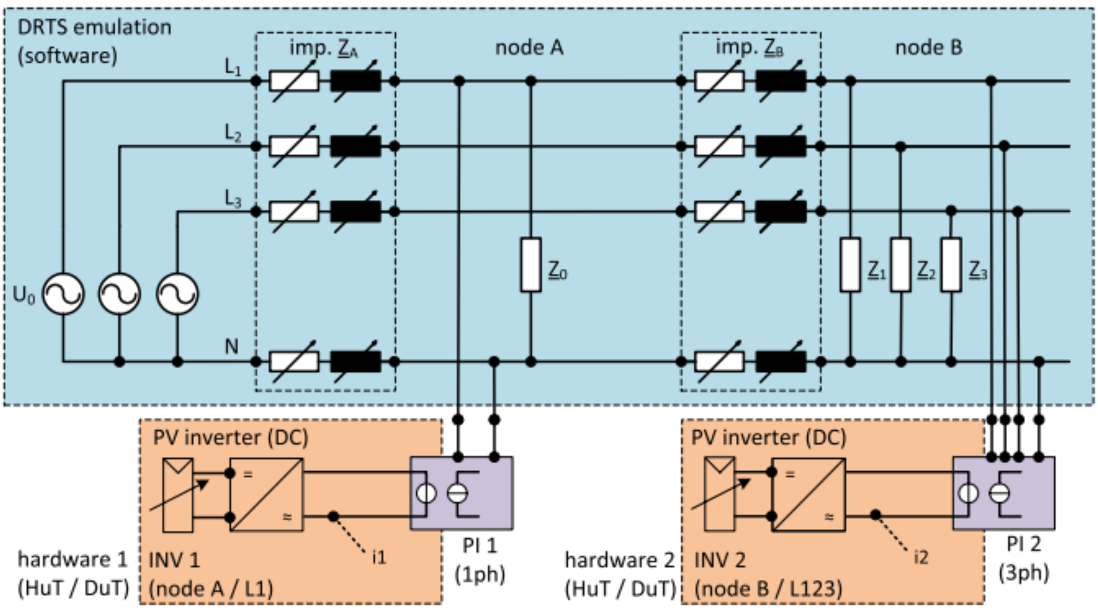

Figure 5 – Power Hardware in the Loop block diagram [40].

Most recently, the proliferation of Open Source Software (OSS) tools for electricity system modelling and the publication of standards for their data interchange has led to much wider adoption of such tools [41] [42]. Using OSS tools and model standardisation, users can contribute features, models can be readily shared between academic and industry users, and simulations can be run on personal computers, in the cloud, or on edge devices regardless of hardware type or operating system. OSS tools have been released for modelling transmission systems, distribution systems, EMTs, and electricity system consumer behaviour and markets – examples of which are given in Table 1 below.

Table 1 – Example OSS projects for electricity system modelling.

OSS Project	**Use Case**	**Software Language**	**Pros / Cons**	**Ref**
PowerModels.jl	Steady-State Power Network Optimization	Julia	Only available in the Julia programming language which is not commonly used, focus is optimal power flow	[43]
PyPSA	Transmission System Modelling	Python	Widely used but more suited to bulk power systems problems than distribution and losses	[44]
OpenDSS	Distribution System Modelling	Delphi	Implementations available in multiple languages, widely used in academia	[45]
AMIRIS	Electricity System Markets	Java	Focus is mostly on transactions, pricing, and markets of electrity	[46]

2.3.1 Energy System Scenarios

Energy System Scenarios (ESS) are long-term forecasts which provide “a qualitative storyline [and] quantitative metrics” to describe how generation and load profiles are expected to be impacted by wider societal changes [47].

ESS are often grouped into sets, reflecting differing policy landscapes or economic scenarios; these enable “science-based decision-making” by energy system operators in the areas of “energy economy, capacity expansion or power sector planning” [47], [48]. ESS are produced by first selecting an energy system model with the “right level of complexity to accurately represent the problems” which the scenarios are intended to answer, taking into consideration the granularity and time horizon required [49]. Various possible futures of economic and policy landscapes are provided to the model to “generate long-term transformation scenarios for … electricity systems” [49].

The UK National Grid’s Future Energy Scenarios (FES) is a long-term forecast of “the future of energy … [to] 2050” designed to support “network planning, investment decisions and government policy” [50]. It contains four scenarios, three of which lead to net-zero carbon emissions by 2050, and one in which the rate of carbon intensity reduction remains steady, causing net-zero targets to be missed in each year from 2025 onwards [50] as shown in Figure 6.

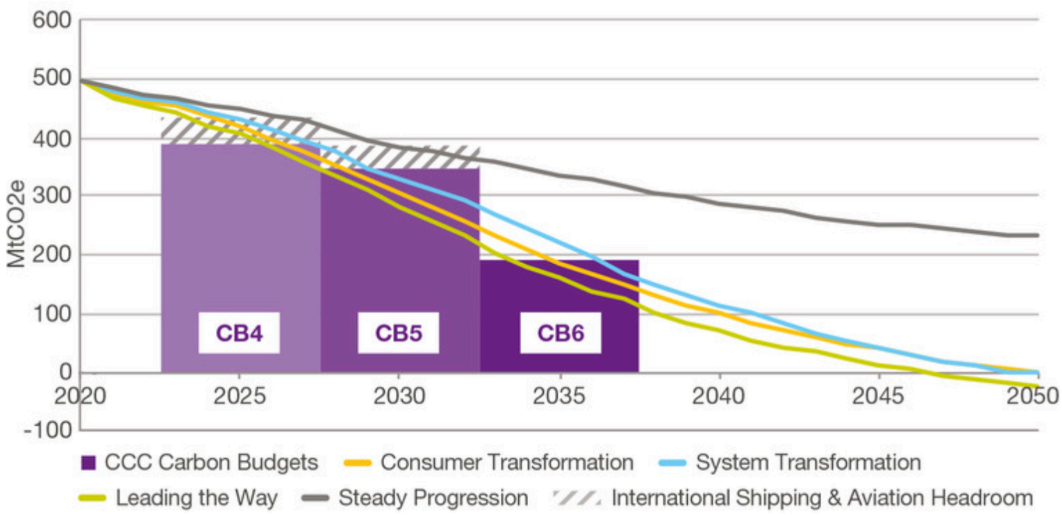

Figure 6 - Future Energy Scenarios carbon intensity [50].

The climate change committee budgets are shown as bars in the figure, with the carbon intensity forecast of all energy consumption in the UK plotted as a line for each scenario. In FES, estimates of total annual energy consumption are disaggregated into residential, heating, transport, and industrial and commercial loads for the years 2020 and 2050.

Table 2 below summarises the electricity portion of the forecasts.

Table 2 – Annual electricity demand scenarios (TWh) (summarised from [50]).

Scenario	**Residential**	**Heating**	**Transport**	**Industrial & Commercial**
2020	74	23	1	163
Consumer Transformation 2050	57	87	*102*	246
System Transformation 2050	63	54	*94*	173
Leading the Way 2050	45	77	*95*	197
Steady Progression 2050	75	50	*101*	179

This shows that whilst residential, industrial, and commercial demand is expected to remain steady, heating load will double or triple, and transport load will increase by a factor of around 100 in all scenarios. Each DNO additionally publishes its own Distribution Future Energy Scenarios (DFES), expanding upon the national FES by providing increased granularity local for an identical set of scenarios [51]. The research question addressed in this thesis will leverage ESS scenarios and forecasts to investigate the implications of the proposed distribution substation flexibility schemes.

2.3.2 Smart Grid

Smart Grids (SG) are electricity systems comprising digital 'information management, control, sensing, communication, and field devices to coordinate multiple processes' [52], whereas traditionally such systems relied on analogue, electromechanical, manual or overall less co-ordinated techniques and processes. The purpose of SG are to enable applications 'for dealing with new grid challenges that have arisen by the introduction of renewable energies' [53], and also for enabling the electrification of heat and transport which can then be supplied by that renewable energy.

2.3.2.1 Reinforcement and Deferral

To support the demand for the charging of Evs, it has been projected that 'by 2050 a third of low voltage (LV) grids in the UK would need reinforcements' [54]. Reinforcement may be required for any or all of the current-carrying equipment including lines, feeders, busbars, switchgear and transformers [55]. Such reinforcement is costly in terms of asset procurement, civil enabling works (for example buried feeder cables), labour, and temporary measures to prevent customer supply interruptions.

Transformers are often the choke point for reinforcement; lines and feeders are typically well oversized initially, and the load is distributed along their length over which excess heat generated can more readily be dissipated, whilst transformers carry the entire load of a distribution substation, and are more easily damaged by overloading.

Existing reinforcement and mitigation techniques include the construction of new additional substations onto the existing distribution network [56], new feeders to spatially distribute load amongst substations [57], use of EVs as a resource of backup power [58], and 'managed charging and strategic charger placement' [59].

As a result, DNOs are seeking to 'defer expensive grid reinforcement' [60] until as far into the future as possible by leveraging flexibility in energy demand and storage which can be enabled by SG technologies. Blended distribution network planning strategies combining targeted reinforcement with deferral techniques including network reconfiguration and 'dispatchable … renewable generators and energy storage units' have also been modelled [61].

2.3.2.2 Flexibility

Flexibility, defined as 'controlled power adjustment sustained for a required duration' [54] to regulate the 'supply-demand balance to adapt to the fluctuating output of variable renewable energy' [62] resources, may be used by DNOs to defer reinforcement as LCT loads increase by 'load smoothing and peak shaving' [63], whilst maximising utilisation of renewable generation. Several specific techniques for implementing flexibility have been both proposed and implemented.

Demand Side Response (DSR) involves controlling 'loads of the final users such that the overall demand is more convenient for the supply side' [64]. Vehicle to Grid (V2G), defined as the 'bidirectional flow of energy between … EVs and the grid' [65], seeks to control a DNOs' customers' EVs by taking advantage of their energy storage function to return energy to the grid when required by the DNO. Grid connected 'coordinated battery deployment at the street or building complex level' [63] is energy storage installed by customers, then partially signalled by the DNO for 'load smoothing and … peak shaving' [63] purposes.

The common feature across the above-described flexibility technology is the requirement for assets owned by DNO customers to be made available for control by the DNO; this of course requires incentives “to encourage market participation” [66]. Specific challenges in successfully delivering flexibility schemes require solving ‘technical, economic, regulatory, and user-related’ [54] barriers; this can be of particular difficultly in non-vertically integrated markets such as the UK, where energy generation, retail, transmission, and distribution are all provided by separate entities.

2.4 Focus of Thesis

The motivation of this thesis is to investigate a pre-emptive transformer reinforcement and flexibility strategy for distribution substations, which may be implemented by DNOs to benefit customers, whilst avoiding the barriers of directly involving customer installations in the provision of flexibility. Pre-emptive upgrading of distribution substation transformer capacity in locations where significant additional LCT load is expected can relieve pressure of the procurement and labour challenges to reinforcement, by spreading the rollout out over a longer duration than reactive reinforcement.

As transformers are often the first item to require reinforcement in a distribution network, and existing practise is to replace an overloaded transformer with one of a higher rating, here we consider an alternative approach. Provisioning additional transformer(s) in parallel with a substation’s existing transformer, instead of removal and replacement of the same with a larger capacity unit:

a) Removes the need for early decommissioning of an otherwise serviceable asset.

b) Increases redundancy of equipment, thus improving reliability indices in the face of asset failure in service.

c) Enables increasing LV capacity without increasing the mass of the individual transformers, significant for pole-mount installations with transformer weight limits. For pad-mounted installations, although additional space would be required, vertical stacking could be considered.

d) Allow assets to be moved around the network if locational LCT demand differs from that forecasted; for example a parallel transformer rarely energised over the course of a year could be shifted to an overloaded site, subject to transport and and installation cost considerations.

e) Most significantly, unlocks the potential for DNO-side flexibility in switching individual transformers in and out of service to manage losses, voltage levels, harmonics propagation, and phase imbalance. We will refer to this technique as Distribution Substation Dynamic Reconfiguration (DSDR) in this thesis.

The following sections will explore the academic literature in answering the research question ‘Are DSDR algorithms a viable method for enabling net-zero, by producing DNO side flexibility following pre-emptive reinforcement?’

The concept of varying the number of transformers in service was discussed in a 1987 transformer operation handbook, with the proposed objective being reduction of losses, and the switching decision to ‘connect another transformer when those in service are at half load’ [67]. The conclusion at that time was that it was ‘out of the question to make constant adjustments’ i.e., to vary the number of transformers in service, but that it could be done either daily during peak load hours, or seasonally – for example during winter.

It is most likely this conclusion was reached because the technology required for dynamic substation reconfiguration was not widely available or economic to deploy; also because distribution-connected LCTs such as EV and PV, which cause intermittent load and generation, power quality disturbances, and phase imbalances were not yet in widespread use.

At the present time, objectives which can be addressed by DSDR such as enabling widespread EV connectivity at LV whilst minimising losses, power quality disturbances and transformer overheating have become of utmost practical interest; meanwhile equipment required for DSDR such as automated circuit breakers, digital instrumentation, and edge computing are widely available.

2.5 Reconfiguration and Optimisation of Distribution Systems

A suite of methods is described in the literature for managing substation capacity, efficiency, and power quality under dynamically changing load conditions; these can broadly be divided into those involving reconfiguration and those involving power electronics. Reconfiguration methods tend to offer quantised steps, relatively infrequent switching at a minute or hourly timescale, and no appreciable switching losses, whilst power electronics methods tend to be continually adjustable in sub-second time ranges, but produce switching losses which must be taken into account [68] [69].

2.5.1.1 Distribution Networks

Distribution Network Reconfiguration (DNR), referred to as Dynamic Reconfiguration (DR) when used in response to changing loads [70], has been defined as ‘changing the operating structure of a distribution system … by resetting the status of line switches’ [71]. A simplified network topology demonstrating DNR is shown in Figure 7, which illustrates a ring feeder section comprising lines ‘q’, ‘r’, ‘s’, and ‘t’, with a flexible normally open point.

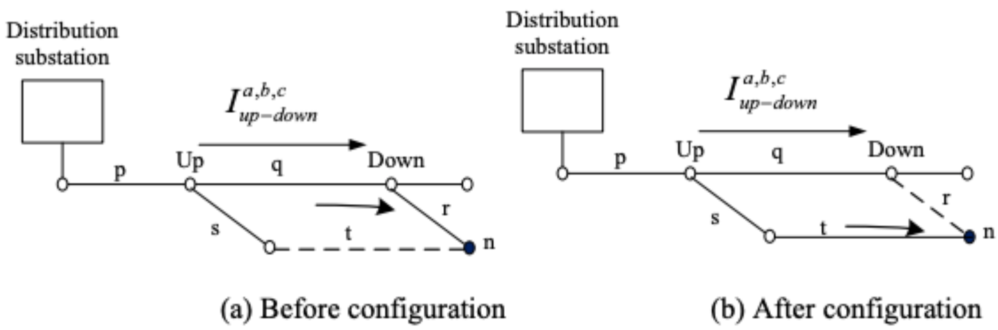

Figure 7 - Simplified network topology demonstrating DNR [72].

The isolating switches between feeder sections are represented by circles at the nodes, and it is here that loads are connected. Feeder sections are represented by solid lines for those in the energised state, and dashed lines for de-energised. Subfigure (a) shows section ‘t’ disconnected, meaning that section of feeder has open switches either end so that power flow is routed *around* the section to reach node n.

In subfigure (b), section ‘t’ has been switched back in allowing power to flow through it to node n, whilst section ‘r’ has been disconnected to maintain the radial topology of the network.

DNR has traditionally been implemented by maintaining the network topology in a radial circuit configuration through Branch Exchange (BE), which ‘converts the radial grid to a ring grid’ momentarily, before the ‘radial structure is restored by opening some other lines of the network’ [73]; successive BE switching operations are modelled or performed to arrive at an optimal or heuristic solution for the objective function(s) under consideration.

The technique has been proposed to optimise a wide variety of objective, including to minimise network losses [70], to reduce risk of voltage violations when DG outputs change unpredictably [71], to manage ‘component condition and substation reliability’ [74], for ‘minimising the annual energy losses considering the variability in active and reactive power demand and distributed generation’ [75], and to improve power quality by reducing voltage harmonics and sags [72].

Further, applications have been proposed in the areas of increasing hosting capacity for PV systems in distribution networks with harmonic pollution [76], minimising curtailment of PV generation [77], and to minimise a distribution network’s load on the transmission system in the presence of intermittent DG and unbalanced loads [78].

2.5.1.2 Distribution Substations

A switchable transformer, containing windings in a reconfigurable arrangement, was proposed in [79]. The transformer’s primary and secondary windings comprise four winding subsections, and are controlled by three switches to configure the sections into series, parallel or conventional arrangements by means of a fixed threshold algorithm.

Phase switching, which aims to balance loads amongst each of the three phases by transferring loads between phases at reconfiguration switches, was been proposed for installation on electricity customer premises and at the substation [80]. Switching decisions are made according to a network model and measured currents, with either a scheduled switching profile or dynamic decision making in near real-time.

Power electronics Soft Open Points (SOPs) [68] have been utilised to share capacity between substations by flexibly controlling power flows between feeders emanating from distinct substations at their meeting points, which would otherwise remain electrically disconnected from each other under normal network operating conditions. These are power electronic devices, which introduce additional losses into a substation, consisting of fixed losses, switching losses and conduction losses.

The method differs markedly from the parallel transformer reconfiguration method proposed in this thesis, principally as DSDR involves reinforcement of the LV network flexibly (i.e. increasing LV capacity), whilst SOP involves flexibly sharing the existing capacity between usually isolated sections of the LV network.

2.5.2 Parallel Transformers and Algorithms

The operation of railway traction transformers in parallel to manage 'reliability, availability, and flexibility of the supply system' was explored in [81], which also considered non-parallel mode and single transformer mode of operation for dual-transformer substations. As the 'maximum efficiency is achieved at a load level ranging from 40 to 50%', this threshold in relation to the average loading caused by train headway patterns was proposed to determine in which mode to operate the substation for minimal losses, which resulted in losses reductions of up to 6.52%.

Dynamic switching of transformers in real-time was not considered; Figure 8 shows the three fixed operational modes taken into consideration, where normally open switches are represented by the unfilled squares and normally closed as shaded squares. Section (a) shows the two transformers feeding separate loads which are not connected, referred to as non-parallel mode. Section (b) shows the two transformers operating in parallel to shared loads. Section (c) shows one transformer switched out of circuit, with the other feeding all loads.

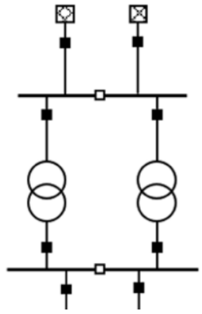

(a) Non-Parallel

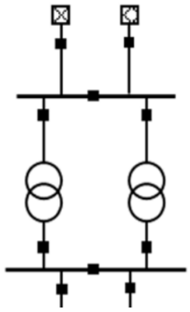

(b) Parallel

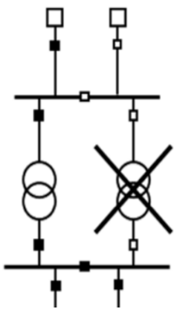

(c) Single-Transformer

Figure 8 – Configuration modes for parallel transformers [81].

Operation of GSP and primary distribution substations with multiple parallel transformers to 'minimise annual energy losses while avoiding frequent transformer switching' was investigated in [82]. A constraint-based optimisation algorithm, applicable to balanced or unbalanced, sinusoidal or harmonic loads was proposed [82]. Frequent transformer switching was avoided by either including constraints that either enforced a minimum up-time for a transformer after it had been switched on, or by directly constraining the number of switching operations during a given time span.

The limitations of the approach proposed is that substation loading forecasts are required in advance of optimisation, and the entire switching schedule for a substation is optimised ahead-of-time rather than in real-time.

2.5.3 Prior Innovation Trials

A number of DNO projects in the UK have trialled innovations of concepts related to DSDR.

2.5.3.1 Low Energy Automated Networks

Southern Electric Power Distribution's Low Energy Automated Networks (LEAN) project targeted 'switching off one in a pair of transformers in selected primary substations', along with reconfiguration of associated network topology for maintaining redundancy, to 'avoid fixed iron losses'. Substation transformer losses were reduced by 25-30% over the 12-month trial period at two substations, compared with full-time parallel operation. The algorithm used to determine the switching point was a pre-determined fixed threshold of half the substation's rated load. Pre- and post-trial testing of the transformers including Sweep Frequency Response Analysis (SFRA) [83] and Dissolved Gas Analysis [84] (DGA) demonstrated that the transformer health was not impacted by regular switching. [85]

Figure 9 shows one of the substations which was included in the trial. It is a primary distribution substation operating at 33 kV / 11 kV, with two pad-mounted transformers usually operating in parallel for operational resilience. [85]

Figure 9 - LEAN trial substation [85].

2.5.3.2 Customer Load Active System Services

Electricity North West's Customer Load Active System Services (CLASS) project trialled a range of innovative methods for Demand Response (DR) [86] in distribution system primary substations by means of voltage control.

One of the approaches involved 'opening one of a pair of primary transformer circuit breakers', which by increasing the substation's impedance causes a voltage drop which in turn causes customer loads to draw less power. This phenomenon was in turn used to provide Frequency Response (FR) [87] services to the transmission system. [88]

2.5.3.3 Celsius

Electricity North West's Celsius project trialled 'cost-effective approaches to managing potentially excessive temperatures at distribution substations'. The motivation for the work was to determine whether existing LV substation transformer reinforcement could be avoided by fitting transformer cooling interventions, enabling them to handle the increased loads presented by EV and Heat Pump (HP) loads; this would 'maximises the use of existing assets'.

Passive cooling interventions trialled included solar shades and anti-solar paint for outdoor transformers, and additional enclosure vents for indoor transformers. The active cooling interventions trialled were positive pressure air-flow, which forced fresh air over the transformer, and negative pressure extraction to draw warm air away from the transformer. It was found that passive cooling released an additional 6% of capacity from the substation, whilst active cooling released up to 23% additional capacity. [89]

2.5.4 Optimisation Objectives

There are several optimisation opportunities available after a substation has been upgraded to DSDR, each with a particular objective; these will be considered next.

2.5.4.1 Losses

Technical losses – those losses of energy between source and load caused by DNO equipment within the electricity distribution system - are a prominent topic for consideration due to their contribution to the standing charge portion of every consumer's electricity bill.

Transformer losses are split into no-load losses, which occur whenever a transformer is energised, and load losses which are a function of electrical power being drawn from the transformer. DSDR algorithms offer the capability to manage both types of losses, by adjusting the number of transformers in service within a substation dynamically according to load.

2.5.4.2 Harmonics

Hamonic pollution of the voltage supplied to customers by an electricity distribution network, formed by components of the voltage signal at multiples of the fundamental frequency, has regulatory implications for DNOs, can cause damage to customer equipment, and can increases losses in transformer cores.

The cause of harmonic voltage on the supply is from harmonic currents being drawn by customer equipment – typically loads with power electronics converters such as EVs – through the impedance between the load and source. As the substation transformer represents a significant proportion of this impedance, multiple transformers in parallel at the substation will have the effect of reducing source impedance, and therefore reducing the harmonic pollution of supply voltage by harmonic loads. DSDR algorithms can manage harmonic voltages at the substation level, and therefore at all customers downstream of that substation, by managing substation impedance through reconfiguration.

2.5.4.3 Phase Imbalance and Transformer Insulation Ageing

A widespread problem in LV distribution networks is load imbalance between the phases, which causes the more heavily loaded winding of the distribution transformer to run hotter than the remaining two. As a result, the paper insulation on that winding ages faster, which can lead to accelerated failure of the said transformer. It is a nontrivial task to rebalance the phases on a substation which supplies domestic customers, as these are usually provided with single phase services connected to a particular phase on the LV feeder when the main is laid, and before the customer's load pattern is known.

A variation of DSDR that in addition to switching substation topology, also switches phase connections whilst a transformer is temporarily de-energised, would enable this load imbalance ageing effect to be shared evenly between transformer windings.

2.5.4.4 Frequency Support by Conservation Voltage Reduction

Flexibility services to support frequency stability of the transmission system by rapidly reducing demand (or increasing generation) at times of unexpected events, such as a tripping circuit breaker at a generating station or interconnector, are currently provided by energy customers, storage operators, or fast responding generation assets.

By switching from parallel to single operation of a DSDR substation during such events, and thereby increasing substation impedance, any resistive loads of downstream customers can be caused to reduce their instantaneous demand – a technique known as Conservation Voltage Reduction (CVR) [90]. This would allow DNO's to aggregate and provide frequency support services directly to the transmission operator without any end customer involvement.

2.6 Summary

This chapter has introduced the background to electricity distribution, and its place within the wider electricity infrastructure. Substation assets, including transformers which are the focus of this thesis, and the challenges they face in the transition to Net-Zero have been discussed. A high-level review of smart grid was followed by a discussion of the focus of this thesis and the research question to be addressed. This led into a more detailed review of the specific topics most relevant to DSDR, followed by a review of relevant innovation trials which have been undertaken on UK distribution networks.

It was determined that the concept of reinforcement of final (LV) distribution substations to cope with Net-Zero related loading by a combination of installing additional parallel transformers rather than uprating the existing, and switching the transformers dynamically according to load, has yet to be researched. It was found that existing reinforcement methods focus on new construction such as feeders and substations, or on flexibility such as demand response and vehicle to grid. As a result, there is very little to be found in the literature on existing algorithms for parallel transformers aside from the threshold algorithm as used in prior innovation trials on medium voltage parallel substations, which was reviewed in this chapter.

The proposed technique has potential applications in losses management, system resilience, harmonics management and phase imbalance, and frequency response and asset condition management as demonstrated by prior similar projects. There is a clear knowledge gap in the development of novel algorithms for managing parallel low voltage distribution substations in the face of changing and increasing load due to EV and other LCT. This thesis addresses this by providing a testbed for the evaluation and validation of such algorithms, a novel model-based algorithm to improve the substation efficiency optimisation achieved by the threshold algorithm, and implementation of a baseline using the incumbent algorithm so that improvements in this area can be quantified.

The remainder of this thesis will explore DSDR in more detail, commencing with the following chapter which will describe the modelling and software work undertaken.

3 Digital Twin of a Reconfigurable Distribution Substation

3.1 Introduction

The previous chapter described how the electrification of heat and transport due to net zero targets over the next few years are expected to cause large scale increases in the electrical demand on low voltage distribution substations. The proposed novel solution here seeks to address this challenge by effectively monitoring, understanding, and preparing substations for this change through a combination of pre-emptive parallel transformer reinforcement, and post-reinforcement real-time substation reconfiguration for optimal operation.

In this chapter, a digital twin model of the post-reinforcement substation is developed, which will be used to rapidly develop the optimisation algorithms required to implement the solution. The outcome is, according to the literature, the first, complete DSDR DT capable of performing experiments in real time, which can operate either entirely virtually by simulating substation load flow, or integrate with physical instruments in a bench top scale model DSDR substation, to accelerate the route to pilot trials and ultimately business-as-usual of this solution.

3.1.1 Generic Reconfigurable Distribution Substation Model

A specification for a generic DSDR model, on which new reconfiguration algorithms may be developed, evaluated, and benchmarked as required is introduced. This will model a distribution substation which is reconfigurable into single operation mode, representing either the substation before reconfiguration or when operation with a single transformer is selected by the algorithm, and into parallel mode – selectable by the algorithm after reinforcement.

The generic DSDR model includes an instrumentation system for measurement of substation load flow, a controllable load as a means of playing back test case load profiles, and a control system for dynamically switching topology during experiments. The generic DSDR model is intended to represent a real world substation, and the Digital Twin (DT) model described in this chapter is designed to comply with the generic DSDR model; by this approach, algorithms developed using the DT model are readily transferrable into pilot trials and beyond for Business as Usual (BaU) deployments.

The requirements for the generic DSDR model which are introduced below seek to ensure a seamless transfer of DSDR between development using models and deployment into real-world substations.

3.1.1.1 Functional Requirements

Functional requirements for the generic substation model produced in this thesis are introduced next.

3.1.1.1.1 Real time, stepwise operation

The generic model will operate in real-time, and at multiples of real-time, with the capability to extract measurements and perform topological reconfiguration after each load-profile step. Both electricity load profiles and real-time substation monitoring systems are typically temporally monotonic – having a fixed time step – so it is reasonable to run optimisation algorithms and apply topological changes in line with each time step. During algorithm development, it is desirable to reproduce load profiles, and therefore run algorithms and apply their outputs, at a much increased rate; this models real-time operation whilst allowing for rapid algorithm evaluation.

3.1.1.1.2 Transferrable to pilot trials

The generic model will be directly transferrable to pilot trials, for example at distribution system test sites operating at normal electricity distribution voltages such as the Power Network Demonstration Centre [91]. To achieve this, the classes of instrumentation and actuators available at these sites will be considered when implementing DSDR models to ensure compatibility.

3.1.1.1.3 Representative of a final distribution substation

The generic DSDR model's topology will mirror that of a pre- or post-reinforced DNO final distribution substation. These typically operate with an 11 kV primary, transforming the electricity supply to the end customer utilisation voltage of 0.4 kV, and are initially constructed with a single transformer for supplying domestic and small commercial loads.

The overarching research question tackled in this thesis concerns the reinforcement of such substations by installation of additional switched transformer capacity alongside the existing, then controlling the number of transformers active at each load step in real-time to optimise substation efficiency.

3.1.1.1.4 PC-based control with remote connectivity

As a reconfigurable substation's algorithmic control should be capable of operating on generic computing hardware, the implementation of the generic DSDR model will be designed to be computer platform independent. It will also enable remote dial-in control, so that the controlling computer and an operators' computers may be separately located.

3.1.1.2 Limitations

Some limitations are applied here to the generic DSDR model, in order that physical implementations may be constructed for a reasonable cost and therefore be accessible as an algorithm development platform to as wide a range of researchers as possible.

3.1.1.2.1 Number of phases

The distribution substation will be represented with a single-phase system, as this reduces the size and cost of physical DSDR scale model implementations, whilst remaining operationally equivalent to a real-world three-phase distribution system from the perspective of algorithm development.

3.1.1.2.2 Number of transformers

The generic DSDR substation comprises two transformers, each individually switchable, to represent a single transformer site that has been reinforced with a dynamic substation reconfiguration capability. Additional parallel transformers, resulting from further rounds of reinforcement, are possible in real-world substations, but considering such a case during algorithm development adds unnecessary cost to physical models and pilot trials.

3.1.1.3 Substation Model

The generic substation topology designed in this chapter for the development of DSDR algorithms is shown in Figure 10 as a Single Line Diagram (SLD) [92]; this substation model will be implemented as a Digital Twin (DT) [93] model.

Digital Twins (DTs) are defined as a real-time virtual representation of a physical asset, including a simulation of some of that asset's attributes [93]. The DT presented in this chapter follows this accepted definition, with an additional capability to operate entirely in simulation mode, and to do so faster than real-time, which enables rapid evaluation of proposed algorithms.

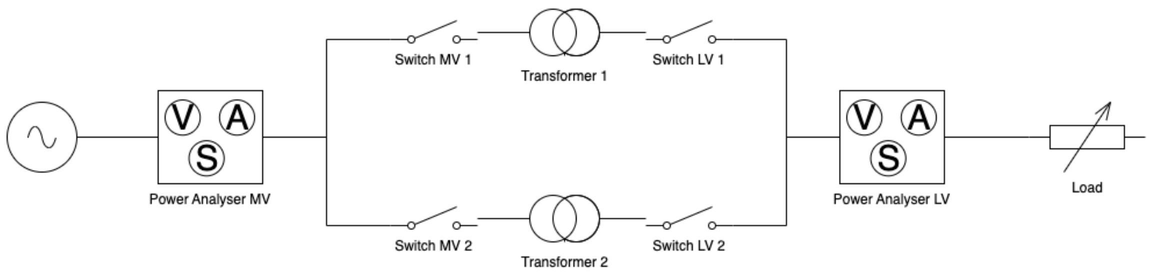

Figure 10 - Distribution Substation Dynamic Reconfiguration (DSDR) generic topology.

The SLD in Figure 10 is shown from left-to-right with respect to the source and load, beginning with an AC voltage source modelled as an infinite bus [94] of negligible supply impedance. This source represents the MV level of a final distribution substation; the nominal voltage will be scaled down from the typical 11 kV in a UK substation, to a safe LV level suitable for benchtop scale models as described in Chapter 4.

Just before the two circuit branches which feed parallel distribution transformers, a power analyser node is positioned to record the MV voltage (V), current (I) and complex power (S). After the branch node, identical branch circuits consist of an MV switch, an MV/LV distribution transformer, and then an LV switch, before both branches recombine. An LV power analyser records the substation's output which feeds a controllable load; for field trials of DSDR, this load represents actual substation demand rather than the controlled load used during virtual and bench experiments.

The proceeding section will build upon the DSDR generic topology and the accepted architecture of a general purpose digital twin, to develop a software framework for the DSDR digital twin including the functional requirements, and considering the limitations introduced in this section.

3.2 Digital Twin Software Design

3.2.1 Introduction

Building from the generic DSDR model, a DT DSDR substation model is developed, designed for rapid development and evaluation of reconfiguration algorithms. The DT implements a software equivalent of a real-world substation operating in real-time, which can also be interfaced to a physical substation for use with scale models and in field pilot trials.

The software implementing the DT model will be designed to be readily extensible, including for additional models such as thermal performance, different classes of algorithm such as those which respond to external signals either from a market or the transmission operator, instruments with extended functionality such as Phasor Measurement Units (PMU) [95] or Continuous Point on Wave (CPOW) [96], and new actuators such as Soft Open Points (SOP) [68].

Such extensibility sets apart the proposed DT model from existing work, both as a new research tool for the benchmarking of DSDR algorithms, and as an operational tool for deploying such algorithms in real-world environments. The development of DSDR is in response to the reinforcement challenges faced by today's electricity distribution networks, as consumer demand rapidly increases with the electrification of heat and transport. Over the remaining sub-sections, suitable software packages are selected with which to implement the components of the DSDR DT.

3.2.2 Software Selection

To implement a general DT architecture, two classes of software component are required [93]. An orchestrator is used to control the capture, processing, and storage of real time data, and a simulator is used to model the behaviour of one or more aspects of the physical system represented by the DT. A general DT software architecture illustrating this concept is shown in Figure 11 below.

Figure 11 - General DT Architecture.

On the left of the diagram, the 'External Systems' block represents both software which is not part of the core DT real-time functionality, such as data storage systems, and hardware with which the DT may communicate, such as sensors connected to the physical asset which the DT twins. These are interfaced to the DT through the Orchestrator component, which is responsible for real-time communications, coordination, and user interaction. The Simulator component of the DT, shown at the right of the figure, is responsible for modelling in real-time one or more parameters of the physical system represented by the digital twin, in response to system state collected by the orchestrator from external systems.

As an illustrative example, a digital twin of a vehicle may receive real-time velocity data from sensors on a real car, and the simulator component of its DT may model the real-time tyre wear on the vehicle. In this chapter, a DT to represent a DSDR substation is implemented. Here, the real-time electrical power demand on a substation is stored in load profiles external to the orchestrator, the real-time power losses in that substation are modelled by the simulator, and an algorithm actor also external to the DT's real-time orchestrator makes real-time decisions about the substation's topological configuration to optimise power losses.

In the following chapter, the DSDR DT is extended to interface with a bench-top physical scale model substation, both to validate the simulator's load-flow accuracy and the performance of optimisation algorithms to be developed, and to demonstrate how the DSDR DT would be used for pilot trials in a real substation. Section 3.2.2.1 below reviews the functional requirements and performs software selection for the orchestrator and simulator components of a DSDR DT.

3.2.2.1 DT Orchestrator

The orchestration component of the DT will be responsible for a number of over-arching tasks, coordinating them to ensure real-time operation, as listed below:

- Interfacing with data sources such as the test load profiles to be played back during an experiment.
- Supervision of the simulation engine which models the substation, including initialising it with model parameters.
- Running experiments and algorithms in or at a multiple of real-time, ensuring that an algorithm run completes and its output is implemented between each load step change.
- Receiving instructions from an operator on which experiments to run, such as which load profile to play back and which algorithm to implement.
- Presenting live results to a user as each experiment is in progress, and announcing the conclusion of each experiment.

The functional requirements for the orchestrator to deliver these tasks are elaborated upon below, so that a suitable programming language for the DT orchestrator implementation may be selected. Firstly, the communications function of the orchestrator will be implemented such that it can interface with laboratory and field instruments. This means that after being used to develop new algorithms, for validation of those algorithms the DT may be used to supervise a physical scale model of DSDR which contains standard benchtop instruments. Following successful bench validation, the algorithm may then be further deployed into field trials using the DT, interfacing with standard field instruments. In all cases, the instruments referred to include those for measuring load flows within the substation, and actuating the changes in desired substation configuration.

The DT orchestrator will accommodate the development of new algorithms via a software plug-in methodology [97, p.]. In this way, any modified or newly developed algorithms may be readily implemented and evaluated with reduced development effort, by making them available as plug-ins to the DT orchestrator without needing to edit the orchestrator software itself.

As the DT orchestrator's subroutines will need to execute asynchronously so as to not block each other during real-time operation, they will be implemented as asynchronous daemon processes [98]. The DT orchestrator will execute experiments queued by a user in real-time or at multiples of real-time, without further interaction from the user. During algorithm development, an algorithm and load profile will be selected by the user; however, for deployment to pilot trials, the user only need select an algorithm, which will then operate on the load changes experienced at a real-world substation. To facilitate such pilot trial deployment, the DT user will be able to connect to the orchestrator from a remote computer, meaning several substations may be controlled from a central location.

3.2.2.1.1 Candidate Languages

A suitable software tool chain with which to build the DT orchestrator is required. The literature reveals that the most commonly utilised software programming languages within this field [99] are MATLAB [100], C/C++ [101] and Python [102]. These solutions are evaluated against the above requirements (section 3.2.2.1) in Table 3 below.

Table 3 – Candidate software language evaluation.

	Software Language		
Requirement	**MATLAB**	**Python**	**C/C++**
Communications protocols for bench and field instruments	Y[1]	Y	Y
Algorithm implementation as plugin	Y	Y	N
Asynchronous execution	Y	Y	Y
Real-time, unattended run-time	Y[1]	Y	Y
Remote overview and control	Y[1]	Y	Y

MATLAB is widely used for modelling and simulation within academia. It aims to simplify the development of algorithms as software plugins through Simulink subsystems, and real-time operation as a DT is possible with additional proprietary hardware such as (SpeedGoat™).

[1] Proprietary hardware required for real-time unattended remote communication with instruments

Python is a general-purpose interpreted programming language, making it inherently cross-platform; it natively supports real-time operation through multi-processing and the wide availability of communication protocol libraries for bench and field instruments. Python's ability to execute directly from source code without compilation lends itself to the iterative development of algorithms as software plugins.

C, and its related object-oriented language C++, are low level programming languages well suited to the development of real-time systems. However, as compiled languages, rapid development and iteration of algorithms developed as plugins would not be possible should C/C++ be used to develop the DT orchestrator. The Python programming language best meets the requirements for a DT orchestrator, and will be used for its implementation, as described in section 3.2.3.

3.2.2.2 DT Simulator

The simulator component of the DT will be responsible for running and solving a load flow [103] within the modelled substation after each load change or substation reconfiguration. After each solve, the DT orchestrator gets access to the powers, voltages, and currents at each node in the modelled substation. In this way, the impact of the algorithm's decision (output) on the objective to be optimised may be immediately quantified. Next, a review of the functional requirements for a DT simulator is carried out, and a suitable load flow package for its implementation is selected.

Whilst the DT simulator will initially be developed using a single-phase circuit model for simplicity, this should be extendable to three-phase circuit models to support use in pilot trials. Therefore, the load flow package will need to accommodate both single and three phase circuit models. Further, as the Python programming language was selected in section 3.2.2.1.1 for implementation of the DT orchestrator, a load flow package will be selected for the DT simulator which is compatible with software written in Python.

During experiment runs, a user selected load profile will be played back by the DT one load step at a time, and between each iteration the DT simulator and algorithm executor will each perform their respective runs. A DT simulator package is selected which can single-step through load settings, rather than needing to be provided with an entire load profile in advance.

This also means the chosen package will be suitable for pilot trials, where the load changes in real time according to user demand, and so is also not known in advance of each experiment.

To mitigate frequent switching (also known as short-cycling), the algorithm (whether threshold or model-based) is given the opportunity by the orchestrator to switch substation topology once per load step, which represents half-hourly time segments. If this were not the case, and the algorithms were instead allowed to reconfigure the substation continuously, the algorithms themselves would need to take responsibility for preventing frequent switching; for example, by the use of a set-back check to only allow a reconfiguration after a fixed duration had elapsed since the last, or a dead-band to prevent further reconfiguration unless the load changes more than a set amount since the last. Should this unnecessary frequent switching prevention responsibility be transferred in future from the orchestrator to the algorithms, it would be prudent to undertake simulation case-studies to ensure an equal level of effectiveness as limiting reconfiguration to fixed time-steps.

During algorithm development, the DT will run on a personal computer, whilst after transition to pilot trials it would run either on a substation server or in the cloud. The load flow simulation package will be selected to be suitable for each of these computational environments. From the DSDR topology of Figure 10, the DT simulator's model will contain a number of circuit nodes such as transformers, a grid connection point, and busbars which connect to the outgoing LV feeders.

The DT orchestrator will be expecting to receive measured voltages, currents, and powers at each of these nodes, at each time step of the experiment, so that it can both provide this data as input to the specified algorithm, and store it in a database for post-experiment evaluation of the algorithm's performance. A load flow package for the DT simulator component will be selected with the capabilities of calculating these measurements at each load step, exposing them to the DT orchestrator in a format suitable for immediate use by the algorithm, and for archival throughout the experiment.

3.2.2.2.1 Candidate Simulation Packages

Let us consider suitable candidate load flow software packages for electricity distribution load flow simulation with regard to the requirements discussed above in section 3.2.2.2, selecting the most suitable to use as the DT simulator component. From the literature, load-flow simulation for electricity distribution systems is commonly implemented using Simulink [104], OpenDSS [105], Power Models Distribution [43], or Power Factory [106]. These are compared for suitability for the DT simulator component in Table 4.

Table 4 – Simulation package evaluation.

Requirement	Simulink	OpenDSS	Power Models Distribution	Power Factory
Single Phase / Three Phase circuits	Y	Y	Y	Y
Interface with Python software	Y	Y	N	Y
Step-wise simulation	Y	Y	Y	Y
Deployable on PC, server, and cloud	N	Y	Y	N
Historian integration and real-time outputs	N	Y	Y	Y

Simulink [104] is a graphical model-based design component of MATLAB [100], and makes models easy to reason due to its visual user experience. Although widely used within academia, and within industry for offline studies, Simulink lacks those features which are desirable in a real-time DT, as it is intended to be run on a user's PC, performing offline simulations.

OpenDSS [105] is an open-source text-based modelling tool, which targets simulations for integration of renewables technologies into electricity distribution systems as its major use-case. It is therefore intended to be suitable for both single-phase and three-phase balanced and unbalanced circuits, and to solve load-flows in single steps. This enables real-time interactions with other software packages, for example generation forecasting or decision-making algorithms. The open-source nature of OpenDSS has led to implementations and connectors for many programming languages, including MATLAB and Python.

Power Models Distribution is a “package for modelling unbalanced power networks” [43], which is implemented in the Julia programming language. Whilst suitable for general use as a load flow simulator within DTs, its lack of an interface to the Python programming language, selected for the DT orchestrator, is a limiting factor. PowerFactory is a commercial package for “analysing generation, transmission, distribution and industrial systems” [106], which in common with MATLAB targets use from a user’s PC. This would limit its use in developing the DT, which should be deployable either to substation servers, or cloud environments, for real-time operation in pilot trials.

As OpenDSS meets all of the requirements, it will be used to develop the load-flow simulation component of the DT. A discussion of the OpenDSS model created is given in section 3.3.

3.2.2.3 Software Architecture

A software architecture for implementing the DSDR DT, which extends the general DT architecture of Figure 11 by defining the external system blocks included in addition to the simulation and orchestration components, is introduced below in Figure 12. The overall function of the DSDR DT is to model a distribution substation whose topology can be controlled in real-time by an optimisation algorithm, post reinforcement with parallel transformers.

As the DSDR DT will initially be used to develop DSDR optimisation algorithms by performing multiple series of experiments, the orchestrator component in this context is better described as an experiment runner, which is shown to the lower left of Figure 12. This orchestrates the systems external to the core DT components so that they may interact with the DT in real time; including retrieval and playing back of load profiles from data storage, communicating load flow and instructions to and from any algorithm which has been ‘plugged in’, and persistence of real-time data into archival data storage for later analysis. Supervision of the circuit simulation component, and retrieval of its real-time simulation results throughout each experiment, is also handled by the experiment runner.

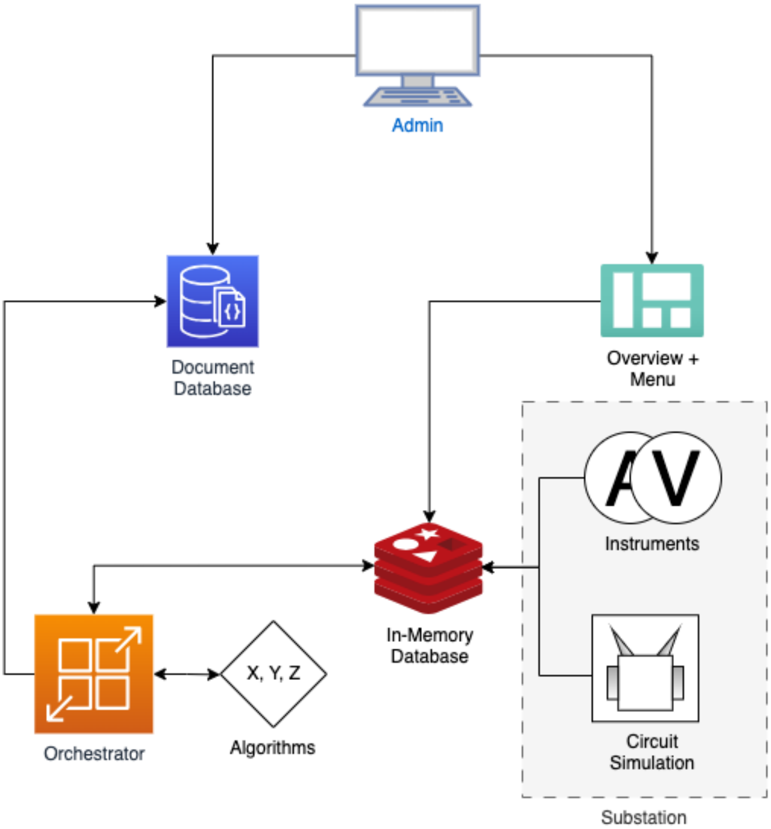

Figure 12 – Software Architecture for DSDR Digital Twin.

The algorithms block to the right of the experiment runner represents the optimisation algorithm, which may either be under development in a research setting, or evaluation and validation in a pilot trial setting. As each algorithm can be developed as a plug-in software component, it is external to the core DT functionality and supervised by the experiment runner. At each time-step of the DT's operation during an experiment, real-time operational state including load flow and the present topological configuration is passed from experiment runner to algorithm, and an instruction for the optimal configuration is then returned from algorithm to experiment runner.

An in-memory database, shown above and to the right of the algorithms block, stores the current instruction from the algorithm, which is placed into it via the experiment runner. From here, the circuit simulation component shown to the lower right of the figure can access these instructions and reconfigure the topology of its circuit model accordingly, before re-running the load-flow simulation.

The results of each load flow are pushed back into the in-memory database, which acts as the communications channel between DT orchestrator and DT simulator. The latest load-flow results are also picked up from the in-memory database by the instruments block shown above the circuit simulation. Here, these are transformed into virtual instruments, which represent the real-time load flow data as measurement from a bench or field instrument, and streamed back into the in-memory database. This capability facilitates integration of the DSDR DT with DSDR benchtop scale models, and with real-world DSDR pilot trial substations.

Shown at the top of the diagram, an administrator's computer is used to monitor experiments in real-time by reading virtual instrument readings. The overview and menu block shown to the centre right presents a text user interface for this to the user, and may be accessed locally, or remotely over a network. This block also allows a user to upload load profiles into storage for use during experiments, retrieve past results after experiments, and manually control the virtual instruments. Finally, the document database block shown to the centre left of the diagram is responsible for persisting load profile and experiment results data; therefore, it can be accessed by both the user and the experiment runner.

3.2.3 Software Architecture Implementation

3.2.3.1 Introduction

From the DSDR DT architecture of 3.2.2.3, the software classes required for its implementation using Object Oriented Programming (OOP) are introduced here. A generic virtual instrument class will be responsible for exposing measurement results from the simulation engine as Virtual Instruments (VI), fully compatible with standard bench instruments used in the benchtop scale model introduced in the following chapter. This class will be sub-classed by the AC source, AC load, AC power meter, and reconfiguration switch instrument classes.

A circuit simulator class will wrap the OpenDSS load-flow modeller, interfacing it with the in-memory database. An experiment runner class will act as the supervisor of all real-time operations, configuring and synchronising the non-core DT components as required for each experiment.

A generic algorithms class provides an interface to the DT orchestrator for real-time transfer of substation measurement data, and algorithm output instructions for substation reconfiguration. Concrete algorithm implementations will then be plugged in as class methods to the generic algorithm class, as discussed in chapter 5. The in-memory database and document database blocks of Figure 12 are not required, as implementations of these are available as existing open-source software projects. Therefore, these are installed, configured, and instantiated by the DT, rather than implemented from source.

3.2.3.2 Open-Source Components

Below, suitable open-source software components with which to build the DSDR DT are identified.

3.2.3.2.1 In-Memory Database

The in-memory database block of Figure 12 will act as a communications channel, storing the latest measurements and commands in real-time, and exposing these so that any other functional block can read them. An in-memory database is the most suitable type of database for this application, as it can be used as shared memory for fast data transfer, with multiple services consuming the same data independently, and without consuming disk I/O capacity.

As the most popular open-source in-memory database, Redis [107] will be used for this functional block. Redis is a key-value store, which will be used of streaming real-time measurements between the simulation engine and virtual power analyser instruments, for passing reconfiguration commands to the virtual reconfiguration actuators, and for triggering the simulation engine on each load step or substation topology change.

3.2.3.2.2 Document Database

The document database block shown in Figure 12 will provide data persistence, namely storing load profiles for use during experiments, and substation state at each time-step of completed experiments. Document databases allow the storage of data without any defined schema, making this choice the most suitable for persisting DSDR DT data, where new virtual instruments or algorithm inputs and outputs may require altering the schema during algorithm development cycles.

For the DSDR DT, MongoDB [108], the most popular no-SQL database, will be used as the document database. MongoDB stores data a sets of documents containing key-value pairs which can be nested, making it the ideal choice to persist the key-value real-time substation state latest values held in the in-memory database at each time step of DSDR experiments.

3.2.3.3 Components Implemented in Source Code

Here the detailed design for implementation of those blocks from Figure 12 which need to be implemented from source as new Python classes is presented. Each class is briefly introduced to review the functionality it provides; its operation is described using software flow control diagrams for each method of the class; and finally, the operations described by each diagram are discussed.

3.2.3.3.1 Algorithm Class

An algorithm class, shown in Figure 13, will implements the framework within which decision-making algorithms can be developed, and then plugged-in as OOP methods. In line with the research question addressed in this thesis, such algorithms will aim to optimise the efficiency, i.e., minimise the power losses, of a DSDR substation, whilst maintaining reliable operation. Future work will develop algorithms targeting optimisation of other parameters such as phase balancing, harmonics management, and grid support.

Further, as the driving motivation at the present time of substation reinforcement preparations is the expected proliferation of electric vehicles, designing the algorithm base class to be extendable through OOP plug-in methods, and loosely coupled to the DT orchestrator through an in-memory database, unlocks potential for future plug-in algorithms to access data at each time step about electric vehicles connected to the substation and their state of charge.

By such extension, the DSDR DT developed here can form the basis of a general-purpose future smart substation DT. The OOP class described here will collect and pass to the algorithm plug-in methods all real-time substation state at each time step of an experiment.

Beginning with the flow diagram at the top of Figure 13, the class initialises by loading the in-memory database connection details from the configuration module described in section 3.2.3.3.4, and establishing a connection to the database. Algorithms plugged in as OOP methods to this class will use the in-memory database connection to push reconfiguration instructions for the substation, for example 'switch on transformer 1, switch off transformer 2', if that is the optimal configuration determined for the currently executing time-step. The second flow diagram describes how substation state measurements from the latest time-step are provided.

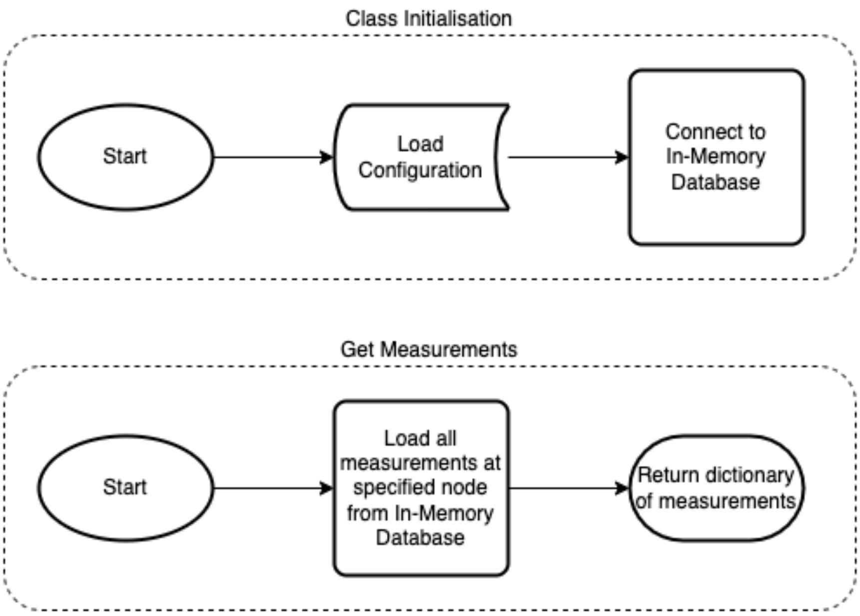

Figure 13 – Algorithm generic class.

An algorithm implementation method may call the 'get measurements' method, specifying the node of interest, and the method will use the in-memory database connection to retrieve all substation states relating to that node. The latest measurement states will have earlier been pushed to the in-memory database by the instruments class, which it retrieves either from physical instruments connected to the DT, or from load-flow results produced by the DT simulation block. The algorithm methods plugged-in to this base class are introduced in chapter 5, and the results they achieve in chapter 6.

3.2.3.3.2 Instruments Classes

Here the instrument OOP software classes for the DSDR DT are described. These communicate with both the physical bench instruments, and with their Virtual Instrument (VI) counterparts, which operate on the same parameters but for the simulated substation.

As all instruments will share much common functionality, OOP inheritance is employed by designing a base instrument class to implement this, and a set of sub-classes which each represent an interface to a specific physical instrument.

3.2.3.3.2.1 Instrument Base Class

The base instrument class design is shown in Figure 14; it is responsible for the common routines used by all instrument specific sub-class implementations, for example, each instrument requires a connection to the in-memory database to where it can write its readings, so the base class implements the logic of creating this connection. For class initialisation, which will be repeated by each instrument implementation class due to OOP inheritance, the base class becomes a Python thread by itself inheriting from the built-in threading class.

By this mechanism, all instrument classes will operate independently of each other, in real-time. The connection with the in-memory database will be used for streaming data between instrument and DT orchestrator, opening a communications channel to the physical or virtual instrument using the NI VISA [109] library, and initialisation is complete. Subsequently, the thread enters a forever loop, therefore becoming a daemon thread, in which instrument readings are collected and instrument commands are handled.

The remaining methods of Figure 14 define how the readings are requested from each instrument using the NI VISA library, how to retrieve commands queued for an instrument, and how to transmit those commands to each instrument.

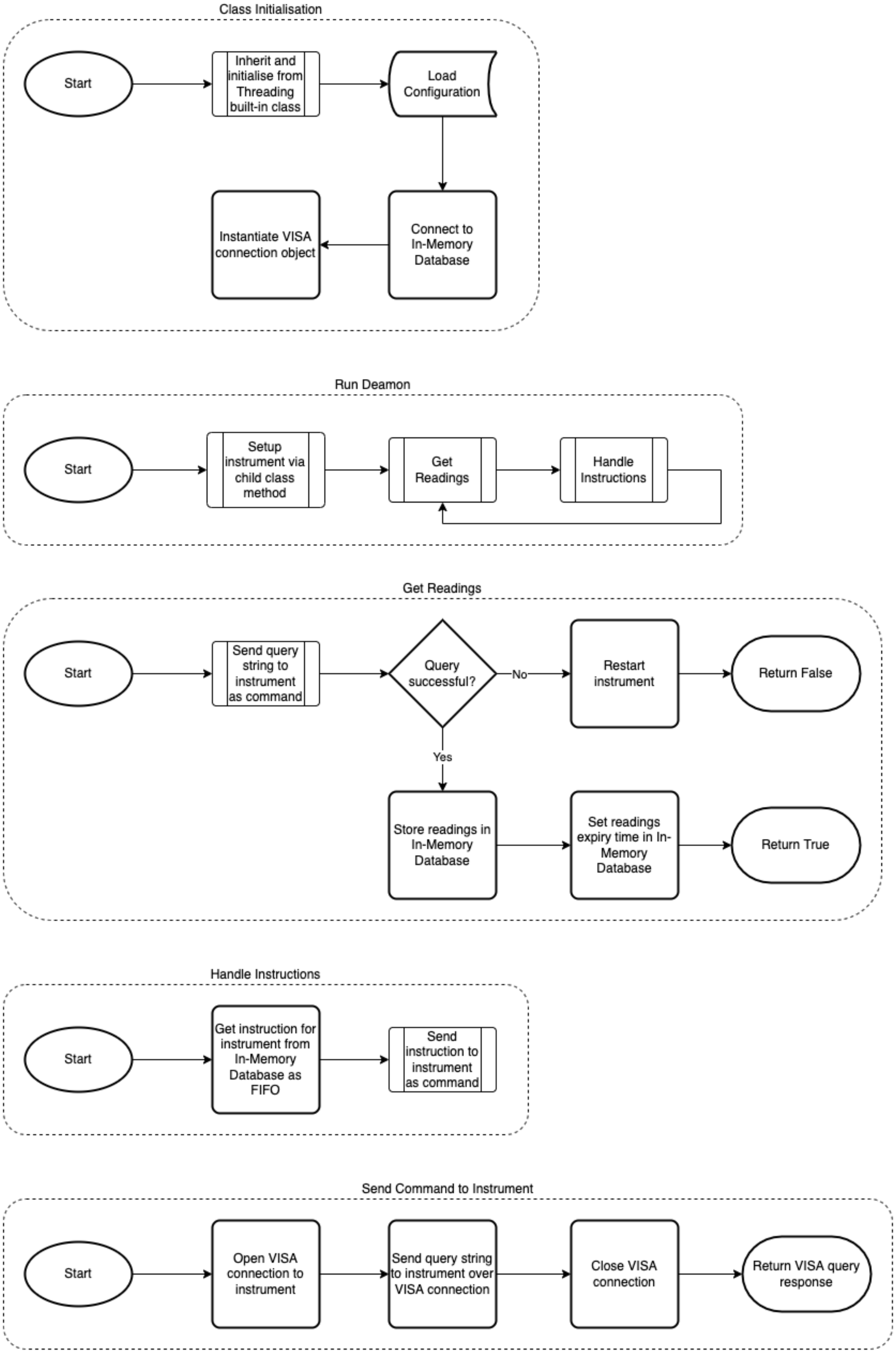

Figure 14 – Instrument base class.

3.2.3.3.2.2 Analyser Sub-Class

The analyser instrument sub-class, with its specific set of flow diagrams and a detailed description of their operation is presented. For reasons of brevity, the remaining instrument sub-class implementations will be described by highlighting only those aspects which differ from the analyser implementation, and without their flow diagrams. The analyser instrument sub-class of Figure 15 enables communications and control between a virtual or physical bench power analyser and the DT orchestrator. The Tektronix PA1000 and Newton's 4th PA1530 instruments are supported, and this is readily extendable to any other power analyser. OOP inheritance from the instrument base class provides the generic DSDR DT instrument methods, including concurrent real-time operation as a deamon thread – this is shown in the uppermost flow diagram.

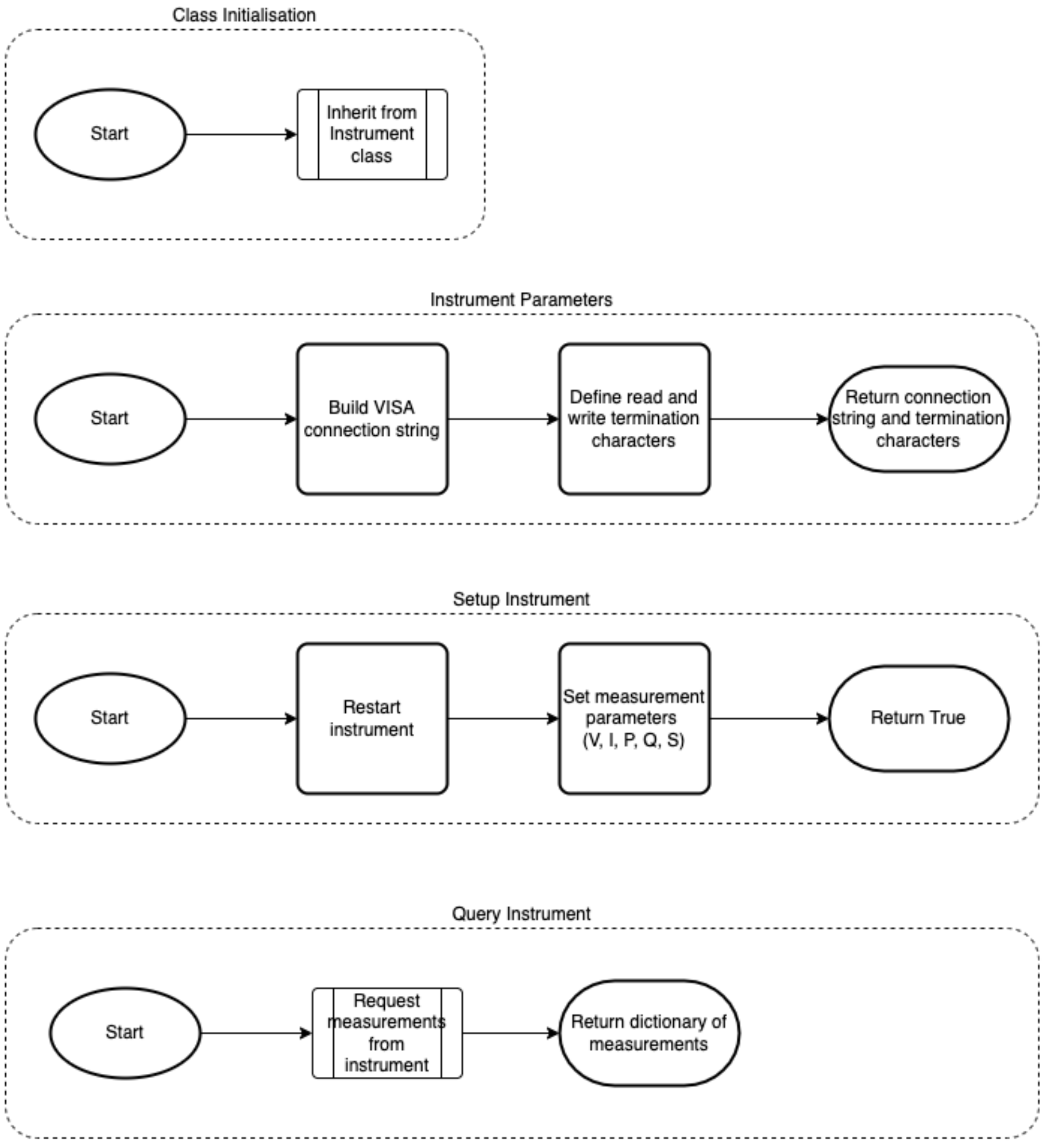

Figure 15 – Analyser instrument class.

Moving downwards through the figure, the instrument base class's NI VISA connection is utilised to define the communications protocol with the instrument. Firstly, an appropriate VISA Resource Name [110] is selected according to the communications channel and protocol specified in the instrument's datasheet, and use that to build a connection string for the Python NI VISA library. For the PA100 instrument, this takes the following form.

TCPIP0::{self.host}::{self.port}::SOCKET

Where 'TCPIP0' specifies use of the TCP/IP physical layer, host and port will be taken from instance variables, and 'SOCKET' specifies that a raw TCP/IP socket will be the communications protocol used. The PA100 instrument datasheet also specifies that data transmitted from the instrument will terminate with a newline character, and commands to the instrument should terminate with the same; therefore these options are set on the NI VISA connection for the instrument, and instrument connection set-up completed.

The third flow diagram from the top of Figure 15 illustrates the procedure for establishing initial communications with the instrument and preparing it for use during DSDR experiments. The analyser is restarted, to return it to a default state, by issuing the instrument specific 'restart' command over the NI VISA connection – for the PA1000 this is '*RST\n', where '\n' represents the newline character terminating the command. To conclude setting up the instrument for DSDR experiments, the parameters that need to be measured at each time-step – voltage, current, real power, reactive power, and apparent power – are configured into the instrument by issuing commands.

Finally, the OOP method is constructed, which will be called each time the instrument base class requests a set of readings from the instrument. The logic implemented is for the 'send measurements' command to be sent to the instrument – ':FRD?' for the PA1000. The response from the instrument is converted from a string into a set of keys and values, known in python as a dictionary, be returned to the calling method of the base-class.

3.2.3.3.2.3 Relay Controller Sub-Class

The relay controller implements the communications channel for the DT to a virtual or physical DSDR switcher panel, which will reconfigure the substation's topology according to algorithm outputs.

The Brainboxes ED-538 ethernet relay is supported by this class, and like the analyser sub-class this can be extended to any bench or field switching device. Querying the instrument returns the relay state for each transformer – i.e. ‘open’ or ‘closed’ – which describes the substation’s configuration state. The class also responds to commands to open or close a particular transformer’s relay by issuing the appropriate command.

3.2.3.3.2.4 Load Bank Sub-Class

The load bank instrument sub-class connects the DSDR to an AC electronic load, enabling load profiles to be played back through the substation in real time throughout each experiment. The class support the ETPS ELPA3250 programmable AC load instrument, and acts as both an actuator to draw the specified load current from the substation, and a meter which can read back the voltage and current at the load side of the substation.

3.2.3.3.2.5 Power Supply Sub-Class

The power supply sub-class implements communications with a programmable AC voltage source, supporting the BK Precision 9801 instrument initially. This type of instrument will be used during experiments to emulate a grid supply to the substation, providing a stable source of power with configurable frequency and voltage.

3.2.3.3.3 DT Orchestrator Module

The DT orchestrator module, shown in Figure 16, will be responsible for setting up and maintaining the real-time operation of the DT, whether an experiment is running or not. This module will be the first to run when the DT starts, and will bootstrap the operation of all other modules within the DT, ensuring all physical or virtual instruments remain online so that experiments can run. When started, the orchestrator will determine whether the real-time operation of the substation will be achieved from virtual or physical instruments, and will initiate connections to those accordingly. After this, it will monitor status of all instruments, restarting them if connectivity is lost.

3.2.3.3.4 Configuration Module

Many of the base classes, sub-classes, and modules within the DSDR DT will require shared states, which may be set by the user before starting the DT, but which will not change whilst the DT is running; database connection parameters being one example of this.

A configuration module will be implemented, which exposes common constants to all classes and modules which import the module.

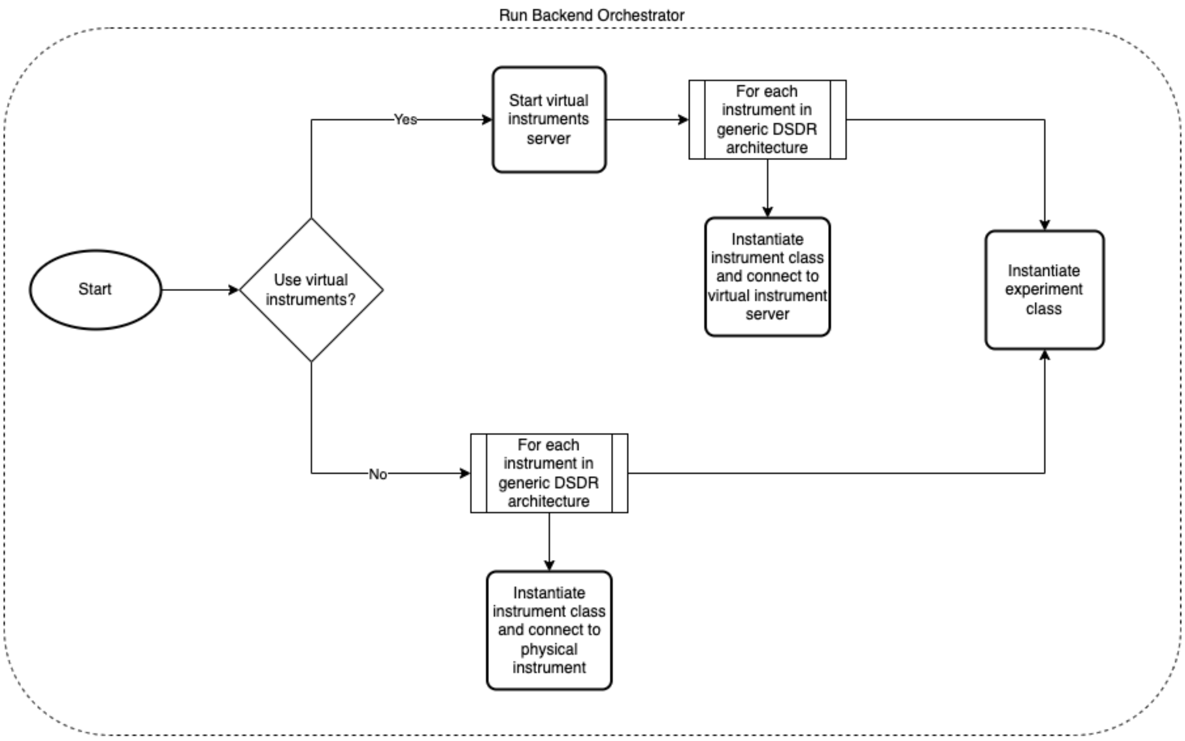

Figure 16 – Backend Orchestrator module.

Here is also the ideal place to provide synchronisation primitives – these variables which may be changed atomically by any other module or class instance, such that others can be kept aware of DT state – for example, 'model running'. The configuration module will be implemented as shown in Figure 17. Global configuration parameters are initialised from default values, which are then overridden from environment variables if they are defined. All constants will then be exposed as standard python variables as attributes of the module, named in all capitals as is the convention for constants in Python.

3.2.3.3.5 Experiment Runner Class

Next, the experiment runner class, which will run each of the DSDR experiments in real-time, coordinating the playing back of a load profile, execution of an algorithm at each time step, reconfiguration of the substation, and storing of results is designed. The logic shown in Figure 18 describes two flows – initialisation of the class, which happens when the DSDR DT starts, and the running of an experiment, which happens once for each experiment queued by a user.

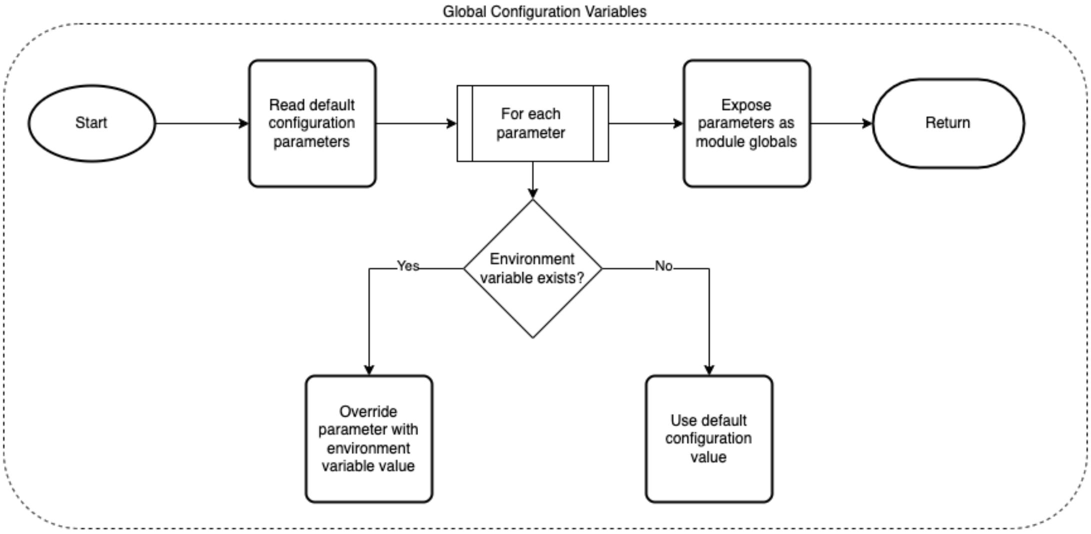

Figure 17 – Configuration module.

Beginning with the initialisation stage, the class inherits from python's threading class to convert to a daemon thread, load the connection parameters for the document database and in-memory database, establish connections to both of these, and then create an instance of the algorithm class that can be called during experiments each time an algorithm execution is required.

The lower flow diagram shows how experiments will be run; each experiment is assigned a unique identifier, before stepping through each time-step of a user-specified load profile recalled from the document database, setting the load current and running the algorithm at each step, then pushing the instantaneous results from all instruments to the document database, tagged by experiment identifier and load step.

3.2.3.3.6 Virtual Instrument Server Classes

From Figure 12, the instruments class will virtualise bench instruments within the DSDR, such that they become twins of physical instruments which may be installed inside a DSDR substation or within a DSDR physical scale model. By this mechanism, the DSDR DT may be operated either entirely virtually with all substation operation simulated, or within an actual substation with physical instruments taking measurements. In both modes, DT operation including the algorithms remain identical, enabling seamless transition from research and development into pilot trials, and beyond to business-as-usual DSDR operation.

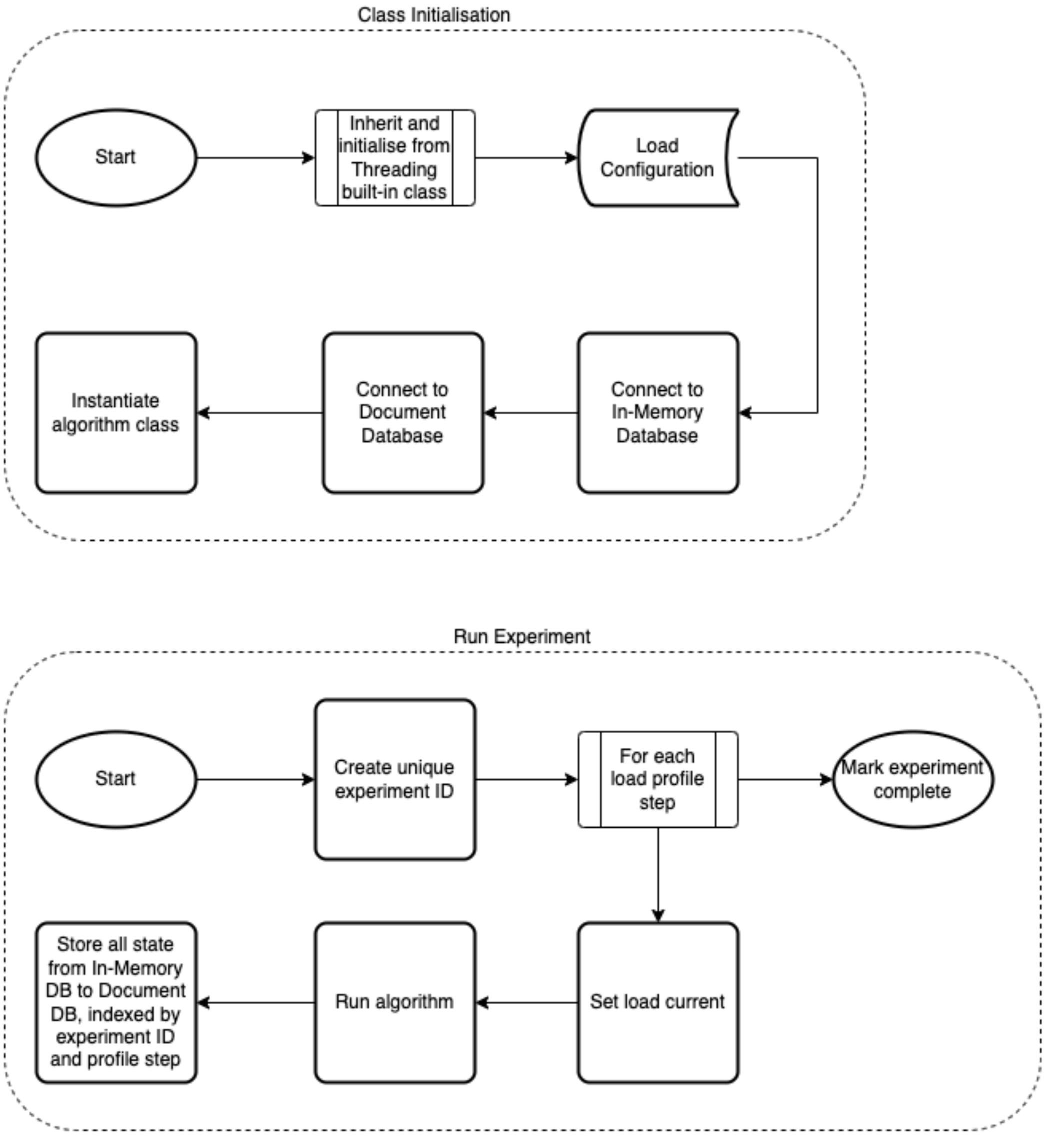

Figure 18 – Experiment Runner class.

Two simple classes are needed to create the VI's; a 'mock instruments' class which collects the appropriate substation simulation results from a specified node of the DSDR substation model, and an 'instrument server' class which presents those results as instrument measurements acting a TCP/IP host server.

The mock instruments class contains a method for each VI to be emulated, which is called by the instrument server each time an NI VISA command arrives for that instrument from the in-memory database. If the command requests to take a reading, the results of the latest substation simulation are read from the in-memory database, converted into the command response format specified by the instrument's datasheet, and return to the method caller.

For commands which were intended to set the state of the instrument (e.g. to operate a reconfiguration switch, or select a voltage measurement range), the new state is pushed to the in-memory database. From here, it can be accessed by the instrument for use in processing any future commands, and by the substation simulation engine in solving a load-flow.

The Instrument server class starts a TCP/IP host server for each VI, listening on the same port as the physical instrument. This receives any traffic for the physical instruments from their instrument class, and redirects it to the correct VI from the mock instruments class. In this way, the algorithm remains naïve as to whether it is interacting with physical or virtual instruments, and so the DSDR DT may be used with physical, virtual, or a hybrid of instruments.

3.2.3.3.7 Circuit Simulation Class

Here a design for the ‘simulator’ block first introduced in Figure 11 – a fundamental component of a generic DT – targeting the simulation of a DSDR substation is produced, to create a DSDR-specific DT. The purpose of the circuit simulation class is to perform a load flow for all nodes of the DSDR substation at each time step of an experiment. To achieve this, the OpenDSS simulation engine selected in Table 4 is wrapped in a python class operating as a daemon thread. The three flow diagrams implementing this – initialisation, daemon operation, and model execution – are shown in Figure 19 and described below.

During initialisation, shown in the uppermost flow diagram, the class is set up as a daemon thread through inheritance, before loading the OpenDSS model file describing the parameters of the substation (see section 3.3.3 for its derivation).

Next, a connection to the in-memory database is set up after loading its connection parameters; it is through this connection that load-flow execution events will be triggered, and where it’s results will be streamed. Therefore, a synchronisation event is registered to trigger each time the live substation state changes, as recorded in the in-memory database; this could be, for example, the substation load changing, or its topological configuration switching.

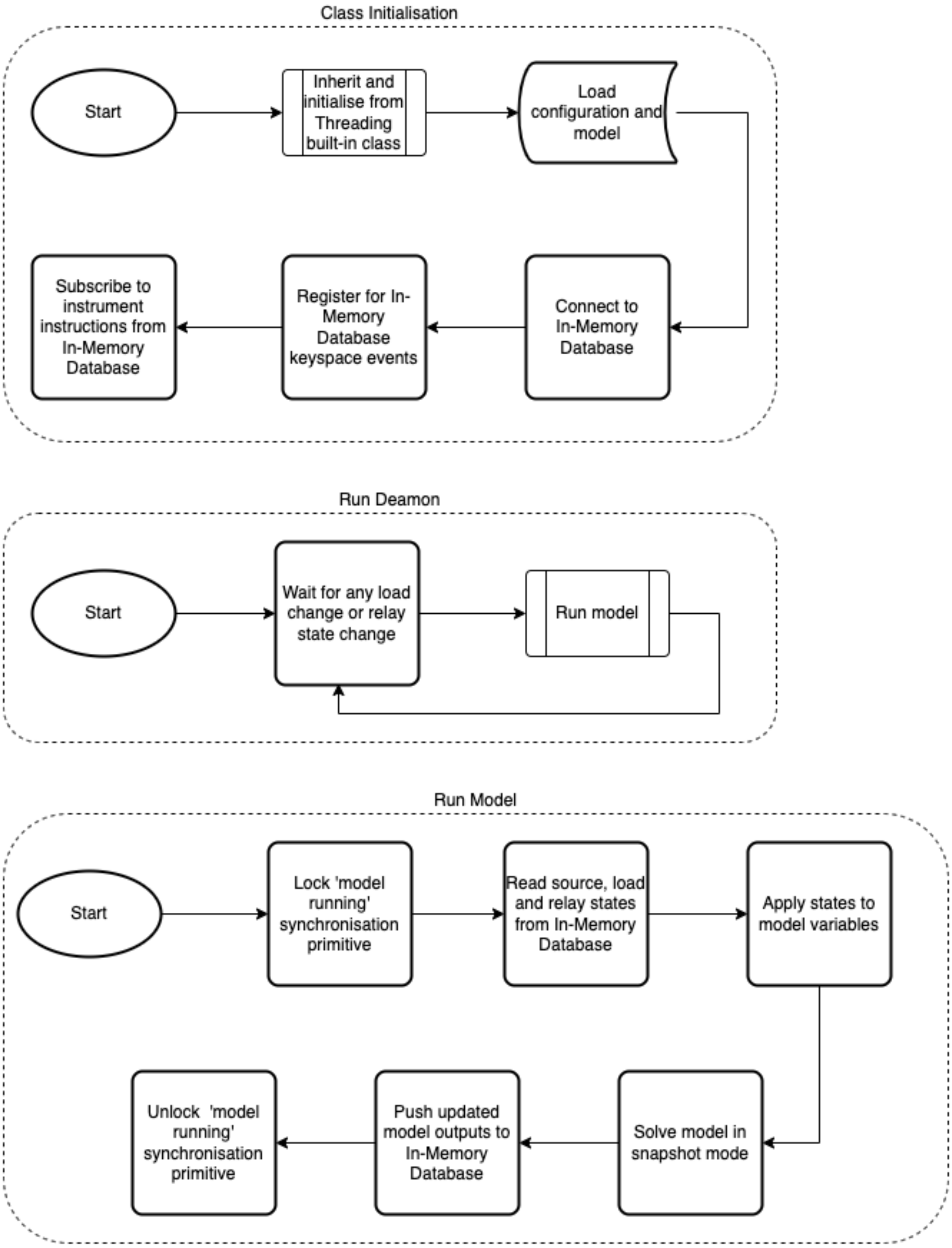

Figure 19 – Circuit Simulation class.

The second flow diagram shows the daemon thread entered by the class after the above initialisation is completed – here, the circuit simulator sits idle until substation state changes, for example when the load increases or decreases.

When this happens, the synchronisation event to run a load-flow is triggered, and the 'run model' method shown in the flow diagram lowermost in the figure is called. This method sets a global indicator that a simulation run is in progress before each load flow runs, and clears the indicator afterwards, enabling other modules to synchronise with these events. Next, the DT substation state is retrieved from the in-memory database, including the real-time load and configured topology, and a load flow is run using the python OpenDSS library [111]. Results from the load-flow run are then sent to the in-memory database, overwriting the previous iteration's results.

3.2.4 Summary

In this section, a python based digital twin software framework for a DSDR substation is implemented. Beginning with a generic DT software architecture, this is developed into an architecture diagram comprising the functional blocks required for a DSDR DT which can be used in virtual, physical, or hybrid modes of DT operation. Suitable software languages and libraries were selected for implementation of the DSDR DT, and those components which would need to be developed from source code were identified, designed, and implemented. Source code for all software produced can be found within the project's GitHub repository[2]. In the following section, the OpenDSS model to be used for simulation of load-flow within the DSDR substation will be developed.

3.3 OpenDSS Model Derivation

3.3.1 Introduction

In this section, a digitised model of the DSDR substation, in a format to suit the OpenDSS simulation package selected for the DSDR DT in section 3.2.2.2.1 is designed and presented. The accepted equivalent circuit models for distribution transformers are explained and used to construct the model of a parallel transformer reconfigurable final distribution substation and derive the process of parameterising it. The result is a text-based digitised OpenDSS DSDR model which will be used by the DSDR DT simulation component to perform load flow analysis in real time during experiments, to develop DSDR optimisation algorithms.

[2] https://github.com/bimec/DSDR (contact author for access)

3.3.2 Equivalent Transformer Models

Here the standard distribution transformer models, used to develop the DSDR substation of Figure 10 into an OpenDSS model are introduced.

3.3.2.1 Full equivalent circuit

Figure 20 shows the full equivalent electrical circuit model of a distribution transformer, with port V1 representing the higher voltage terminals, and port V2 the lower voltage terminals [34].

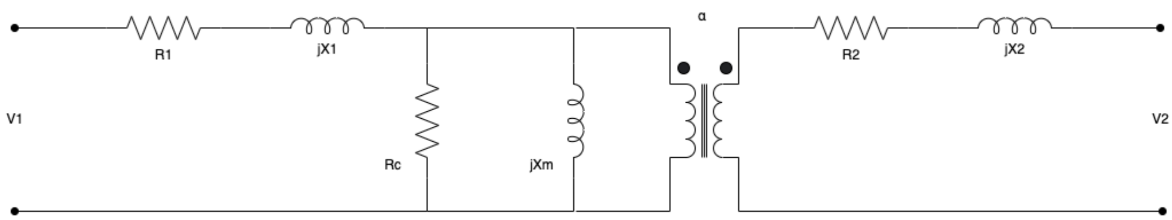

Figure 20 - Transformer equivalent circuit.

This model may be used to determine a transformer's operating parameters such as load voltage regulation, iron losses, copper losses, and magnetising current. Reduced versions of this model, as described in the following sections, may be used to simplify such computations, whilst extensions to the model may be made for simulating phenomena such as component temperatures [112] or frequency response [113].

Table 5 lists the model parameters, which are further described below. The transformer winding ratio (α) is shown as a parameter of the ideal transformer element in the model circuit, and represents the quotient of higher voltage winding (primary) turns Np to lower voltage winding (secondary) turns Ns, as shown in Eq. 1.

$$\alpha = \frac{N_p}{N_s} \qquad \textit{Eq. 1}$$

Where:

- α is the nominal transformer winding ratio
- N_p is the integer quantity of turns in the transformer's primary winding

- N_s is the integer quantity of turns in the transformer's secondary winding

Table 5 - Parameters of transformer full equivalent circuit.

Parameter	**Unit**	**Description**
R_1	Ohms	Primary winding resistance
jX_1	Ohms	Primary winding reactance
R_c	Ohms	No-load loss resistance
jX_m	Ohms	Magnetising reactance
R_2	Ohms	Secondary winding resistance
jX_2	Ohms	Secondary winding reactance
α	Ratio	Primary to Secondary Transformer winding ratio
Phases	Qty	Number of phases
Windings	Qty	Number of windings per phase

The circuit segment to the left of the ideal transformer represents the transformer primary, to which magnetising current reactance (jX_m) and iron loss resistance (R_c) are arbitrarily assigned as a simplification. In a physical transformer, these are in fact artefacts of the transformer's core and its electromagnetic interactions with the windings. The segment to the right of the ideal transformer represents the secondary, lower voltage winding and terminals.

Components R_1 and jX_1model the primary side winding resistance and winding inductive reactance, which affect the primary side's contribution to copper loss and voltage regulation respectively; $R_2$and jX_2serve the same purpose in modelling the transformer's secondary windings.

3.3.2.2 Reduced equivalent circuit referred to primary

The equivalent circuit model above may be referred to the transformer's primary, which is useful in computing the transformer's operating losses and efficiency for a particular load [67]. The resistances of both the primary and secondary windings are combined and then referred to the primary winding according to Eq. 2. Total winding inductive reactance may be combined as referred to the primary according using Eq. 3, although this parameter is not required in determining transformer losses, as the ideal inductor is a lossless element.

$$R_{eq_1} = R_1 + \alpha^2 R_2 \qquad \textit{Eq. 2}$$

$$jX_{eq_1} = jX_1 + \alpha^2 jX_2 \qquad \textit{Eq. 3}$$

Where:

- R_{eq_1} is combined winding resistance referred to the primary side in ohms
- $R_1$is primary winding resistance in ohms
- R_2 is secondary winding resistance in ohms
- α is the nominal transformer winding ratio
- jX_{eq_1} is combined winding reactance referred to the primary side, in ohms
- jX_1 is primary winding reactance in ohms
- jX_2 is secondary winding reactance in ohms

Parameter R_c and jX_mremain unchanged from the model in Figure 20, as they remain in the same position in the primary section of the equivalent circuit. Finally, a load impedance R_L is placed across port V_2' , which represents the secondary voltage referred to the primary as determined by Eq. 4, and the model is constructed as shown in Figure 21.

$$V_2' = V_2\, \alpha \qquad \textit{Eq. 4}$$

Where:

- V_2' is secondary winding voltage referred to the primary side, in volts
- V_2 is actual secondary winding voltage in volts
- α is the nominal transformer winding ratio

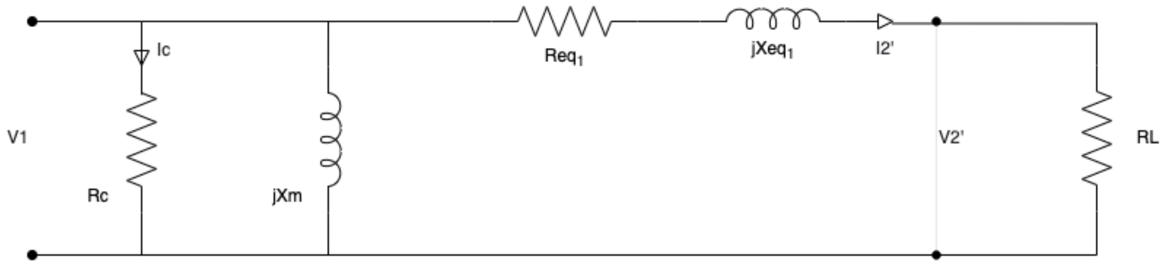

Figure 21 – Transformer equivalent circuit referred to primary.

A summary of the components in the equivalent circuit model referred to the primary is given in Table 6.

Table 6 – Parameters of equivalent circuit referred to primary.

Parameter	**Unit**	**Description**
R_{eq_1}	Ohms	Equivalent winding resistance
jX_{eq_1}	Ohms	Equivalent winding reactance
R_c	Ohms	No-load loss resistance
jX_m	Ohms	Magnetising reactance
R_L	Ohms	Load resistance

3.3.2.3 Reduced equivalent circuit referred to secondary

Similarly, the original equivalent model may be referred to the secondary, which is convenient for computing a transformer's voltage regulation for a certain load. Iron loss resistance and magnetising current reactance, which were specified in relation to the primary side in Figure 20, may be referred to the secondary to become R_c' and jX_m', given by Eq. 5 and Eq. 6.

$$R_c' = \frac{R_c}{\alpha^2} \quad \text{Eq. 5}$$

$$jX_m' = \frac{jX_m}{\alpha^2} \quad \text{Eq. 6}$$

Where:

- R_c' is iron loss resistance in the transformer's core, referred to the secondary winding, in ohms

- R_c is iron loss resistance when modelled as shunting the primary side of the transformer, in ohms
- α is the nominal transformer winding ratio
- jX'_m is the magnetising current reactance in the transformer's core, referred to the secondary winding, in ohms
- jX_m is the magnetising current reactance when modelled as shunting the primary side of the transformer, in ohms

Primary and secondary winding resistances and reactances are once again combined, but are now referred to the secondary winding by Eq. 7 and Eq. 8.

$$R_{eq_2} = \frac{R_1}{\alpha^2} + R_2 \tag{Eq. 7}$$

$$jX_{eq_2} = \frac{jX_1}{\alpha^2} + jX_2 \tag{Eq. 8}$$

Where:

- R_{eq_2} is combined winding resistance referred to the secondary side, in ohms
- R_1 is primary winding resistance in ohms
- R_2 is secondary winding resistance in ohms
- α is the nominal transformer winding ratio
- jX_{eq_2} is combined winding reactance referred to the secondary side, in ohms
- jX_1 is primary winding reactance in ohms
- jX_2 is secondary winding reactance in ohms

Adding a load impedance to the model yields the equivalent circuit model shown in Figure 22, now with the primary voltage V'_1 referred to the secondary.

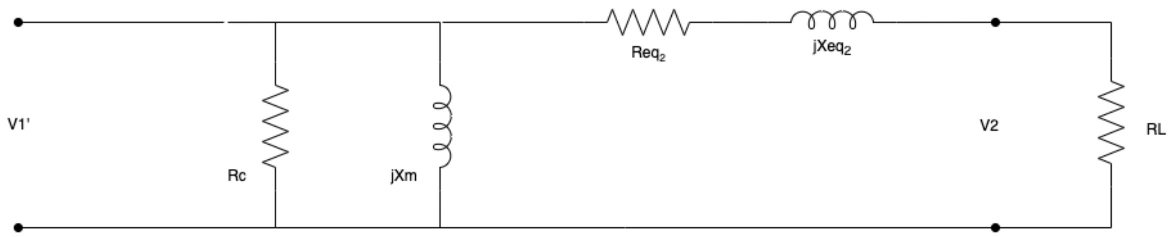

Figure 22 - Transformer equivalent circuit referred to secondary.

The parameters of the equivalent transformer model referred to the secondary side are given in Table 7.

Table 7 - Parameters of equivalent circuit referred to secondary.

Parameter	**Unit**	**Description**
R_{eq_2}	Ohms	Equivalent winding resistance
jX_{eq_2}	Ohms	Equivalent winding reactance
R_c	Ohms	No-load loss resistance
jX_m	Ohms	Magnetising reactance
R_L	Qty	Load resistance

The transformer equivalent circuits described above are utilised in the remainder of this chapter and in chapter 4, to construct, parameterise, and validate DT and BTSM models of a parallel transformer reconfigurable final distribution substation.

3.3.3 Digitised Substation Model

The reference substation described in Figure 10 was digitised by describing it using OpenDSS syntax to create a DT model. This consists of a plaintext file listing the required circuit components, including all connections and values.

3.3.3.1 Substation Topology

A modification to some circuit components (but not the topology) of Figure 10 was necessary to digitise the model. All required switches were implemented as OpenDSS lines, which may be set to be 'open' or 'closed' during a simulation in order to model ideal switches.

Connections between all components were implemented as lines with a length of 1m. A Single Line Diagram (SLD) representation of the digitised model is shown in Figure *23*, including component numbers for reference, with the full model listings given in appendix section 10.1.2.

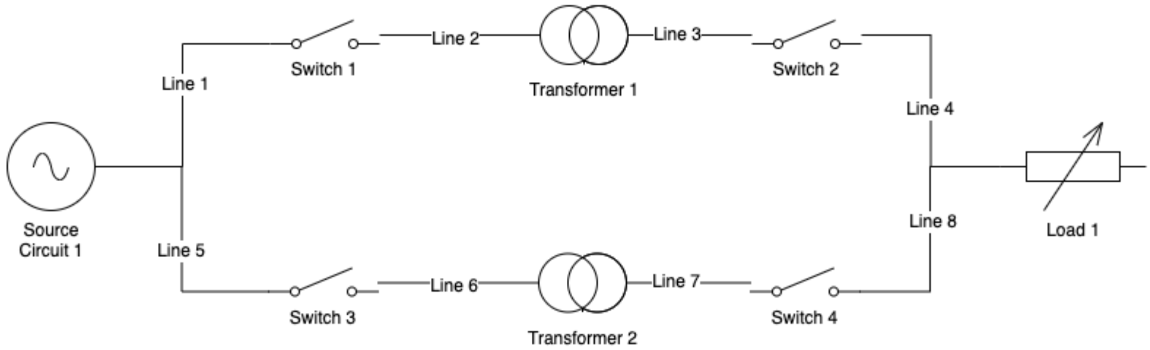

Figure 23 – DSDR OpenDSS model topology.

The OpenDSS components used in the DT model are shown in Table 8, cross referenced against the generic component types of Figure 10. Power analyser measurements in OpenDSS may be extracted from any component during simulation, therefore instruments are not explicitly required within the model itself.

Table 8 – OpenDSS model components.

Generic Component	**OpenDSS Component Type**
Source	Circuit
Line	Line
Node	Bus
Switch	Line
Transformer	Transformer
Load	Load

A number of global parameters, which remain fixed during simulation runs, are also defined within the model as listed in Table 9. Frequency is set at 50 Hz to represent a UK DNO system (but can be changed to suit other regions, e.g. 60 Hz for USA); MV and LV nominal voltages are set at 230 V and 24 V respectively to match the bench top scale model substation presented in chapter 4, along with single phase operation, and the simulation mode is set to single-step operation so that topology may be externally altered between each solve. The OpenDSS model parameters required for each transformer are listed in Table 10, each of which remain static throughout each simulation run.

Table 9 - Model global parameters.

OpenDSS Parameter	**Unit**	**Setting**	**Description**
DefaultBaseFrequency	Hz	50	Base frequency for PU purposes
baseKV	Kilovolts	0.23	Source operation voltage (phase)
Frequency	Hz	50	Source operation frequency
Phases	Qty	1	Source number of phases
Voltagebases	Kilovolts	0.4 (MV) 0.04 (LV)	Base voltages for PU purposes (line)
Mode	N/A	Snap	Solve mode of simulation

The number of phases and windings, MV and LV voltages, and nominal power rating are set to match the physical scale model design of chapter 4, whilst transformer impedances, rated losses, and magnetising current are extracted from measurements made of each transformer in the scale model as also described in chapter 4. Load type 1 (constant P and constant Q) was specified in the model, to suit generic substation load profiles.

Table 10 - Model transformer parameters.

Parameter	**Unit**	**Description**
phases	Qty	Number of phases
windings	Qty	Number of windings
kvs	[kV, kV]	Primary and secondary nominal voltages
kvas	[kVA, kVA]	Primary and secondary nominal power
%Noloadloss	%	Rated no-load loss
XHL	%	Equivalent winding reactance
%Rs	[%, %]	Primary and secondary winding resistances
%imag	%	Magnetising current

Table 11 lists the load types available within OpenDSS. Load parameters described as constant are those which may be adjusted during simulation runs, whilst fixed load parameters may not.

Table 11 –OpenDSS Load Types [114].

OpenDSS Load Model	Description
1	Constant P and constant Q
2	Constant Z
3	Constant P and quadratic Q
4	Exponential P and Q
5	Constant I
6	Constant P and fixed Q
7	Fixed reactance
8	ZIP (constant Z, I, and P combination)

3.3.3.2 Model Parameter Derivation

Transformer no-load losses (parameter '%Noloadloss' from Table 10) are required by OpenDSS to be expressed as a percentage of nameplate rated complex power S_{BASE}, and are determined using Eq. 9.

$$\%Noloadloss = \frac{P_C}{S_{BASE}} = \frac{V_1^2 / R_C}{S_{BASE}} \qquad \text{Eq. 9}$$

Where:

- P_C is the rated no-loss power at nominal supply voltage V_1, in watts
- S_{BASE} is the transformer's nameplate rated complex power, in volt-amperes
- V_1 is the nominal supply voltage in volts
- R_C is iron loss resistance when modelled as shunting the primary side of the transformer, in ohms

Equivalent winding reactance (parameter XHL from Table 10), expressed as the percentage combined winding reactances referred to the primary against rated base impedance, is extracted using Eq. 10.

$$XHL = \%jX_{eq_1} = \frac{jX_{eq_1}}{Z_{BASE\,1}} = \frac{jX_1 + \alpha^2\, jX_2}{V_1^2 / S_{BASE}} \qquad \text{Eq. 10}$$

Where:

- XHL is percentage equivalent winding reactance in ohms
- $\%jX_{eq_1}$ is percentage combined winding reactance referred to the primary
- $jX_{eq_1}$is combined winding reactance referred to the primary side, in ohms
- Z_{BASE_1} is the primary base impedance at nominal supply voltage, in ohms
- jX_1 is primary winding reactance in ohms
- α is the nominal transformer winding ratio
- $jX_2$is secondary winding reactance in ohms
- V_1 is the nominal supply voltage in volts
- S_{BASE} is the transformer's nameplate rated complex power in volt-amperes

Winding resistances for the primary and secondary windings (vector parameter %Rs from Table 10), expressed as a percentage over base impedance referred to the respective galvanic side of the transformer, are extracted using Eq. 11 and Eq. 12 respectively.

$$\%R1 = \frac{R_1}{Z_{BASE_1}} = \frac{R_1}{V_1^2 / S_{BASE}} \qquad \text{Eq. 11}$$

Where:

- %R1 is primary winding percentage resistance
- R_1 is primary winding resistance in ohms
- Z_{BASE_1} is the primary base impedance at nominal supply voltage V1, in ohms
- V_1 is the nominal supply voltage, in volts
- S_{BASE} is the transformer's nameplate rated complex power, in volt-amperes

$$\%R2 = \frac{R_2}{Z_{BASE_2}} = \frac{R_2}{V_2^2 / S_{BASE}} \qquad \text{Eq. 12}$$

Where:

- %R2 is secondary winding percentage resistance
- R_2 is secondary winding resistance in ohms
- $Z_{BASE\,2}$ is the primary base impedance at nominal secondary open circuit voltage, in ohms
- V_2 is nominal secondary open circuit voltage in volts
- S_{BASE} is the transformer's nameplate rated complex power in volt-amperes

Magnetising current (parameter %imag from Table 10), expressed as the percentage of magnetising current against base current, as referred to the primary, is extracted using Eq. 13.

$$\%imag = \frac{I_M}{I_{BASE_1}} = \frac{V_1/_{jXm_1}}{S_{BASE}/_{V_1}} \qquad \text{Eq. 13}$$

Where:

- $\%imag$ is percentage magnetising current
- I_M is actual magnetising current in amps
- I_{BASE_1} is primary base current at nominal supply voltage in volts
- V_1 is the nominal supply voltage in volts
- jXm_1 is the magnetising current reactance when modelled as shunting the primary side of the transformer, in ohms
- S_{BASE} is the transformer's nameplate rated complex power, in volt-amperes

3.3.3.3 Model file implementation

Next an OpenDSS model file is created to represent the digitised DSDR substation of Figure *23*, using the parameters derived in section 3.3.3.2. The result will be a plain text file in OpenDSS format, describing the nodes and connections of a DSDR substation, ready to be parameterised in chapter 4, and then used for load-flow simulations during experiments in chapter 5.

Below, each line of the model source code is presented, relating it to the entities shown in Figure *23*, and further discuss how parameters are found. Variable parameters to be determined by calculation are shown with the placeholder <parameter_name> style, and all OpenDSS commands used are taken from the OpenDSS user manual [114]. Source code will be highlighted using the following style:

```
Example OpenDSS source code
```

Let us first set up the constant parameters, which will not change between experiments, and describe the nominal ratings of the substation and its grid supply.

Frequency is set to 50 Hz, to suit modelling of UK and European substations:

```
Set DefaultBaseFrequency=50
```

A grid supply to the substation is set up, with parameters set to match the bench top scale model introduced in the following chapter and as discussed in section 3.3.3.1. The primary voltage is set to 230 V, 50 Hz, single phase:

```
new circuit.circuit1 baseKV=0.230 bus1=mainSource pu=1.0 frequency=50 phases=1
```

Voltage bases, on which percentage results will be reported after each load flow run, are set at 0.4 kV and 0.04 kV line to line:

```
set voltagebases = [0.4, 0.04] !line voltages
```

Next, the upper branch circuit of Figure *23*, which controls one of the two transformers in the reference DSDR substation, is defined. Line 1 is defined as connecting the grid supply to the substation with the primary side reconfiguration switch in this branch:

```
new line.line1 bus1=mainSource bus2=Switch1Input phases=1 length=1 units=m
```

Switch 1 is also implemented as a line in OpenDSS, with its ‘switch’ attribute set to give it the behaviour of a switch:

```
new line.switch1 bus1=Switch1Input bus2=Switch1Output phases=1 length=1
units=m switch=true
```

Line 2 connects the primary reconfiguration switch of the upper branch circuit to Transformer 1:

```
new line.line2 bus1=Switch1Output bus2=transformer1_hv phases=1 length=1
units=m
```

Next, the transformer of the upper branch, providing the parameter placeholders to be calculated as discussed in section 3.3.3.2 is defined. V1_kv and V2_kv will represent the primary and secondary nominal voltages of the transformer, whilst S1_kva and S2_kva will represent its rated complex power.

Rated no-load loss, equivalent winding reactance, winding resistance and magnetising current parameter placeholders will be calculated in the following chapter when parameterising the substation to a bench top scale model DSDR substation:

```
New transformer.T1 phases=1 windings=2 buses=[transformer1_hv
transformer1_lv]
~ kvs=[<V1_kv> <v2_kv] kvas=[S1_kva s2_kva]
~ %Noloadloss=<rated_no_load_loss>
~ XHL=<equivalent_winding_reactance>
~ %Rs = [<primary_winding_resistance> <87econdary_winding_resistance>]
~ %imag=<magnetising_current>
```

Defining the secondary reconfiguration switch and its connecting lines in the same manner as the primary reconfiguration switch, except that Line 4 is set up to be connected to the substation’s load, yet to be declared:

```
new line.line3 bus1=transformer1_lv bus2=Switch2Input phases=1 length=1
units=m
new line.switch2 bus1=Switch2Input bus2=Switch2Output phases=1 length=1
units=m switch=true
new line.line4 bus1=Switch2Output bus2=load_bus phases=1 length=1 units=m
```

The lower branch circuit of Figure *23* is defined in the same way as the upper branch;

```
new line.line5 bus1=mainSource bus2=Switch3Input phases=1 length=1 units=m
new line.switch3 bus1=Switch3Input bus2=Switch3Output phases=1 length=1 units=m switch=true
new line.line6 bus1=Switch3Output bus2=transformer2_hv phases=1 length=1 units=m

New transformer.T2 phases=1 windings=2 buses=[transformer2_hv transformer2_lv]
~ kvs=[<V1_kv> <v2_kv] kvas=[S1_kva s2_kva]
~ %Noloadloss=<rated_no_load_loss>
~ XHL=<equivalent_winding_reactance>
~ %Rs = [<primary_winding_resistance> <seondary_winding_resistance>]
~ %imag=<magnetising_current>


new line.line7 bus1=transformer2_lv bus2=Switch4Input phases=1 length=1 units=m
new line.switch4 bus1=Switch4Input bus2=Switch4Output phases=1 length=1 units=m switch=true
new line.line8 bus1=Switch4Output bus2=load_bus phases=1 length=1 units=m
```

Penultimately, the load demand on the secondary side of the substation is defined with an adjustable load of OpenDSS load type 1 (see Table 11); this means the load can be set in terms of real power and power factor, and will not change with voltage.

Setting the power factor to unity initially, and using the placeholder ‘load_kw’ for load power, to be set dynamically during experiments:

```
new load.load1 bus1=load_bus phases=1 kv=0.024 kw=<load_kw> pf=1.0 model=1
~ Vminpu=0.8 Vmaxpu=1.2
```

Finally, the solving mode is set to ‘snap’, which means that a load-flow can be performed after each load change, at the request of the circuit simulation class described in section 3.2.3.3.7:

```
solve mode=snap
```

3.3.4 Summary

In this section, the derivation of an OpenDSS model was completed, to produce a digitised model of the DSDR substation for use by the circuit simulation class of the DSDR digital twin.

Calculations for parameterising the model were developed from standard transformer equivalent circuits, to transform these into the parameter formats specified in the OpenDSS user manual. In the next chapter, the model developed here will be parameterised to and validated against at bench top scale model DSDR substation.

3.4 Summary

This chapter implemented a DT model of a DSDR reference reconfigurable substation. The concept of a generic DSDR substation was developed, the functional requirements for its implementation were identified, and an SLD representation was produced from which to build the digitised model. It then reviewed the definition of a generic digital twin and developed this into a software architecture for a DSDR DT, before selecting suitable software and simulation packages with which to implement it.

The logic and source code for a complete DSDR DT solution which can be used to develop optimisation algorithms by running experiments in real time was produced, and OpenDSS source code that solves load-flows for the reconfigurable substation was derived from equivalent transformer models to generate a digitised substation model. In the following chapter, a bench top scale model of the DSDR substation is developed, against which the DSDR DT is parameterised and then validated.

4 Bench Top Scale Model of a Reconfigurable Distribution Substation

4.1 Introduction

In the previous chapter, a software-based DT model of a DSDR substation was built, for the development of optimisation algorithms which can be applied after a substation has been pre-emptively reinforced. An advantage of digital twin models compared with conventional offline simulations is that DTs are designed to interface in real-time with the physical systems they model. This chapter presents the design and construction of a physical Bench Top Scale Model (BTSM) of a DSDR substation, and interfacing it such that the optimisation algorithms under development run within the DT software whilst measuring and applying their reconfigurations to the BTSM hardware in real-time.

The BTSM described herein is a scaled down physical model of a real distribution substation. It is designed so that it may be constructed on a workbench in any power systems laboratory, uses standard benchtop measurement instruments, and can emulate either a pre-reinforcement substation, or one that has been pre-emptively reinforced with DSDR reconfiguration equipment.

The development of a BTSM for the DSDR substation has two prime motivations with respect to impact on applied research. Firstly, it enables validation of DSDR optimisation algorithms to take place on physical hardware and in real time, which greatly assists in building confidence by DNO's in the case for Business-as-Usual (BaU) deployments of DSDR to their actual substations. Secondly, it provides a suitable platform on which to develop the interfaces with field-grade instruments in pre-field trials of DSDR, creating a defined route to pilot trials for DSDR algorithms at dedicated facilities such as the Power Network Demonstration Centre [91].

With respect to academic impact, the BTSM developed in this chapter, through use of widely available off-the-shelf components and bench instruments, provides a standardised test-bed for the development and reproducible benchmarking of DSDR optimisation algorithms. The design and implementation of a BTSM is discussed in section 4.2, to produce a DSDR validation tool that can be readily constructed on an experiment bench at any research facility's power systems laboratory.

Here, wiring schematics and control system block diagrams are introduced, and a BTSM is constructed from an equipment list provided. Section 4.3 deals with measuring the as-built BTSM, parameterising an instance of the DSDR DT such that the two models produce equivalent results, and ensuring the correctness, reproducibility, and matching between the two models. This is achieved through hand calculations based on equivalent circuit diagrams, measurements made with bench instruments, and playback of test load profiles for cross-checking voltage regulation and substation efficiency at the full range of operational loads.

4.2 Design and Implementation

4.2.1 Introduction

This section develops, from the DSDR generic topology introduced in the previous chapter, a physical scale model of a distribution substation. The model described in this chapter is designed to be readily constructed on an experiment bench at any research facility power systems laboratory, therefore it is referred to herein as the Bench Top Scale Model (BTSM) of a DSDR substation.

The immediate purpose of the BTSM is to validate that the DSDR DT software developed in chapter 3 can operate and communicate in real-time with physical instruments and actuators in a substation, giving equivalent results when compared against the simulated substation. Further, the research and development context to development of a BTSM is to prepare for the rollout of DSDR to pilot trials and business-as-usual deployments, by demonstrating that optimisation algorithms developed in the simulated DSDR DT environment are transferrable to real-world substations for pilot trials.

The topics within this section are arranged as follows; the wiring schematic of the BTSM is introduced in section 4.2.2, then the equipment required for its construction is set out in section 4.2.3. Methods for controlling the BTSM, and its instrumentation using the DSDR DT software developed in the previous chapter, are discussed in section 4.2.4; finally, the implementation and verification of a BSTM in a typical power laboratory are described in section 4.2.5.

4.2.2 Wiring Schematic

Firstly, a wiring schematic is developed for the BTSM based on the DSDR generic SLD introduced in chapter 3, to describe both the electrical connections between electric power components and the communications connections of the control and instrumentation components. Figure 24 shows the electrical connections with solid black lines, and the communication links with dashed red lines. The overall architecture of a DSDR substation is apparent by observing the solid lines depicting two circuit branches, each with a transformer configured in or out by a pair of switches.

Starting at the top left of the diagram, a computer running the DSDR DT software interfaces to the instruments in the BTSM via an Ethernet cable and LAN switch. This allows the DT software, running in hardware target mode, to read measurements from the physical instruments and send reconfiguration commands to actuators within the BTSM in real-time.

The AC source shown to the centre top of the figure is set to 230 V / 50 Hz, and can optionally be connected to the experiment control system if power supply adjustment mid-experiment is required. All remaining instruments labelled on the diagram are connected via Ethernet cable to the LAN switch for automated control by the DT. These include the two power analyser channels, which measure voltage, current, and power at the higher voltage and lower voltage side of the substation, the AC load which reproduces demand load profiles, and reconfiguration relays which perform transformer switching by actuating the contactors controlling each transformer.

Finally, the two transformers shown in the centre of the diagram, each connected within their own reconfiguration circuit branch, step down the 230 V scaled primary supply voltage to the 24 V scaled load voltage. These are not directly connected to any instrument, as they represent scale models of standard electricity distribution transformers, which do not have on-board instrumentation in most real-world final distribution substations.

Addressing the safety aspects of constructing such a design, electrical power connections will be made using insulated test leads with 4mm touch-safe connectors rated at 1 kV; further, the AC source voltage being set to 230 V builds in a significant safety margin with respect to the test lead rating.

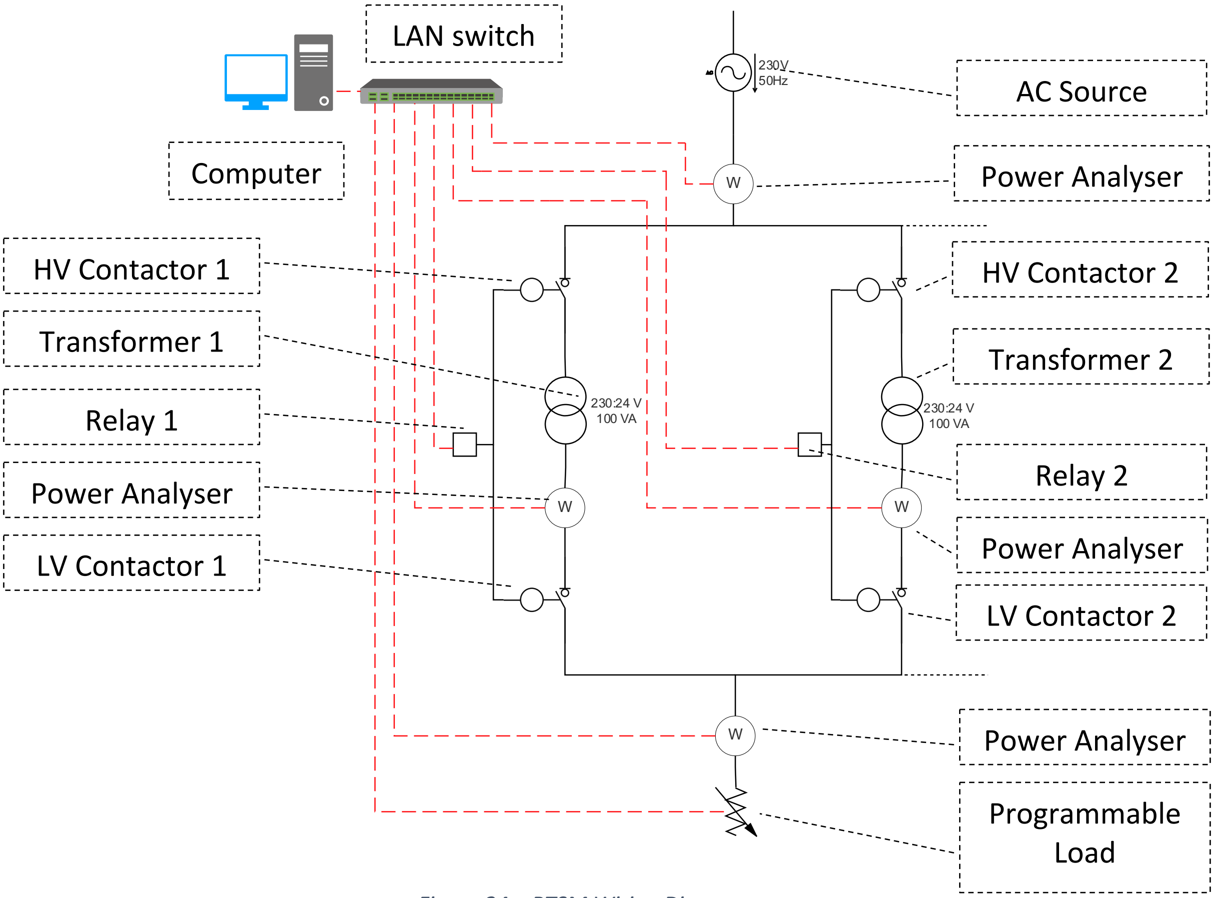

Figure 24 – BTSM Wiring Diagram.

Use of Ethernet cables between the computer and instruments further protects the communications systems from mains voltages, as LAN ports to which these cables connect are electrically isolated from the conductors within those cables.

4.2.3 Equipment

Next, suitable equipment is identified in Table 12 for constructing the BTSM according to Figure 24 using items available within the power laboratories at London South Bank University; equivalent apparatus is expected to be available in power laboratories at other research institutions, such that the BTSM can readily be replicated.

Table 12 - Equipment List for BTSM Design.

Function	Manufacturer	Model	Rating	Qty
Transformer	Block	STS-100/23/24	100 VA	2
Power Supply	RS-Pro	136-8308	24 V / 30 W	1
Relay	Brainboxes	ED-538	5 A / 30 V	1
Indicator	Schneider Electric	A9E18335	12 V – 48 V	2
Contactor	Schneider Electric	LC1D18BD	18 A / 24 V coil	2
AC Source	BK Precision	9801	300 VA	1
Power Analyser	Newton's 4th	PPA1530	20 A / 1000 V	1
AC Load	ETPS	ELPA-3250	20A / 60 V / 300 W	1
LAN Switch	Netgear	GS308	8 Ports	1
Ethernet to Serial adapter	Brainboxes	ES-701	4 x RS 232 ports	1
Ethernet cable	N/A	N/A	Cat-5	5
Insulated test lead	N/A	N/A	1000 V / 20 A	20

The items listed above are combined into functional groups as described in the following sub-sections, and are connected to each other using insulated test leads, which facilities tool-less connection and provides safety protection from dangerous voltages.

4.2.3.1 Transformers

The transformers, which act as scale models of distribution transformers in a real substation, were each grouped with a protective cartridge fuse on the primary, as shown in Figure 25.

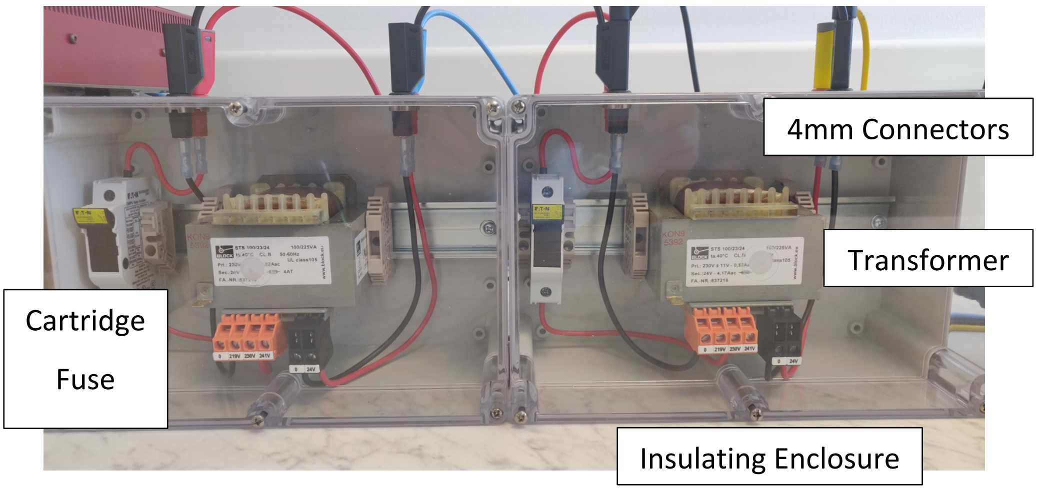

Figure 25 – Bench Top Scale Model (BTSM) transformers.

They were also fitted into insulated enclosures, complete with safety 4mm connectors, to provide touch safety for the operator. This arrangement is convenient as transformers can then be easily removed from the experimental setup for parameterisation measurements, and replaced back into the experiment with ease, without disturbing any electrical connections.

The terminals of each 4mm safety connector which pass through the enclosures were labelled with respect to primary or secondary winding, and phase or neutral polarity, to avoid connection errors when doing so.

The transformers used in the BTSM are of the dry type, which manages the hardware cost and complexity of constructing the BTSM; they are therefore suitable for modelling the electrical behaviour of distribution transformers. For the future addition of a thermal modelling component into the DT, the standard model for oil immersed transformers from BS IEC 60076-7:2018 [115] would be most suitable, as distribution final transformers are typical of the Oil Natural Air Natural (ONAN) cooling type.

However, for validation of future thermal modelling results using the BTSM, the dry-type thermal model from IEC 60076-12:2008 [116] would be most suitable.

4.2.3.2 Power Supply, Relays, Indicators and Contactors

The 24 V DC power supply, relays, indicators, and contactors listed in Table 12 were combined into a DSDR reconfiguration switcher panel, which is shown in Figure 26. The purpose of the panel is to reconfigure the DSDR substation’s topology by switching transformers in or out, according to commands received from the DT software over the Ethernet connection.

Further, a pre-reinforcement substation can be modelled using the BTSM, for benchmarking against post-reinforcement smart operation, by disabling one of the contactor outputs (either within the DSDR DT software or by physical disconnection).

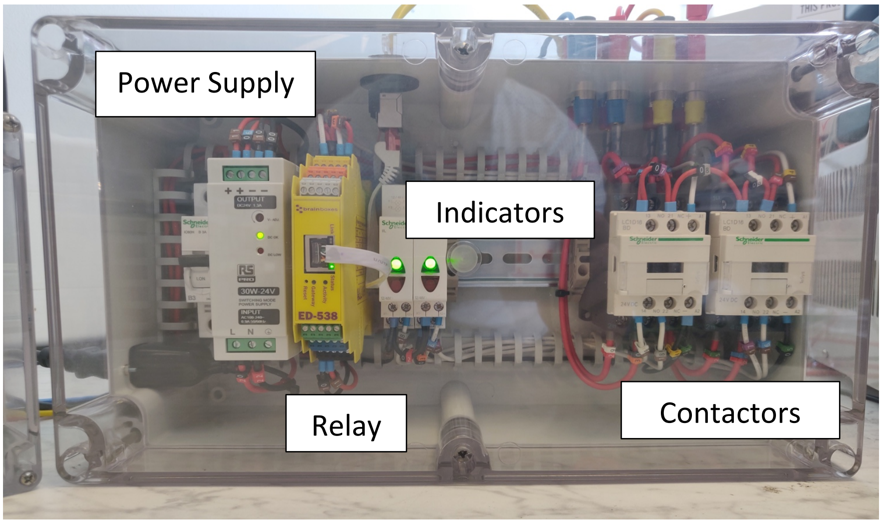

Figure 26 – Substation reconfiguration panel.

The power supply, protected by a miniature circuit breaker, supplies power to the panel's control circuits consisting of the relay, indicators, and contactors. The relay is of the Ethernet controlled type; it latches into the closed position when first energised, and subsequently processes commands received at its Ethernet port to latch each output into the correct position.

Reconfiguration switching instructions are received from the DT software, and the relay contacts (outputs) operate the indicator lamps to display the status of each controlled transformer (red for on, green for off), and simultaneously the coils (input) of the contactors. Each contactor controls one transformer, by switching both the primary and secondary windings through its contacts (outputs), as indicated in each circuit branch of Figure 24.

The components of the reconfiguration switcher panel are mounted on a DIN rail within an insulated enclosure to keep them securely fixed, and are connected to the other components of the BTSM using 4mm safety connectors, which ensures that the experiment is touch-safe for the operator. Mains power for the input of the 24V power supply is brought into the enclosure via a kettle lead bulkhead connector seen to the left of Figure 26, and Ethernet is passed through the enclosure to the relay using an RJ-45 bulkhead adapter seen to the top-centre of the figure.

4.2.3.3 AC Source, Power Analyser, and AC Load

The bench instruments within the BTSM – the AC Source, Power Analyser, and AC Load – are considered here as a functional group, as they each interface both with the power system of the scale model DSDR, and exchange measurements and commands with the DSDR DT over a digital communications bus.

In the laboratory based BTSM constructed in section 4.2.5, these instruments are included within the experiment by stacking them together on the bench. By comparison, at a pilot trial deployment of the DSDR DT, field instruments would be used as shown in Figure 27. These would typically either be mounted adjacent to existing switchgear (subfigure a), or rack mounted (subfigure b).

(a) *GridKey ™ field power analyser installed within a substation, measuring individual feeder voltages and currents* [117]

(b) *SEL 3555 ™ substation automation controller, rack mountable, which controls relays and contains a real-time processor* [118, p. 3555]

Figure 27 - Field instruments suitable for DSDR pilot trials.

The AC source, which models a grid supply to the scale model substation, was implemented using a BK Precision 9801 ™ power supply with a 300 VA capacity as shown in Figure 28a, set at 230 V and 50 Hz output. The phase and neutral electrical connections were brought out from the instrument to the reconfiguration switcher according to the wiring diagram of Figure 24, via a BS1363 plug-top to 4mm safety connector adapter.

Power analyser capability was provided by a Newton's 4th PPA1530 ™ bench power analyser instrument as seen in Figure 28b, utilising two of its three channels. The first channel measures voltage, current, and power at the primary side of the substation – the uppermost power analyser of Figure 24 – with the second channel measuring the same quantities at the secondary side (output) of the substation.

The instrument was also configured to measure substation efficiency between channels 1 and 2 in real time, displaying this as a percentage on its user interface, and exposing it via Ethernet connection to the DSDR DT software.

The final instrument, an AC load as shown in Figure 28c, is the ETPS ELPA3250 ™ programmable load bank – used within the BTSM for replaying load profiles through the DSDR substation during experiments. Its RS232 communications interface is converted to Ethernet using the serial to Ethernet adapter listed in Table 12, enabling it to communicate with the DSDR DT software.

(a) (b) (c)

Figure 28 – BTSM Instruments – a) BK Precision 9801 AC Source, b) Newton's 4th PPA1530 Power Analyser, c) ETPS ELPA3250 programmable AC Load.

4.2.3.4 LAN Switch

The final item of equipment, a LAN switch, provides a marshalling point at which Ethernet cables from all instruments, and the reconfiguration switcher panel, connect to a PC running the DSDR DT software. The following subsection describes in further detail how this equipment is controlled from an operator's PC, and how real-time measurements are streamed to the DSDR DT software.

4.2.4 Control and Instrumentation

The control and instrumentation methodology for the BTSM leverages on re-use of the DSDR DT software developed in the previous chapter. With only minor changes to its configuration, the DSDR DT application is capable of retrieving substation state measurements from the physical instruments within the BTSM, and issuing reconfiguration commands to its actuators, in real-time. The optimisation algorithms developed using the DSDR DT would then control the BTSM, without any changes to their operation, and without being aware that the substation being controlled had been swapped from virtual to physical. Figure 29 below depicts the integration of the DSDR DT software application with the BTSM instruments in block diagram form.

Beginning with the DSDR DT software at the left of the figure, an operator may view substation state and queue experiments from a PC which is running the application, and is also connected to the LAN switch via Ethernet cable. The software functional blocks consisting of frontend, logic control, backend, and databases map to the software modules described in full detail in the previous chapter.

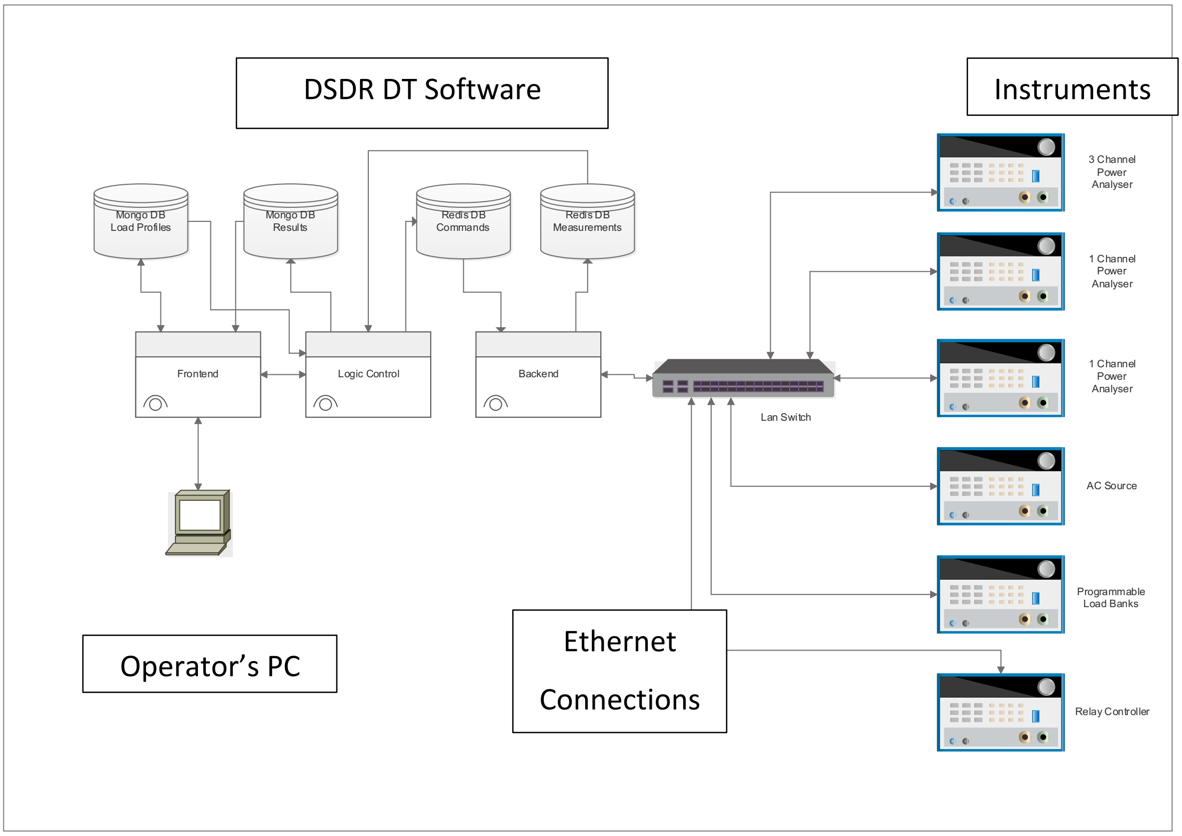

Figure 29 – BTSM experiment control system.

To the centre of the diagram is shown the LAN switch, connecting all instruments and actuators to the PC running the DSDR DT application, with communications over Ethernet cables. This switch is unmanaged, and as the instruments are set with fixed IP addresses, it is also transparent as far as the DT is concerned. Should remote control of the BTSM or a pilot trial DSDR deployment be desired, the switch could be replaced with a router set up to port-forward TCP requests from the operator's PC to the instruments, or the local PC may could be remotely connected to from the operator's location using a Virtual Private Network (VPN) [119].

The instruments and actuators shown to the right of the figure are those described in detail in section 4.2.3 above, which are in turn connected to the power system of the BTSM according to Figure 24. The benefits of the approach described in this section include the ability to develop optimisation algorithms on a DSDR DT model with a simulated substation, then rapidly deploy them to the BTSM for validation prior to pilot trial. Use of the DSDR DT software to run experiments on the BTSM also provides scope to include additional simulations into the DT. These would run on top of measurements made by the physical BTSM instrument, such as transformer internal temperature modelling and ageing rate.

The following section describes how the BTSM wiring diagram of section 4.2.2, experimental apparatus of section 4.2.3, and experiment control scheme of this section were combined to construct a BTSM set up.

4.2.5 Bench Set Up

The as-built BTSM, set up in a laboratory at London South Bank University, can be seen in Figure 30 below, with the equipment groupings of section 4.2.3 labelled on the photograph. An oscilloscope including current and voltage probes is used for waveform verification at substation input and output, and the additional branch-circuit power analysers of Figure 24 are included for load flow verification purposes.

Further, spare AC loads of differing ratings are wired in parallel with the instrument listed in Table 12, to enable increased substation capacity if desired. All additions are optional extras to the BTSM, and were not connected to the DSDR DT application for the work described in this thesis.

On the front panels of the bench instruments to the right of the figure, and at the top of the transformer and reconfiguration switcher panels to the left of the figure, can be seen the insulated test leads - complete with 4mm safety connectors - implementing the power system conductors of the wiring diagram from Figure 24. The Ethernet cables and LAN switch are connected to rear of the instruments; one from each instrument to the switch, and one from the switch to operator's PC.

With the arrangement shown, instruments may be read and controlled manually via their front panels, which is useful during experiment set up, and remotely via the DSDR DT application from the operator's PC. During setting up and initial energisation of the BTSM, the oscilloscope - shown on top of the other bench instruments - with the voltage and current probes shown on the bench in front of the instruments, are also very useful in confirming the waveforms at substation input and output are as expected. The oscilloscope channels were set up as shown in Table 13, to observe these at the BTSM substation's primary and secondary connections.

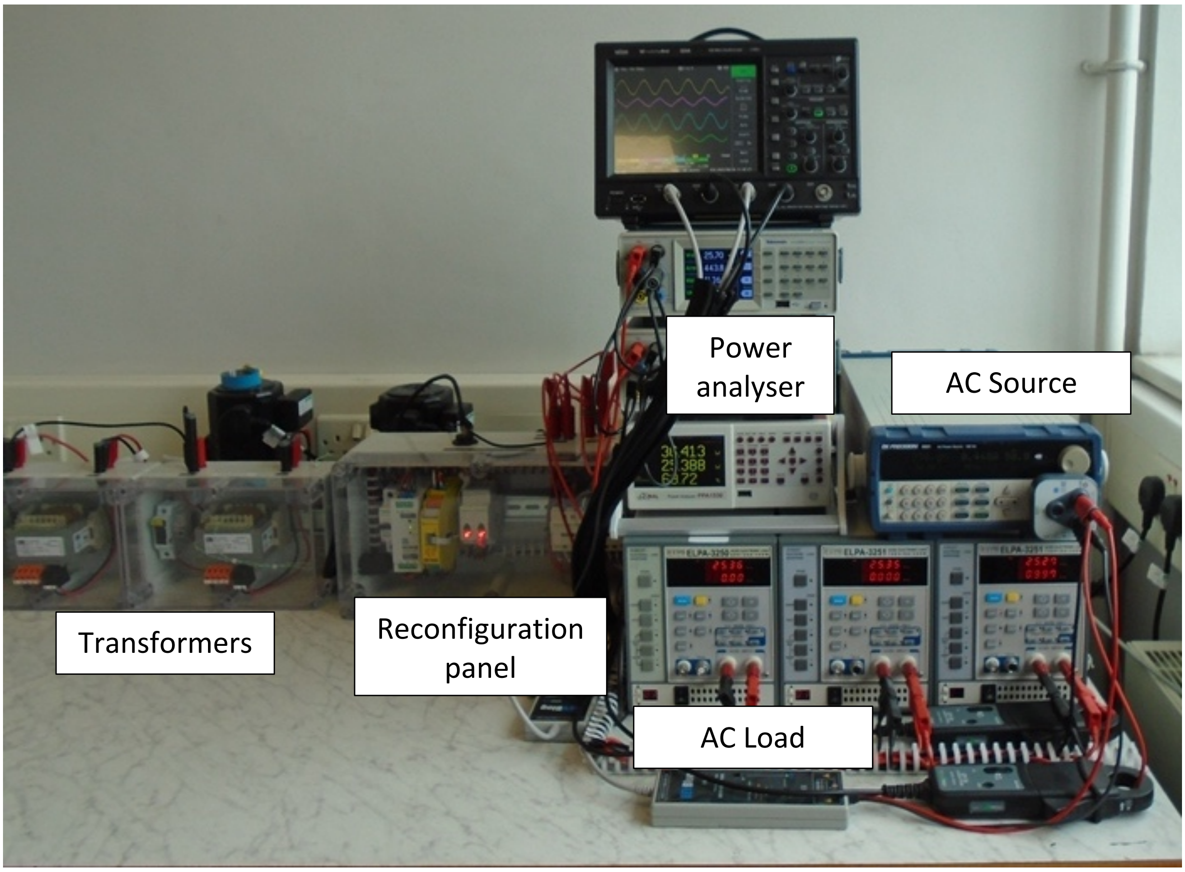

Figure 30 – BTSM set up on laboratory work bench.

Table 13 – Oscilloscope channel settings for initial verification of BTSM.

Substation Node	Type	Channel	Trace Colour	Probe Type
Primary input	Voltage	1	Yellow	Differential
Primary input	Current	2	Pink	Clamp
Secondary output	Voltage	3	Blue	Differential
Secondary output	Current	4	Green	Clamp

At initial power on of the BTSM, both circuit branches of the DSDR (and therefore both transformers) are switched in by the reconfiguration switcher by default, and the load drawn by the AC loads is set to zero by default. The waveforms observed on the oscilloscope under these start-up conditions are shown in Figure 31 below with RMS measurements at the bottom of the image. The measurements indicated by the oscilloscope are not used during experiments, and are for indication only due to the relatively large measurement uncertainty of differential and clamp probes.

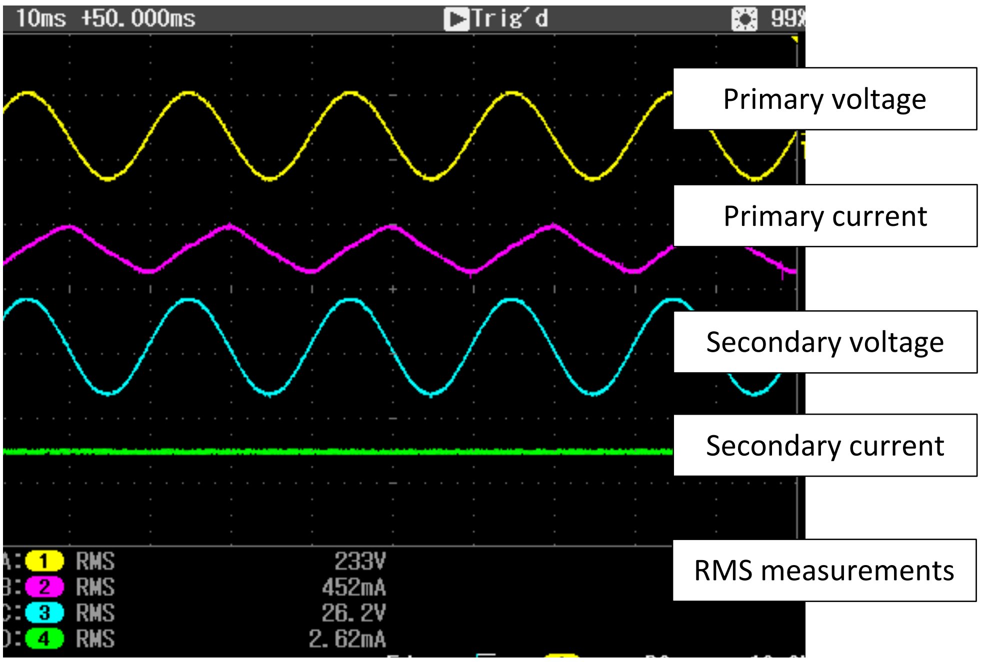

Figure 31 – BTSM waveforms at initial power on.

Primary voltage is a clean sinusoid of around 230 V, indicating the AC source is set up and functioning correctly, whilst the primary current shows the typical harmonic pollution of a transformer magnetising current waveform producing a near triangle wave.

Secondary voltage is also a clean sinusoid as expected, and measures close to 26 V, the rated open-circuit voltage of the transformers in the BTSM. Secondary current is close to zero, the residual few milliamps measured by the oscilloscope resulting from the input noise of the oscilloscope channel and current clamp probe, indicating the AC load is set to zero as expected.

Next, the AC load was manually set to the full load power of the substation with both transformers in circuit – 200 W – producing the oscillographs shown in Figure 32. Primary and secondary voltage waveforms remain sinusoidal, with secondary voltage having reduced to close to 24 V, as expected for the rating of the transformers at full load. Secondary current is sinusoidal and in phase with secondary voltage, indicating that the AC load is performing as expected.

Finally, primary current now exhibits significantly reduced harmonic pollution, as the load current through the transformer dominates the magnetising current at each transformer's primary winding.

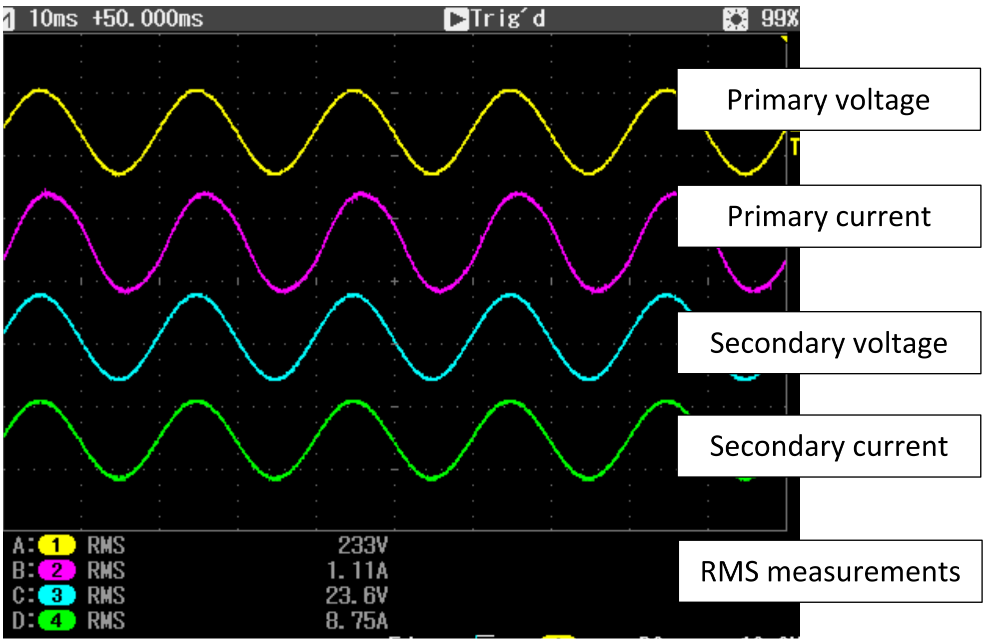

Figure 32 - BTSM waveforms at full load.

The BTSM is now ready to be operated by the DSDR DT software, which will initially be used to validate that the measurements made by the physical bench top instruments within the BTSM, and the virtual instruments within the DT, are equivalent and well matched.

4.2.6 Summary

This section has introduced the design, construction, and initial verification of a bench-top scale model (BTSM) DSDR substation. The BTSM will be a vital tool in validating smart substation optimisation algorithms, developed within a virtual DT simulated substation, against a real-time environment containing physical instruments and transformers. Wiring schematics and a list of required equipment were produced, which enable the BTSM to be replicated in any power systems laboratory; it was shown how the DSDR DT software application can interface and control the BTSM in real-time using Ethernet communications; and a BTSM implementation was constructed and validated in a laboratory setting.

The following section will detail the parameterisation process used to match an instance of the DSDR DT developed in the previous chapter to the BTSM implementation constructed in this section. The resulting DSDT DT model parameters will then be used to validate that both models of a DSDR substation (DT and BTSM) produce equivalent measurements, so that optimisation algorithms can be reliably and rapidly iteratively developed and evaluated using the DT, then validated and prepared for pilot trials using the BTSM.

4.3 Parameterisation and Validation

This chapter deals with ensuring the “correctness”, reproducibility, and matching between the BTSM and DT models, so that they can later be depended upon for the development and validation of DSDR optimisation algorithms. In section 4.3.1, the parameters of the BTSM model are measured, and used to populate the DT’s transformer model. Section 4.3.2 uses calculations based on the classical equivalent circuit models of a transformer to validate measured values of magnetising current, voltage regulation, and power losses of the BTSM. Finally, the BTSM and the parameterised DT models are validated by cross checking against each other in section 4.3.3.

4.3.1 Component Parameterisation

Component parameterisation for a DSDR model is the process of acquiring measurements from physical transformers, and then applying those to the virtual transformer model within the DSDR DT.

In the remainder of this chapter, the transformers of the BTSM implementation constructed in the laboratory as described in section 4.2.5 will be parameterised so that an instance of the DSDR DT application can be created which closely matches the operation of the BTSM. For pilot trial deployments, the parameterisation measurements would be carried out on physical transformers at a real distribution substation, or taken from the datasheet or factory test data, then applied to the DT using the method described here.

4.3.1.1 Equipment

Parameter measurement of transformers is carried out using standard equipment available in a power laboratory to perform the Open Circuit Test (OCT) and Short Circuit Test (SCT) [120] on each transformer; a continuously adjustable, stable AC voltage source, and a power analyser measuring voltage, current, and phase angle. The equipment listed in Table 14 was used for these tests on the BTSM described in section 4.2.5.

Table 14 – Transformer parameter test equipment.

Type	**Make**	**Model**	**Rating**
Variable Transformer	Aldetronics	ITV-15	1.5 kVa
AC Source	Thurlby Thandar	AC1000	1 kW
Power Analyser	Newton's 4th	PPA5520	10 A
Breakout Box	Tektronix	BB1000-UK	20 A

The variable transformer and AC source instruments were used in combination to form a stable and adjustable AC voltage; this providing a clean, stable sinusoidal voltage, and the variable transformer making the same continuously adjustable, to suit the OCT and SCT procedures described below in sections 4.3.1.3 and 4.3.1.4. The breakout box was used to adapt the power analyser's connections to suit the variable transformer's output connections.

4.3.1.2 Devices Under Test

The two scale-model distribution transformers from Table 12 were each removed from the BTSM in turn, to become the Device Under Test (DUT) for OCT and SCT, and then replaced into the BTSM; their specifications are shown in Table 15, taken from the manufacturer's datasheet given in appendix section 10.1.1.

Although transformers may be of identical design, and equal voltage, current, and frequency ratings, manufacturing tolerances and operating conditions will lead to expected variations in the measurements carried out. The OCT process used to measure each transformer is described next.

4.3.1.3 Open Circuit Test

The Open Circuit Test (OCT) procedure was carried out using the test circuit shown in Figure *33* and the experimental setup shown in Figure *34*, to measure each DUT transformer's rated no-load loss and magnetising current.

These will later be transformed into the '%Noloadloss' and '%imag' parameters expected by the OpenDSS model within the DSDR DT in section 4.3.1.7. During the OCT, a pure sinusoidal voltage produced by the AC source was adjusted to the DUT transformer's nominal secondary rating using the variable transformer with the connections shown in Figure *33*; as the variable transformer is connected on the supply side of the power analyser instrument, it's losses would not affect the measurement.

Table 15 – Scale Model Transformer Details.

Attribute	**Value**	**Unit**
Manufacturer	Block	
Model	STS	
Power Rating	100	VA
Phases	1	
Windings	2	
Primary Voltage	230	V
Secondary Voltage	24	V
Cooling Type	Air Natural (AN)	
Dielectric	Dry Type	
Frequency	50 – 60	Hz

The supplied voltage, current, and power as measured by the power analyser instrument at the secondary winding were recorded, with the primary winding being left as an open circuit.

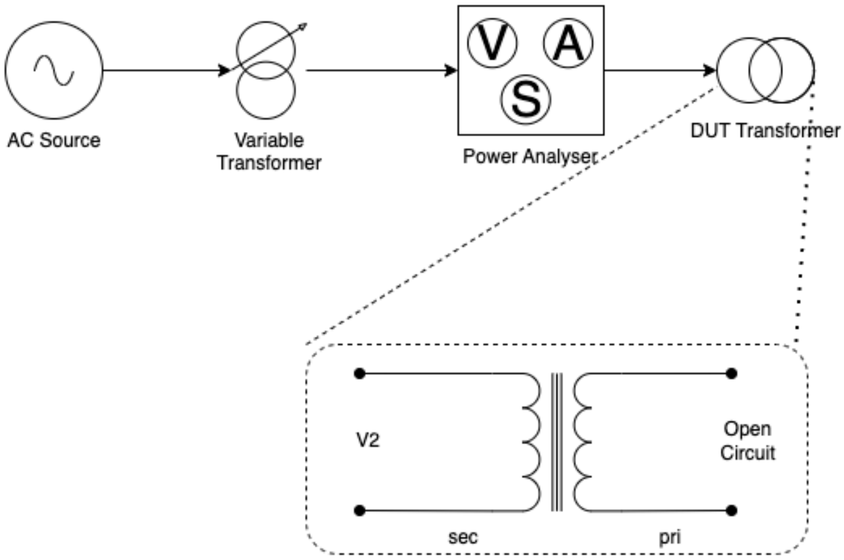

Figure 33 - Transformer Open Circuit Test Schematic.

As the no-load loss and magnetising current are a phenomena of the transformer's iron core, the choice of winding to energise during the OCT is arbitrary; however, the secondary winding permits the test to be performed at a lower voltage and so is preferred. Figure *34* shows the OCT being performed on one of the DUT transformers, with the equipment listed in Table 14 labelled on the diagram.

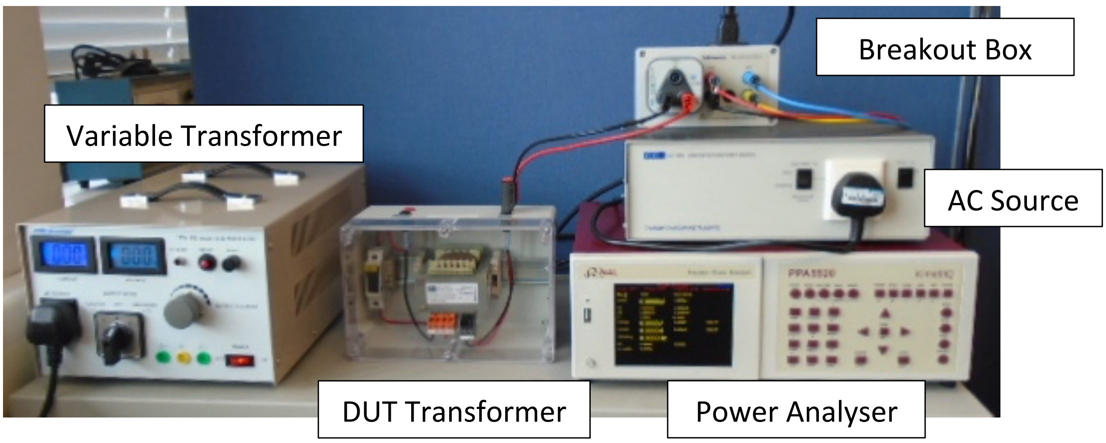

Figure 34 - Open Circuit Test (OCT) Setup.

It can be seen from the photograph that the 4mm safety connectors to the top left of the DUT transformer enclosure were left unconnected, to form the open circuit at the primary winding. The results were recorded for both DUT's – given in section 4.3.1.5 – and the parameterisation proceeded with the remaining tests.

4.3.1.4 Short Circuit Test

Next, the SCT procedure was carried out using the test circuit shown in Figure *35*, to measure each DUT transformer's combined winding resistances and winding reactances. These will be used to determine the 'XHL' and '%Rs' parameters of the digitised substation model in section 4.3.1.7.

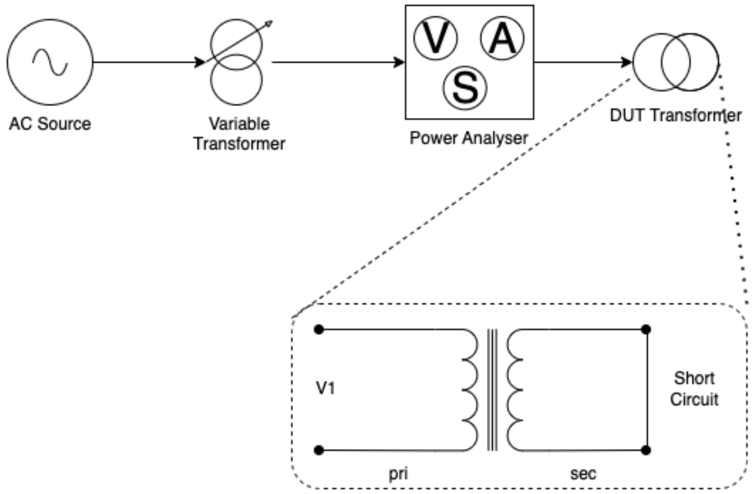

Figure 35 *- Transformer Short Circuit Test Schematic.*

The secondary winding was shorted, as this allows the test to be performed at a lower (primary) current than shorting the primary; a pure sinusoidal voltage connected to the primary winding adjusted to the magnitude at which the primary winding rated current was attained. The supplied voltage, current, and power at the primary terminals are recorded in section 4.3.1.5, and the experimental setup for the SCT is shown in Figure *36* below.

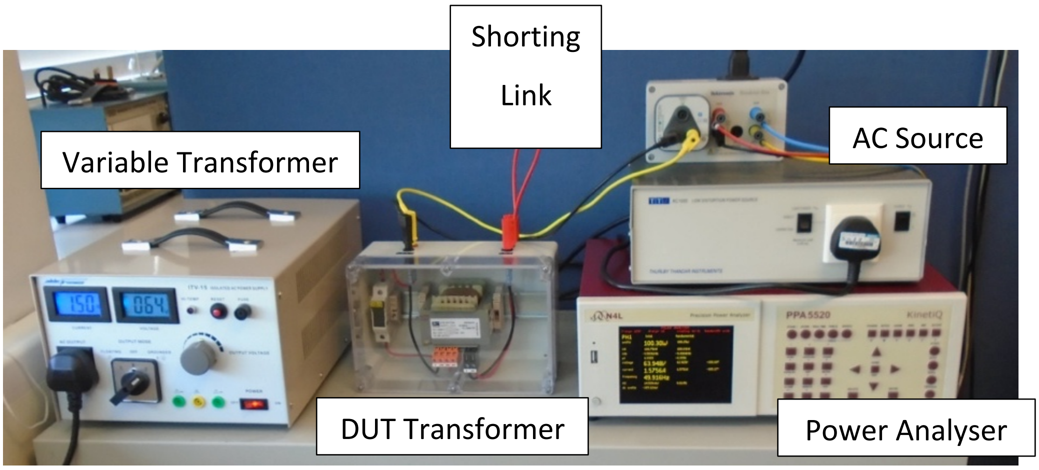

Figure 36 *- Short Circuit Test (SCT) Setup.*

For the SCT, the AC supply is connected to the DUT's primary winding, and a shorting link is in place across the secondary terminals as can be seen in the photograph.

4.3.1.5 Measurements

The OCT and SCT measurement results for both DUT transformers are listed in Table 16.

Table 16 – DUT Transformer test results.

	Open Circuit Test		**Short Circuit Test**		
Parameter	**DUT 1**	**DUT 2**	**DUT 1**	**DUT 2**	**Unit**
P	5.040	4.377	10.921	10.393	W
|S|	45.246	38.689	10.974	10.445	VA
jQ	44.96	38.441	1.077	1.041	VAr
p.f.	0.111	0.113	0.995	0.995	N/A
Vrms	23.979	23.994	20.878	20.089	V
I	1.887	1.612	0.526	0.520	A

Where:

- P is real power in watts
- |S| is apparent power in volt-amperes
- jQ is reactive power in volt-amperes reactive
- p.f. is phase angle of the current signal with respect to the voltage signal (no units)
- Vrms is root mean square magnitude of the voltage signal in volts
- I is current in amps

The complex power (P and jQ) measurements from each DUT's OCT results confirm that a variation in both no-load loss and magnetising current exists between otherwise identical model transformers; this is likely due to variations in the iron cores arising from manufacturing tolerances. Winding resistances and reactances as measured during the SCTs, which are easier to control during manufacture, were very closely matched between the two DUTs.

Turns ratio was measured by connecting the second channel of the power analyser to the open primary winding during each OCT, yielding the results shown in Table 17. The turns ratios of the two DUT's were very closely matched, as expected, because controlling the number of winding turns during manufacture is easily achieved.

Table 17 – Measured DUT turns ratios.

DUT	Primary Voltage	Secondary Voltage	Turns Ratio (α)
1	230.312 V	25.9516 V	8.875
2	230.361 V	25.9780 V	8.867

The open circuit secondary voltage is notably designed to be greater than the rated secondary voltage given in the datasheet, which is to allow for voltage regulation when each transformer operates at rated load. Next, the measurements performed in this section will be used to determine equivalent circuit parameters for each DUT transformer of the BTSM, so that they can be used within the digitised DSDR DT model.

4.3.1.6 Equivalent Circuit Parameter Calculation

To extract each DUT's equivalent circuit parameters, the measured voltages, currents and powers recorded during OCT and SCT were used in conjunction with the equivalent circuit for each test. Figure 37 shows the OCT equivalent circuit, with voltage being applied to the transformer secondary. Winding resistance and reactance are omitted due to their negligible contributions to no-load loss and magnetising current.

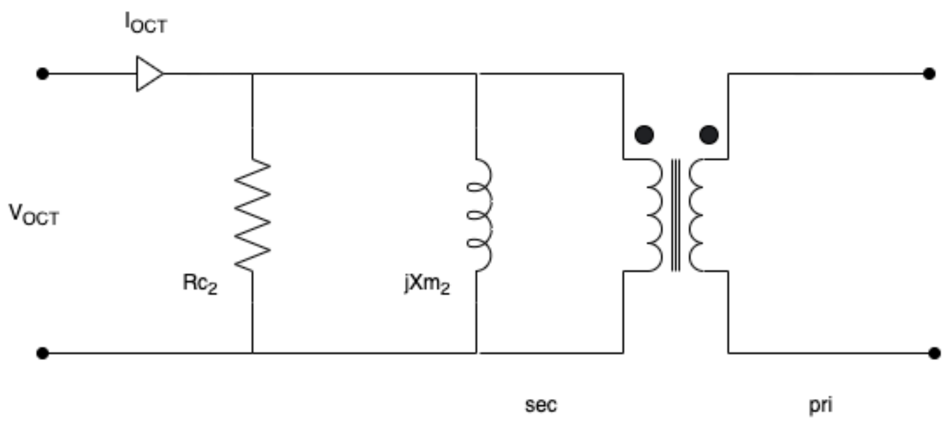

Figure 37 - OCT Equivalent Circuit.

No-load losses were calculated as referred to the secondary using Eq. 14.

$$R_{c_2} = \frac{V_{OCT}^2}{P_{OCT}} \qquad \text{Eq. 14}$$

Where:

- R_{c_2} is iron loss resistance when modelled as shunting the secondary side of the transformer, in ohms
- V_{OCT} is voltage applied to the secondary winding during the OCT, in volts
- P_{OCT} is real power absorbed by the transformer during the OCT, in watts

The result was referred back to the primary using Eq. 15.

$$R_{c_1} = a^2 R_{c_2} \quad \text{Eq. 15}$$

Where:

- R_{c_1} is iron loss resistance when modelled as shunting the primary side of the transformer, in ohms
- α is the nominal transformer winding ratio
- R_{c_2} is iron loss resistance when modelled as shunting the secondary side of the transformer, in ohms

Similarly, the magnetising current was calculated for the secondary and referred to the primary side using Eq. 16.

$$jX_{m_1} = a^2 \frac{V_{OCT}^2}{-jQ_{OCT}} \quad \text{Eq. 16}$$

Where:

- α is the nominal transformer winding ratio
- jX_{m_1} is the magnetising current reactance when modelled as shunting the primary side of the transformer, in amps
- V_{OCT} is voltage applied to the secondary winding during the OCT, in volts
- jQ_{OCT} is reactive power of the transformer during the OCT, in volt-amperes reactive

Figure 38 shows the SCT equivalent circuit referred to the primary side. Here, no-load loss resistance and magnetising current reactance are omitted, as they have no effect upon winding impedance.

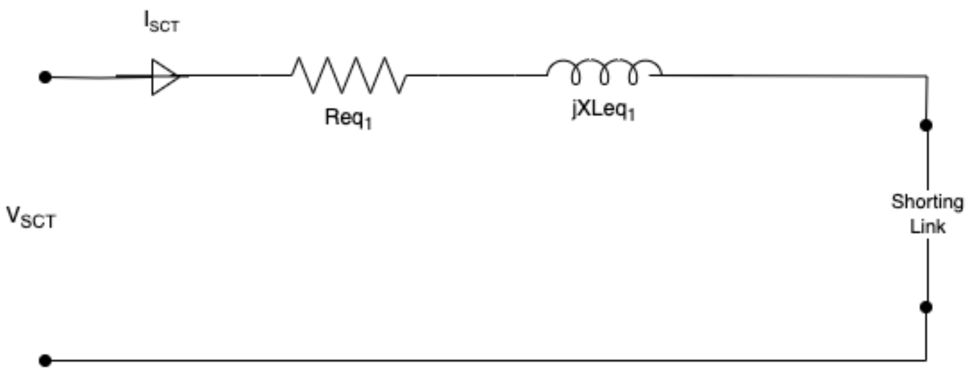

Figure 38 - SCT equivalent circuit referred to the primary side.

Combined equivalent resistances were calculated and then divided equally, as a reasonable assumption [120], between the primary and secondary sides accounting for turns ratio, using Eq. 17 and Eq. 18.

$$R_{eq_1} = \frac{P_{SCT}}{I_{SCT}^2} \qquad \textit{Eq. 17}$$

$$R_1 = \frac{R_{eq_1}}{2}, \qquad R_2 = \frac{R_1}{a^2} \qquad \textit{Eq. 18}$$

Where:

- R_{eq_1} is combined resistance of windings referred to the primary side, in ohms
- P_{SCT} is real power absorbed by the transformer during the SCT, in watts
- I_{SCT} is primary current drawn by the transformer during the SCT, in amps
- R_1 is the portion of combined winding resistance assigned to the primary winding, in ohms
- R_2 is the portion of combined winding resistance assigned to the secondary winding, referred to the secondary side, in ohms
- α is the nominal transformer winding ratio

Primary and secondary winding reactances were determined using Eq. 19 and Eq. 20.

$$jX_{eq_1} = \frac{-jQ_{SCT}}{I_{SCT}^2} \quad \text{Eq. 19}$$

$$jX_1 = \frac{jX_{eq_1}}{2}, \qquad JX_2 = \frac{jX_1}{a^2} \quad \text{Eq. 20}$$

Where:

- jX_{eq_1} is combined reactance of windings referred to the primary side, in ohms
- jQ_{SCT} is reactive power at the transformer during the SCT, in volt-amperes reactive
- I_{SCT} is primary current drawn by the transformer during the SCT, in amps
- jX_1 is the portion of combined winding reactance assigned to the primary winding, in ohms
- JX_2 is the portion of combined winding reactance assigned to the secondary winding, referred to the secondary side, in ohms
- α is the nominal transformer winding ratio

The extracted equivalent circuit parameters, calculated as described above, for each DUT are listed in Table 18. As expected for identical model DUTs, all parameters are well matched, with the only notable deviations being no-load loss resistance and magnetising current reactance, as discussed in section 4.3.1.5.

Next, the analogue equivalent circuit parameters calculated in Table 12 are transformed into OpenDSS digitised model parameters to suit the DSDR DT's substation simulator component.

Table 18 – DUT equivalent circuit parameters from OCT and SCT measurements.

Parameter	**Symbol**	**Unit**	**DUT 1**	**DUT 2**
Primary winding resistance	R_1	Ohms	19.765	19.212
Primary winding reactance	jX_1	Ohms	1.940	1.948
No-load loss resistance[3]	R_c	Ohms	8986.04	10341.47
Magnetising current reactance[3]	jX_m	Ohms	1007.33	1177.55
Secondary winding resistance	R_2	Ohms	0.251	0.244
Secondary winding reactance	jX_2	Ohms	0.0246	0.0248
Combined winding resistance[3]	R_{eq_1}	Ohms	39.53	38.436
Combined winding reactance[3]	jX_{eq_1}	Ohms	3.88	3.90

4.3.1.7 Digitised Model Parameter Calculation

Extracted OpenDSS transformer parameters are calculated from the measurements in Table 18, using the method set out in the previous chapter (section 3.3.2 - Model Parameter Derivation). The resulting digitised transformer model parameters for both DUTs are given below in Table 19.

Table 19 – Extracted OpenDSS transformer parameters.

OpenDSS Parameter	**Unit**	**DUT 1**	**DUT 2**
phases	Qty	1	1
windings	Qty	2	2
Kvs [pri, sec]	[kV, kV]	[0.230, 0.026]	[0.230, 0.026]
Kvas [pri, sec]	[kVA, kVA]	[0.1, 0.1]	[0.1, 0.1]
%Noloadloss	%	5.887	5.115
XHL	%	0.733	0.737
%Rs [pri, sec]	[%, %]	[3.736, 3.713]	[3.632, 3.609]
%imag	%	52.515	44.923

Where:

- Phases is the quantity of AC phases (windings) at each side of the transformer
- Windings it the total number of windings at the transformer

[3] As referred to primary

- Kvs is a vector of nominal windings voltage ratings
- Kvs is a vector of nominal windings apparent power ratings
- %Noloadloss is the measured no-load loss power as a percentage of rated power
- XHL is measured total reactance of the windings as percentage of rated base reactance
- %Rs is a vector of resistance of each winding as percentage of base resistance
- %imag is measured magnetising current as a percentage of rated base current

These values were used to complete the OpenDSS DSDR substation model, as listed below. Initiate a new model, set the system frequency, and specify a single phase 230V source:

```
Clear

Set DefaultBaseFrequency=50

new circuit.circuit1 baseKV=0.230 bus1=mainSource pu=1.0 frequency=50
phases=1

set voltagebases = [0.4, 0.04] !line voltages
```

Set up the lines and switches on the primary side of transformer 1:

```
!#################### LEFT BRANCH ################################
new line.line1 bus1=mainSource bus2=Switch1Input phases=1 length=1 units=m

new line.switch1 bus1=Switch1Input bus2=Switch1Output phases=1 length=1
units=m switch=true

new line.line2 bus1=Switch1Output bus2=transformer1_hv phases=1 length=1
units=m
```

Declare the measured parameters of transformer 1 as listed in Table 19:

```
New transformer.T1 phases=1 windings=2 buses=[transformer1_hv
transformer1_lv]
~ kvs=[0.230 0.026] kvas=[0.1 0.1]
~ %Noloadloss=5.887
~ XHL=0.733
~ %Rs = [3.736, 3.713]
~ %imag=52.515
```

Set up the lines and switches on the secondary side of transformer 1:

```
new line.line3 bus1=transformer1_lv bus2=Switch2Input phases=1 length=1 units=m

new line.switch2 bus1=Switch2Input bus2=Switch2Output phases=1 length=1 units=m switch=true

new line.line4 bus1=Switch2Output bus2=load_bus phases=1 length=1 units=m
```

Set up the lines and switches on the primary side of transformer 2:

```
!#################### RIGHT BRANCH ################################
new line.line5 bus1=mainSource bus2=Switch3Input phases=1 length=1 units=m

new line.switch3 bus1=Switch3Input bus2=Switch3Output phases=1 length=1 units=m switch=true

new line.line6 bus1=Switch3Output bus2=transformer2_hv phases=1 length=1 units=m
```

Declare the measured parameters of transformer 2 as listed in Table 19

```
New transformer.T2 phases=1 windings=2 buses=[transformer2_hv transformer2_lv]
~ kvs=[0.230 0.026] kvas=[0.1 0.1]
~ %Noloadloss=5.115
~ XHL=0.737
~ %Rs = [3.632 3.609]
~ %imag=44.923
```

Set up the lines and switches on the secondary side of transformer 2:

```
new line.line7 bus1=transformer2_lv bus2=Switch4Input phases=1 length=1 units=m

new line.switch4 bus1=Switch4Input bus2=Switch4Output phases=1 length=1 units=m switch=true

new line.line8 bus1=Switch4Output bus2=load_bus phases=1 length=1 units=m
```

Set up the adjustable load, common to both transformers' secondary, and prepare model for single-step solving:

```
!#################### LOADS ################################
new load.load1 bus1=load_bus phases=1 kv=0.024 kw=0.2 pf=1.0 model=1
~ Vminpu=0.8 Vmaxpu=1.2

solve mode=snap
```

4.3.1.8 Summary

An OpenDSS model of the BTSM transformers was produced in this section, by measurement of the transformers using the Open Circuit and Short Circuit tests, use of classical transformer equivalent circuit models to extract the ideal component parameters in analogue form, and conversion of these into digitised parameters to suit the model. The following sub-sections will see the validation of the BTSM and DSDR DT with above model file against manual measurements taken at run-time operation of the BTSM.

Once the equivalence of DSDR DT and BTSM results has been established, these will be utilised in the remaining chapters in the delivery of experiments for the rapid development and physical validation of optimisation algorithms for smart, reconfiguration substations.

4.3.2 Manual Validation

4.3.2.1 Calculations

Here, the measured performance of transformer DUT 1 at the no-load and full-load operating points is compared with the manually calculated expected values based on the equivalent circuit parameters determined in section 4.3.1.6. Validations are performed for no-load current, full-load voltage regulation and full-load losses.

4.3.2.1.1 No-load Current

Constructing the reduced equivalent circuit as referred to the transformer's primary side, with the experimental parameters determined in section 4.3.1.6 and with zero load impedance, yields the diagram shown in Figure 39. Current, $I_c =$ in the core loss component R_c, which shunts and is in phase with the primary voltage, is given by $I_c = \frac{V_1}{R_c} = \frac{230\ \angle 0°}{8986.04\ \angle 0°} = 0.0256\ \angle 0°\ A$.

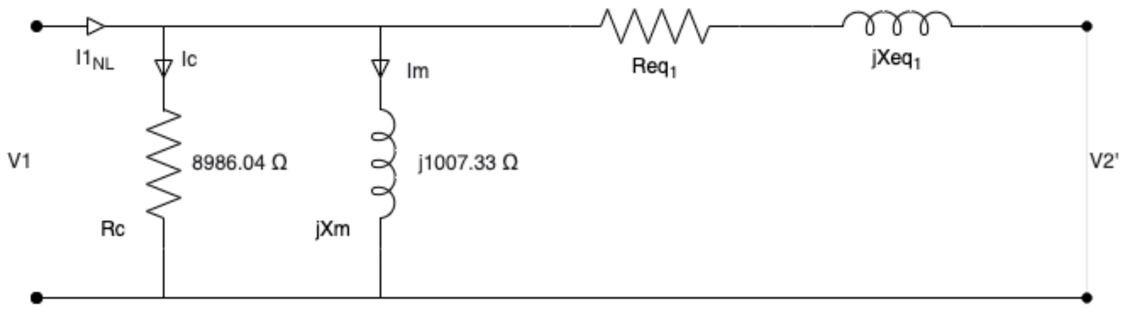

Figure 39 – Equivalent circuit for no-load current calculation.

Equivalently, current, $I_m$in the core magnetising component jX_m, which shunts and is in quadrature with the primary voltage, is given by

$I_m = \frac{V_1}{jX_m} = \frac{230\ \angle 0°}{1007.33\ \angle 90°} = 0.228 \angle -90°\ A$. The absolute vector sum of these currents $I_{1_{NL}}$ is given by $\left| I_{1_{NL}} \right| = \sqrt{I_c^2 + I_m^2} = 0.230\ A$, which will later be compared with the measured value of no-load current.

4.3.2.1.2 Full-load voltage regulation

Constructing the reduced equivalent circuit, electrically referred to the secondary, with the experimental parameters determined in section 4.3.1.6 and with a secondary terminal impedance producing full rated load, yields the diagram shown in Figure 40. Core loss resistance and magnetising current impedance are not required for the calculation, so are omitted.

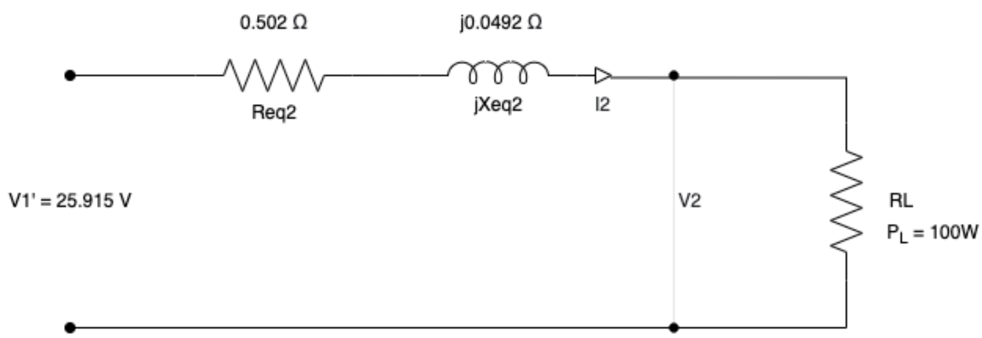

Figure 40 – Equivalent circuit for full load voltage regulation calculation.

Primary rated voltage referred to the secondary is given by $V_1' = \frac{V_{1_{rated}}}{\alpha} = 25.915$ V. Using Kirchhoff's Voltage Law (KVL) [121] for the loops of the circuit through V_1', R_{eq_2}, jX_{eq_2}, and V_2 enables construction of the voltage triangle in Figure 41, taking V_2 as a reference.

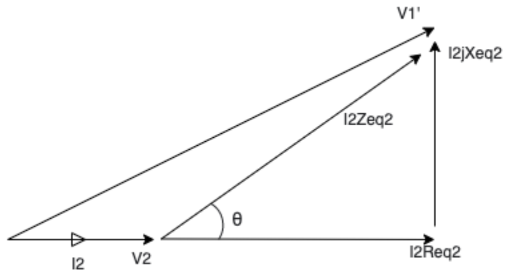

Figure 41 – Voltage triangle for full load voltage regulation calculation.

Combining winding resistance and reactance into a complex impedance gives $Z_{eq_2} = \sqrt{R_{eq_2}^2 + jX_{eq_2}^2}\ \angle tan^{-1}\left(\frac{jX_{eq_2}}{R_{eq_2}}\right) = 0.504\ \angle 5.60°\ \Omega$, giving the angle theta. The left hand side (LHS) of Figure 41 may then be redrawn as Figure 42, with the absolute volt drop across the impedance given by $\left|I_2 Z_{eq_2}\right| = 0.504\frac{100}{V_2} = \frac{50.4}{V_2}$.

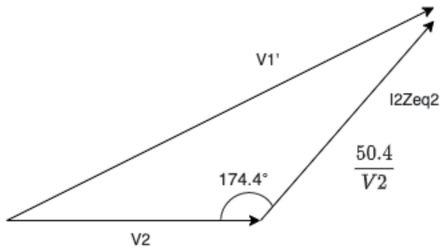

Figure 42 – Voltage triangle of transformer voltage to suit solving by cosine rule.

Substituting V_2 for x and applying the cosine rule, $25.915^2 = x^2 + \frac{50.4}{x} - 2x\ \frac{50.4}{x}\cos 174.4°$, which has roots $x = -23.807, x = -2.117, x = 2.117, x = 23.807$. It can be assumed that secondary voltage under full load V_2= 23.807 V is the only reasonable solution, as the DUT has a rated secondary voltage of 24V. This result will be compared with the measured value of full-load voltage.

4.3.2.1.3 Full-load losses

Constructing the reduced equivalent circuit with full load as referred to the secondary, and with calculated full-load voltage referred to the secondary $V_{2_{FL}}' = V_{2_{FL}}\,\alpha = (23.8073)(8.875) = 211.29\ V$, yields the circuit shown in Figure 43.

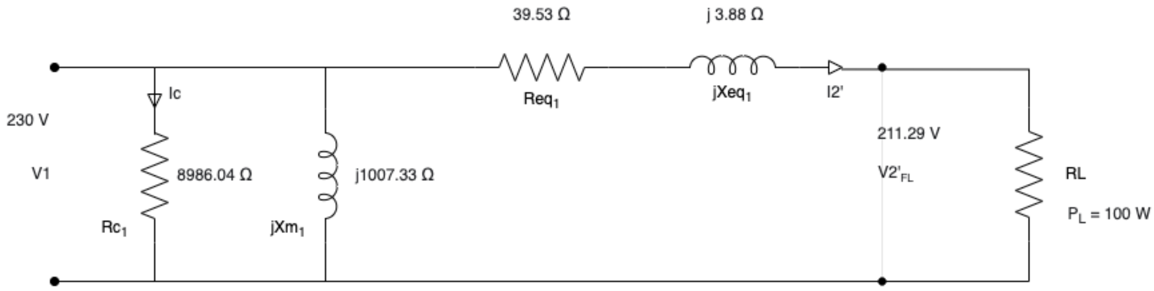

Figure 43 - Equivalent circuit for full load losses calculation.

Resistance required for operation at full load given the expected voltage regulation is calculated by $R_L = \frac{V2{\prime}_{FL}{}^2}{P_L} = \frac{211.29^2}{100} = 446.43\ \Omega$, enabling determination of current I2' through the winding resistances as $I2' = \frac{V2{\prime}_{FL}}{R_L} = \frac{211.29}{446.43} = 0.473\ \angle 0°\ A$. Copper losses, P_{cu}in the windings are thus $P_{cu} = I2'^2\ Req_1 = (0.473)^2(39.53) = 8.844\ W$.

Core losses $P_c$are determined by $P_c = \frac{V_1^2}{R_c} = \frac{230^2}{8986.04} = 5.887\ W$, and summing the losses yields $Losses_{FL} = P_{cu} + P_c = 14.731\ W$, which will be compared with measured losses of the DUT under full load.

4.3.2.2 Measurements

The input and output parameters of DUT 1 at the two operating points of most interest for validation – no-load and full-load – were measured with a power analyser. Supply power was provided at rated voltage from a sinusoidal voltage source, with a sinusoidal in-phase load drawn by a programmable AC load; the measurement set-up and instruments are shown in Figure 44.

The parameters measured were real power, apparent power, reactive power (calculated), power factor, voltage and current. Raw measurement data from these tests can be found in appendix section 10.1.3.

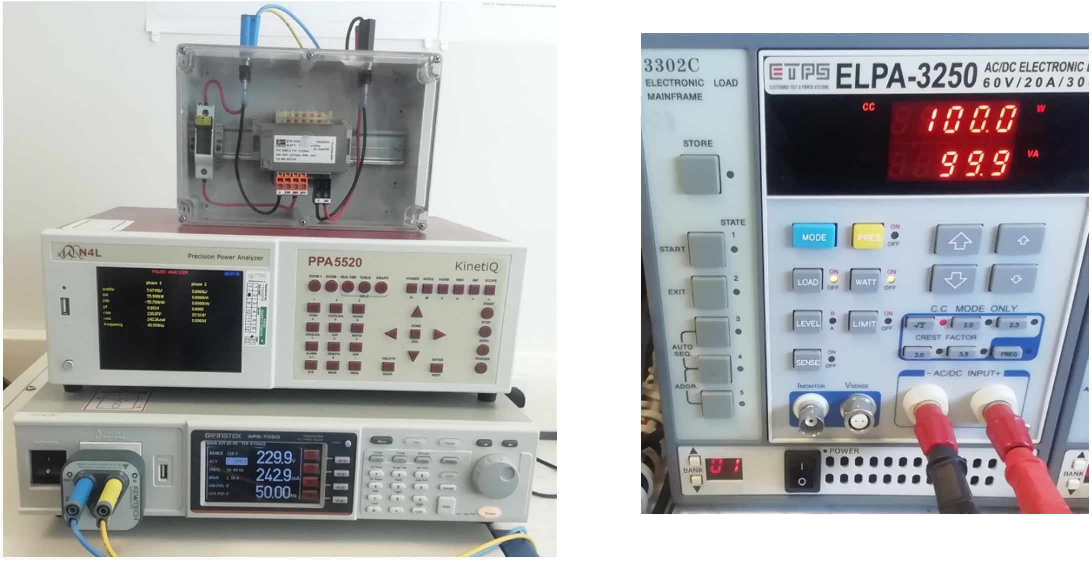

(a) (b)

Figure 44 – a) DUT measurements at no-load and full load with b) programmable load.

4.3.2.2.1 No Load

The measurements recorded at no-load are given in Table 20.

Table 20 – No-load DUT 1 measurement results.

Parameter	Primary	Secondary	Unit
P	5.655	0.0	W
|S|	55.900	0.0	VA
jQ	55.613	0.0	VAr
p.f.	0.101	0.0	-
Vrms	230.01	25.920	V
I	0.243	0.0	A

Where:

- P is real power absorbed by the transformer or load
- |S| is apparent power absorbed by the transformer or load
- jQ is reactive power absorbed by the transformer or load
- p.f. (power factor) is the ratio of real power to apparent power
- Vrms is the root mean square value of the voltage signal
- I is the root mean square value of the current signal

As expected for an unloaded transformer, all output measurements are zero except for voltage, and the input power factor is close to zero.

4.3.2.2.2 Full Load

The measurements recorded at full-load are given in Table 21.

Table 21 - Full-load DUT 1 measurement results.

Parameter	**Primary**	**Secondary**	**Unit**
P	114.60	100.04	W
|S|	125.57	100.06	VA
jQ	51.328	2.000	VAr
p.f.	0.913	0.999	-
Vrms	230.05	23.806	V
I	0.546	4.203	A

Where:

- P is real power absorbed by the transformer or load
- |S| is apparent power absorbed by the transformer or load
- jQ is reactive power absorbed by the transformer or load
- p.f. (power factor) is the ratio of real power to apparent power
- Vrms is the root mean square value of the voltage signal
- I is the root mean square value of the current signal

As expected for a transformer operating at rated power with a resistive load, input power factor is close to unity, and output reactive power is negligible.

4.3.2.3 Validations

The calculated values for no-load current, full-load voltage regulation, and full-load losses from section 4.3.2.1 are next compared with measured values from section 4.3.2.2, in Table 22 below.

Table 22 – DUT 1 measured vs calculated values at no-load and full load.

Validation	Calculated Value	Measured Value	Error
No-load current	0.230 A	0.243 A	-5.35 %
Full-load voltage regulation	23.807 V	23.806 V	0.004 %
Full-load losses	14.73 W	14.56 W	1.15 %

As seen in Figure 31, the actual magnetising (no-load) current as measured by the power analyser is not a pure sinusoidal signal, but contains harmonic components in additional to the fundamental. This effect is due to saturation of the transformer's iron core, a phenomenon not modelled in the classical transformer equivalent circuits used to produce the calculated value (Figure 39), and not problematic for the optimisation algorithms developed in the following chapters.

These harmonics increase the measured current in the wideband signal measured by the power analyser, accounting for the -5.35 % residual in the calculated value of no-load current in Table 22. Full-load voltage regulation and full-load losses, being sinusoidal and not affected by core saturation, are very well matched between the equivalent circuit model calculated values and the measured values of Table 22.

This sub-section has shown that the difference between calculated and measured values are within the uncertainties of the instruments and the measurements taken, demonstrating "correctness" in the results of the parameterisation process. Next, the power, voltage, and current measurements of the BTSM and DSDR DT models will be compared at no-load and full-load operation of the substation, in all substation reconfiguration states, to further demonstrate the equivalence of the two model paradigms under dynamic conditions.

4.3.3 Models Validation

The DT and BTSM were validated by means of cross-checking their measurements under identical configuration and load states. Each model was operated in single-transformer mode with each DUT, and in parallel mode, under both no-load and full load conditions. This allowed comparisons to be made between the operating voltage, current, and power at the substation input node and output node.

4.3.3.1 DT Measurements

Figure 45 and Figure 46 show the DT status screen when operating DUT 1 in single mode at no-load and full-load conditions respectively.

```
Instruments
        controller:     {'tx_1': '1', 'tx_2': '0'}
        source          {'V': '230.0', 'f': '50.0', 'I': '0.2269', 'P': '-7.8279', 'pf': '-0.15'}
        tx1 primary:    {'V': '229.9416', 'I': '0.2276', 'W': '7.8219', 'VAr': '51.7575', 'VA': '52.3452'}
        tx2 primary:    {'V': '0.0', 'I': '0.0', 'W': '0.0', 'VAr': '0.0', 'VA': '0.0'}
        substation:     {'Input_W': '7.8279', 'Output_W': '0.0', 'Efficiency_%': '0.0'}
        load            {'Bank': '0', 'Wave': '0', 'Load_on': '0', 'I': '0.0', 'V': '25.7622'}
```

Figure 45 - DT measurement for single operation mode using DUT 1 at no-load.

```
Instruments
        controller:     {'tx_1': '1', 'tx_2': '0'}
        source          {'V': '230.0', 'f': '50.0', 'I': '0.5606', 'P': '-119.3079', 'pf': '-0.9253'}
        tx1 primary:    {'V': '229.8877', 'I': '0.5609', 'W': '119.2711', 'VAr': '49.0009', 'VA': '128.9445'}
        tx2 primary:    {'V': '0.0', 'I': '0.0', 'W': '0.0', 'VAr': '0.0', 'VA': '0.0'}
        substation:     {'Input_W': '119.3079', 'Output_W': '99.8368', 'Efficiency_%': '83.68'}
        load            {'Bank': '0', 'Wave': '0', 'Load_on': '1', 'I': '4.3287', 'V': '23.0641'}
```

Figure 46 - DT measurement for single operation mode using DUT 1 at full-load.

The two figures above are snapshots of the DSDR DT operator's view of the application software whilst an experiment is in progress. Each line represents either a virtual or physical instrument, depending upon the mode of operation, followed by the instantaneous measurements recorded by that instrument at the substation node to which it is connected.

The 'controller' instrument is the substation reconfiguration controller, and its measurements are the Boolean switching states of each transformer ('tx_1' and 'tx_2'), i.e. whether they are current switched into or out of the substation's circuits. The 'source' instrument represents the grid supply to the substation, with the voltage and frequency measurements shown first – these remain stable throughout each experiment. Measured current, real power, and power factor are also shown, which change dynamically as the substation's load and configuration changes throughout each experiment.

Next, the measured parameters at the primary side of each transformer ('tx_1' and 'tx_2'), if available, are shown. These are always available when in virtual instrument mode, and are optional in BTSM mode, but are generally useful for validation only and are not required by the optimisation algorithms.

The ‘substation’ instrument represents the two-channel power analyser connected at substation input and output, and displays measured power at both of these nodes, in addition to the substation’s real-time efficiency given by the two measurements.

Finally, the ‘load’ instrument represents the programmable AC load instrument connected to the substation’s output. Displayed first are the load type (named ‘Bank’ and ‘Wave’ on the ETPS ELPA-3250 instrument) which set the mode to AC and the load type to constant current – these do not change throughout or between experiments. Next, the load state is displayed as a Boolean, indicating whether the instrument is set to sink power (1) or remain in standby (0); this is followed by the dynamic measurements of current and voltage made by the programmable load at its input.

Equivalent results for DUT 2 can be found in appendix section 10.1.5. Figure 48 and Figure 49 show the DT status screen when operating in parallel mode under both load conditions.

```
Instruments
        controller:     {'tx_1': '1', 'tx_2': '1'}
        source          {'V': '230.0', 'f': '50.0', 'I': '0.4217', 'P': '-14.3053', 'pf': '-0.1475'}
        tx1 primary:    {'V': '229.9446', 'I': '0.2145', 'W': '8.382', 'VAr': '48.5983', 'VA': '49.3159'}
        tx2 primary:    {'V': '229.947', 'I': '0.2083', 'W': '5.9129', 'VAr': '47.5429', 'VA': '47.9092'}
        substation:     {'Input_W': '14.3053', 'Output_W': '0.0', 'Efficiency_%': '0.0'}
        load            {'Bank': '0', 'Wave': '0', 'Load_on': '0', 'I': '0.0', 'V': '25.781'}
```

Figure 47 - DT measurement for parallel operation mode at no-load.

```
Instruments
        controller:     {'tx_1': '1', 'tx_2': '1'}
        source          {'V': '230.0', 'f': '50.0', 'I': '1.1025', 'P': '-236.3365', 'pf': '-0.932'}
        tx1 primary:    {'V': '229.8914', 'I': '0.5517', 'W': '118.2307', 'VAr': '45.9408', 'VA': '126.8426'}
        tx2 primary:    {'V': '229.8915', 'I': '0.5511', 'W': '118.0347', 'VAr': '46.0295', 'VA': '126.6922'}
        substation:     {'Input_W': '236.3365', 'Output_W': '199.1942', 'Efficiency_%': '84.284'}
        load            {'Bank': '0', 'Wave': '0', 'Load_on': '1', 'I': '8.6139', 'V': '23.1248'}
```

Figure 48 - DT measurement for parallel operation mode at full-load.

The measured values at no-load and full-load for the DT were as expected, and are compared with those from the BTSM in Table 24 and Table 25.

4.3.3.2 BTSM Measurements

The same set of measurements as described in section 4.3.3.1 were performed on the BTSM, and results captured directly from its two-channel power analyser. Figure 49 shows the instrument’s front panel whilst recording single-mode operation of the substation with DUT 1 switched in. Equivalent figures for DUT 2 can be found in appendix section 10.1.5.3, and all results are compared with those of the DSDR DT in Table 24 and Table 25.

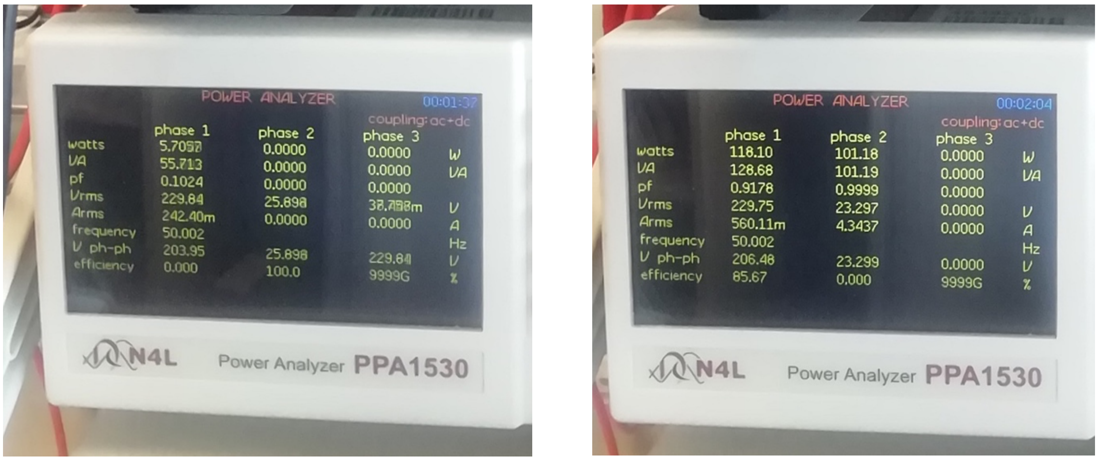

(a) (b)

Figure 49 - BTSM measurement for DUT 1 single operation at a) no-load and b) full-load.

The instrument screens above show the view from the BTSM operator's perspective at the bench whilst an experiment is in progress, who can observe instantaneous readings either from the instrument front panels, or from the DSDR DT application software as seen in Figure 45 for example. Channel 1 on the analyser was connected to the substation input node, with channel 2 connected to the output node. The PPA1530 instrument shown in the photographs organises measurements as a table, with channels organised into columns (named 'phases'), and measurands into rows.

For BTSM experiments, the instrument is configured to record, display, and expose to the DSDR DT software the quantities described in Table 23. Figure *50* shows the power analyser instrument screens with the substation reconfigured for parallel operation, for a) no-load and b) full-load settings of the programmable load.

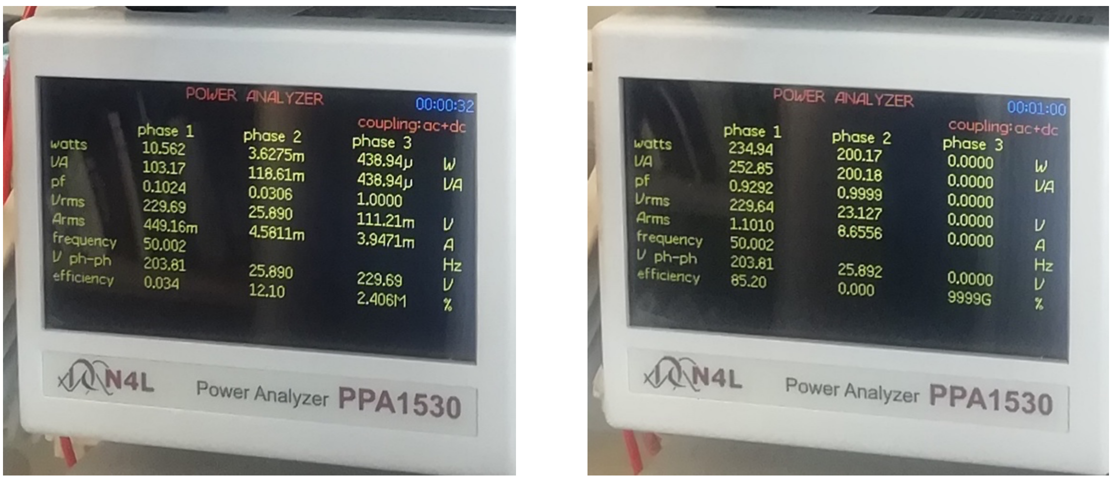

(a) (b)

Figure 50 - BTSM measurement for parallel operation a) no-load and b) full-load.

Table 23 - Power Analyser Measurands for BTSM Experiments.

Label	Measurand	Unit
Watts	Real Power	W
VA	Apparent Power	VA
Pf	Power Factor	-
Vrms	Root Mean Square Voltage	V
Arms	Root Mean Square Current	A
Frequency	Voltage frequency	Hz
V ph-ph	Line voltage	V
Efficiency	Quotient of channel 2 and channel 1 real powers	%

Next, the resulting measurements under both no-load and full-load conditions, and at all configuration topologies, will be presented and discussed.

4.3.3.3 Comparison of Measurements between DT and BTSM

The measurements from both the parameterised DSDR DT and the BTSM models under single-transformer operation are shown in Table 24 for DUT 1.

Table 24 – DT and BTSM validation for single operation mode using DUT 1.

		Input			Output		
Load	**Model**	**P**	**V**	**I**	**P**	**V**	**I**
No-load	DT	7.828 W	230.0 V	0.227 A	0.0 W	25.76 V	0.0 A
	BTSM	5.806 W	229.8 V	0.242 A	0.0 W	25.90 V	0.0 A
	Residuals	*25.83 %*	*0.09%*	*-6.61%*	*0.0%*	*-0.54%*	*0.0%*
Full-load	DT	119.3 W	230.0 V	0.561 A	99.84 W	23.06 V	4.33 A
	BTSM	118.1 W	229.8 V	0.560 A	101.2 W	23.30 V	4.34 A
	Residuals	*1.01%*	*0.09%*	*0.18%*	*1.36%*	*-1.04%*	*-0.23%*

At each set-point, the voltage, power, and current were recorded at substation input and output. For the DT model, these are simulated using the OpenDSS transformer parameters extracted in section 4.3.1.7, whilst for the BTSM they are measured directly using the power analyser instrument.

The parameters used to model each transformer in OpenDSS fit within two categories; those which dominate at no-load and are extracted from OCT measurements; and those which dominate at high loads, extracted from SCT measurements. Analysing the residuals between both models at the extremes of each transformer's rated operating regime – no-load and full-load – therefore serves to accentuate any errors produced within the OpenDSS simulation. Residuals at full-load are very small, indicating that the BTSM and DT models are extremely well matched at this operating point. At no-load, the transformer input current residual between models exhibits a level of mismatch that whilst not insignificant, would be expected for a model which does not include transformer core saturation (DT), and a power analyser that does include wideband measurement of the harmonics in the current signal caused by that saturation (BTSM).

The error in current measurements at no-load also causes mismatch of power measurements between the models at no-load; whilst this at first may seem significant in percentage terms between measurements, in percentage terms of rated transformer power it is actually far less significant, and is not expected to adversely affect the development and performance of optimisation algorithms. To confirm this finding, the uncertainties of substation efficiency between BTSM and DT models in a continuum of operating points between no-load and full-load will be verified in section 4.3.3.4. Table 25 below shows the equivalent measurements from both models under single-transformer operation for DUT 2.

Table 25 – DT and BTSM validation for single operation mode using DUT 2.

		Input			**Output**		
Load	**Model**	**P**	**V**	**I**	**P**	**V**	**I**
No-load	DT	6.50 W	230.0 V	0.194 A	0.0 W	25.80 V	0.0 A
	BTSM	4.93 W	229.75 V	0.207 A	0.0 W	25.91 V	0.0 A
	Residuals	*24.15%*	*0.11%*	*-6.70%*	*0.0%*	*-0.43%*	*0.0%*
Full-load	DT	117.7 W	230.0 V	0.545 A	99.84 W	23.17 V	4.31 A
	BTSM	117.5 W	229.89 V	0.546 A	100.2 W	23.08 V	4.34 A
	Residuals	*0.17%*	*0.05%*	*-0.18%*	*-0.36%*	*0.39%*	*-0.70%*

The residuals at full-load were again very small, and those of the input measurements at no-load of the same order as for DUT 1, validating the parameterisation method as valid and reproducible. Measurements for both models in parallel mode are shown in Table 26.

Table 26 – DT and BTSM validation for parallel operation mode.

		Input			Output		
Load	**Model**	**P**	**V**	**I**	**P**	**V**	**I**
No load	DT	14.31 W	230.0 V	0.422 A	0.0 W	25.78 V	0.0 A
	BTSM	10.56 W	229.7 V	0.449 A	0.004 W	25.89 V	0.005 A
	Residuals	*26.21%*	*0.13%*	*-6.40%*	*0.0%*	*-0.43%*	*0.0%*
Full load	DT	236.3 W	230.0 V	1.103 A	199.2 W	23.12 V	8.614 A
	BTSM	234.9 W	229.64 V	1.101 A	200.2 W	23.13 V	8.656 A
	Residuals	*0.59%*	*0.16%*	*0.18%*	*-0.50%*	*-0.04%*	*-0.49%*

For the substation operating with parallel transformers, as each BTSM transformer is rated at 100W, full-load has now increased to 200W.

Similarly for the results obtained under single transformer operation, all measurement residuals at full-load with parallel transformer operation were minimal. Likewise, the residuals of input current and power at no-load exhibit similar magnitude errors to that of single transformer operation, and once again this is not expected to present a problem for the optimisation algorithms presented in later chapters. Next, the ‘experiment runner’ feature of the DT application software will be leveraged, to automate an extended validation of the matching between the BTSM and parameterised DSDR DT models over the full range of substation loads.

4.3.3.4 Validation Over Full Range of Substation Loads

As a final validation step, performance over the entire range of loads were validated in substation parallel operation mode for the DT and BTSM models. This was achieved by playing back a test load profile, consisting of a linear ramp between no-load and full-load over 48 steps, as described below.

4.3.3.4.1 Preparation of ramp test load profile

Load profiles for use by the DSDR DT software are stored as documents within the DT's MongoDB [108] document database. The data format is a flat (non-nested) Javascript Object Notation (JSON) [122] object, in which the keys represent the time steps and can be any numeric type (to ensure they sort correctly), and the values represent the load factor (the quotient of instantaneous load to rated load). A linear function with 48 equal values between zero and one, with keys in timestamp format from 00:30 hours to 00:00 hours, was produced in the expected JSON format and stored in the DT's document database with the profile name 'ramp'. A snippet of the resulting database document is shown in Figure 51, with the first few time steps and load factor values.


```
  _id: ObjectId('63208b4c2ecc223179c34eea')
  name: "Test Functions"
v data: Object
  v ramp: Object
      00:30:00: 0
      01:00:00: 0.021
      01:30:00: 0.043
      02:00:00: 0.064
      02:30:00: 0.085
      03:00:00: 0.106
      03:30:00: 0.128
      04:00:00: 0.149
      04:30:00: 0.17
```


Figure 51 – Snippet of ramp test load profile in JSON format.

A time series plot of the ramp test load profile to illustrate the concept is shown below in Figure 52. When this load profile is replayed through both the BTSM and DT models, measurements from the respective bench instruments and virtual instruments of the physical substation and virtual substation will be captured at many points in the normal operating range of the substation. Next, the DSDR DT software menu interface will be used to launch a playback of the load profile on both the BTSM and DT models.

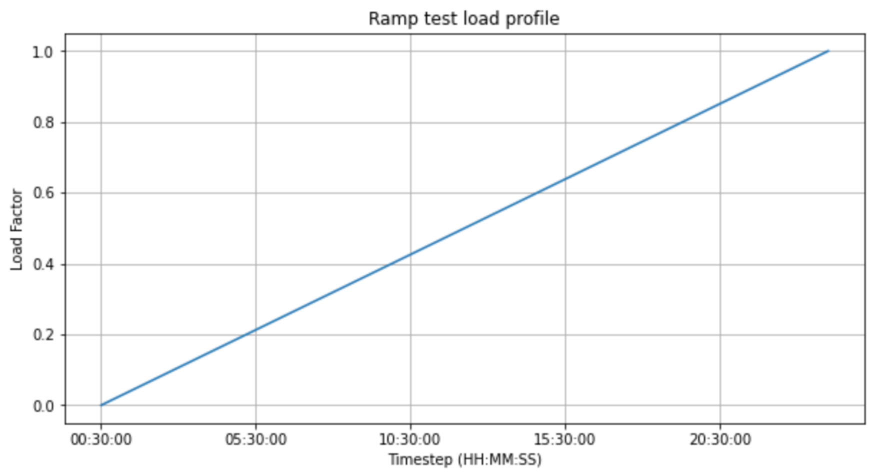

Figure 52 – Ramp test profile.

4.3.3.4.2 Launching ramp test experiment using DSDR DT software menu

The DSDR DT software is first launched by the operator, with configuration initially set to run experiments on the virtual substation; then, the process described below is subsequently repeated with the DSDR DT software configured to use the physical BTSM substation for the experiment. The operator is presented with a main menu as the primary user interface to the DSDR DT software, from where the 'Play load profile' option is selected as shown in Figure 53.

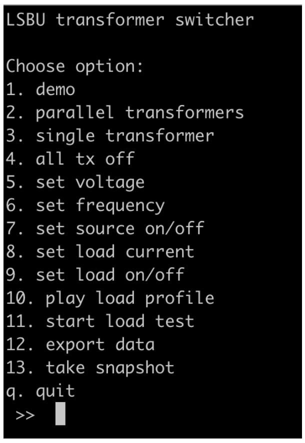

Figure 53 - Main menu.

The operator will then be prompted to select a profile group ('Test Functions' in this case), and a load profile ('ramp' in this case), as shown in Figure 54 (a) and (b) respectively.

(a) Profile group (b) Load profile

Figure 54 – Selecting a load profile.

Finally, a scaling factor is chosen to convert the normalised set of load-factors within the load profile into concrete values of current magnitude, as shown in Figure 55a. In this exercise, the substation has a rated total power of 200 W at 24 V, yielding a scaling factor of 8.33 A. The time step in seconds is also specified as shown in Figure 55b. This is the period at which the time steps in the load profile will be replayed in real-time through the model under test during the experiment – 10 s was chosen here, meaning the experiment will complete in 480 s.

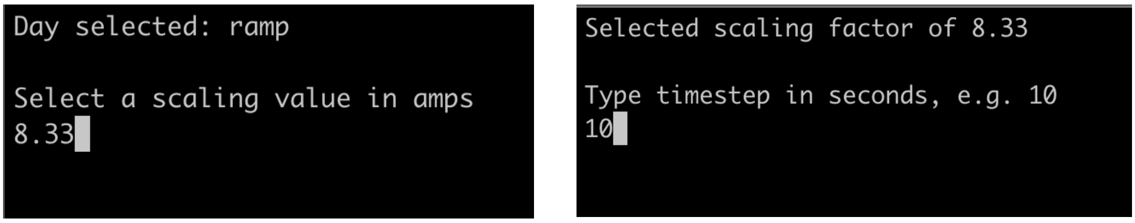

(a) Scaling factor (b) Time step

Figure 55 – Selecting scaling factor and time step for real-time profile playback.

All measurement points from each instrument at each time step – can be extracted from the document database for analysis as discussed next.

4.3.3.4.3 Ramp test validation results

Measurements were extracted for the substation output voltage vs load, as produced by the BTSM and DT models over their full operating range, with the results plotted in Figure 56 below. The chart shows that as expected, due to the voltage regulation phenomena of the transformers caused by their impedances, substation output voltage reduces as load on the substation increases. The effect is apparent in both the function of output voltage simulated by the DT, and that measured within the BTSM; both models are consistent. This measurement was made with the substation configured in parallel mode, this being the most arduous case to accurately model due to possibility for circulating currents between the transformers; results for individual transformers are therefore omitted for brevity.

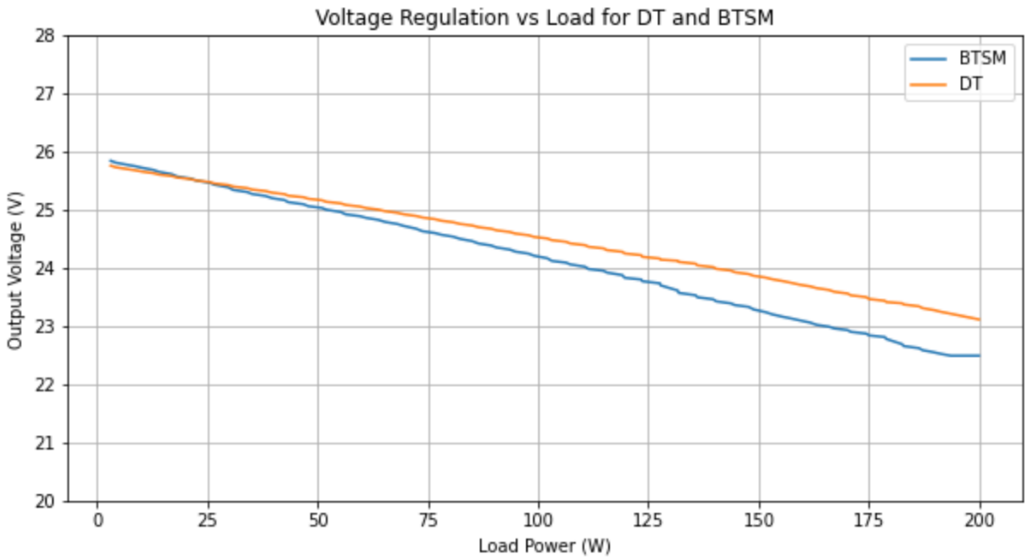

Figure 56 – Substation Voltage Regulation Over Full Range.

The effect of load voltage regulation appears slightly more pronounced in the BTSM than the DT, due to additional impedance introduced by the test leads and connections, in series with the transformers in the BSTM circuits.

The overall result shown in Figure 56 demonstrates that the BTSM was measured accurately, the DT model was parameterised correctly, and that the instruments performed well for the duration of each experiment over the full range of possible DSDR substation loading.

Measurement of substation efficiency versus load for both models at the full range of operational set points was also extracted from the document database after the automated validation experiments, and these results are shown in Figure *57* below.
At low substation loads, iron loss in the transformer's cores - which remains constant - is responsible for the majority of losses. Around this operating point, efficiency is lowest as most of the power drawn by the transformer is to supply its internal iron losses.

As substation load increases, copper loss in the windings - which increases with the square of load current - begins to dominate the total losses. Substation efficiency also begins to increase, as the proportion of power drawn by the transformer to supply its connected load dominates that drawn to supply the fixed iron loss and variable copper loss.
Efficiency begins to wane as the transformer approaches its rated load, as the copper losses become significant due to their I^2R term. Above rated load, efficiency would begin to drop rapidly, and the heat generated in the windings by copper losses would cause damage to their paper insulating layers.

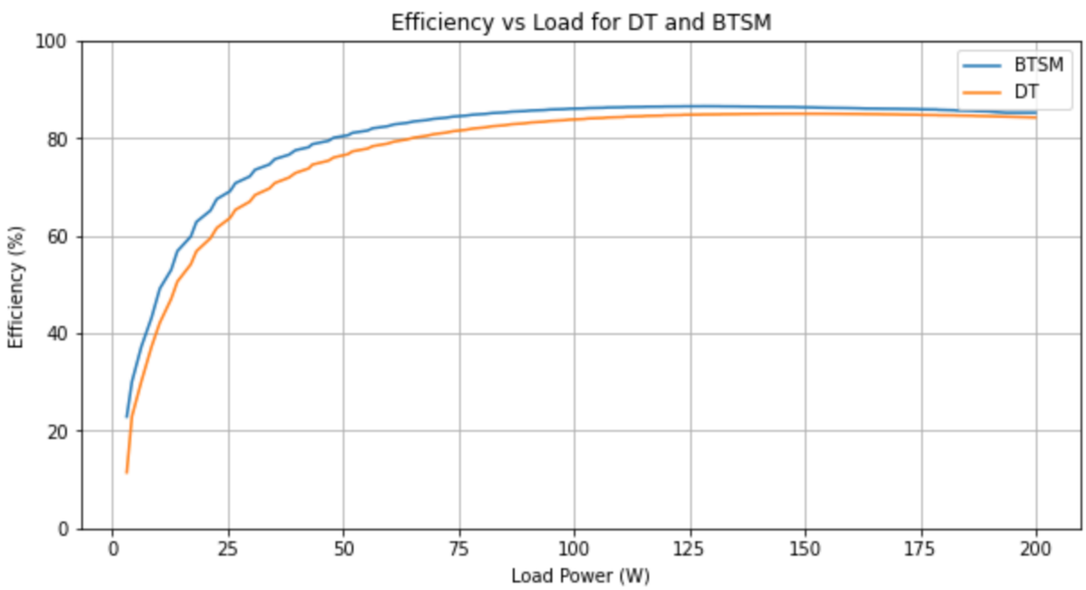

Figure 57 - Substation Efficiency Over Full Range.

The substation operating efficiency was shown to be well matched between DT and BTSM models, with negligible residual and no artefacts or anomalous values evident in the results. It can be concluded from the extended validation described in this section that the parameterisation of the DT model to the measurements of the BTSM, and the performance of both, are satisfactory for the development of optimisation algorithms targeting substation efficiency over the full range of rated substation loads.

4.3.3.4.3.1 Harmonics and Magnetic Flux

A further point to consider is the effect of harmonics on (and caused by) the magnetic flux in the transformer's core, the current in the windings, and losses. The transformer's magnetising current is non-linear due to the magnetic hysteresis of flux in the core, and this by definition causes some harmonic iron losses at the no-load condition. Additionally, if the load current drawn from the transformer contains harmonics, due to skin effect a higher proportion of current flows at the surface of the winding conductors than the centre.

This effect causes not only additional copper losses, but also increased heating of the winding conductors, which can in turn shorten the winding insulation service life. Bulk core losses are considered (but not separately from the other no-load losses) in the OpenDSS transformer model through the parameter '%Noloadloss', which includes the magnetising current losses attributable to flux hysteresis. Winding insulation thermal degradation, whether caused by harmonic loads and skin effect or otherwise, is not part of the OpenDSS transformer model, but could be considered in future through co-simulation with a thermal modelling tool. Transformer losses due to iron core losses with respect to flux are explored by simulation studies in [123] and [124].

4.3.4 Summary

This section described the process used to parameterise the DSDR Digital Twin (DT) model to match the Bench-Top Scale Model (BTSM), and then to validate both models individually and against each other. Parameterisation of the DSDR DT was undertaken by measuring the BTSM's transformers using the Open Circuit Test (OCT) and Short Circuit Test (SCT) methods, extracting the measurements into transformer equivalent circuit component values, then transforming these into the form required by the OpenDSS digital model of a distribution transformer.

Next, one of the measured BTSM transformers was set to operate at no-load and full-load whilst connected to a power analyser, so that the measurements of magnetising current, voltage regulation, and power losses could be validated against manual computations of the expected values.

The DT model was parameterised using the OpenDSS values determined from measurement of the BTSM transformers, then instantaneous power, voltage, and current measurements produced by the two models at no-load and full-load were cross-checked against each other. Finally, the substation power losses and voltage regulation for both models at the full range of loads were compared by using the DSDR DT software to playback a ramp load profile. It was demonstrated that the OCT / SCT measurements and resulting equivalent circuit parameters were consistent and reproducible, and that the BTSM and DT models were well matched with respect to each other. A small error was found to be present when digitally modelling the transformer's magnetising current at low loads, which is not expected to adversely affect the development of optimisation algorithms using the validated models.

4.4 Summary

Bench Top Scale Model (BTSM), extended from the Distribution System Dynamic Reconfiguration (DSDR) substation introduced earlier in this thesis. The BTSM complements the Digital Twin (DT) DSDR model by providing a platform on which substation optimisation algorithms developed within a software simulated environment can be evaluated on physical hardware in real-time, and proven ready for field pilot trials and business-as-usual deployments.

The blueprints for a BTSM were laid out using the foundations of the generic DSDR substation, describing it by wiring schematics, control and instrumentation block diagrams, and a bill of equipment. An implementation of the BTSM was physically constructed using off-the-shelf components and instruments, demonstrating the practicality of the design. Analysis of the BTSM's equivalent circuit model and measurement of its physical parameters followed, to create an instance of the DT model which was parameterised with equivalence to the constructed BTSM.

Extensive validation of the matching between the BTSM and DT using bench instrument measurements, manual calculations, and ramp load profile playback has demonstrated accurate equivalence of the substation power efficiency and voltage regulation results produced by the two models. The benefit is that DSDR algorithms may be rapidly developed in parallel and at accelerated load profile playback rates using the DT simulated environment, with confidence that they will perform equivalently when validated in real-world environments.

The BTSM will be used as a standard testbed for the development and benchmarking of DSDR optimisation algorithms in research contexts, with a clearly established route to use within DNO's distribution substations. This is the first demonstration of paired digital twin and benchtop-scale reconfigurable distribution substation models, and the approach has applications in not only the rapid development of energy efficiency algorithms, but also in topics including Conservation Voltage Reduction (CVR) [125], dynamic phase re-balancing [126], and non-traditional substation reinforcement strategies.

The following chapter will set out the experiments to be performed on the BTSM and DT models during the development and evaluation of each new optimisation algorithm, including the energy system scenarios and load profiles to be investigated.

5 Experiments on Distribution Substation Dynamic Reconfiguration

5.1 Introduction

The previous chapter introduced the bench top scale model to be used in experiments for evaluating new parallel transformer algorithms. This chapter describes those experiments performed using the previously introduced DSDR models for the development, evaluation, and validation of new Smart Grid (SG) algorithms. The focus is on the optimisation of substations reinforced with DSDR to unlock net-zero objectives, such as the mass connection of EVs.

To date, dynamic reconfiguration of distribution substations has been trialled only at primary substations which already contained parallel transformers [85]. The experiments described herein seek to investigate the DSDR reinforcement and optimisation of final distribution substations, where the majority of EV's will be connected, with newly proposed algorithms which offer numerous advantages to existing practice.

Section 5.2 outlines the scope and limitations of the experiments proposed in the proceeding sections, seeking to make best use of the DT and BTSM models presented chapter 4. Section 5.3 explains how Energy System Scenarios (ESS) will be leveraged to tailor the experiments to the expected change in electricity demand and load shapes towards the net-zero target year 2050. Sections 5.4 and 5.5 discuss the Low Carbon Technologies (LCT), load profiles, and reinforcement strategies which are available, and selects those to be used within the experiments.

Public sources of data for the above are introduced, whilst the objectives, measurement metrics, benchmarks and test cases of the proposed algorithms are described in sections 5.6 and 5.7, which also outlines the process to be followed for each experiment.

5.2 Scope and limitations

5.2.1 Introduction

This section discusses the factors affecting the scope of the DSDR experiments to be performed, and any limitations which will be applied to manage these.

5.2.2 Aggregation of single consumer load profiles

Demand profiles in a Low Voltage (LV) distribution network as seen from the Point of Common Coupling (PCC) of a final substation serving multiple customers represent an aggregation of the loads of each customer, as expected from the application of Kirchhoff's Current Law (KCL).

As each individual customer's daily load profile differs from all others dependant on customer activity, even between similar days, for example a weekday in spring, the substation's demand profile is predominantly stochastic. Modelling this phenomenon for the experiments described in this chapter would serve to smooth the load profiles, meaning that the algorithms could not be developed or evaluated on a worst-case scenario.

To avoid this, single load profiles – such as for one domestic property – will be scaled linearly according to each scenario, without introducing temporal or magnitude stochasticity when building composite load profiles. Similarly, customer or natural events that create extremely rare load profile fluctuations, such as the uptick when many customers boil their kettle simultaneously as a sporting event concludes will be excluded, as the efficiency algorithms under development are expected to have the greatest effect during normal daily loads rather than targeting low probability, high impact events.

5.2.3 Power quality

Loads on a real substation consist not only of real power but also reactive power, and in addition contain signals at harmonic multiples of the fundamental power frequency. As this work focuses on the load profiles of dwellings, which are unlikely to contain significant reactive or harmonic content, it is reasonable to exclude these power quality phenomena from the experimental load profiles. They may however be of interest in future derivative works, especially those that consider commercial and industrial customer loads.

5.2.4 Operation of parallel transformers

Traditional power systems engineering practice holds that transformers operated in parallel should be of similar rating and percentage impedance, so that loads are equally shared between them.

The transformers used in the BTSM described in chapter 4 follow this principle, likewise the parameters of the transformer which were used to construct the DT model described in chapter 3. However, the design of the BTSM and DT models do not enforce this constraint, enabling the trial of alternate modes of operation in future works.

5.2.5 Measurement uncertainty

When conducting experiments on the BTSM, measurement error in the obtained load flow readings can affect both repeatability between runs, and validation against DT results. These uncertainties can be divided into systematic and stochastic errors, which should be accounted for when planning experiments and analysing their results. Systematic errors are fixed offsets in the measurements recorded by physical instruments in the BTSM system, such as current transducers – these will not change between experiment runs, but may be apparent as variations between DT and BTSM results.

Stochastic errors are non-deterministic noise added to each measurement reading, caused for example by physical effects on the signal being measured within the instruments Analogue to Digital Converter (ADC), and will cause differences in identical measurements taken at differing times, such as when an identical experiment is repeated.

To faithfully represent real-world measurement uncertainties, the manufacturers' datasheet specifications for systematic and stochastic errors for each instrument are implemented in the DT model, but may also be disabled for each experiment. In order to maintain repeatability whilst developing and evaluating optimisation algorithms, the bulk of the experiments will be performed using the DT model, with instrument uncertainty disabled. A subset of results will then be validated using BTSM experiments, with allowances made for expected uncertainties.

5.2.6 Summary

To summarise the scope and limitations when planning DSDR experiments, uncertainties could be introduced both when aggregating load profiles and using physical instruments in the BTSM, but this will be minimised by using linear scaling of single customer load profiles, and by focusing initial algorithm evaluation on DT model experiments.

Power measurements will focus on real power at the fundamental frequency – a suitable approach for distribution networks of domestic customers – and the transformers in each experimental model will be a matched pair to mitigate unbalanced load sharing.

5.3 Scenarios

5.3.1 Introduction

As introduced in chapter 2, Energy System Scenarios (ESS) are long-term forecasts of energy generation and load trends for a range of societal, economic and policy states. ESS are published at global [127], national [50], and regional [51] levels, with increasing granularity but reducing generality respectively. It is therefore desirable when defining experiment inputs for the development and evaluation of novel DSDR algorithms to select an ESS with sufficient detail for the problem being modelled, but which is also applicable across a range of DSO regions where the technology could be deployed.

ESS are used in this work to extract two types of data essential for the development and evaluation of a DSDR reinforcement strategy. Firstly, ESS forecast the increase in overall electrical demand on an annual basis, which is used to understand when, and how much, reinforcement of distribution systems including substations will be required for continued reliable operation and ability to service that demand. Secondly, ESS contain predictions about the classes of load that will drive the increase in demand, and the shape of the load drawn by each class. Such load shape data is used to construct the composite load profiles used to develop, evaluate, and validate these DSDR algorithms.

This section will identify sources of ESS data appropriate for synthesising future scenarios, in which DSDR reinforcement can be applied to electricity distribution networks as an enabling technology towards the wider societal goal of Net Zero by 2050. There will be a focus on domestic base load, as this applies to the vast majority of Distribution System Operator (DSO) final substations, and Electric Vehicle (EV) charging loads, as these are likely to rapidly increase as the UK heads towards the 2030 ban on Internal Combustion Engine (ICE) vehicles. The following ESS are evaluated for suitability of informing DSDR algorithm development; World Energy Scenarios [127], Future Energy Scenarios [50], and Distribution Future Energy Scenarios [51], which are listed in Table 27. Consensus findings shared by all three ESS will be used to plan the experiments in this chapter.

Table 27 – Energy System Scenarios evaluated for experiment planning.

ESS	Publisher	Scale	Granularity
World Energy Scenarios [127]	World Energy Council	Global	Subcontinent
Future Energy Scenarios [50]	National Grid ESO	National (UK)	National
Distribution Future Energy Scenarios [51]	UK Power Networks	Regional (South-East England)	LSOA

5.3.2 Sources of Scenario Data

5.3.2.1 World Energy Scenarios

The World Energy Scenarios (WES) [127], compiled by the World Energy Council (WEC), sets out the three likely routes for the "transformation of the energy sector by 2040" [127], and forecasts the effects of each scenario on energy supply, demand, and CO2 emissions until 2060. WES findings are described at the global scale, with the results grouped into seventeen world regions.

WES is based on a multi-regional model which determines "least-cost configurations of the global energy system from resource extraction to energy end uses". The three scenarios presented are those resulting from a market-driven approach, a government-driven approach, and an approach prioritising national interests (also referred to as protectionism); the key drivers are a slowdown in population growth, Evs overtaking ICE vehicles, and an increasing share of wind and PV in the generation mix.

Across all scenarios WES forecasts that energy demand will grow by up to a third by 2060 – the majority of this by 2030 – and that the electricity share of that demand increases compared with all other energy vectors (e.g., oil and gas). It also found that "digitally smart grid control mechanisms" would be required to manage electricity network losses in the face of these changes, to enable "a mobility revolution building on electric drives" [127].

5.3.2.2 Future Energy Scenarios

National Grid's (NG) report Future Energy Scenarios (FES) [50] is an ESS covering the United Kingdom (UK) to year 2050, based on a whole energy system view model of consumer behaviour including domestic heating, household appliance, and road transport energy use. The four scenarios considered are summarised in Table 28 below, with the key drivers of each being electrification and hydrogen for heating and transport, and energy efficiency measures for buildings.

Table 28 – National Grid's Future Energy Scenario Names.

Scenario Name	**Key Changes towards Net Zero**
Consumer Transformation	Change in how energy is used
System Transformation	Change in how energy is generated and supplied
Leading the Way	Technology and investment
Steady Progression	Slow decarbonisation to 73% of 1990 levels

Consumer Transformation achieves Net Zero (NZ) primarily by changes in consumer behaviour and flexibility, for example by consuming less energy overall, or by doing so at times when ample renewable energy is available. System Transformation also achieves NZ, but by focusing change on the energy supply side, for example by replacing natural gas with hydrogen as a fuel source. Leading the Way blends these two approaches by investing in high consumer engagement and world-leading technology to achieve NZ. Finally, Steady Progression minimises investment and interventions to that required to reduce CO2 emissions gradually towards a finite limit but does not achieve NZ by 2050.

FES found that across all NZ scenarios distributed generation is set to proliferate widely – with "ten times more solar PV on rooftops by 2050", demand from electrical appliances decreases, and one quarter of EV's will provide grid flexibility services. With respect to baseline residential heat and appliance demand, although the scenario findings diverge widely when all energy vectors are considered, there is consensus that electrical demand increases steadily and modestly, by between 20% and 50% over a thirty-year period as shown in Figure 58.

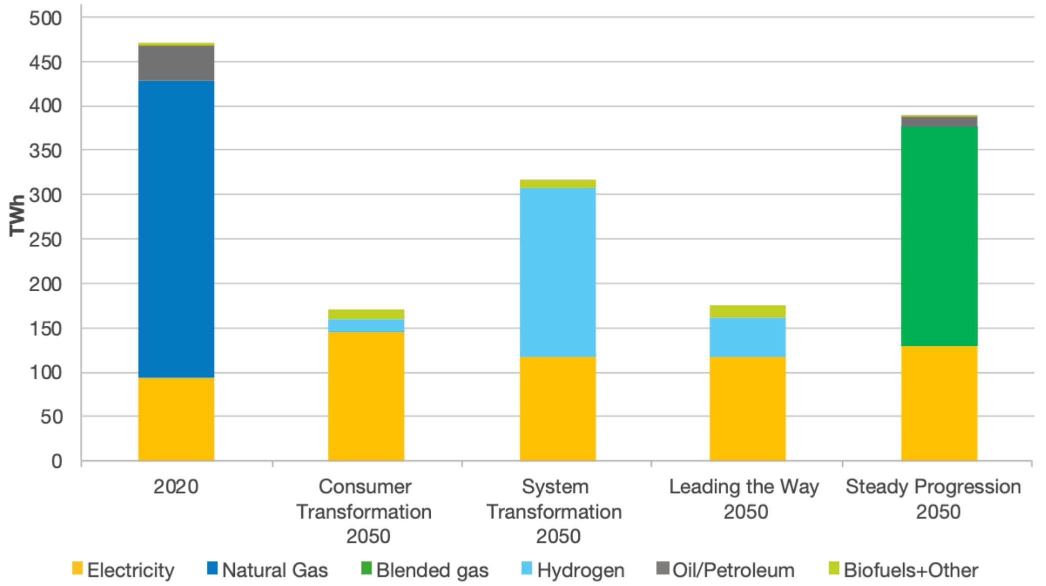

Figure 58 – FES annual residential energy demand for heat and appliances [50].

The forecasts for road transport energy demand are quite different to that of heating and appliance loads; firstly, as shown in Figure 59 below, across all scenarios around 30 million Evs will be in use on the UK's roads, the majority of them appearing in the decade between 2025 and 2035 for all NZ compliant scenarios.

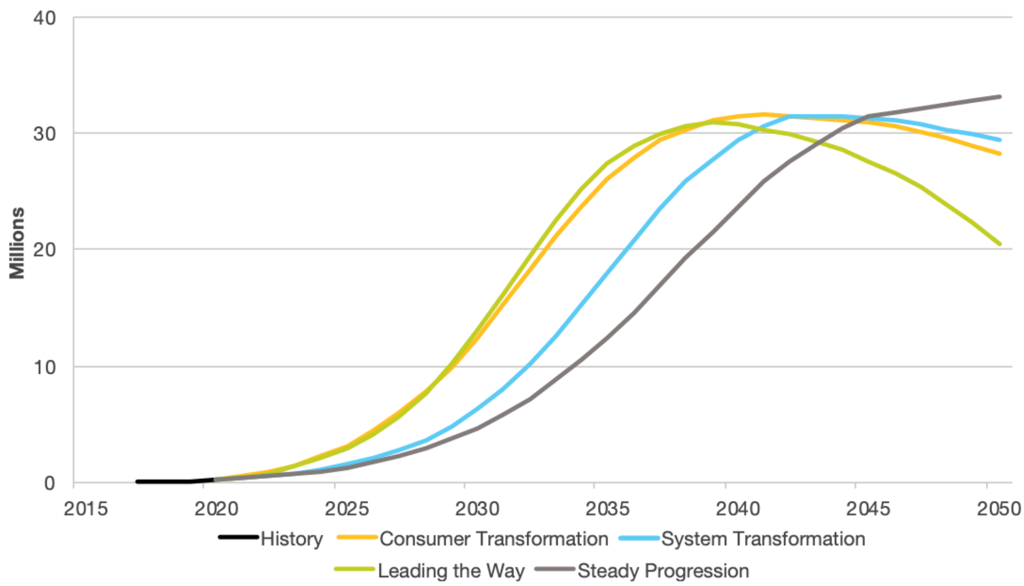

Figure 59 – FES number of Evs on the road [50].

The second major differentiator in the forecasts of road transport load is that all four scenarios agree that this will add around 100 TWh of annual electrical load to the UK energy system, as shown in Figure 60.

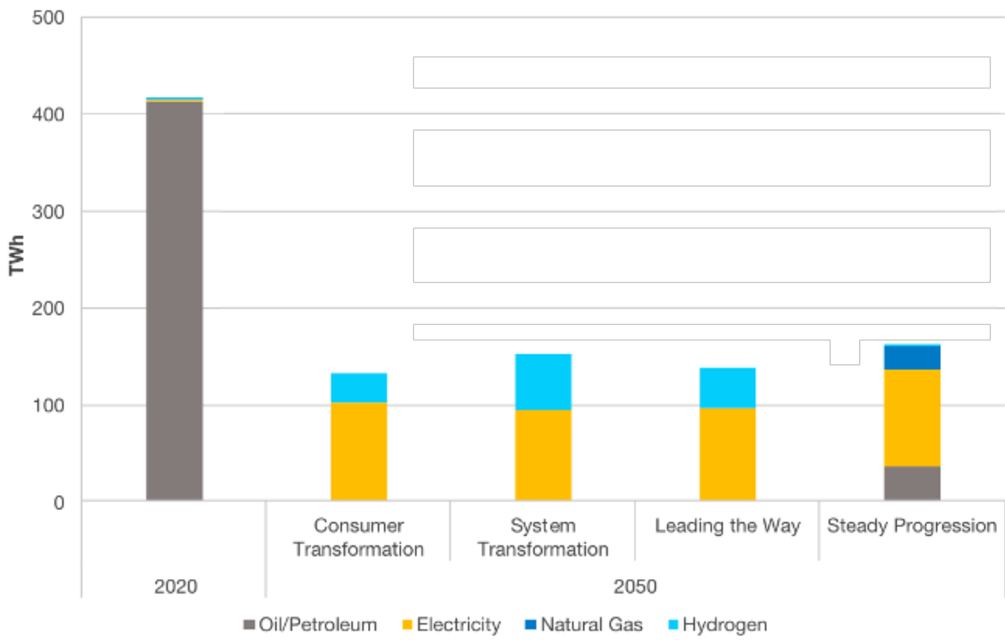

Figure 60 – FES road transport annual energy demand [50].

To summarise, Evs will create approximately 100% additional load on top of the existing heating and appliance base load, the majority of it within a single decade, whilst heating and appliance base load itself will increase by a maximum of 50% over three decades.

5.3.2.3 Distribution Future Energy Scenarios

Distribution Future Energy Scenarios (DFES) [51] by UK Power Networks (UKPN) has the most detailed spatial granularity of the three ESS, covering London and the South East UK down to the Lower Super Output Area (LSOA) level to the year 2050. Its model tracks building stock growth, appliance energy efficiency, air conditioning behaviour, low-carbon transport, and decarbonised heating, all applied over the same set of scenarios as FES. They key drivers include distributed generation, local battery energy storage, and flexibility services.

DFES's major relevant findings were that for transport, uptake of Evs will be a dominant factor in demand increase, driven by reducing EV battery costs; for heating, gas boilers will be replaced by either heat pumps or hydrogen boilers (but which technology will dominate is still an unknown); and that uptake of rooftop solar will be exceptionally high.

5.3.3 Summary

The ESS review shows that baseline heating and appliance electrical demand will increase by 20% - 50% over 30 years. By planning long-term reinforcement strategies, DNO's are experienced at dealing with this type of steady load growth. However, the ESS also shows that the electrification of transport – ~30 million new Evs on the UK's roads by 2040 – will add another 100% to the existing heating and appliance base load over a short period.

Coupled with the stochastic nature of where and when those EV's will charge, how much they will be offset by distributed generation, and how they will participate in flexibility (which may in any case support the national grid rather than local distribution), the preparation of distribution substations to enable rapid EV proliferation is a challenge that existing DNO reinforcement methods are not well suited to. It is clear that Evs are the near-term dominant factor in a significant and rapid load increase, and therefore these DSDR experiments are planned to evaluate the newly developed algorithms before and after EV loads, both with and without the requisite substation reinforcements.

5.4 Load profiles

5.4.1 Introduction

This section builds on the scenarios driving the need for substation reinforcement identified in section 5.3, to identify sources for the individual Load Profiles (LPs) of the demand behind the scenarios. Whilst the timescale of ESS are in years or decades, electricity distribution load profiles are on a timescale of hours and days. More formally, a load profile is a set of evenly spaced temporal load magnitude values drawn by an electricity customer, for a particular demand type, during a specific season, over a fixed period.

The UK industry standard for load profiles uses half-hourly measurements over the course of one whole day, yielding 48 load values in kW [128]; these are produced either from averaged measured real-world data, or generated from a bottom-up demand model of a typical electricity customer or technology type. LP's suitable for developing and evaluating DSDR algorithms for domestic base load and electric vehicle load, according to the scenarios described in section 5.3 will be identified, standardised, and combined in this section.

5.4.2 Domestic

LPs for base load are measured, prepared, and released by Elexon as 'Electricity User Load Profiles' [128]. These are half-hourly one-day profiles grouped by customer type, tariff mode, season, and day-of-week. The customer types (referred to as 'Profile Descriptions' in the Elexon dataset [128]) available are shown in Table 29.

Table 29 – Profile descriptions for Elexon 'Electricity User Load Profiles' data [128].

Profile No.	**Profile Description**
1	Domestic Unrestricted (single rate)
2	Domestic Economy 7 (two rate)
3	Non-Domestic Unrestricted (single rate)
4	Non-Domestic Non-Maximum Demand Economy 7 type (two rate)
5	Non-Domestic Maximum Demand Customers with Load Factor 0-20%
6	Non-Domestic Maximum Demand Customers with Load Factor 20-30%
7	Non-Domestic Maximum Demand Customers with Load Factor 30-40%
8	Non-Domestic Maximum Demand Customers with Load Factor >40%

5.4.2.1 Customer Types

Domestic customer types are subdivided in to single and dual rate tariffs, with Economy 7 (profile 2, dual rate) typical for flats without a natural gas connection, using night storage heaters for comfort heating and dual immersion heaters for domestic hot water production. The remaining population of domestic customers (i.e., flats *with* natural gas connections, terraced, semi-detached, and detached houses), are represented by the single rate domestic profile 2. Profiles 3 and 4 – non-domestic but without a specified load factor – refer to small commercial customers with and without Economy 7 tariffs respectively, such as high street shops.

All of the profile descriptions discussed hitherto are likely to be connected at Low Voltage (LV) to the nearest final distribution substation, with domestic single rate (profile 1) representing the vast majority of customers. The remaining profiles – numbered 5 through 8 – are described as 'Maximum Demand Customers'; these are light industrial customers such as warehouses or wholesale stores with an agreed maximum demand up to 100 kW.

They are likely to be connected to the distribution system via a dedicated supply transformer, often shared between a few customers such as on an industrial estate. As this work intends to target DSDR algorithm development towards the largest subset of final distribution substations – which is those supplying domestic customers at the single rate – base load will be established based on profile number 1 – Domestic Unrestricted.

5.4.2.2 Day Types

The daily load profiles are also grouped by 'Day Type' into weekdays, Saturday, and Sundays, as shown in Table 30; each has an associated two or three letter code, used as abbreviations within the dataset [128].

Table 30 – Day types for Elexon 'Electricity User Load Profiles' data [128].

Day Type	Day Type Code
Weekdays	WD
Saturdays	SAT
Sundays	SUN

5.4.2.3 Seasons

The final data split of the Elexon LPs is by season; these are three of the four traditional seasons of spring, autumn, and winter, with the summer season subdivided into summer and high summer. The definitions and durations of these seasons are given in Table 31, along with their abbreviations.

5.4.2.4 Summary

The Elexon single-tariff domestic load profiles [128], representative of the domestic heating and appliance load connected to the majority of final distribution substations, will be used to develop and evaluate new DSDR algorithms with respect to base load. Algorithm performance for each of the three day-types and each of the five season-types from Table 30 and Table 31 respectively yields fifteen permutations of base load daily load profile.

Table 31 – Season types for Elexon 'Electricity User Load Profiles' data [128].

Code	Season	Start	End	Weeks
WTR	Winter	Day of clock change from BST to GMT in October	Day preceding clock change from GMT to BST in March;	21
SPR	Spring	Day of clock change from GMT to BST in March	Friday preceding the start of the summer period	7
SMR	Summer	Sixteenth Saturday before the August bank Holiday	After ten weeks	10
HSR	High Summer	Sixth Saturday before August Bank Holiday	Sunday following August Bank Holiday	6
AUT	Autumn	Monday following the August Bank Holiday	Day preceding the clock change from BST to GMT in October	8

5.4.3 Electric Vehicles (EV)

LPs for EV charging have been made available by Electricity North West Limited (ENWL), generated by stochastic modelling of recorded real-world EV charging session start times and demanded energy per session [129]. They are in the form of one hundred daily profiles, with a five-minute sampling period, each representing an individual Electric Vehicle Charging Point (EVCP) instantaneous demand in kW. A representative sample of five of these EVCP profiles is shown in Figure 61.

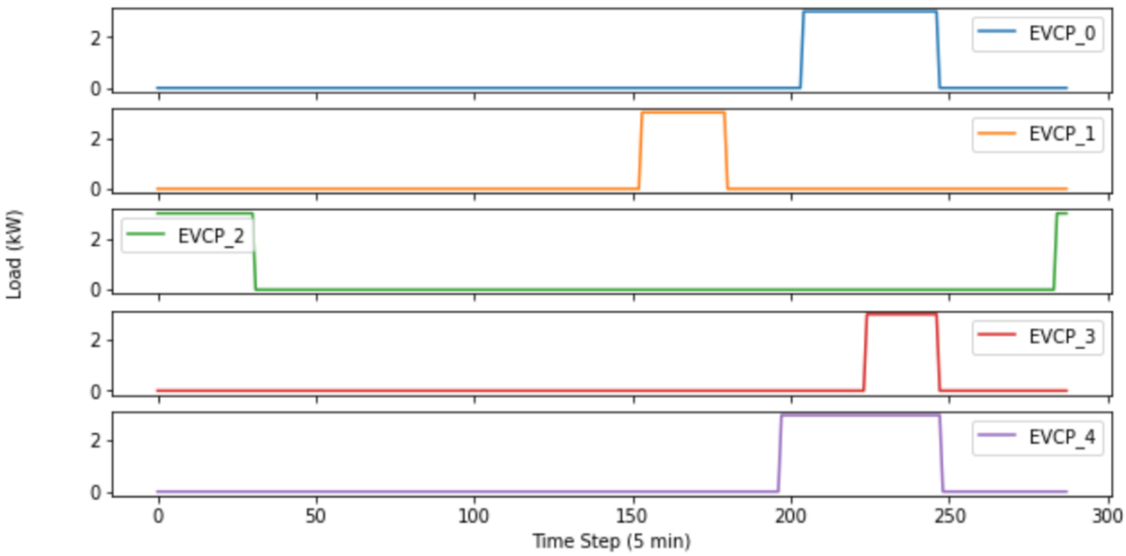

Figure 61 – ENWL EV load profile data sample of first five charging points [1].

Each EVCP typically has one charging session per day, but that charging session start time, and the quantity of energy required based on battery state of charge, are stochastic. As the DSDR experiments require aggregated load profiles as seen at the substation level, pre-processing of the EV LPs is necessary to create an average daily EV profile at half hourly sampling period that can be combined with the domestic base load identified in section 5.4.2; this process will be discussed next.

5.4.4 Load Profile Data Pre-Processing for Use in DSDR Experiments

The DSDR real-time software designed in chapter 3 reproduces LPs into each experiment from a document database, where they are stored as sets of timestamp and load magnitude pairs in collections grouped by demand such as base load or EV load, and type such as Autumn Weekday, seen in Figure 62 below.

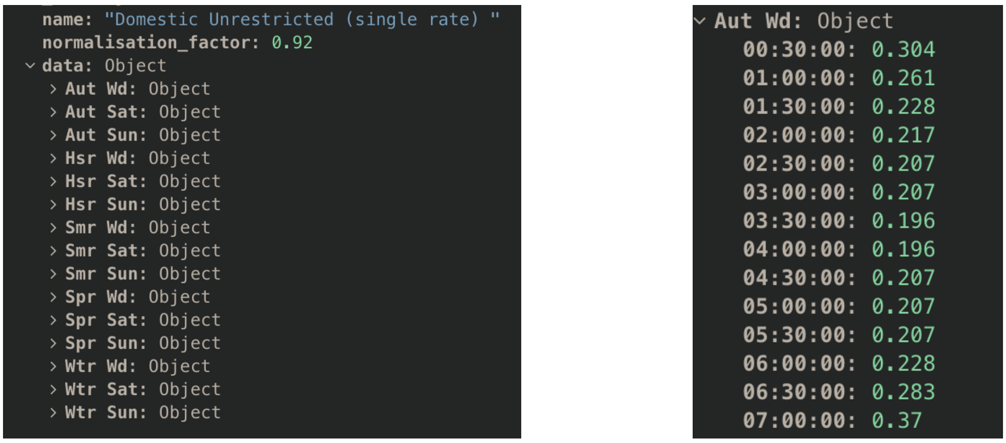

(a) (b)

Figure 62 – DSDR software database format for load profiles a) demand type group and b) daily profile.

Each collection of profiles is linearly normalised such that the peak load magnitude across all profiles in the demand type group has a value of 1.0; the scalar by which all profiles in the collection were divided to achieve this (i.e., the original peak value across all profiles in the group) is stored along with the collection as the normalisation factor. Aside from these requirements, the length and sampling period of each profile is entirely flexible.

This subsection describes the process of transforming the Elexon domestic [128] and ENWL EV [129] load profiles from the format in which they are released, into a common format such that they may be combined and loaded in to the DSDR document database to perform the experiments.

5.4.4.1 Domestic Base Load Profiles

The Elexon LPs [128] are provided as a spreadsheet, with one worksheet per demand type, one column per compound season-day type, forty-eight rows of half-hourly timestamps, and instantaneous demand values in kW, as shown in Figure 63.

	A	B	C	D	E	F	
1	Time	Aut Wd	Aut Sat	Aut Sun	Hsr Wd	Hsr Sat	Hsr !
2	00:30	0.28	0.31	0.35	0.29	0.31	
3	01:00	0.24	0.27	0.3	0.25	0.27	
4	01:30	0.21	0.24	0.24	0.22	0.23	
5	02:00	0.2	0.22	0.22	0.21	0.22	
6	02:30	0.19	0.2	0.21	0.2	0.21	
7	03:00	0.19	0.19	0.2	0.19	0.2	
8	03:30	0.18	0.19	0.19	0.19	0.19	
9	04:00	0.18	0.19	0.19	0.19	0.2	
10	04:30	0.19	0.19	0.19	0.19	0.19	
11	05:00	0.19	0.19	0.18	0.19	0.2	
12	05:30	0.19	0.19	0.19	0.2	0.2	
13	06:00	0.21	0.2	0.2	0.21	0.2	
14	06:30	0.26	0.23	0.2	0.24	0.22	
15	07:00	0.34	0.27	0.22	0.3	0.26	
16	07:30	0.43	0.33	0.27	0.37	0.33	
17	08:00	0.5	0.4	0.32	0.39	0.35	

Figure 63 – Domestic base load profile raw data format [128].

To extract the domestic single tariff load profile from its associated worksheet, the normalisation factor is determined as the cell with the greatest kW load value, and all cells in the sheet are divided by that normalisation factor. This yields the normalised set of fifteen load profiles separated by season-day type as shown in Figure 64; the data is then loaded into the DSDR document database and stored separately for later combining with EVCP LPs.

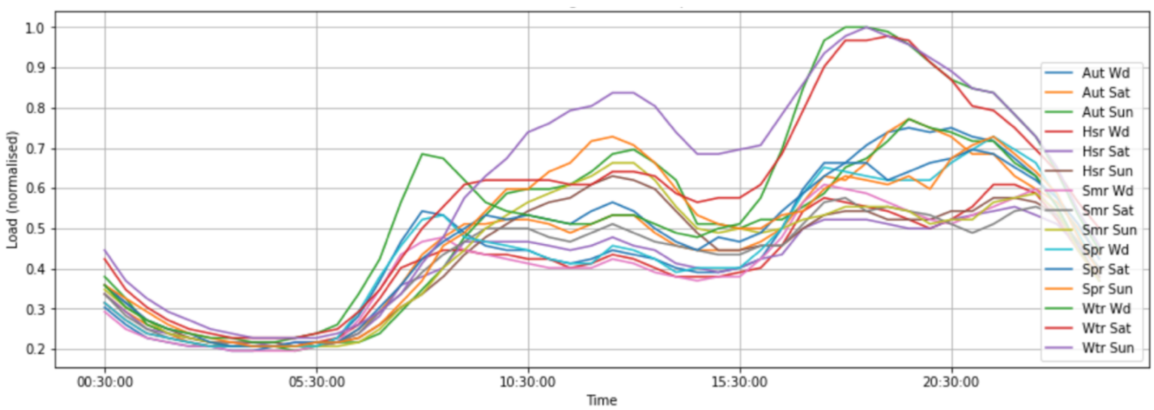

Figure 64 – Normalised domestic single rate load profiles for all day and season types [128].

The profiles demonstrate the evening pickup in load when dinners are being cooked, and the low background load overnight when most appliances are in standby mode – legend abbreviations are taken from Table 30 and Table 31.

5.4.4.2 Electric Vehicle Charge Point Load Profiles

The ENWL EV [129] load profiles are provided as a matrix of one hundred columns representing distinct EVCP, two hundred and eighty eight rows representing time steps in five minute intervals, and a kW load value in each matrix element; a sample of which is seen in Figure 65.

	0	**1**	**2**	**3**	**4**	**5**	**6**	**7**	**8**	**9**	**...**	**90**	**91**	**92**	**93**	**94**	**95**	**96**	**97**	**98**	**99**
0	0	0	3	0	0	3	3	0	3	3	...	0	3	0	0	3	3	3	3	3	0
1	0	0	3	0	0	3	3	0	3	3	...	0	3	0	0	3	3	3	3	3	0
2	0	0	3	0	0	3	3	0	3	3	...	0	3	0	0	3	3	3	3	3	0
3	0	0	3	0	0	3	3	0	3	3	...	0	0	0	0	3	3	3	3	3	0
4	0	0	3	0	0	3	3	0	3	3	...	0	0	0	0	3	3	3	3	3	0
...	...	...	...	...	...	...	...	...	...	...	...	...	...	...	...	...	...	...	...	...	...
283	0	0	0	0	0	3	3	0	3	3	...	0	3	0	0	3	3	3	3	3	0
284	0	0	3	0	0	3	3	0	3	3	...	0	3	0	0	3	3	3	3	3	0
285	0	0	3	0	0	3	3	0	3	3	...	0	3	0	0	3	3	3	3	3	0
286	0	0	3	0	0	3	3	0	3	3	...	0	3	0	0	3	3	3	3	3	0
287	0	0	3	0	0	3	3	0	3	3	...	0	3	0	0	3	3	3	3	3	0

Figure 65 – EV load profile raw data format [129].

The EVCP monitored in the field trials from which this data was collected were rated at 3 kW, which is the value of the nonzero matrix elements. Further processing of these individual EVCP profiles into a normalised, aggregated EV load profile will remove any bias introduced by this homogenous set of EVCP ratings, as demonstrated below. First, the matrix is summed row-wise, producing a column vector of aggregated EV After Diversity Demand (ADD) from the columns representing individual EVCP loads.

The rows are resampled from five-minutely to half-hourly, timestamps labels are added, the maximum value is noted, and the load is normalised by dividing all values by the maximum, yielding the LP shown in Figure 66 below.

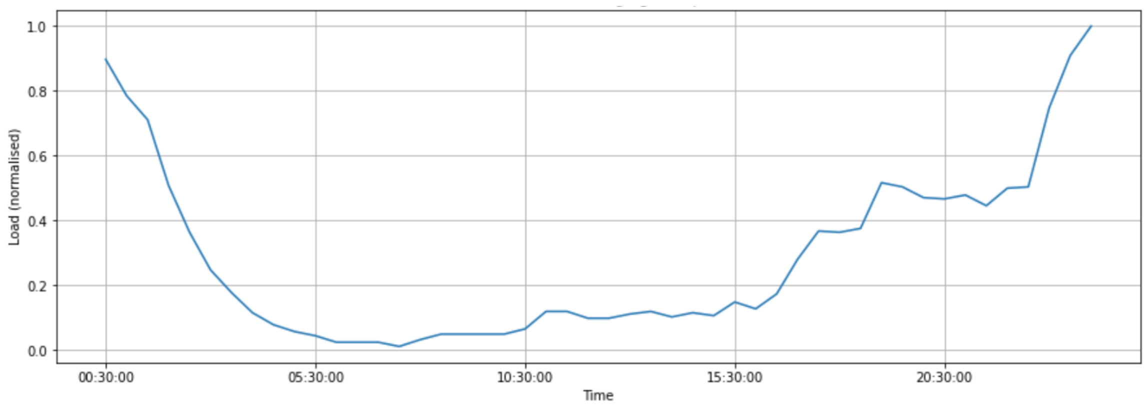

Figure 66 – Normalised electric vehicle charging load profile.

As expected, the aggregated EV LP sees demand pickup occur in the evening, when drivers return home and place their vehicles on charge. As for the domestic LPs, the data is loaded into the DSDR document database, and also stored so it can be combined with base load for each experiment.

5.4.5 Summary

This section identified load profile data sources for domestic base and electric vehicle charging demand, which can be later combined and scaled according to the ESS demand growth forecasts identified in section 5.3. The available data was pre-processed for this, then loaded into the document database of the DSDR software developed in chapter 3. The following section will introduce the topic of substation reinforcement methods, and identify those most suitable for use with DSDR optimisation algorithms.

5.5 Reinforcement methods

5.5.1 Introduction

Electricity distribution system reinforcement refers to a capital investment which upgrades the capacity of equipment in a distribution network. This section identifies existing reinforcement methods and alternatives, identifies where DSDR reinforcement sits amongst those, and of the four variations of DSDR reinforcement selects the most suitable for the DSDR optimisation algorithms experiments planned in this chapter. Traditional reinforcement is currently achieved by replacing existing cables or transformers with equipment of a higher rating [130], and is made necessary either because actual demand has increased to the limits of existing equipment ratings, or is likely to in the near future.

A DSDR substation reinforcement strategy provides a new method of reinforcing substations; rather than remove (i.e., scrap or recycle) an existing transformer when reinforcement becomes necessary, a DSDR reinforcement would install an additional transformer in parallel with the existing, whilst providing both with on-load switching control equipment.

Challenges when rapidly deploying traditional reinforcement in anticipation of mass EV adoption include bottlenecks in skilled labour and equipment supply chains, cost justification of significant capital expenditure, and risk of targeting the wrong substations with reinforcement with respect to where the additional EV load materialises. Although reinforcement decisions are backed by surveys and forecasting, EV uptake can take place much more quickly than these anticipate, particularly in response to government incentives which are often announced without much notice.

5.5.1.1 Pre-Reinforcement

Furthermore, as EV's are mobile loads by nature, reinforcement needs can move between areas somewhat unexpectedly, therefore pre-reinforcement without full commitment to permanent reinforcement is worthwhile investigating. Whilst pre-emptive reinforcement as proposed in this thesis does require commitment of labour and switchgear before a load materialises, transformers can be moved between substations as load solidifies, in the case that planning forecasts were inaccurate. That being said, pre-reinforcement activities should nonetheless be supported by uncertainty and forecasting studies of EV uptake and charging behaviour patterns, to try to ensure a targeted investment in new distribution assets.

5.5.1.2 Alternative methods to pre-reinforcement

Alternative methods which aim to defer traditional reinforcement comprise flexibility services provided by customers, and active network management by DNOs. Examples of the former include Demand Side Response (DSR) [131] which asks consumers to reduce demand during periods when equipment is overloaded, and Vehicle to Grid (V2G) [132] which returns energy from EVs to the LV distribution system during the same periods.

Techniques forming the latter include Soft Open Points (SOP) [68] to route power flow away from heavily load equipment, and grid connected Battery Energy Storage Systems (BESS) [13] to smooth load curves drawn through equipment. The challenges in deploying flexibility include implementing real-time signalling and incentives across a large pool of customers, and the challenges with active network management include designing, installing, and maintaining the necessary power electronics systems as well as regulatory framework limitations around DNO's owning energy storage assets.

DSDR aims to ameliorate the above challenges by unlocking flexible pre-emptive reinforcement, whilst avoiding the use of power electronics solutions, ultimately delivering optimisation at a local agent level for each substation. Below, the DSDR reinforcement variations are discussed, and the most suitable approach for this work is identified for the experiments.

5.5.2 Matched transformer

In the matched transformer approach to DSDR reinforcement, a second transformer of equal rating is connected in parallel with the existing single substation transformer, and both are provided with on-load controlled switching. As both transformers are of identical rating and design, impedance mismatch between the transformers will be minimal and therefore the load sharing between them should be close to equal when the substation is operating in parallel mode.

5.5.3 Low loss transformer

In the low loss transformer variation, a second transformer of equal rating, but of low loss design is connected in parallel with the existing transformer, and both are capable of being switched. Low loss transformers comprise high-performance core materials and oversized winding conductors, meaning that there would likely be an impedance mismatch between the transformers, leading to the low loss transformer likely carrying a higher proportion of the load when operating in parallel with the substation's original transformer.

5.5.4 Big-little architecture

In the big-little architecture, an existing transformer is supplemented by an additional transformer of higher rating, connected in parallel, with both transformers switchable.

Whilst this approach may be suitable for reinforcing substations where the load is expected to be more than double the substation's initial rating, similar to the above variation it would be challenging to ensure ideal load sharing between the transformers in the ratio of their respective ratings.

5.5.5 Unswitched transformer

In the final variation, the existing transformer is left uncontrolled (i.e., permanently on-load), whilst an additional transformer with switch control and of equal rating is connected in parallel. Whilst this variation minimises the requirement to disturb switchgear arrangements to the existing transformer, it reduces the scope of optimisation algorithms which then only switch one transformer instead of both.

5.5.6 Summary

This section considered the definition of traditional reinforcement on electricity distribution networks, the alternatives to traditional reinforcement including DNO-side active network management, customer-side flexibility, and the newly introduced technique of DSDR reinforcement. Four variations of DSDR reinforcement were identified.

For best load-sharing between parallel transformers and maximum flexibility afforded to optimisation algorithms, it was concluded that the DSDR experiments in this work will adopt the matched transformer DSDR technique, whereby an existing final distribution substation with a single transformer is reinforced with an equal rated additional transformer operating in parallel, with both transformers switchable in service by a DSDR algorithm.

5.6 Selected Optimisation objectives

In chapter 2, four potential optimisation objectives of DSDR substations were identified, with various beneficiaries including the DNO operating the substation, the customers supplied by the substation, and the transmission system operator from whom the substation is ultimately supplied. An objective function which minimises total substation losses, when scaled to many substations, has the potential to reduce customer bills as well as defer the construction of new power plants which would otherwise be required as losses increase with the EV rollout.

It can be readily modelled by both the DT and BTSM, and the value proposition for deploying in real-world scenarios is quantifiable as the cost of wholesale energy consumed by losses is well defined. Managing harmonics using DSDR would be most applicable to substations already with a relatively high supply impedance, i.e., in a rural location, therefore would have a positive impact but only on a subset of all final distribution substations.

Whilst the DT simulation engine could readily model harmonics, implementing controllable harmonically polluted loads in the BTSM would require a special type of electronic load which is prohibitively expensive [133].

Similarly, phase imbalance optimisation through DSDR would have the greatest impact only on urban substations, as rural distribution networks have ready access to overhead lines where the phases can be rebalanced. In addition, constructing a BTSM for three phase operation in order to validate the developed algorithms would require an upgrade to three-phase bench instruments, adding significant cost.

Finally, DSDR algorithms aiming to provide frequency support to the transmission system, whilst applicable to all final substations, would have a positive impact only on occasions when a deleterious event occurs on the transmission system, making their value proposition difficult to quantify. It follows therefore that the initial, and most impactful, set of algorithms to be developed for DSDR substations should be targeted towards managing substation losses.

5.7 Experimental Procedure

5.7.1 Introduction

This section describes the metrics and test cases used to evaluate the developed algorithm performance, the two algorithms which will be evaluated, and the process by which this will be achieved.

5.7.2 Measurement Metrics and Benchmarks

Since the objective function for DSDR development in this work – minimising technical losses – is now selected, in order to evaluate the developed algorithms, it is beneficial to define the metrics which will measure how effectively each algorithm performs during experiments. Transformer technical losses are typically measured in terms of real power (kW, MW etc.) and energy (kWh, MWh etc.), however for DSDR algorithm evaluation, using these as metrics would make it difficult to compare results between substations with transformers of different ratings. An alternative approach is to measure algorithm performance based on the total efficiency of the DSDR substation. Instantaneous substation efficiency, which is recorded for every time step in the experiments, is given in Eq. 2.

$$\eta_{substation} = \frac{P_{out}}{P_{in}} \qquad \textit{Eq. 21}$$

Where:

- $\eta_{substation}$ is total substation efficiency in %
- P_{out} is total real power at substation secondary in Watts
- P_{in} is total real power at substation primary in Watts

To aggregate substation efficiency over all the time steps of the load profile played back during an experiment, it is reasonable to take the mean of the instantaneous substation efficiency measurements as given in Eq. 22.

$$\eta_{avg} = \frac{1}{N_{steps}} \sum_{n=1}^{N_{steps}} \eta_{substation} \qquad \textit{Eq. 22}$$

Where:

- η_{avg} is mean substation efficiency in %
- N_{steps} is the integer number of time steps in the experiment
- $\eta_{substation}$ is total substation efficiency in %

Results of each experiment, regardless of model used (DT or BTSM) or algorithm selected, is quantified in terms of mean efficiency difference versus the identical experiment with no algorithm (i.e., both transformers in service for each time step). Using this method, algorithm results from the DT and BTSM experiments can be readily compared with future real-world pilot trial results, and also scaled up to estimate impact for entire DNO regions, or national energy systems.

5.7.3 Test cases

Next, the test cases which will model the combination of independent variables for each experiment are considered. Experiments are carried out against these test cases to illustrate the implications on substation losses of traditional versus DSDR reinforcement strategies. The independent variables are as follows.

5.7.3.1 Energy System Scenarios

Three scenario years are considered, which divide conveniently into 15-year intervals from the base year 2020 from FES [50], the year 2035 by when the 2030 ICE ban will have taken effect leading to a near peak in Evs on the UK roads as seen in Figure 59, and the year 2050 by which Net Zero emissions is targeted for the UK [134]. From section 5.4, the growth in the two load types most heavily impacting the majority of final distribution transformers is considered, those being domestic base load and EV charging load. Table 32 shows the load growth in both of these categories for years 2020, 2035, and 2050 according to the consensus of the majority of ESS cases.

Table 32 – Electricity system scenario cases for 2020, 2035, and 2050 with respect to final distribution substations.

Description	**Scenario Year**	**Base Load**	**EV Load**	**Abbreviation**
Base Year	2020	66.7% original substation rating	Negligible	BY
ICE Ban Effect	2035	83.35% original substation rating	100% original substation rating	IB
Net Zero	2050	100% original substation rating	100% original substation rating	NZ

It is assumed that existing substations are sized to cope with the steady growth in base load without any reinforcement out to Net Zero year 2050; therefore using the 50% base load growth between 2020 and 2050 from FES [50], base load at 2050 is set at 100% substation rating, and 2020 at 66.7% substation rating. Base load for year 2035 is linearly interpolated between that for year 2020 and 2050 as 83.35% substation rating; in all cases this being with reference to the rating of the single MV/LV transformer in a non-reinforced substation.

From Figure 59 and Figure 60, EV load was negligible in year 2020, but for the two highest uptake scenarios in FES [50] is forecast to have almost peaked by 2035, by which time it's magnitude will be equal to that of the base load in 2020, where it also remains at 2050.

It is therefore clear from the ESS evaluated in section 5.3 that total load on a typical UK final distribution substation may well reach 183.35% of its original rating by 2035, and 200% by 2050, necessitating urgent attention to reinforcement and / or flexibility amelioration methods in the next few years.

5.7.3.2 Reinforcement Strategies

The reinforcement cases considered will be that of no-reinforcement, i.e., if no action is taken by the DNO; and DSDR reinforcement, with switchable parallel transformers. These are listed in Table 33 below.

Table 33 – Reinforcement strategy cases.

Case	**Description**	**Abbreviation**
Base Case	Original substation with single transformer	BC
DSDR Reinforcement	Parallel transformers with switching control	DR

A third possible reinforcement case of traditional reinforcement with replacement of the existing transformer with one of a higher rating is effectively accounted for in the no-algorithm case described in the following subsection.

5.7.3.3 Algorithms

The optimisation algorithm cases to best tested on each DSDR experiment are given in Table 34, with full technical details of each discussed fully in chapter 6.

Table 34 – Algorithm cases.

Algorithm	Description	Abbreviation
No Algorithm	Both transformers remain switched in for all load steps	NA
Threshold Algorithm	Random transformer switched out at low load	TA
Model Based Algorithm	Transformers switched to most efficient topology according to OpenDSS simulation of each permutation	MB

The first test case is with no algorithm, whereby both transformers remain in service throughout load profile playback; this case requires no inputs, and is expected to produce similar results to the case where the DNO upgrades the capacity of a substation but does not implement DSDR switching. The threshold algorithm case requires an input of real-time load on the substation, and switches one randomly selected transformer off when that load is below a pre-set threshold. Finally, the model-based algorithm case also requires the real-time load as input, but could also accept additional parameters in future iterations such as harmonic content of load; it runs OpenDSS simulations for all switching permutations of the DSDR substation, to determine that with the lowest losses.

5.7.3.4 Models

The two models on which experiments will be performed are shown in Table 35.

Table 35 – Model cases.

Model	Description	Abbreviation
Digital Twin	Software-based representation of DSDR substation	DT
Bench Top Scale Model	Scaled down physical model of DSDR substation	BTSM

These are the DT model, as described in chapter 3, on which each permutation of experiment will be performed, and the BTSM described in chapter 4, on which a subset of the experiments will have their algorithm performance verified.

5.8 Summary

This chapter extended the work described in chapters 3 and 4 where the DT and BTSM were introduced, to explain how they are utilised to demonstrate the real-world value of DSDR to final distribution substations in unlocking the electrification of transport. The sale of ICE vehicles will stop in 2030, and it was found that this will double the load on existing LV substations within a few years, necessitating widescale reinforcement. DSDR enables the smooth rollout of reinforcement, managing losses and reducing scrapping of existing transformers in the face of uncertainty in EV demand at the postcode level, ultimately assisting towards the UK reaching net zero carbon emissions by 2050.

The following chapter introduces implementations of the existing threshold algorithm, and of the novel model-based algorithm, to be used in combination with the experiments described in this chapter.

6 Algorithms

The previous chapter outlined the experiments to be performed on the DT and BTSM for a range of scenarios, in order to evaluate the existing threshold algorithm against the novel proposed model-based algorithm. This chapter describes the implementation of both of these algorithms for parallel transformer distribution substations.

6.1 Introduction

Two classes of DSDR optimisation algorithm are describe in this chapter. These share a common objective function - namely to minimise the real power consumed by technical losses in the DSDR substation – however they are distinct with respect to technical approach, configurability, and extensibility. The threshold algorithm detailed in section 6.2 controls the single or parallel operation of by direct comparison between measured substation load and a threshold value, whilst the model-based algorithm of section 6.3 uses the measured load in combination with a digital simulation of the substation to select single or parallel operation. Each experiment will be repeated for each algorithm, and their performance at reducing substation losses evaluated according to the metrics defined in section 5.7.

6.2 Threshold Algorithm

The threshold algorithm, shown in Figure 67, is based on [135] from industry innovation trials in MV distribution networks. It's development for a DT and BTSM is novel, and will enable testing in a variety of LV use-cases not available in the existing real-world LV networks, such as parallel transformer substations. It uses binary decision logic to select a heuristically efficient reconfiguration state of the substation at each load step. A threshold value of substation load in kVA, about which the substation will change its configuration between single or parallel mode, is loaded from configuration. This can optionally be set for each experiment, but is usually 50% of the substations total kVA rating in accordance with [67].

At each load step, the total substation load is retrieved from the power analyser placed at that node. Should this load be greater than the pre-set threshold value, a command is issued to the reconfiguration switches that the substation be placed into parallel operation mode. Otherwise, a reconfiguration command for single transformer operation is issued.

In that case, experimental repeatability is attained through an additional logical fork which commands the most recently used single transformer to remain energised if the substation was already in single operation mode from the previous load step, otherwise commanding the least recently used transformer if the substation was previously in parallel operating mode. This prevents frequent switching between transformers during periods of low load.

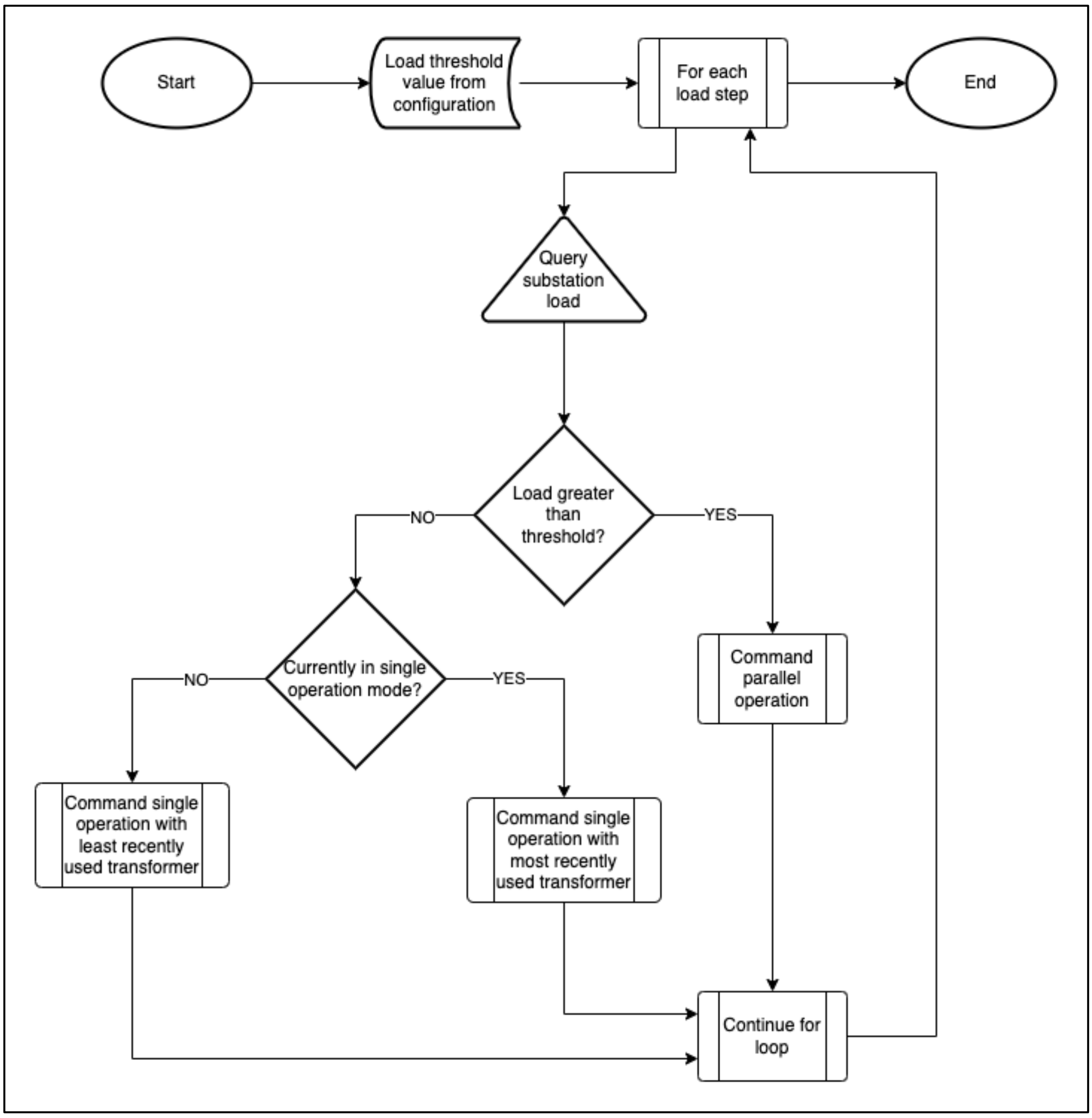

Figure 67 - Threshold algorithm flow chart.

The benefits of the threshold algorithm include that it is simple to reason about, and is of low computational complexity such that is may be implemented in systems with minimal processing capacity. Its existing trials in medium voltage parallel substations provide a basis for validation and comparison across voltage and power levels, and a baseline for the benchmarking of improved DSDR algorithms such as the model-based algorithm described next.

6.3 Model-Based Algorithm

The model-based algorithm, shown in Figure 68, uses OpenDSS simulations of the substation in each reconfiguration state to select the theoretically optimal single or parallel operating mode. It is the novel algorithm proposed in this thesis, drawing together the accelerated real-time use of DTs and physical evaluation of algorithm results on BTSMs.

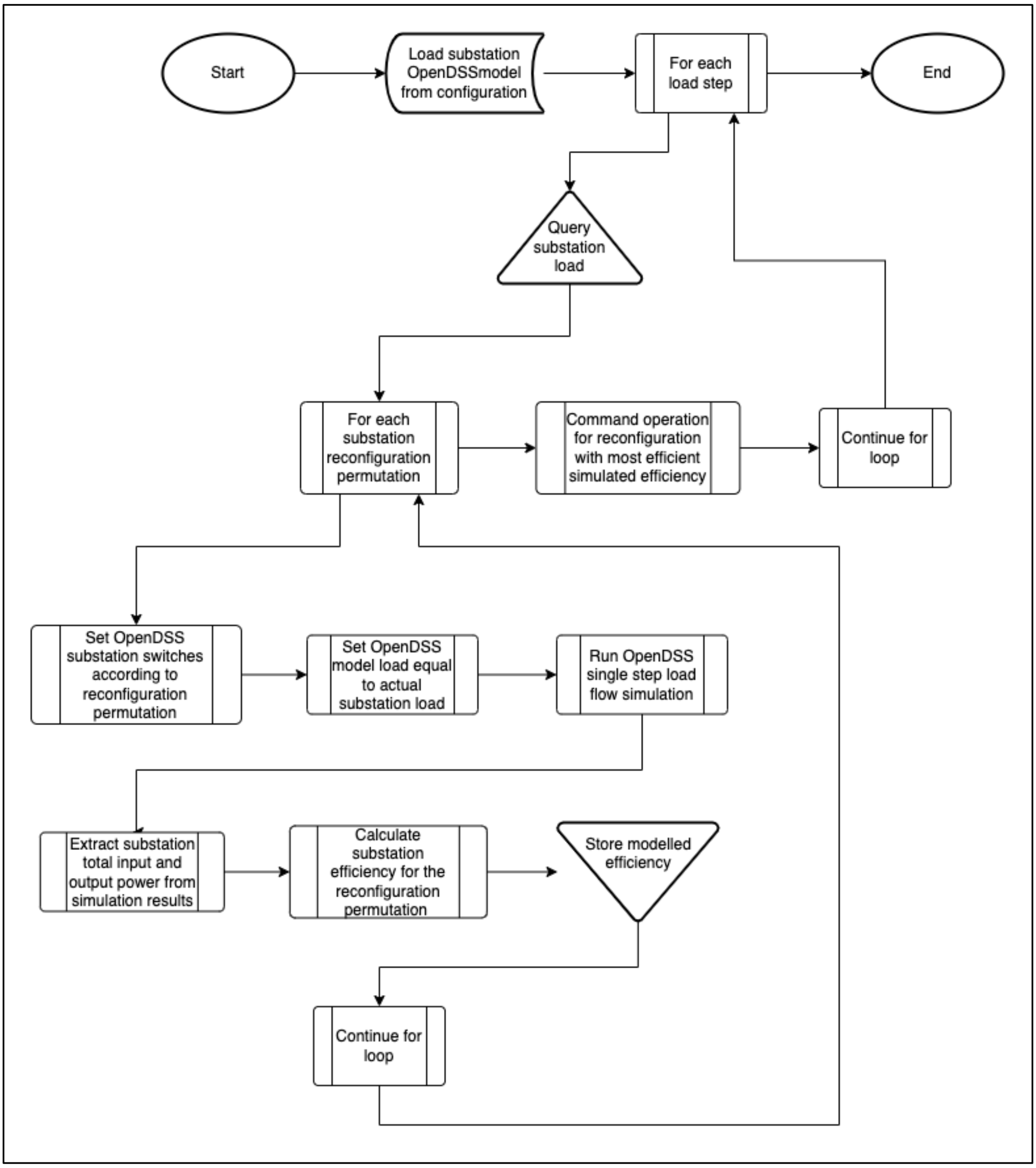

Figure 68 – Model-based algorithm flow chart.

During algorithm initialisation, a parameterised digital model of the substation identical to that described in chapter 3 is loaded, in preparation for running load flow simulations during algorithm operation. At each load step, as for the threshold algorithm, total substation load is retrieved.

The model-based algorithm then iterates over each reconfiguration permutation of the substation, i.e. single mode with transformer one, single mode with transformer two, and parallel mode. One obvious advantage of this approach is that substations with an arbitrary number of switchable parallel transformers (i.e. not just two) can be modelled and therefore controlled by this algorithm, opening a route for seamless future substation reinforcement should it become required.

At each iteration, an OpenDSS load flow is performed to determine the modelled substation efficiency at the actual operating load. In this way, the algorithm evaluates both individual and combined transformer losses at each load step for the particular loading condition, to calculate an optimal configuration of the substation in which losses will be minimised. Finally, the reconfiguration permutation which yielded the highest modelled substation efficiency is commanded onto the actual substation.

6.4 Experimental Process

DSDR experiments to evaluate the algorithms described will be performed on the DT model for each combination of test cases described in section 5.7.3, and quantified according to the efficiency measurement metrics derived in section 5.7. As load profile playback on the BTSM is slower to allow for instrument settling time, and a wait period between experiments is necessary to allow the transformers to cool to ambient temperature for experimental repeatability, a subset of the same experiments will be performed on the BTSM for validation of results.

6.5 Summary

Two DSDR algorithms – threshold and model-based – were designed, and an experimental plan to evaluate and validate those with suitable metrics was established.

Benefits of the model-based algorithm are that it can command the theoretical optimum efficiency of the substation at each load step, can readily be adapted to optimise alternative (or multiple) additional objective functions, and is suitable for an arbitrary number of transformers within a substation.

Future work to extend the model-based algorithm for improved accuracy could see the including of modelling thermal effects on winding resistance (and therefore copper losses and ergo transformer efficiency). For the DT experiments, this would involve including a discrete-time model of transformer winding temperature with respect to ambient temperature, initial winding temperature, and load current, a calculation of winding resistance adjusted for winding temperature, and updating of the OpenDSS winding resistance parameter at each load step.

For the BTSM experiments however, whilst winding temperature could easily be measured from the scale model transformers using a thermocouple, experiments would need to be slowed down considerably to allow for a steady-state settled temperature to be achieved at each new load step. Further points to be considered for algorithm completeness could include transformer degradation, modelled over a large fleet of transformers and EVs in the presence of microgrids, a simulation framework for which is introduced in a recent simulation study [136], and management of harmonic currents drawn by LCT loads by optimising substation total impedance through transformer parallel switching.

The following chapter will present the results of DSDR experiments performed on a permutation set of scenario years, reinforcement strategies, algorithms, and models, as a demonstration of DSDR's value and readiness for pilot trial in real distribution systems. It will include efficiency improvements achieved by the novel model-based algorithm, over the threshold algorithm implemented for benchmarking.

7 Results and Discussion

7.1 Introduction

The previous chapter outlined the operation of the threshold and model-based algorithms implemented so far. This chapter presents the results of the experiments performed to evaluate these algorithms. In section 7.2, the experiment load profiles derived from combining domestic base load and EV charging are presented, along with information on which experiments were run. Section 7.3 leverages several graphical analyses to present the DT algorithm evaluation results.

Results are presented throughout in terms of substation efficiency which is a percentage, rather than in losses which are a physical quantity (e.g. W), as this provides for a better intuition for comparison of the scale model results here (rated at 200 W) and how the algorithms would be expected to perform on a real-world substation (rated at 100’s of kW). Finally, section 7.4 draws conclusions about model and algorithm performance during the experiments, and sets out proposed improvements to each of these.

7.2 Combined Load Profiles and Set of Experiments

7.2.1 Introduction

In this section, the results of combining domestic base and electric vehicle load profiles to represent the three scenario years under consideration are presented. Normalised with respect to original substation power rating, Base Year 2020 consists of 66.7% base load with no EV load; ICE Ban Effect Year 2035 is a combination of 83.35% base load with 100% EV load; and Net Zero Year 2050 has 100% of each load type. The set of experiments which were performed on the DT and BTSM are also described in this section.

7.2.2 Load Profiles

A load profile describes the temporal energy demand placed on an electricity system, and may be aggregated on the basis of an appliance type (EV, HP), a consumer type (domestic, commercial), a substation, or a grid supply point [137]. Load profiles are used for sizing assets such as transformers, feeders and switchgear, and may be described in terms of their Maximum Demand (MD) – the highest sample - and Load Factor (LF) which is shown in Eq. 23 [128].

$$LF = \frac{Total\ Demand\ (kWh)}{Maximum\ Demand\ (kW) * \ Sampling\ Duration\ (hours)} \quad \text{Eq. 23}$$

7.2.2.1 Domestic, Commercial, and Industrial Loads

The classic set of UK half-hourly domestic, commercial and industrial load profiles used by DNOs were compiled by Elexon after 'recording and analysing Half-Hourly demand data from a representative sample of customers' [128], the types of which are shown in Table 36. These profiles are a measure of the average electricity consumption pattern separated by customer type, day (weekday, Saturday, Sunday), and season (spring, summer, high summer, autumn, winter). Two-rate customers are those who receive cheaper electricity during the night for electrical heating and hot water purposes.

Table 36 – Standard UK load profile customer types [128].

Profile Class	Customer Type
1	Domestic Unrestricted (single rate)
2	Domestic Economy 7 (two rate)
3	Non-Domestic Unrestricted (single rate)
4	Non-Domestic Non-Maximum Demand Economy 7 type (two rate)
5	Non-Domestic Maximum Demand Customers with Load Factor 0-20%
6	Non-Domestic Maximum Demand Customers with Load Factor 20-30%
7	Non-Domestic Maximum Demand Customers with Load Factor 30-40%
8	Non-Domestic Maximum Demand Customers with Load Factor >40%

Profile classes one, two, and three for an Autumn Weekday are shown in Figure 69 below, which highlights electric storage heating load during night-time (orange curve), and high commercial energy demand during office hours (grey curve).

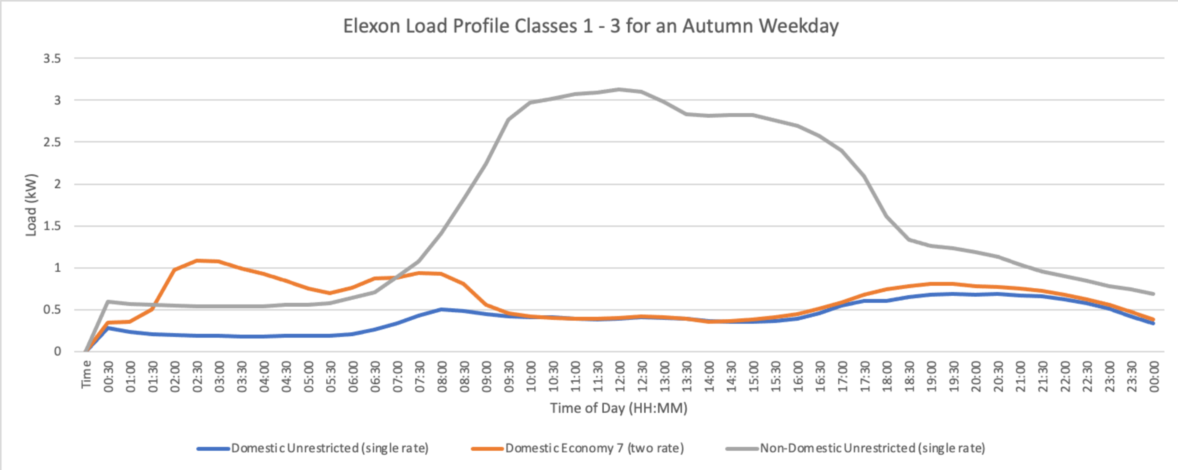

Figure 69 - Example Standard load profiles – plotted from data in [128].

7.2.2.2 Electric Vehicle Charging Loads

Electric Vehicle (EV) charging loads are of particular interest at present due to the proliferation of EVs, meaning that their 'integration in the power system is becoming a crucial issue' [138]. Electric Vehicle Charging Point (EVCP) load profiles may be taken from 'surveys, ICE/EV trials and charger trials' [138] data; around sixty such datasets have been released publicly [139].

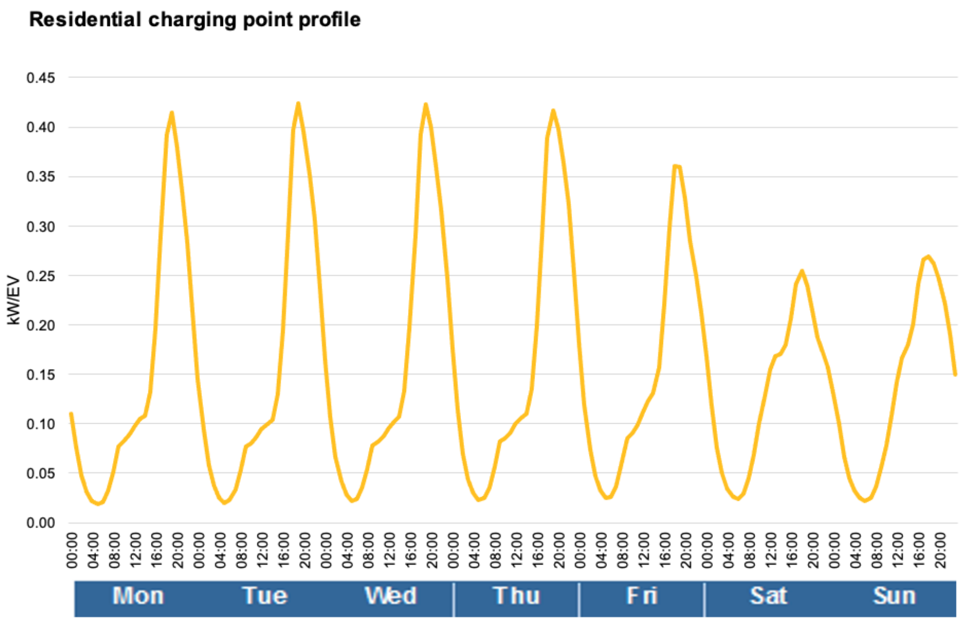

Figure 70 - Average weekly charging profiles for residential EVCP [140].

In addition, models leveraging 'statistical characterization to stochastic processes and machine learning' [139], which have been composed from those datasets, may be utilised to synthesise new EV load profiles for specific scenarios.

National Grid's Future Energy Scenarios 2019 [140] includes average weekly charging profiles for residential, workplace and public EVCP. It can be seen that most load was drawn in the evenings and overnight; also that the average load per EVCP is much lower than the standard rating of domestic EVCP, meaning that there was a low utilisation of EVCP's in the sample data.

EV loads may also be dynamically managed through the use of smart charging, which can be utilised to manage effects on the transmission and distribution systems of mass simultaneous, uncontrolled charging events by signalling to EV's when they should charge [141].

7.2.2.3 All Season Days

The combined load profiles for each season-day are shown below in Figures 71 - 73; the dashed reference lines represent 100% of the original substation rating, to which the load amplitude values are normalised.

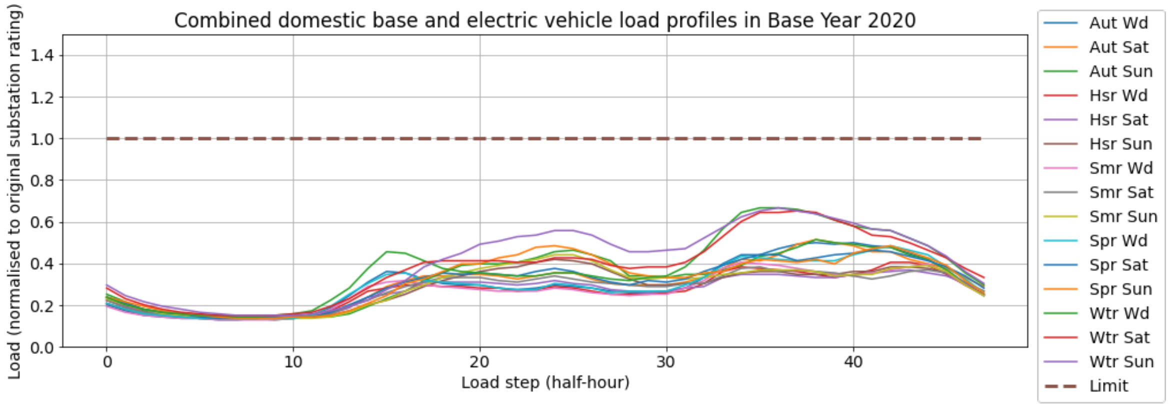

Figure 71 – Combined load profile for each season-day in Base Year 2020.

Figure 71 demonstrates that in the base year, substation load remains below the substation's power rating for each time step of every season day by a comfortable margin. Under such conditions, there is little requirement to reinforce a substation unless significant additional load is expected to materialise imminently, such as the connection of new homes.

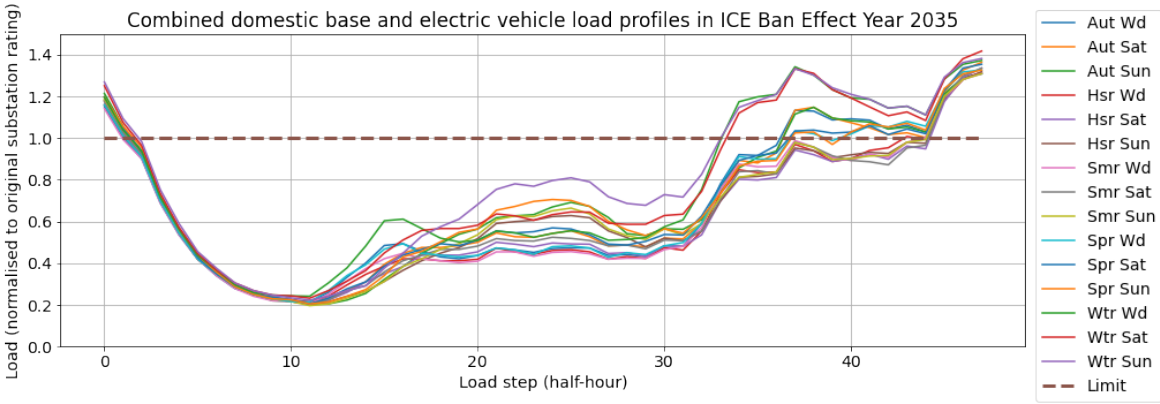

Figure 72 - Combined load profile for each season-day in ICE Ban Effect Year 2035.

By 2035, the proliferation of EV's and their associated charging load is expected to cause substation load profiles in all season-days to exceed the power rating of the substation by up to 40% from the late evening until the early morning, as seen in Figure 72. During winter, additional overloads of between 20% - 30% are expected from late afternoon to late evening.

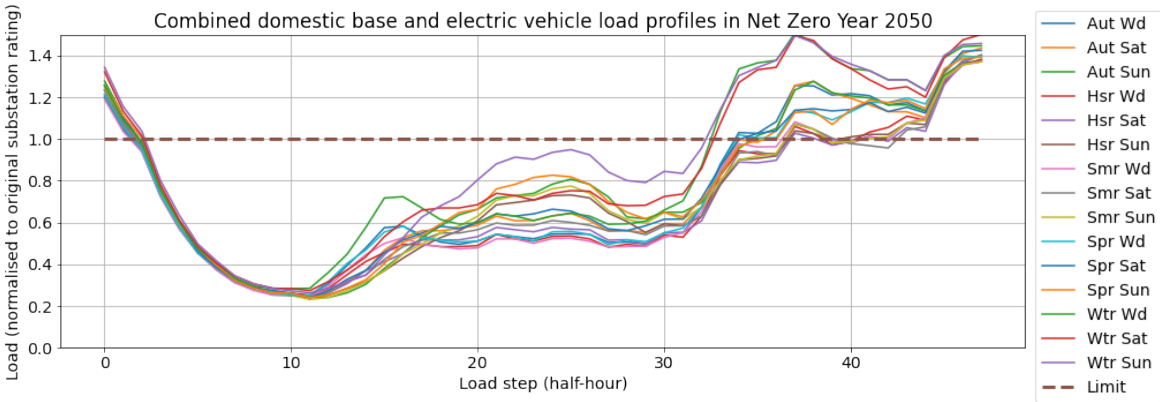

Figure 73 - Combined load profile for each season-day in Net Zero Year 2050.

As seen in Figure 73, by 2050 the substation load profiles are similar to those seen in 2035, with overloads in every season-day, and these exceeding 40% of substation rating during winter.

7.2.3 Experiments Performed

As planned in the previous chapter, the full set of experiments combining scenario-years, season-days, algorithms, and reinforcement scenarios were performed on the DT model in order to thoroughly evaluate algorithm performance under the widest possible range of operating conditions.

The playback of load profiles through the BTSM proceeds far slower than on the DT, as in order to provide repeatability, delay time must be included between each load step whilst instrument measurements settle, and between experiments whilst the transformers cool to ambient temperature. Therefore, a subset of experiment combinations were performed on the BTSM with the purpose of validating algorithm performance under the most onerous (winter) substation operating conditions.

Table 37 lists the experiment combinations performed on both models; a total of 21 sets of experiments were performed, formed of three scenario-years, four algorithm and reinforcement states, two experimental models, five seasons, and three day types.
This comprised the playback of 207 daily load profiles with a total of 9,936 load steps, yielding 317,952 individual data points which are analysed and presented in this chapter. The experiments with single transformer operation, representing the case where a substation is not reinforced to cope with increased load, were omitted from the BTSM experiments to avoid overloading the scale model transformers.

7.2.4 Summary

The combined load profiles seen in section 7.2.2.3 show that a substation originally sized to cope with steady increases in domestic base load until 2050 can now be expected to experience serious overloads by 2035 due to the upcoming proliferation of EV's. Three major approaches are possible to address these overloads – use flexibility services to shift load away from peaks where ratings are exceeded [54]; use power electronics and / or local energy storage to supply some of the load at peak times from another substation or from batteries [68], [142]; or reinforce the substation to increase it's maximum power rating [143].

By inspection of Figure 73, during winter months there is little delta in the areas of the load curves which lie above and below the reference line, meaning a very high percentage of all load would need to be flexible for the first approach to be successful. Using battery energy storage presents a similar challenge, as the battery storage would be charged during periods of low load; whilst transferring power from nearby substations assumes they are not also simultaneously overloaded, which cannot be guaranteed with the expected large uptake of EV's.

The combined load profiles presented in this chapter clearly demonstrate a requirement for reinforcement in the very near future, and therefore justify the work in this thesis to optimise the operation of that reinforcement, such that it may be carried out pre-emptively with minimal detriment from technical losses.

The results presented in this chapter are an analysis of the 207 daily load profiles, 9,936 load steps, and 317,952 data points yielded by the experiments performed on the DT and BTSM. The following section presents an evaluation of the efficiency optimisation results achieved by the threshold and model-based algorithms, as substations become progressively more overloaded by EV charging in each scenario year.

7.3 Algorithm Evaluation using Digital Twin Model

Table 37 shows the experiments performed for this thesis.

7.3.1 Substation efficiencies per scenario year

The substation operating efficiencies at each half-hourly load step are overlaid for each season-day. Reference lines are drawn at the maximum and minimum efficiency observed for each scenario year, across all algorithms.

Table 37 – DSDR Algorithm Evaluation and Validation Experiments Performed on DT and BTSM.

Scenario	Year	Algorithm	Model	Seasons	No. of Season-Days
Net Zero	2050	Threshold	Bench Top	Winter	3
Net Zero	2050	Model-Based	Bench Top	Winter	3
Net Zero	2050	None	Bench Top	Winter	3
Base	2020	Threshold	Bench Top	Winter	3
Base	2020	Model-Based	Bench Top	Winter	3
Base	2020	None	Bench Top	Winter	3
ICE Ban Effect	2035	Threshold	Bench Top	Winter	3
ICE Ban Effect	2035	Model-Based	Bench Top	Winter	3
ICE Ban Effect	2035	None	Bench Top	Winter	3
Base	2020	Threshold	Digital Twin	All	15
ICE Ban Effect	2035	Threshold	Digital Twin	All	15
Net Zero	2050	Threshold	Digital Twin	All	15
Base	2020	Model-Based	Digital Twin	All	15
ICE Ban Effect	2035	Model-Based	Digital Twin	All	15
Net Zero	2050	Model-Based	Digital Twin	All	15
Base	2020	None	Digital Twin	All	15
ICE Ban Effect	2035	None	Digital Twin	All	15
Net Zero	2050	None	Digital Twin	All	15
Base	2020	Single Transformer (TX 1)	Digital Twin	All	15
ICE Ban Effect	2035	Single Transformer (TX 1)	Digital Twin	All	15
Net Zero	2050	Single Transformer (TX 1)	Digital Twin	All	15

7.3.1.1 Base Year

Figure 74 shows the efficiency time series in the Base Year for load profile playback without substation reconfiguration. With no algorithm to optimise the substation's configuration, during the early mornings when demand is low, efficiency for all season-days drops to a minimum of 47.67%. At the highest operating efficiencies achieved during the evening peaks, efficiency peaks at 80.28%.

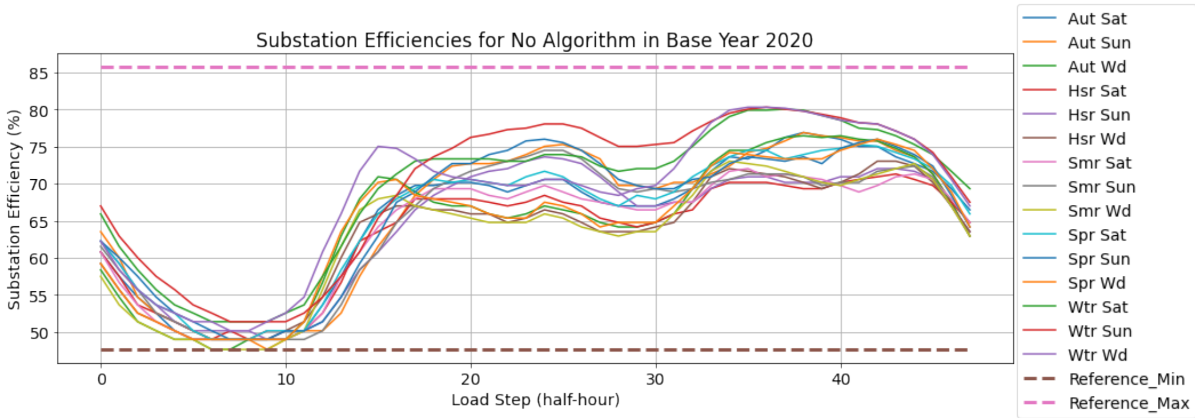

Figure 74 – Daily substation efficiency for all season-days in base year without algorithmic control.

Implementing threshold algorithm control, as shown in Figure 75, lifted the minimum operating efficiency to 62.16%, and also improved the peak efficiency to 84.18%, which was achieved in the evening.

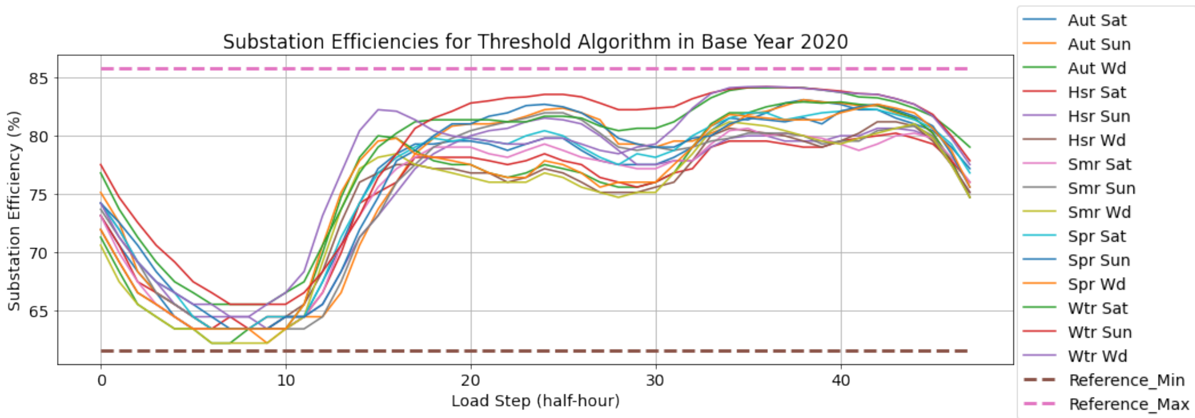

Figure 75 - Daily substation efficiency for all season-days in base year with threshold algorithm control.

Finally, using model-based control boosted the peak efficiency to 85.73%, achieved during both the afternoon and evening periods, as seen in Figure 76 below.

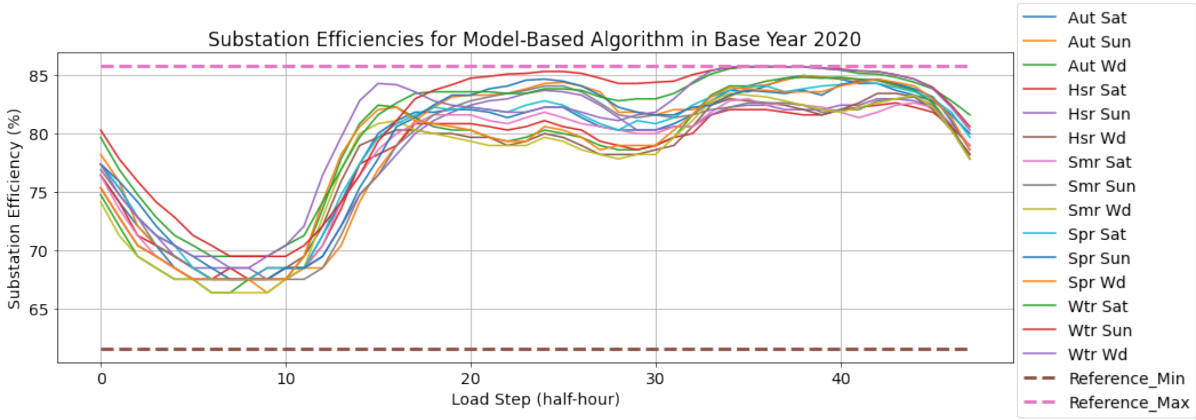

Figure 76 - Daily substation efficiency for all season-days in base year with model-based algorithm control.

7.3.1.2 ICE Ban Effect Year

By 2035, the generally increased load due to EV charging has reduced the under-utilisation of parallel transformers. Peak efficiency was 85.03%; however, whilst operating efficiency over the course of each day was greater than for the previous scenario yeas, minimum efficiency increased to 57.76%.

Without algorithm control, peak efficiency is almost reached overnight when EV load is greatest, but during the remaining periods of morning and afternoon this remains suboptimal, as seen in Figure 77.

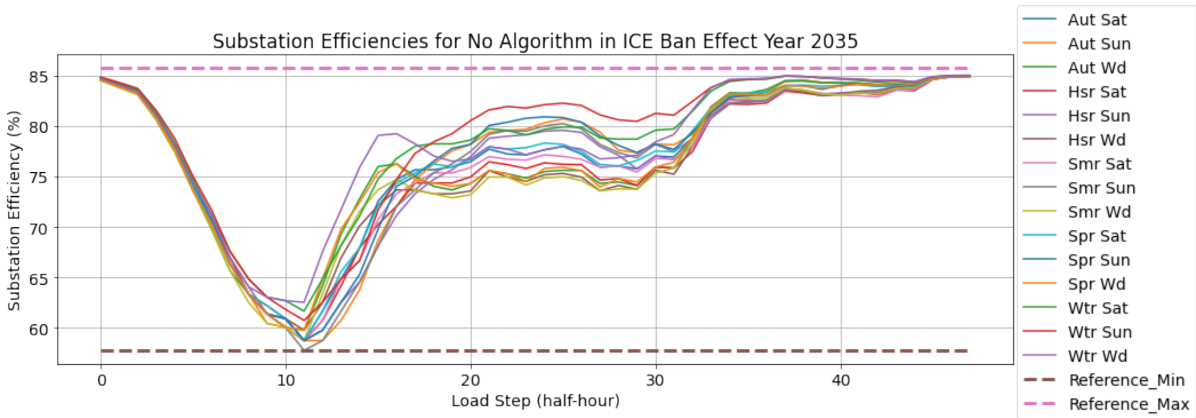

Figure 77 - Daily substation efficiency for all season-days in ICE-ban effect year without algorithmic control.

With the addition of threshold algorithm control, although peak reference efficiency is not attained, it is maintained only very slightly below this level for much of the daytime, evening and overnight period per Figure 78 below.

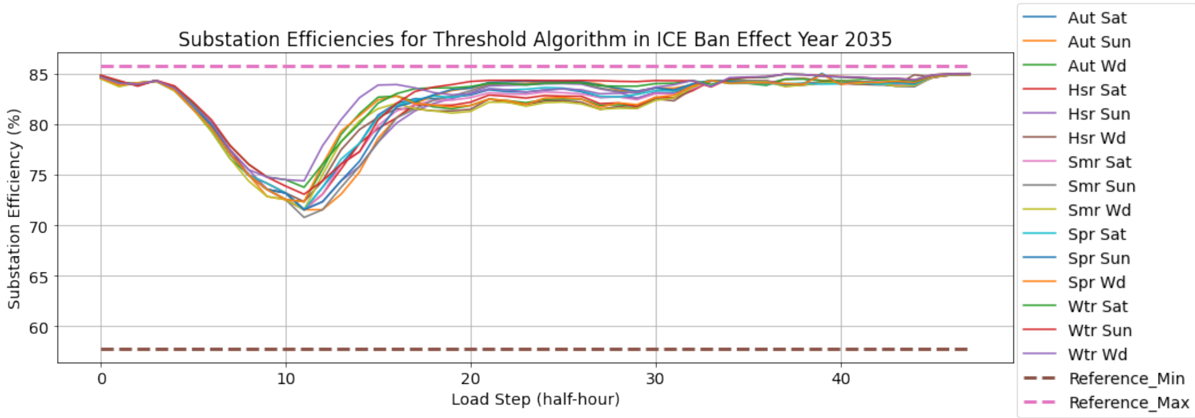

Figure 78 - Daily substation efficiency for all season-days in ICE-ban effect year with threshold algorithm control.

The model-based algorithm further improves substation efficiency in this scenario year as shown in Figure 79, reaching and maintaining a peak above 85% for most season-days and for most time steps except the morning period, which is lightly loaded.

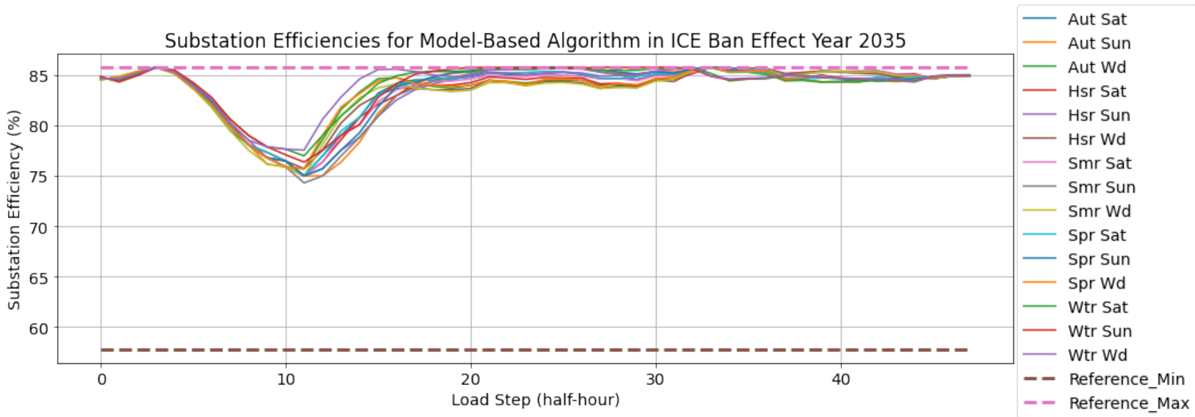

Figure 79 - Daily substation efficiency for all season-days in ICE-ban effect year with model-based algorithm control.

7.3.1.3 Net Zero Year

By the net zero year, both algorithms perform as well as for the ice ban effect year. Figure 80 shows a large drop in efficiency during the lightly loaded early hours.

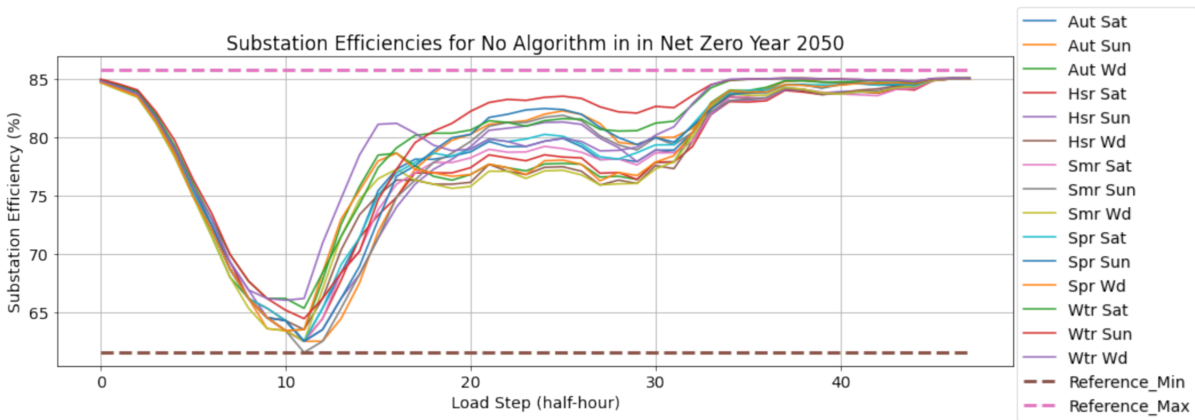

Figure 80 - Daily substation efficiency for all season-days in net-zero year without algorithmic control.

Figure 81 below shows this being corrected by the threshold algorithm.

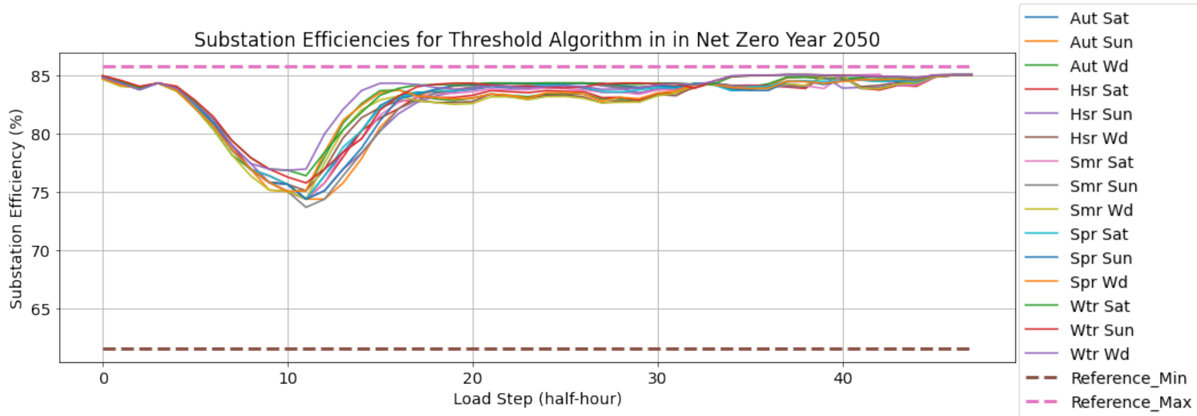

Figure 81 – Daily substation efficiency for all season-days in net-zero year with threshold algorithm control.

Further incremental improvements across the entire range of each day are achieved by the model-based algorithm as seen in Figure 82.

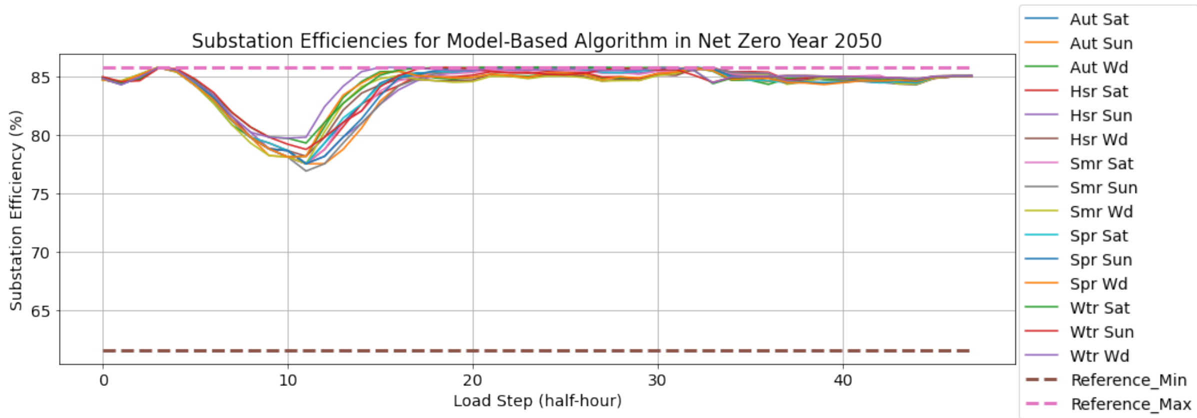

Figure 82 – Daily substation efficiency for all season-days in net-zero year with model-based algorithm control.

7.3.2 Transformer Utilisation by Each Algorithm

This subsection evaluates each transformer, by summing the periods for which single operation mode was commanded by one the algorithms. The bar charts below display the normalised utilisation of transformer 1 (in blue) and transformer 2 (in orange), for the model-based algorithm (left hand subplot) and threshold algorithm (right hand subplot), where normalisation is performed by dividing the on-time of each transformer by the total on-time to yield values in the interval [0.0, 1.0]. The utilisation value for each data point is also labelled above each bar. In the base year, as seen in Figure 83, the model-based algorithm exclusively selects transformer 2 for single operation periods, and the threshold algorithm exclusively selects transformer 1.

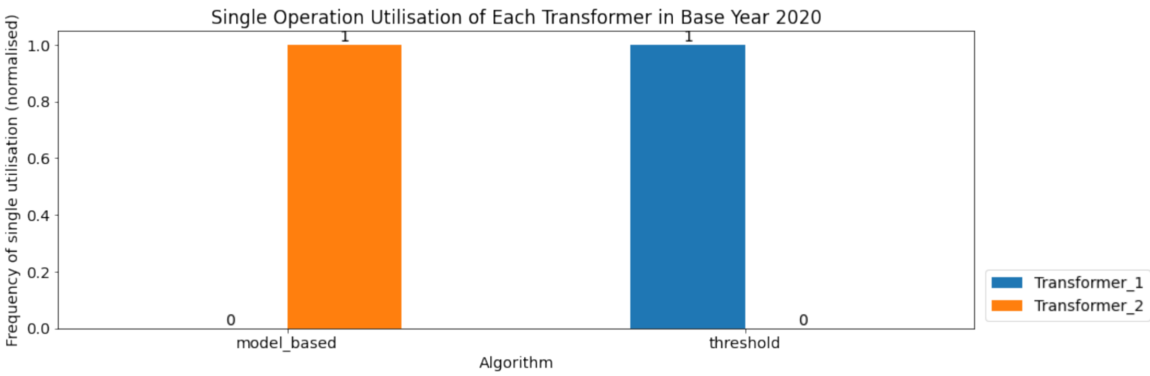

Figure 83 – Transformer utilisation per algorithm in base year.

There is little change in these results for the ICE ban effect year, as shown in Figure 84 below, with only a small utilisation of transformer 2 by the threshold algorithm.

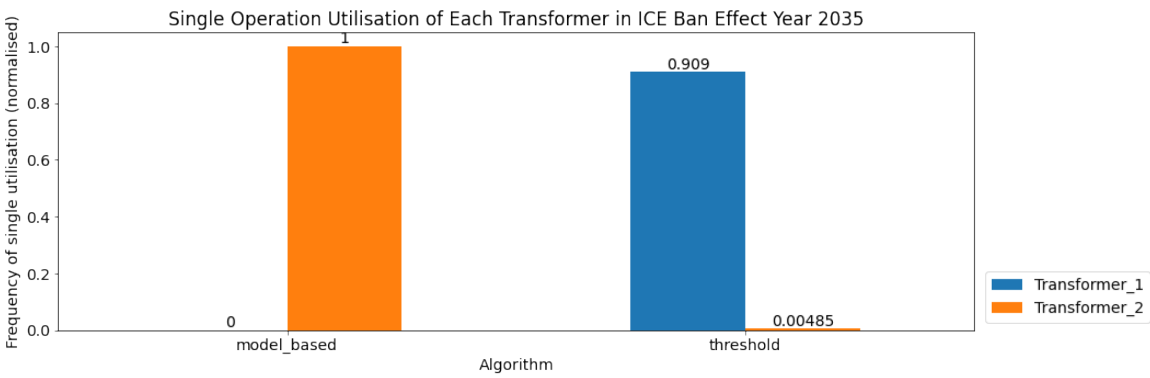

Figure 84 – Transformer utilisation per algorithm in ICE-ban effect year.

A similar result is seen in Figure 85 for the net zero year, with 100% utilisation of transformer 2 by the model-based algorithm and a strong preference for transformer 1 by the threshold algorithm.

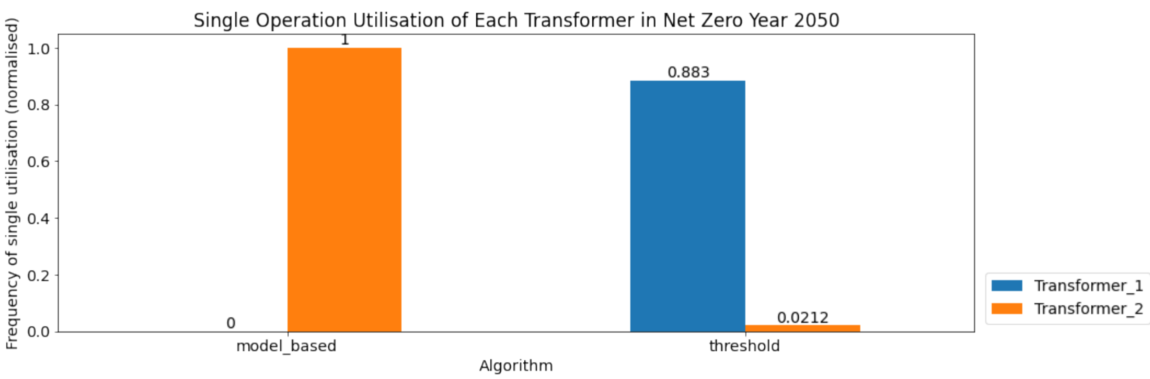

Figure 85 – Transformer utilisation per algorithm in net-zero year.

The model-based algorithm tended to over-utilise transformer 2 (shown in orange) and under-utilise transformer 1 (shown in blue).

This is because the algorithm's model parameters, which were derived from the physical BTSM transformer tests, show that transformer 2 is this slightly more efficient than Transformer 1 when both transformers are out of circuit and at ambient temperature.

Conversely, the threshold algorithm favoured transformer 1. This is due to the implementation detail of the algorithm, whereby it was designed to select transformer 1 for the first and each subsequent contiguous single operation load step. Such preference of both algorithms for a particular transformer during single operation mode is suboptimal, as it may cause unequal ageing of the transformers. Approaches to resolve this phenomenon are proposed in chapter 8.

7.3.3 Day with highest average load

In this subsection, a time series study is performed of the substation's load, efficiency, and reconfiguration state for the season-day with the highest average load – Winter Sunday. This analysis is intended to demonstrate how each algorithm achieves its optimisation results. The duration of each daily load profile experiment is plotted, with half-hourly load steps given on the horizontal axis, experiment settings and mean daily efficiency information provided in the title. Transformer states are represented by 0 for 'off', and 1 for 'on', in the upper two sub-plots. Separate charts are provided for each of the following algorithm and reinforcement states:

- 'Single operation' represents a substation before it has been reinforced, by setting transformer 1 to 'on' and transformer 2 to 'off' for the duration of load profile playback.
- 'No algorithm' represents a post reinforcement substation with parallel transformers, but without application of any DSDR algorithm to optimise the substation's efficiency in real-time, by fixing both transformer 1 and transformer 2 to 'on'.
- 'Threshold algorithm' represents a parallel reinforced substation, with both transformer states controlled by the threshold DSDR algorithm described in chapter 5 to optimise efficiency in real-time.
- 'Model-based algorithm' represents a parallel reinforced substation, as above but controlled by the model-based DSDR algorithm described in chapter 5.

7.3.3.1 Base Year

Figure 86 displays the load and substation efficiency in the base year for the single-operation reconfiguration state, exclusively using Transformer 1; mean efficiency for the winter Sunday was 78.3 %.

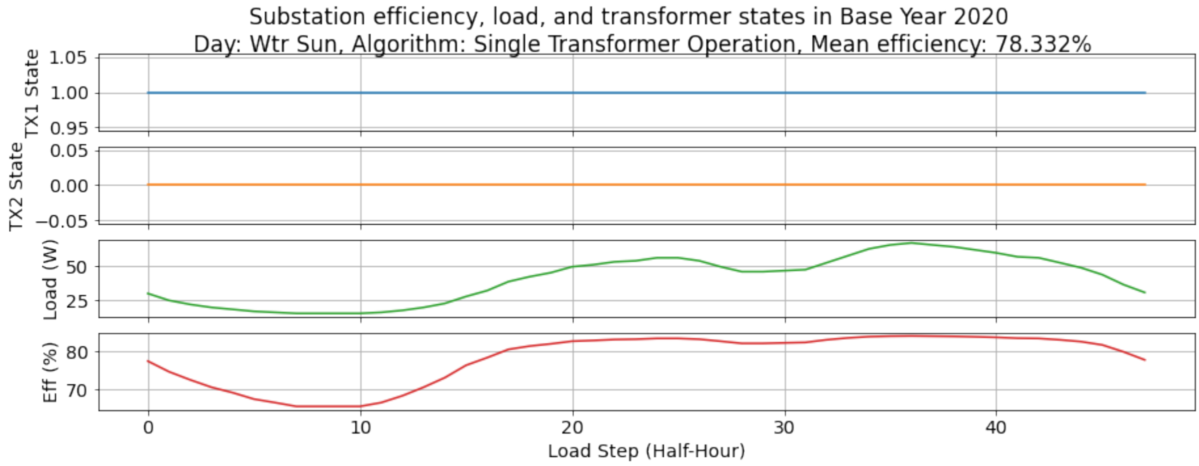

Figure 86 – DT experiment time series results for a Winter Sunday in Base Year with single transformer operation.

Figure 87 below shows the results for the same year and season-day, with reconfiguration state set to parallel and no algorithm running. The load remains below original substation rating for all load steps, and therefore the mean substation efficiency is lower than that achieved in 'single operation' mode above at 69.7%.

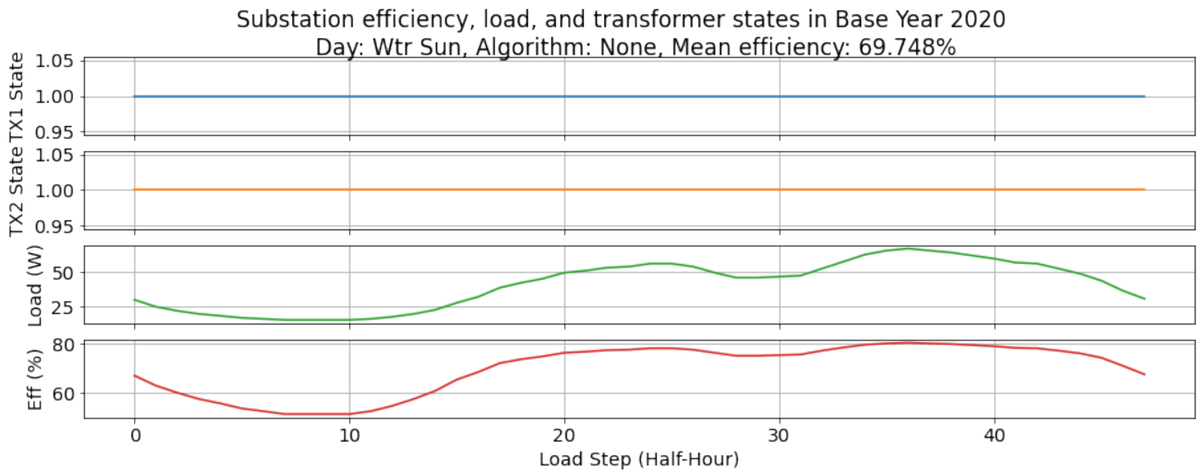

Figure 87 – DT experiment time series results for a Winter Sunday in Base Year with no algorithm.

Applying the threshold algorithm improves mean efficiency to 78.3% (Figure 88 below), which matches that of single-transformer operation, as no periods of parallel transformer operation are required at such low loads.

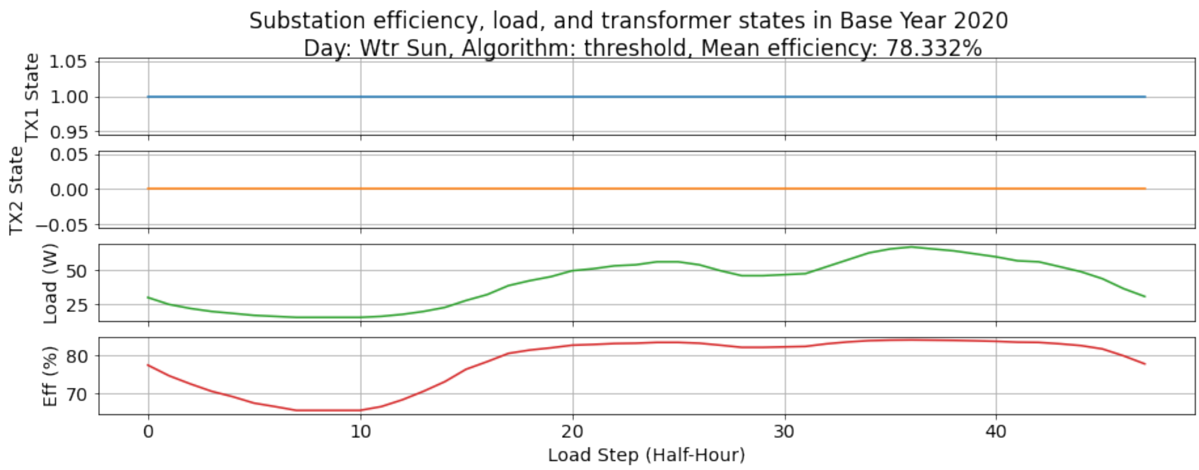

Figure 88 – DT experiment time series results for a Winter Sunday in Base Year with threshold algorithm.

The model-based algorithm results (Figure 89 below) improve overall efficiency to 80.8% by selecting the optimal transformer, whilst still keeping the substation in single operation at each time step. Both algorithms select single transformer operation for each load step; the difference being in which transformer is selected, as discussed in section 7.3.2. The model-based algorithm yields a 2.48% (2DP) overall efficiency improvement over the threshold algorithm, as the model's parameters make it aware of which transformer is the most efficient to use in single operation mode; these parameters are derived from measurements on the BTSM, whose winding resistances vary slightly between physical transformers due to manufacturing tolerances.

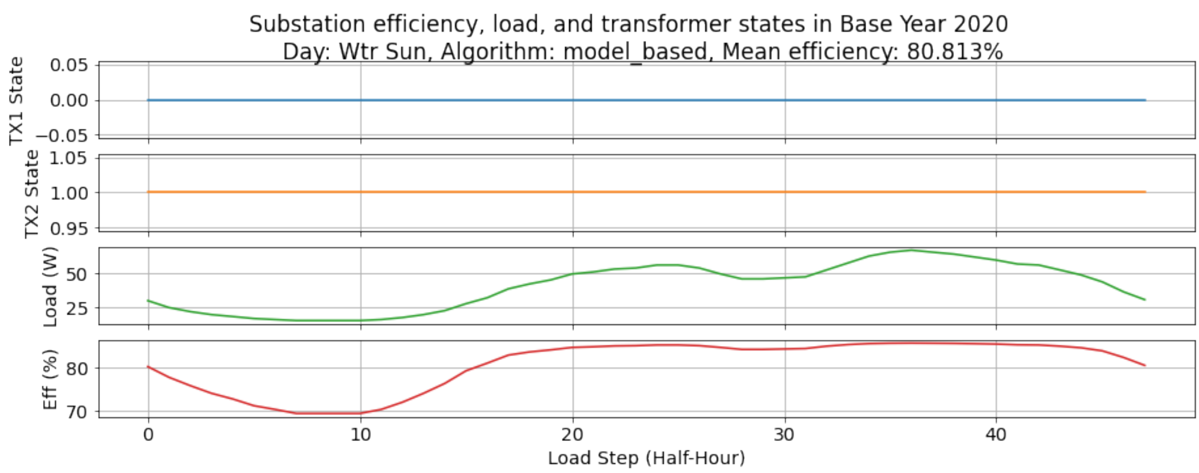

Figure 89 – DT experiment time series results for a Winter Sunday in Base Year with model-based algorithm.

7.3.3.2 ICE Ban Effect Year

In the ICE ban effect year, baseline efficiency can be taken as that from operating with a single transformer as shown in Figure 90 below.

By this year, load has increased due to proliferation of EV's, and exceeds the original substation rating during load steps representing the evening and overnight periods. Therefore, although the 'single transformer operation' experiment achieves mean efficiency of 81.75%, in a real substation with physical transformers rather than a DT model damage would occur to the transformer's winding insulation due to these overloads.

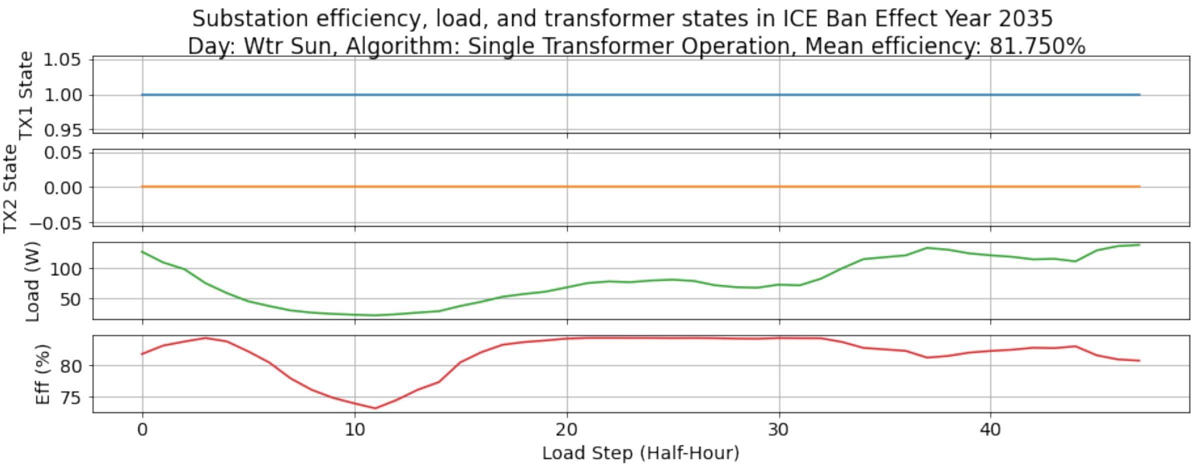

Figure 90 – DT experiment time series results for a Winter Sunday in ICE Ban Effect Year with single transformer operation.

Reinforcing the substation with parallel transformers but without DSDR algorithms, prevents such overloads of transformer windings. However, substation efficiency drops to 78.80%, as shown in Figure 91.

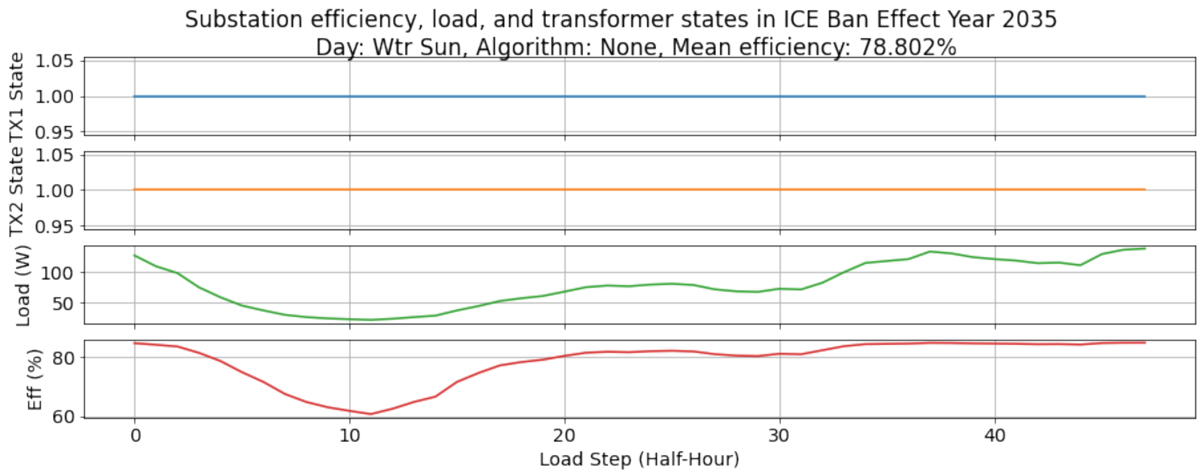

Figure 91 – DT experiment time series results for a Winter Sunday in ICE Ban Effect Year with no algorithm.

Operation of the DSDR substation with the 'threshold' algorithm yielded a 3.82% efficiency improvement over 'no algorithm' (Figure 92) to 82.6%.

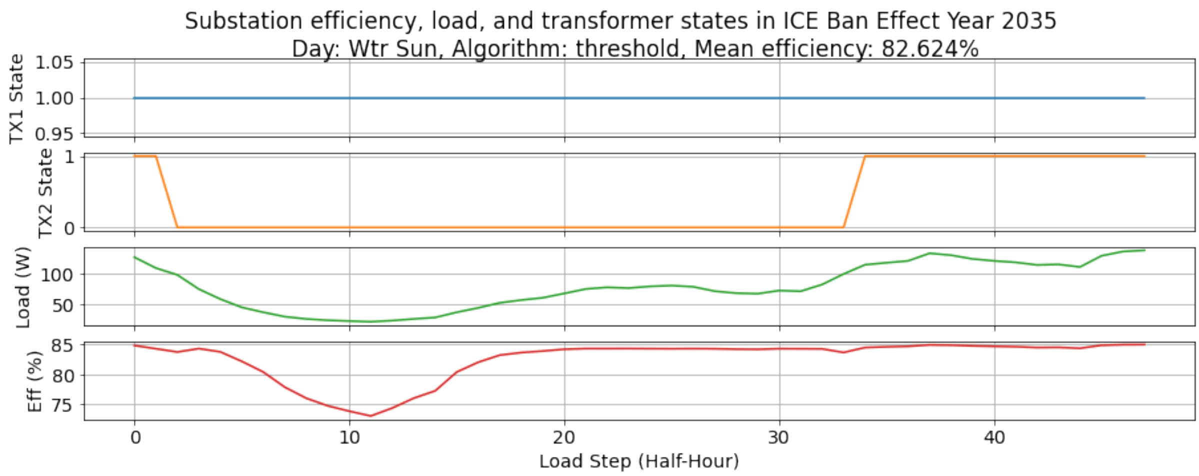

Figure 92 – DT experiment time series results for a Winter Sunday in ICE Ban Effect Year with threshold algorithm.

The ‘model-based’ algorithm improved this result by a further 1.3% to 83.9%, as seen in Figure 93. The application of ‘threshold’ and ‘model-based’ DSDR algorithms to the parallel reinforced substation resulted in mean efficiencies exceeding that achieved both for the pre-reinforcement case and the ‘no algorithm’ reinforcement case; this is the desired outcome of DSDR algorithms.

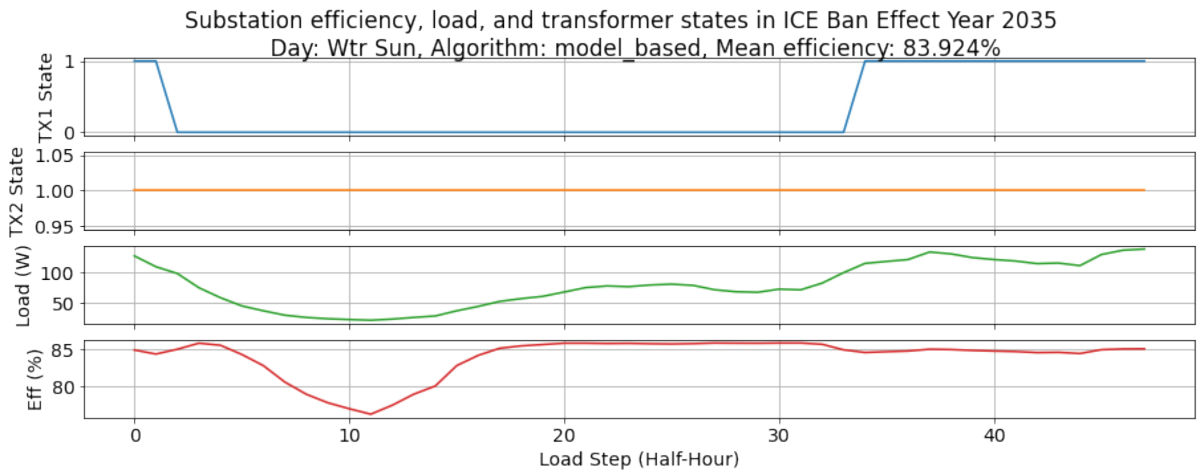

Figure 93 – DT experiment time series results for a Winter Sunday in ICE Ban Effect Year with model-based algorithm.

7.3.3.3 Net Zero Year

Net Zero Year yielded similar results to those of the ICE ban effect year, as the substation’s load profile increased only incrementally in the intervening fifteen years. The ‘threshold’ experiment improved the mean efficiency of the ‘no algorithm’ parallel reinforced substation by 3.02%, and the ‘model-based’ case improved this by a further 1.15%; plots of these results are given in appendix section 10.1.6.

7.3.4 Efficiency per Season-Day grouped by Algorithm for each Scenario Year

In this subsection, an analysis is made of the per-algorithm mean efficiency results for each season-day in the base year, ICE ban effect year, and net zero year experiment sets. In the figures below, the 'no algorithm', 'model-based', and 'threshold' cases are represented by blue, orange, and green bars respectively.

In the Base Year (Figure 94), there is a ~10% increase in daily substation efficiency when controlling a DSDR substation with either of the algorithms compared with uncontrolled parallel operation. This is largely because the load profiles are as-yet unimpacted by EV demand, and as such are most efficiently served by a single transformer. DSDR using the model-based algorithm outperforms that with the threshold algorithm for all season-days.

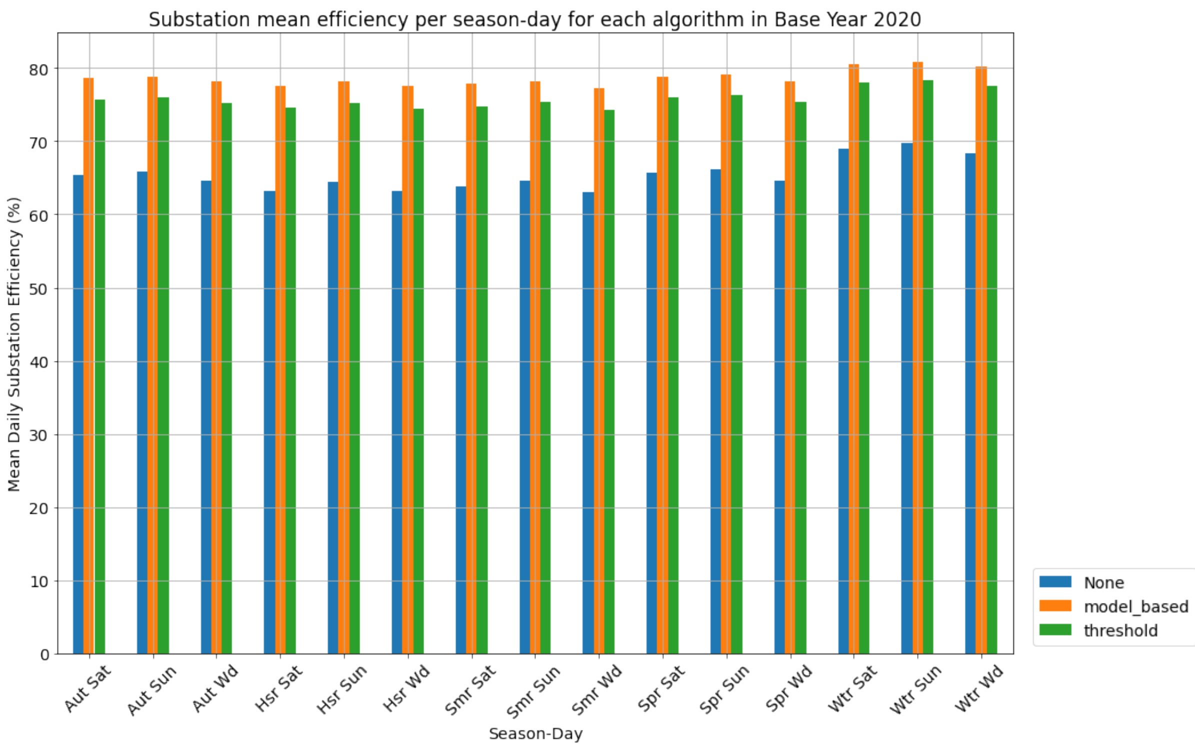

Figure 94 – Mean efficiencies per season-day for each algorithm in Base Year.

In the ICE ban effect year (Figure 95), the model-based algorithm also outperforms the threshold algorithm, both of which improve efficiency of a non-controlled parallel reinforced substation after EV demand is added.

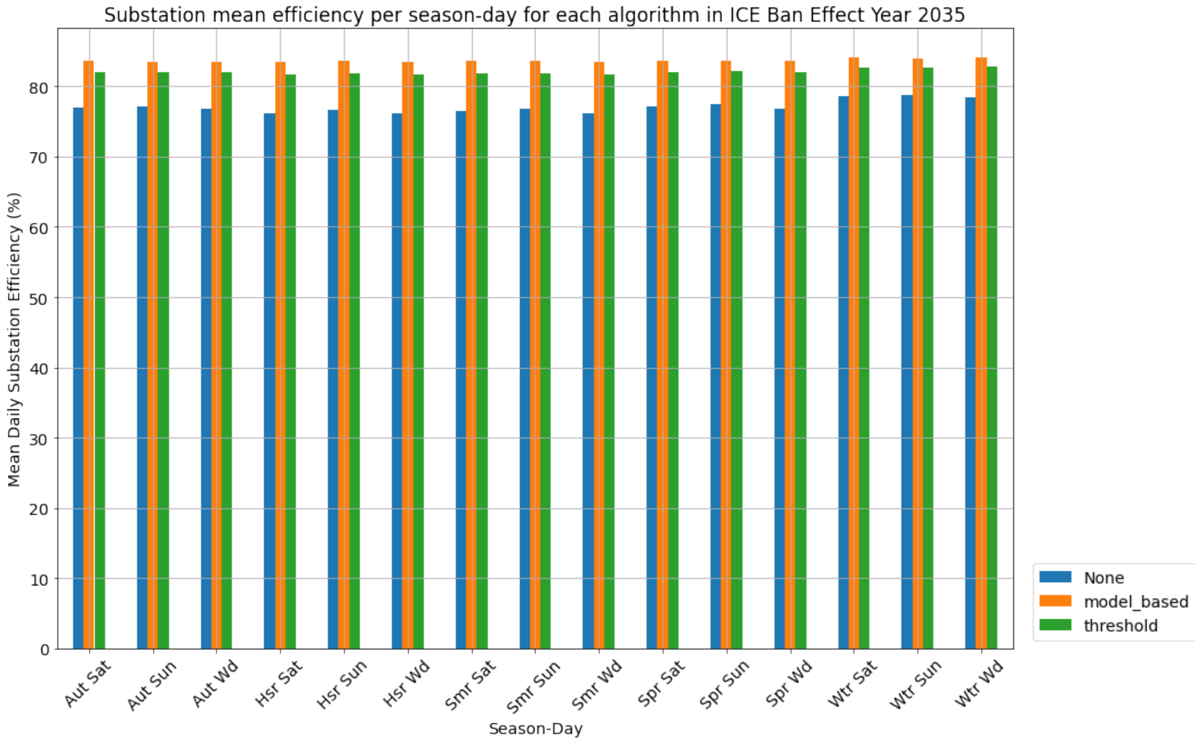

Figure 95 – Mean efficiencies per season-day for each algorithm in ICE Ban Effect Year.

Finally, in the net zero year (Figure 96), as for the preceeding scenario years, results for every season-day are consistest with the highest load day studied in section 7.3.3. Deploying either DSDR algorithm always improves substation efficiency. The model-based algorithm always yields best performance, because it's parameters (see section 3.3.3.2) include the information necessary to simulate and then select the most efficient transformer with which to operate during load steps when single transformer operation is optimal.

7.3.5 Frequency of efficiencies for algorithms in each scenario year

The charts in this subsection demonstrate how each algorithm shifts the operating efficiency of each load step in order to optimise the DSDR substation. Every load step, from all experiments in a scenario year, is placed into one of 40 bins based on substation efficiency, and grouped by DSDR algorithm; the results are presented as histograms. As in section 7.3.4, the 'no algorithm' group is represented by blue frequency bars, 'model-based' by orange, and 'threshold' by green.

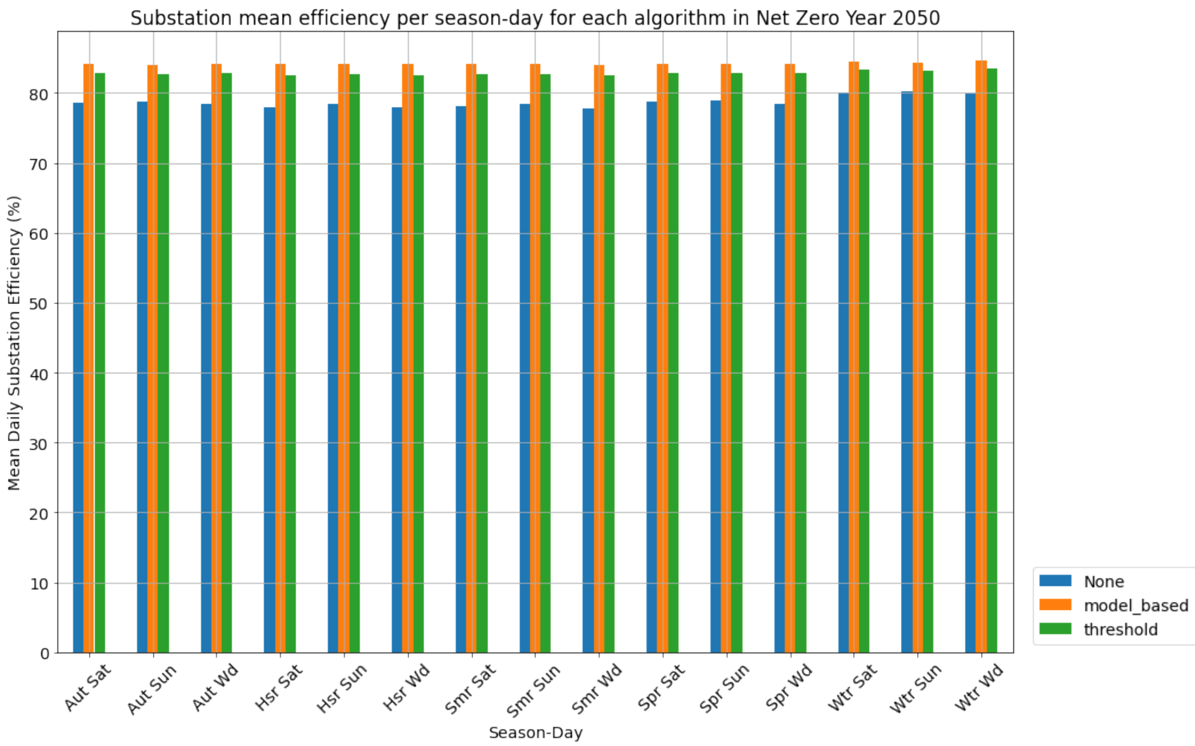

Figure 96 – Mean efficiencies per season-day for each algorithm in Net Zero Year.

Results for the base year (Figure 97) show an efficiency distribution with two distinct peaks for each algorithm case. Referring to the single day experiment time series charts of section 7.2.2.3, this phenomenom can be explained as an artefact of the demand shape before EV proliferation; this is broadly quantised between the overnight period with loads less than one quarter of the original substation rating, and daytime period with loads around half of the original substation rating.

As the base year demand never approaches a level where parallel operation would improve efficiency, each algorithm selects single transformer operating mode for all load steps, whilst the 'no algorithm' always maintains parallel operation. The resulting efficiency of each load step thus closely follows demand, and as at low load a transformer's losses are dominated by iron losses, efficiency is higher in base year for those load steps with higher demand. The 'model-based' and 'threshold' cases each compress and shift load step efficiency frequency to the right by selecting single transformer operation, which improves substation efficiency by reducing iron losses from the second transformer by de-energising it.

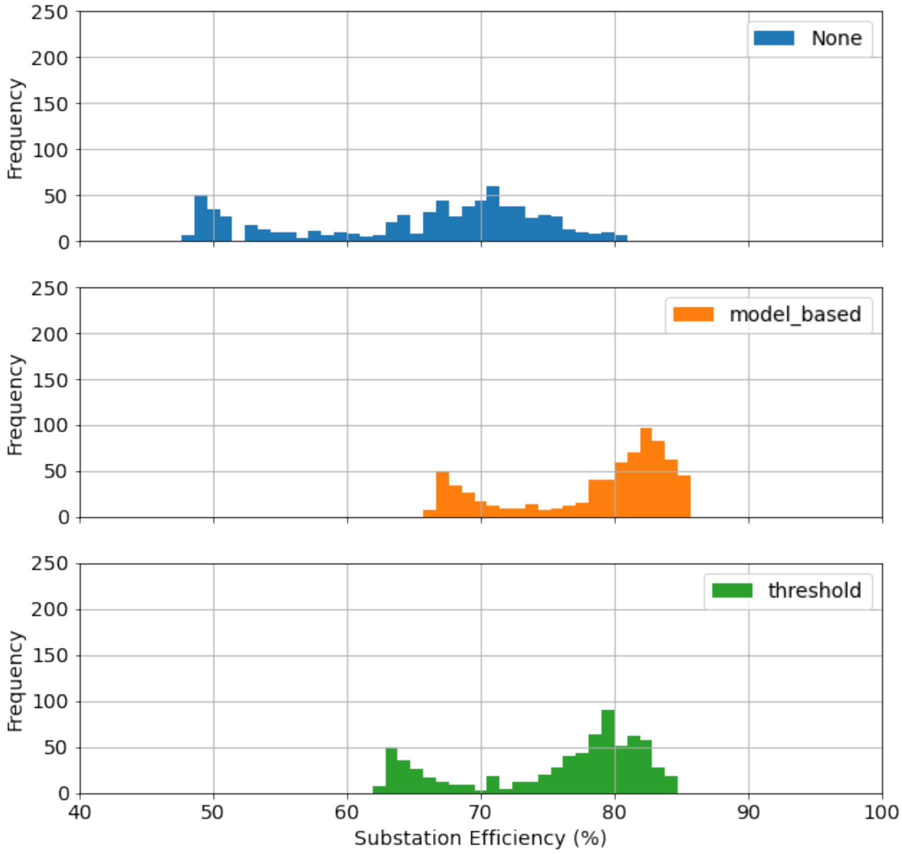

Figure 97 – Substation efficiency frequency for each load step per algorithm in Base Year.

In the ICE ban effect year (Figure 98), load step efficiency frequencies tend to form a skewed single peak with a long left tail regardless of algorithm. This is because, as seen in section 7.3.1.2, the demand profile remains above the region where iron loss dominates efficiency, and is instead most often in the higher-load region where the efficiency slope is relatively flat with respect to load.

The 'model-based' and 'algorithm' cases shorten the left tail, by cutting off the low operating efficiencies for those remaining load steps with relatively low load, by selecting single transformer operation.

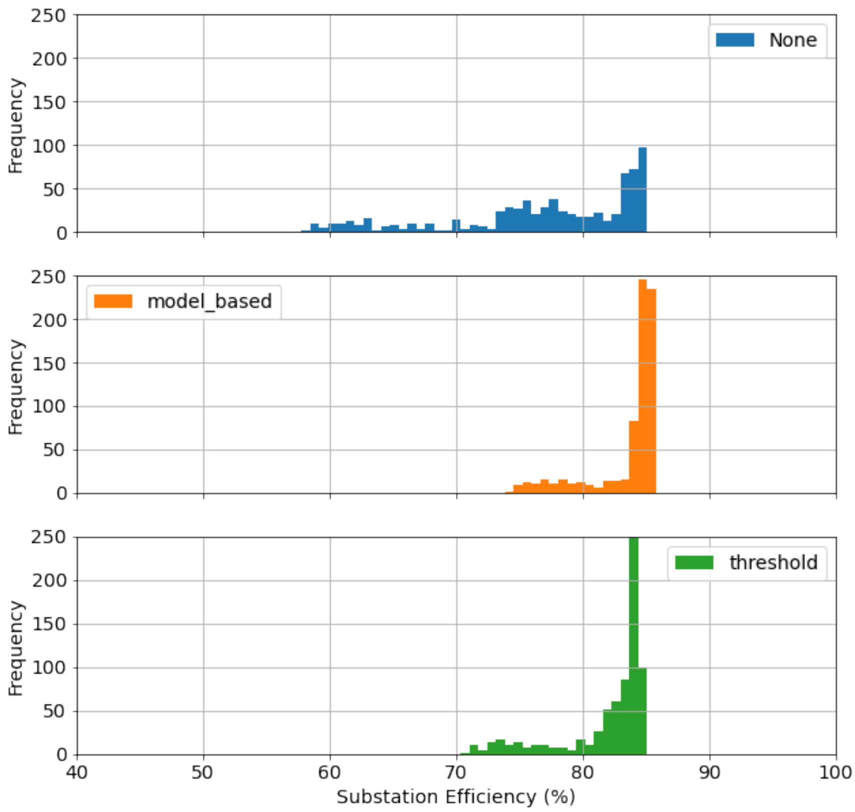

Figure 98 – Substation efficiency frequency for each load step per algorithm in ICE-Ban Effect Year.

Finally, results for the Net Zero Year (Figure 99) are highly correlated with those of the ICE ban effect year, as the load profiles are broadly similar with only a modest increase in EV demand.

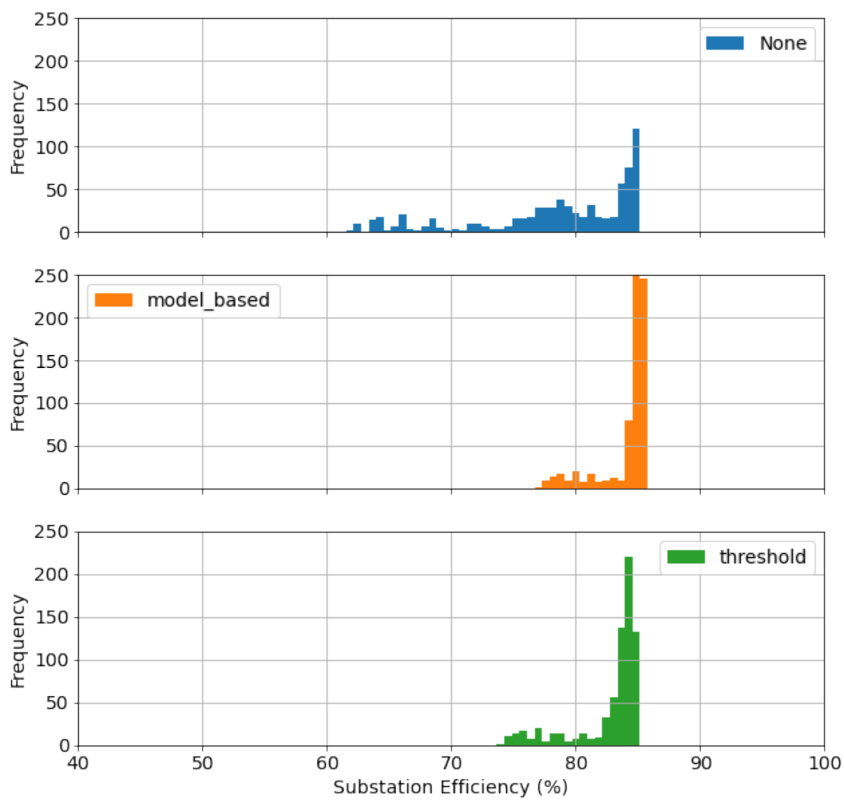

Figure 99 - Substation efficiency frequency for each load step per algorithm in Net Zero Year.

7.3.6 Extrapolating results to full year

This subsection extends the mean substation efficiency of each season-day experiment to a full calendar year, by weighting each result according to the quantity of each day-type per week, and quantity of weeks per season.

Results for each Saturday and Sunday were weighted by a factor of $\frac{1}{7}$, and each weekday by $\frac{5}{7}$, then further weighted for each season before grouping by algorithm and taking the mean. Table 38 shows the seasonal weightings applied, to extrapolate results from each season-day out to a full calendar year.

Table 38 – Seasonal weightings for annual efficiency extrapolation calculations.

Season	Season Code	Weeks per Year	Weighting
Winter	WTR	21	$\frac{21}{52}$
Spring	SPR	7	$\frac{7}{52}$
Summer	SMR	10	$\frac{10}{52}$
High Summer	HSR	6	$\frac{6}{52}$
Autumn	AUT	8	$\frac{8}{52}$

These were calculated according to the quantity of weeks represent by each season, divided by the quantity of weeks per calendar year. The resulting mean annual substation efficiencies are presented in bar chart format for each scenario year, with each bar representing a DSDR algorithm case.

Base year results (Figure 100) show that, as when studying DSDR substation efficiency in individual season-days, the ‘threshold’ case outperforms the ‘no algorithm’ case, and the ‘model-based’ case further improves upon both.

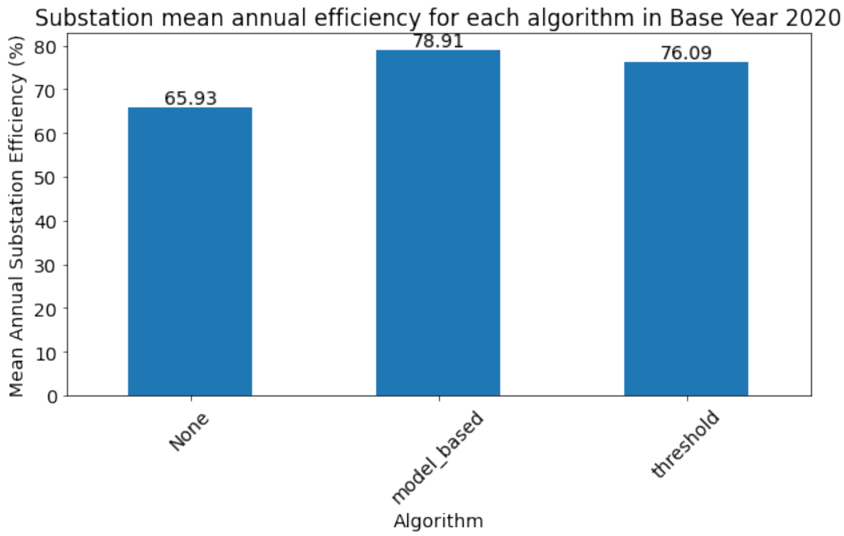

Figure 100 – Substation yearly efficiency per algorithm in Base Year.

Results in the ICE ban effect year (Figure 101) demonstrate the effectiveness of the DSDR algorithms in maintaining high operating efficiency of reinforced substations. The baseline increased for 'no algorithm' increased due to additional load better utilising the parallel transformers, whilst the threshold and model-based algorithms improved upon this by 4.84% and 6.40% respectively.

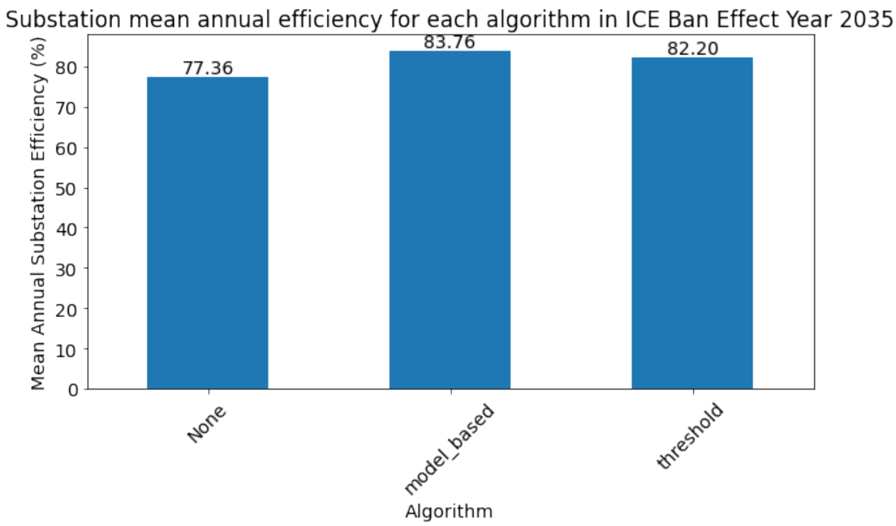

Figure 101 - Substation yearly efficiency per algorithm in ICE-Ban Effect Year.

Finally, results in the net zero year (Figure 102) portray a similar trend to that of the ealier scenario years – the 'threshold' case always outperforms the 'no algorithm' case, and the 'model-based' case always offers best performance.

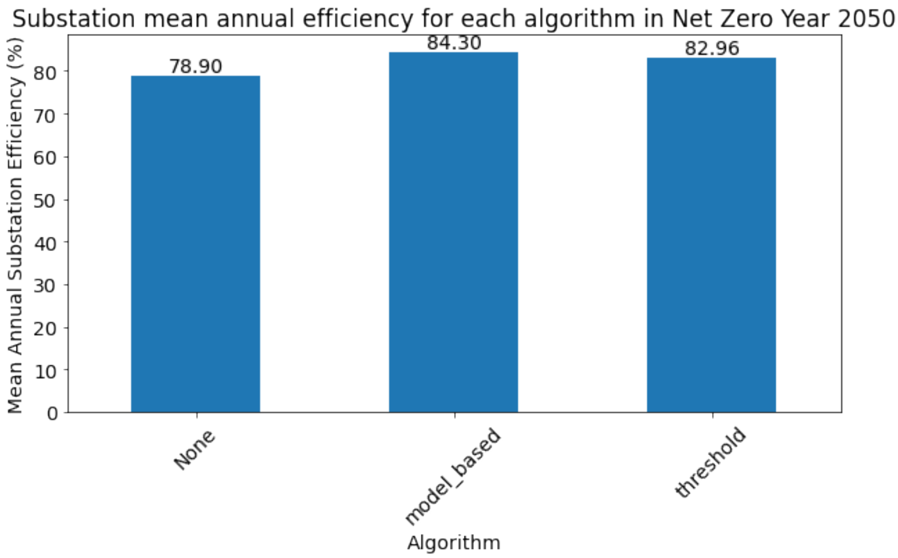

Figure 102 - Substation yearly efficiency per algorithm in Net Zero Year.

This section presented results from DSDR experiments performed using the DT model, over every season-day and scenario year derived in the previous chapter. The analyses within provided a positive evaluation of the two developed DSDR efficiency optimising algorithms, a baseline for validation of algorithm performance using the phsyical BTSM, and insights into improvements which could be made to the algorithms.

7.4 Summary

This chapter has described how combined domestic and EV load profiles were prepared, and the set of experiments they were used in. Improvements to algorithms were proposed, and a thorough examination and cross-comparison of all results was made. The substation efficiency improvement results for the algorithms were evaluated on the DT using:

- Time series operating efficiencies at each load step, overlaid for each season-day
- Utilisation of each transformer during single operation mode load steps
- Substation load, reconfiguration state, and efficiency profiles for Winter Sunday - the season-day with greatest mean load
- Mean substation efficiency per season-day
- Substation load step efficiency histogram
- Substation yearly operating efficiency

A quantitative summary of the mean annual substation efficiency improvements yielded by each algorithm, against the baseline case of 'no algorithm' for each scenario year, is given in Table 39. The results show that DSDR has the potential to improve substation efficiency by greater than 5% as new EV loads proliferate through electricity distribution networks.

Table 39 – Summarised mean annual substation efficiency improvements for threshold and model-based algorithms.

Scenario Year	**Threshold Algorithm Efficiency Improvement**	**Mode-Based Algorithm Efficiency Improvement**
Base 2020	10.16%	12.98%
ICE Ban Effect 2035	4.84%	6.40%
Net-Zero 2050	4.06%	5.40%

After evaluation using the DT, experimental results were then validated using the BSTM, with equivalent data and outcomes obtained. Full experiment results dataset are located in the author's GitHub data repository for the project[4]. The following chapter will draw final conclusions from all work described thus far in the thesis, including scaling up the benefits UK wide.

[4] https://github.com/brownr16/DSDR-data (contact author for access)

8 Conclusions

This work has addressed the pressing need to prepare electricity distribution substations for the expected loads caused by the proliferation of electric vehicles, which itself is driven by the electrification of transport to meet net zero targets. Electric vehicle charging is forecast to double the power demand seen at each low voltage substation, taking existing transformers well above their rated thermal capacity. The Distribution Substation Dynamic Reconfiguration reinforcement method and optimisation algorithms developed within this thesis provide a strategy for the pre-emptive reinforcement of substations likely to be impacted by these changes.

The use of parallel transformers and reconfiguration algorithms enables existing substations to be upgraded ahead of time, without incurring the additional no-load losses usually associated with such an approach. In subsequent years, when significant electric vehicle load arrives on the electricity network downstream of the substation in question, the reconfiguration algorithm ensures the correct number of transformers are energised to manage the connected load within thermal constraints, whilst minimising losses. As electric vehicle charging session behaviour is stochastic, and they can move around to charging locations served by different substations on different days according to available parking spaces, it is vital to deploy a smart, temporally flexible approach to service that load, such as that studied in this work.

8.1 Research contributions

The research contributions described in this work include:

- A digital twin model of the distribution substation dynamic reconfiguration approach to reinforcement, representing a single final distribution substation and capable of producing repeatable results when evaluating optimisation algorithms.
- A bench top scale model of the distribution substation dynamic reconfiguration approach, with parallel single-phase 230:24 V transformers, relays, and measurement instrumentation.
- Distribution substation dynamic reconfiguration software which can run arbitrary optimisation algorithms on both above models.
- An implementation of the threshold algorithm, which requires only load measurement values and operates in real time.

- A model-based algorithm, which operates in real-time and extends the open-source OpenDSS load-flow solver to select the optimal substation configuration through simulated permutations.
- Quantitative results for threshold and model-based algorithm performance in distribution substation dynamic reconfiguration situations across three scenario years.

8.1.1 DSDR Model Performance

8.1.1.1 Digital Twin Model

During algorithm evaluation using the DT, the containerised nature of the model enabled multiple experiments to be performed concurrently on a single computer, by creating additional DT instances. This greatly increased the throughput of experiment load profile playback.

8.1.1.2 Bench Top Scale Model

The BTSM also performed well, producing results that were consistent with those from the DT. Additional losses were observed in the BSTM, resulting from physical effects including transformer winding temperature above ambient temperature, hook-up wire resistance, and instrument shunt resistance.

8.1.2 Algorithm Performance

The threshold algorithm, which achieves its efficiency optimisation by switching in a parallel transformer when the demand exceeds the theoretical threshold of optimal efficiency, greatly improved the operating efficiency of parallel reinforced substations in all scenario years. The model-based algorithm aimed to optimise substation efficiency, by performing a load flow simulation for each reconfiguration permutation according to real-time demand, and selecting the most efficient for each load step. This algorithm was able to incrementally improve upon the substation operating efficiency gains achieved by the threshold algorithm, making it the best performing. Being model-based, it is also possible to supplement the algorithm with additional models, either to improve its performance further or to target alternative or additional optimisation objectives.

The threshold algorithm achieved a 4.06% annual operating efficiency improvement for a DSDR reinforced parallel substation in the net zero year, whilst model-based algorithm achieved a 5.40% efficiency improvement. This 1.34% improvement by the novel model-based algorithm presented here over the existing threshold alogorithm first used in the earlier referenced LEAN project, also implemented here as a benchmark, is a significant step forward. Based on the forecasts of combined domestic and EV charging annual electricity demand of 200 TWh by 2050, this represents a potential saving of 2.68 TWh annually, equivalent to that of a ~300 MW capacity generating station running continuously at full power.

In all years from 2035 onwards, a non-reinforced substation would become overloaded on a daily basis due to EV charging demand, causing overheating and damage to winding insulation. Whilst quantifying the financial costs of such transformer damage, or the financial cost to upgrade susbstations pre-emptively is outside the scope of this work, it is noted in the literature that ‘spending to upgrade electricity networks to support electric vehicles’ can ‘unlock, sustain and increase value in different parts of the economy’ [144]. It is also difficult to apply a cost study in terms of electricity losses to pre-emptive reinforcement, as DNO’s do not pay for losses incurred on their network, but are instead required by their license conditions to minimise them.

During single transformer operation, unequal sharing of on-time between transformers is observed for both algorithms; improvements are proposed in the following subsection to address this issue.

8.2 Future Work

Future work on DSDR will focus on improvement of existing models and algorithms, development of new algorithms, inclusion of additional optimisation objective functions, and exploration of additional load scenarios.

8.2.1 Improvement of Existing Models and Algorithms

Model speed improvements could be realised by adapting the DT, creating an alternate version using agent-based modelling. Load steps would be iterated as soon as each agent (substation model, algorithm etc.) computation is complete. Although such agent-based

DSDR software would not be suitable for deployment in real-world substations due to a lack of real-time operational capability, the resulting increased throughput should enable DSDR algorithm evaluation with very large load profiles (e.g. half-hourly for a full calendar year). A further refinement to the model would be the inclusion of transformer winding temperature calculations, and the effect of this on transformer losses.

To improve threshold algorithm transformer utilisation, a random transformer is selected for the first single operation load step, remains energised for the rest of that single operation group of load steps, but a change between transformers is made in each subsequent block of single operation. For the model-based algorithm, add a thermal model for the transformer windings which updates their winding resistances in the model parameters in real-time according to load. This will have the effect of better tracking the dynamic efficiency of each transformer, which reduces as the windings warm up, thus utilisation between transformers should automatically balance.

8.2.2 New Algorithms

A new class of algorithm based on reinforcement learning could be developed, which should require far less manual parameterisation than the model-based algorithm.

8.2.3 Optimisation Objective Functions

Algorithms could be developed with additional objective functions, including harmonics management and demand-side response through conservation voltage reduction.

8.2.4 Load Scenarios

Additional load scenarios could be explored, including those for heat pumps, distributed generation, flexible EV charging, and bidirectional EV charging.

8.3 Final Remarks

Scaling up the model-based algorithm’s 5.40% efficiency improvement to all final distribution substations across the UK, based on the forecasts of combined domestic and EV charging annual electricity demand of 200 TWh by 2050, DSDR has the potential for ~10 TWh of system efficiency savings.

9 References

[1] 'The Supply System', in *Electricity Distribution Network Design, 2nd Edition (IEE Power) by Lakervi, E. (1905) Paperback*, pp. 1–17.

[2] B. Bowers, 'Michael Faraday', in *A History of Electric Light and Power*, Reprint edition., Stevenage Hertfordshire ; New York: Institution of Engineering and Technology, 1982, pp. 12–24.

[3] P. L. Hannah, 'Pioneers of Lighting and Power', in *Electricity Before Nationalisation: A Study of the Development of the Electricity Supply Industry in Britain to 1948*, 2nd Edition., Baltimore: The Johns Hopkins University Press, 1979, pp. 1–35.

[4] T. Ackermann, G. Andersson, and L. Söder, 'Distributed generation: a definition', *Electric Power Systems Research*, vol. 57, no. 3, pp. 195–204, Apr. 2001, doi: 10.1016/S0378-7796(01)00101-8.

[5] F. Weschenfelder *et al.*, 'A review on the complementarity between grid-connected solar and wind power systems', *Journal of Cleaner Production*, vol. 257, p. 120617, Jun. 2020, doi: 10.1016/j.jclepro.2020.120617.

[6] A. von Meier, *Electric Power Systems: A Conceptual Introduction: 8*, 1st edition. Hoboken, N.J: Wiley-IEEE Press, 2006.

[7] F. Qiu, J. Wang, C. Chen, and J. Tong, 'Optimal Black Start Resource Allocation', *IEEE Transactions on Power Systems*, vol. 31, no. 3, pp. 2493–2494, May 2016, doi: 10.1109/TPWRS.2015.2442918.

[8] M. N. Mansouri, M. F. Mimouni, B. Benghanem, and M. Annabi, 'Simulation model for wind turbine with asynchronous generator interconnected to the electric network', *Renewable Energy*, vol. 29, no. 3, pp. 421–431, Mar. 2004, doi: 10.1016/S0960-1481(03)00225-8.

[9] T. Gönen, 'Transmission System Planning', in *Electric Power Transmission System Engineering: Analysis and Design*, New York: Wiley–Blackwell, 1988, pp. 3–25.

[10] S. Ramar and S. Kuruseelan, 'Power System Structure', in *Power System Analysis*, Delhi: PHI Learning, 2013, pp. 1–2.

[11] R. E. Brown, 'Reliability Metrics and Indices', in *Electric Power Distribution Reliability: 1*, 2nd edition., New York: CRC Press, 2008, pp. 41–102.

[12] B. Bowers, 'Early Supply Schemes', in *A History of Electric Light and Power*, Reprint edition., Stevenage Hertfordshire ; New York: Institution of Engineering and Technology, 1982, pp. 135–150.

[13] J. Aghaei, S. A. Bozorgavari, S. Pirouzi, H. Farahmand, and M. Korpås, 'Flexibility Planning of Distributed Battery Energy Storage Systems in Smart Distribution Networks', *Iran J Sci Technol Trans Electr Eng*, vol. 44, no. 3, pp. 1105–1121, Sep. 2020, doi: 10.1007/s40998-019-00261-z.

[14] F. R. Islam, A. Lallu, K. A. Mamun, K. Prakash, and N. K. Roy, 'Power Quality Improvement of Distribution Network Using BESS and Capacitor Bank', *Journal of Modern Power Systems and Clean Energy*, vol. 9, no. 3, pp. 625–632, May 2021, doi: 10.35833/MPCE.2019.000304.

[15] 'Distribution Substations and LV Networks', in *Electricity Distribution Network Design, 2nd Edition (IEE Power) by Lakervi, E. (1905) Paperback*, pp. 192–208.

[16] R. E. Brown, 'Distribution Systems', in *Electric Power Distribution Reliability: 1*, 2nd edition., New York: CRC Press, 2008, pp. 1–38.

[17] P. Trichakis, P. C. Taylor, P. F. Lyons, and R. Hair, 'Predicting the technical impacts of high levels of small-scale embedded generators on low-voltage networks', *IET Renewable Power Generation*, vol. 2, no. 4, pp. 249–262, Dec. 2008, doi: 10.1049/iet-rpg:20080012.

[18] I. S. Bayram and T. S. Ustun, 'A survey on behind the meter energy management systems in smart grid', *Renewable and Sustainable Energy Reviews*, vol. 72, pp. 1208–1232, May 2017, doi: 10.1016/j.rser.2016.10.034.

[19] S. J. Davis *et al.*, 'Net-zero emissions energy systems', *Science*, vol. 360, no. 6396, p. eaas9793, Jun. 2018, doi: 10.1126/science.aas9793.

[20] S. Conti, S. Raiti, and G. Tina, 'Small-scale embedded generation effect on voltage profile: an analytical method', *IEE Proceedings - Generation, Transmission and Distribution*, vol. 150, no. 1, pp. 78–86, Jan. 2003, doi: 10.1049/ip-gtd:20020739.

[21] N. Hatziargyriou, H. Asano, R. Iravani, and C. Marnay, 'Microgrids', *IEEE Power and Energy Magazine*, vol. 5, no. 4, pp. 78–94, Jul. 2007, doi: 10.1109/MPAE.2007.376583.

[22] K. Gillingham and J. Sweeney, ‘Barriers to implementing low-carbon technologies’, *Clim. Change Econ.*, vol. 03, no. 04, p. 1250019, Nov. 2012, doi: 10.1142/S2010007812500194.

[23] G. Behal, ‘Substation Innovations: The Heart and Brain of the Grid [Guest Editorial]’, *IEEE Power and Energy Magazine*, vol. 17, no. 4, pp. 16–22, Jul. 2019, doi: 10.1109/MPE.2019.2910425.

[24] J. Bhatt, V. Shah, and O. Jani, ‘An instrumentation engineer’s review on smart grid: Critical applications and parameters’, *Renewable and Sustainable Energy Reviews*, vol. 40, pp. 1217–1239, Dec. 2014, doi: 10.1016/j.rser.2014.07.187.

[25] E.-K. Chan and H. Ebenhoh, ‘The implementation and evolution of a SCADA system for a large distribution network’, *IEEE Transactions on Power Systems*, vol. 7, no. 1, pp. 320–326, Feb. 1992, doi: 10.1109/59.141721.

[26] ‘Equipment’, in *Electricity Distribution Network Design, 2nd Edition (IEE Power) by Lakervi, E. (1905) Paperback*, pp. 98–121.

[27] B. Hochart, Ed., ‘Liquid Dielectrics’, in *Power Transformer Handbook*, English ed. edition., London ; Boston: Butterworth-Heinemann Ltd, 1987, pp. 185–202.

[28] B. Li, Z. Hao, S. Li, S. Pan, J. Xiong, and B. Zhang, ‘Response Characteristics of the Buchholz Relay and Novel Non-Electric-Parameter Protection Methods’, *IEEE Transactions on Power Delivery*, vol. 38, no. 6, pp. 4103–4113, Dec. 2023, doi: 10.1109/TPWRD.2023.3321773.

[29] A. Xemard, B. Jurisic, M. Rioual, A. Olivier, and E. Sellin, ‘Interruption of small, medium-voltage transformer current with a vacuum circuit breaker’, *Electric Power Systems Research*, vol. 187, p. 106502, Oct. 2020, doi: 10.1016/j.epsr.2020.106502.

[30] H. W. Dommel, A. Yan, and S. Wei, ‘Harmonics from Transformer Saturation’, *IEEE Transactions on Power Delivery*, vol. 1, no. 2, pp. 209–215, Apr. 1986, doi: 10.1109/TPWRD.1986.4307952.

[31] L. Bolduc, A. Gaudreau, and A. Dutil, ‘Saturation time of transformers under dc excitation’, *Electric Power Systems Research*, vol. 56, no. 2, pp. 95–102, Nov. 2000, doi: 10.1016/S0378-7796(00)00087-0.

[32] R. Hamilton, ‘Analysis of Transformer Inrush Current and Comparison of Harmonic Restraint Methods in Transformer Protection’, *IEEE Transactions on Industry Applications*, vol. 49, no. 4, pp. 1890–1899, Jul. 2013, doi: 10.1109/TIA.2013.2257155.

[33] ‘Three-Phase Transformer Inrush Current Reduction Strategy Based on Prefluxing and Controlled Switching | IEEE Journals & Magazine | IEEE Xplore’. Accessed: Feb. 26, 2024. [Online]. Available: https://ieeexplore.ieee.org/abstract/document/9363173

[34] F. de Leon, A. Farazmand, and P. Joseph, ‘Comparing the T and π Equivalent Circuits for the Calculation of Transformer Inrush Currents’, *IEEE Transactions on Power Delivery*, vol. 27, no. 4, pp. 2390–2398, Oct. 2012, doi: 10.1109/TPWRD.2012.2208229.

[35] G. Lyon, ‘Some experience with a British a.c. network analyser’, *Proceedings of the IEE - Part II: Power Engineering*, vol. 97, no. 60, pp. 697–714, Dec. 1950, doi: 10.1049/pi-2.1950.0199.

[36] J. T. Pender, ‘A Combined Steady-state and Transient a.c. Network Analyser’, *The International Journal of Electrical Engineering & Education*, vol. 6, no. 3, pp. 353–361, Oct. 1968, doi: 10.1177/002072096800600302.

[37] J. Cohn, ‘Transitions from Analog to Digital Computing in Electric Power Systems’, *IEEE Annals Hist. Comput.*, vol. 37, no. 3, pp. 32–43, Jul. 2015, doi: 10.1109/MAHC.2015.37.

[38] J. Mitra and C. Singh, ‘Incorporating the DC load flow model in the decomposition-simulation method of multi-area reliability evaluation’, *IEEE Transactions on Power Systems*, vol. 11, no. 3, pp. 1245–1254, Aug. 1996, doi: 10.1109/59.535596.

[39] J. Mahseredjian, V. Dinavahi, and J. A. Martinez, ‘Simulation Tools for Electromagnetic Transients in Power Systems: Overview and Challenges’, *IEEE Transactions on Power Delivery*, vol. 24, no. 3, pp. 1657–1669, Jul. 2009, doi: 10.1109/TPWRD.2008.2008480.

[40] G. F. Lauss, M. O. Faruque, K. Schoder, C. Dufour, A. Viehweider, and J. Langston, ‘Characteristics and Design of Power Hardware-in-the-Loop Simulations for Electrical Power Systems’, *IEEE Transactions on Industrial Electronics*, vol. 63, no. 1, pp. 406–417, Jan. 2016, doi: 10.1109/TIE.2015.2464308.

[41] M. Groissböck, ‘Are open source energy system optimization tools mature enough for serious use?’, *Renewable and Sustainable Energy Reviews*, vol. 102, pp. 234–248, Mar. 2019, doi: 10.1016/j.rser.2018.11.020.

[42] A. Mercurio, A. Di Giorgio, and P. Cioci, ‘Open-Source Implementation of Monitoring and Controlling Services for EMS/SCADA Systems by Means of Web Services— IEC 61850 and IEC 61970 Standards’, *IEEE Transactions on Power Delivery*, vol. 24, no. 3, pp. 1148–1153, Jul. 2009, doi: 10.1109/TPWRD.2008.2008461.

[43] C. Coffrin, R. Bent, K. Sundar, Y. Ng, and M. Lubin, ‘PowerModels. JL: An Open-Source Framework for Exploring Power Flow Formulations’, in *2018 Power Systems Computation Conference (PSCC)*, Jun. 2018, pp. 1–8. doi: 10.23919/PSCC.2018.8442948.

[44] T. Brown, J. Hörsch, and D. Schlachtberger, ‘PyPSA: Python for Power System Analysis’, *Journal of Open Research Software*, vol. 6, p. 4, Jan. 2018, doi: 10.5334/jors.188.

[45] D. Montenegro, M. Hernandez, and G. A. Ramos, ‘Real time OpenDSS framework for distribution systems simulation and analysis’, in *2012 Sixth IEEE/PES Transmission and Distribution: Latin America Conference and Exposition (T D-LA)*, Sep. 2012, pp. 1–5. doi: 10.1109/TDC-LA.2012.6319069.

[46] M. Reeg *et al.*, ‘AMIRIS: An Agent-Based Simulation Model for the Analysis of Different Support Schemes and Their Effects on Actors Involved in the Integration of Renewable Energies into Energy Markets’, in *2012 23rd International Workshop on Database and Expert Systems Applications*, Sep. 2012, pp. 339–344. doi: 10.1109/DEXA.2012.54.

[47] M. Binsted, G. Iyer, R. Cui, Z. Khan, K. Dorheim, and L. Clarke, ‘Evaluating long-term model-based scenarios of the energy system’, *Energy Strategy Reviews*, vol. 32, p. 100551, Nov. 2020, doi: 10.1016/j.esr.2020.100551.

[48] T. Niet, N. Arianpoo, K. Kuling, and A. S. Wright, ‘Increasing the reliability of energy system scenarios with integrated modelling: a review’, *Environ. Res. Lett.*, vol. 17, no. 4, p. 043006, Mar. 2022, doi: 10.1088/1748-9326/ac5cf5.

[49] ‘Review of model-based electricity system transition scenarios: An analysis for Switzerland, Germany, France, and Italy | Elsevier Enhanced Reader’. Accessed: May 16, 2022. [Online]. Available: https://reader.elsevier.com/reader/sd/pii/S1364032122000314?token=63E584CC08174DB1E92B6C17756E6D4CE854BDE440183CC0C6AA42133A878EF5A16D09BF47E0C8140323D5B95311F2D5&originRegion=eu-west-1&originCreation=20220516040625

[50] ‘Future Energy Scenarios 2021 | National Grid ESO’. Accessed: May 23, 2022. [Online]. Available: https://www.nationalgrideso.com/future-energy/future-energy-scenarios/fes-2021

[51] ‘Distribution Future Energy Scenarios 2022 | UK Power Networks’. Accessed: May 23, 2022. [Online]. Available: https://www.ukpowernetworks.co.uk/future-energy/dfes-2022

[52] O. A. Omitaomu and H. Niu, ‘Artificial Intelligence Techniques in Smart Grid: A Survey’, *Smart Cities*, vol. 4, no. 2, Art. no. 2, Jun. 2021, doi: 10.3390/smartcities4020029.

[53] F. Rohde and S. Hielscher, ‘Smart grids and institutional change: Emerging contestations between organisations over smart energy transitions’, *Energy Research & Social Science*, vol. 74, p. 101974, Apr. 2021, doi: 10.1016/j.erss.2021.101974.

[54] F. Gonzalez Venegas, M. Petit, and Y. Perez, ‘Active integration of electric vehicles into distribution grids: Barriers and frameworks for flexibility services’, *Renewable and Sustainable Energy Reviews*, vol. 145, p. 111060, Jul. 2021, doi: 10.1016/j.rser.2021.111060.

[55] M. Miller, K. Rudion, H. Nägele, and J. Schnaars, ‘A grid reinforcement approach for an optimized planning of high-voltage distribution grids under consideration of line loading indicators’, *IET Renewable Power Generation*, vol. n/a, no. n/a, doi: 10.1049/rpg2.12442.

[56] P. Prakobkaew and S. Sirisumrannukul, ‘Optimization of Electrical Substation Location for Distribution Loss Reduction from Power Demand of Electric Vehicle Charging Stations’, in *2021 5th International Conference on Power and Energy Engineering (ICPEE)*, Dec. 2021, pp. 262–267. doi: 10.1109/ICPEE54380.2021.9662514.

[57] S. Elmallah, A. M. Brockway, and D. Callaway, ‘Can distribution grid infrastructure accommodate residential electrification and electric vehicle adoption in Northern California?’, *Environ. Res.: Infrastruct. Sustain.*, vol. 2, no. 4, p. 045005, Nov. 2022, doi: 10.1088/2634-4505/ac949c.

[58] A. Hussain and P. Musilek, ‘Resilience Enhancement Strategies For and Through Electric Vehicles’, *Sustainable Cities and Society*, vol. 80, p. 103788, May 2022, doi: 10.1016/j.scs.2022.103788.

[59] N. Panossian, M. Muratori, B. Palmintier, A. Meintz, T. Lipman, and K. Moffat, ‘Challenges and Opportunities of Integrating Electric Vehicles in Electricity Distribution Systems’, *Curr Sustainable Renewable Energy Rep*, vol. 9, no. 2, pp. 27–40, Jun. 2022, doi: 10.1007/s40518-022-00201-2.

[60] R. Gupta *et al.*, 'Spatial analysis of distribution grid capacity and costs to enable massive deployment of PV, electric mobility and electric heating', *Applied Energy*, vol. 287, p. 116504, Apr. 2021, doi: 10.1016/j.apenergy.2021.116504.

[61] M. A. Mejia, L. H. Macedo, G. Muñoz-Delgado, J. Contreras, and A. Padilha-Feltrin, 'Medium-term planning of active distribution systems considering voltage-dependent loads, network reconfiguration, and CO2 emissions', *International Journal of Electrical Power & Energy Systems*, vol. 135, p. 107541, Feb. 2022, doi: 10.1016/j.ijepes.2021.107541.

[62] T. Takeshita, H. Aki, K. Kawajiri, and M. Ishida, 'Assessment of utilization of combined heat and power systems to provide grid flexibility alongside variable renewable energy systems', *Energy*, vol. 214, p. 118951, Jan. 2021, doi: 10.1016/j.energy.2020.118951.

[63] J. Mair, K. Suomalainen, D. M. Eyers, and M. W. Jack, 'Sizing domestic batteries for load smoothing and peak shaving based on real-world demand data', *Energy and Buildings*, vol. 247, p. 111109, Sep. 2021, doi: 10.1016/j.enbuild.2021.111109.

[64] E. Guelpa and V. Verda, 'Demand response and other demand side management techniques for district heating: A review', *Energy*, vol. 219, p. 119440, Mar. 2021, doi: 10.1016/j.energy.2020.119440.

[65] B. Bibak and H. Tekiner-Moğulkoç, 'A comprehensive analysis of Vehicle to Grid (V2G) systems and scholarly literature on the application of such systems', *Renewable Energy Focus*, vol. 36, pp. 1–20, Mar. 2021, doi: 10.1016/j.ref.2020.10.001.

[66] C. Gschwendtner, S. R. Sinsel, and A. Stephan, 'Vehicle-to-X (V2X) implementation: An overview of predominate trial configurations and technical, social and regulatory challenges', *Renewable and Sustainable Energy Reviews*, vol. 145, p. 110977, Jul. 2021, doi: 10.1016/j.rser.2021.110977.

[67] B. Hochart, Ed., 'Power Transformer Handbook', in *Power Transformer Handbook*, English ed. edition., London ; Boston: Butterworth-Heinemann Ltd, 1987, pp. 58–61.

[68] W. Cao, J. Wu, N. Jenkins, C. Wang, and T. Green, 'Operating principle of Soft Open Points for electrical distribution network operation', *Applied Energy*, vol. 164, pp. 245–257, Feb. 2016, doi: 10.1016/j.apenergy.2015.12.005.

[69] J. M. Bloemink, 'Distribution-level power electronics : soft open-points', Jul. 2012, doi: 10.25560/17991.

[70] X. Ji, Z. Yin, Y. Zhang, B. Xu, and Q. liu, 'Real-time autonomous dynamic reconfiguration based on deep learning algorithm for distribution network', *Electric Power Systems Research*, vol. 195, p. 107132, Jun. 2021, doi: 10.1016/j.epsr.2021.107132.

[71] Y. Song, Y. Zheng, T. Liu, S. Lei, and D. J. Hill, 'A New Formulation of Distribution Network Reconfiguration for Reducing the Voltage Volatility Induced by Distributed Generation', *IEEE Transactions on Power Systems*, vol. 35, no. 1, pp. 496–507, Jan. 2020, doi: 10.1109/TPWRS.2019.2926317.

[72] Y. Ch, S. K. Goswami, and D. Chatterjee, 'Effect of network reconfiguration on power quality of distribution system', *International Journal of Electrical Power & Energy Systems*, vol. 83, pp. 87–95, Dec. 2016, doi: 10.1016/j.ijepes.2016.03.043.

[73] A. Dejamkhooy, Y. Fathi Khaneghah, and H. Shayeghi, 'Modified branch exchange reconfiguration of active distributed network for simultaneous loss reduction and power quality improvement', *International Transactions on Electrical Energy Systems*, vol. 29, no. 10, p. e12065, 2019, doi: 10.1002/2050-7038.12065.

[74] I. Sarantakos, D. M. Greenwood, J. Yi, S. R. Blake, and P. C. Taylor, 'A method to include component condition and substation reliability into distribution system reconfiguration', *International Journal of Electrical Power & Energy Systems*, vol. 109, pp. 122–138, Jul. 2019, doi: 10.1016/j.ijepes.2019.01.040.

[75] A. M. Tahboub, V. R. Pandi, and H. H. Zeineldin, 'Distribution System Reconfiguration for Annual Energy Loss Reduction Considering Variable Distributed Generation Profiles', *IEEE Transactions on Power Delivery*, vol. 30, no. 4, pp. 1677–1685, Aug. 2015, doi: 10.1109/TPWRD.2015.2424916.

[76] E. Kazemi-Robati, M. S. Sepasian, H. Hafezi, and H. Arasteh, 'PV-hosting-capacity enhancement and power-quality improvement through multiobjective reconfiguration of harmonic-polluted distribution systems', *International Journal of Electrical Power & Energy Systems*, vol. 140, p. 107972, Sep. 2022, doi: 10.1016/j.ijepes.2022.107972.

[77] H. Gao, W. Ma, S. He, L. Wang, and J. Liu, 'Time-segmented Multi-level Reconfiguration in Distribution Network: A Novel Cloud-edge Collaboration Framework', *IEEE Transactions on Smart Grid*, pp. 1–1, 2022, doi: 10.1109/TSG.2022.3156433.

[78] A. Zhou, H. Zhai, M. Yang, and Y. Lin, 'Three-Phase Unbalanced Distribution Network Dynamic Reconfiguration: A Distributionally Robust Approach', *IEEE Transactions on Smart Grid*, pp. 1–1, 2021, doi: 10.1109/TSG.2021.3139763.

[79] H. A. Dharmawan and A. M. Ali, 'Development of switchable transformer research at University of South Australia', *Renewable Energy and Power Quality Journal*, vol. 1, no. 07, pp. 698–703, Apr. 2009, doi: 10.24084/repqj07.477.

[80] L. Cao, G. Feng, X. Cheng, and L. Wang, 'Configuration of smart phase-swapping switches in low-voltage distribution systems based on sequenced participation indices', *Measurement and Control*, p. 0020294020920899, May 2020, doi: 10.1177/0020294020920899.

[81] Z. H. Tan, K. H. Chua, Y. S. Lim, S. Morris, L. Wang, and J. H. Tang, 'Optimal operations of transformers in railway systems with different transformer operation modes and different headway intervals', *International Journal of Electrical Power & Energy Systems*, vol. 127, p. 106631, May 2021, doi: 10.1016/j.ijepes.2020.106631.

[82] D. Jakus, J. Vasilj, R. Čađenović, and P. Sarajčev, 'Optimising the transformer substation topology in order to minimise annual energy losses', *IET Generation, Transmission & Distribution*, vol. 12, no. 6, pp. 1323–1330, 2018, doi: 10.1049/iet-gtd.2017.0721.

[83] R. Khalili Senobari, J. Sadeh, and H. Borsi, 'Frequency response analysis (FRA) of transformers as a tool for fault detection and location: A review', *Electric Power Systems Research*, vol. 155, pp. 172–183, Feb. 2018, doi: 10.1016/j.epsr.2017.10.014.

[84] J. Faiz and M. Soleimani, 'Assessment of computational intelligence and conventional dissolved gas analysis methods for transformer fault diagnosis', *IEEE Transactions on Dielectrics and Electrical Insulation*, vol. 25, no. 5, pp. 1798–1806, Oct. 2018, doi: 10.1109/TDEI.2018.007191.

[85] 'Low Energy Automated Networks (LEAN)', ENA Innovation Portal. Accessed: Jun. 07, 2022. [Online]. Available: https://smarter.energynetworks.org/projects/sset207-01/

[86] A. Srivastava, S. Van Passel, and E. Laes, 'Assessing the success of electricity demand response programs: A meta-analysis', *Energy Research & Social Science*, vol. 40, pp. 110–117, Jun. 2018, doi: 10.1016/j.erss.2017.12.005.

[87] J. Atkinson and I. M. Albayati, 'Impact of the Generation System Parameters on the Frequency Response of the Power System: A UK Grid Case Study', *Electricity*, vol. 2, no. 2, Art. no. 2, Jun. 2021, doi: 10.3390/electricity2020009.

[88] 'Customer Load Active System Services (CLASS)', ENA Innovation Portal. Accessed: Jun. 07, 2022. [Online]. Available: https://smarter.energynetworks.org/projects/enwlt204/

[89] 'Celsius', ENA Innovation Portal. Accessed: Jun. 07, 2022. [Online]. Available: https://smarter.energynetworks.org/projects/enwlen01/

[90] A. El-Shahat, R. J. Haddad, R. Alba-Flores, F. Rios, and Z. Helton, 'Conservation Voltage Reduction Case Study', *IEEE Access*, vol. 8, pp. 55383–55397, 2020, doi: 10.1109/ACCESS.2020.2981694.

[91] C. D. Booth, F. Coffele, and G. M. Burt, 'The Power Networks Demonstration Centre: An environment for accelerated testing, demonstration and validation of existing and novel protection and automation systems', in *12th IET International Conference on Developments in Power System Protection (DPSP 2014)*, Mar. 2014, pp. 1–6. doi: 10.1049/cp.2014.0153.

[92] A. Hussain, M. Aslam, and S. M. Arif, 'A standards-based approach for Auto-drawing single line diagram of multivendor smart distribution systems', *International Journal of Electrical Power & Energy Systems*, vol. 96, pp. 357–367, Mar. 2018, doi: 10.1016/j.ijepes.2017.10.003.

[93] E. VanDerHorn and S. Mahadevan, 'Digital Twin: Generalization, characterization and implementation', *Decision Support Systems*, vol. 145, p. 113524, Jun. 2021, doi: 10.1016/j.dss.2021.113524.

[94] N. Barabanov, J. Schiffer, R. Ortega, and D. Efimov, 'Conditions for Almost Global Attractivity of a Synchronous Generator Connected to an Infinite Bus', *IEEE Transactions on Automatic Control*, vol. 62, no. 10, pp. 4905–4916, Oct. 2017, doi: 10.1109/TAC.2017.2671026.

[95] R. E. Wilson, 'PMUs [phasor measurement unit]', *IEEE Potentials*, vol. 13, no. 2, pp. 26–28, Apr. 1994, doi: 10.1109/45.283885.

[96] S. Murphy, K. Jones, T. Laughner, M. Bariya, and A. Von Meier, ‘Accelerating Artificial Intelligence on the Grid’, in *2020 Clemson University Power Systems Conference (PSC)*, Mar. 2020, pp. 1–7. doi: 10.1109/PSC50246.2020.9131317.

[97] S. Wagner *et al.*, ‘Benefits of Plugin-Based Heuristic Optimization Software Systems’, in *Computer Aided Systems Theory – EUROCAST 2007*, R. Moreno Díaz, F. Pichler, and A. Quesada Arencibia, Eds., in Lecture Notes in Computer Science. Berlin, Heidelberg: Springer, 2007. doi: 10.1007/978-3-540-75867-9_94.

[98] R. Rajkumar, M. Gagliardi, and L. Sha, ‘The real-time publisher/subscriber inter-process communication model for distributed real-time systems: design and implementation’, in *Proceedings Real-Time Technology and Applications Symposium*, May 1995, pp. 66–75. doi: 10.1109/RTTAS.1995.516203.

[99] H. Fangohr, ‘A Comparison of C, MATLAB, and Python as Teaching Languages in Engineering’, in *Computational Science - ICCS 2004*, M. Bubak, G. D. van Albada, P. M. A. Sloot, and J. Dongarra, Eds., in Lecture Notes in Computer Science. Berlin, Heidelberg: Springer, 2004, pp. 1210–1217. doi: 10.1007/978-3-540-25944-2_157.

[100] ‘MATLAB - MathWorks’. Accessed: Jul. 04, 2022. [Online]. Available: https://uk.mathworks.com/products/matlab.html

[101] ‘Standard C++’. Accessed: Jul. 04, 2022. [Online]. Available: https://isocpp.org/

[102] ‘Welcome to Python.org’, Python.org. Accessed: Sep. 26, 2021. [Online]. Available: https://www.python.org/

[103] R. A. M. van Amerongen, ‘A general-purpose version of the fast decoupled load flow’, *IEEE Transactions on Power Systems*, vol. 4, no. 2, pp. 760–770, May 1989, doi: 10.1109/59.193851.

[104] ‘Simulink - Simulation and Model-Based Design’. Accessed: Jul. 04, 2022. [Online]. Available: https://uk.mathworks.com/products/simulink.html

[105] ‘OpenDSS’. Accessed: Jun. 27, 2022. [Online]. Available: https://www.epri.com/pages/sa/opendss

[106] ‘PowerFactory - DIgSILENT’. Accessed: Sep. 14, 2020. [Online]. Available: https://www.digsilent.de/en/powerfactory.html

[107] ‘Redis’, Redis. Accessed: Jul. 04, 2022. [Online]. Available: https://redis.io/

[108] ‘MongoDB | Build Faster. Build Smarter.’, MongoDB. Accessed: Jul. 04, 2022. [Online]. Available: https://www.mongodb.com

[109] ‘NI-VISA Overview’. Accessed: Jul. 05, 2022. [Online]. Available: https://www.ni.com/en-gb/support/documentation/supplemental/06/ni-visa-overview.html

[110] ‘VISA Resource Name Control - NI’. Accessed: Aug. 22, 2022. [Online]. Available: https://www.ni.com/docs/en-US/bundle/labview/page/lvinstio/visa_resource_name_generic.html

[111] D. Krishnamurthy, ‘OpenDSSDirect.py: Python direct-mode interface to OpenDSS’. Accessed: Jul. 04, 2022. [Online]. Available: https://github.com/dss-extensions/OpenDSSDirect.py

[112] G. Swift, T. S. Molinski, and W. Lehn, ‘A fundamental approach to transformer thermal modeling. I. Theory and equivalent circuit’, *IEEE Transactions on Power Delivery*, vol. 16, no. 2, pp. 171–175, Apr. 2001, doi: 10.1109/61.915478.

[113] B. Cogitore, J. P. Keradec, and J. Barbaroux, ‘The two-winding transformer: an experimental method to obtain a wide frequency range equivalent circuit’, *IEEE Transactions on Instrumentation and Measurement*, vol. 43, no. 2, pp. 364–371, Apr. 1994, doi: 10.1109/19.293449.

[114] ‘OpenDSS User Manual’. Accessed: Jul. 07, 2022. [Online]. Available: https://sourceforge.net/p/electricdss/code/HEAD/tree/trunk/Distrib/Doc/OpenDSSManual.pdf

[115] ‘IEC 60076-7:2018 | IEC Webstore’. Accessed: Jan. 03, 2024. [Online]. Available: https://webstore.iec.ch/publication/34351

[116] ‘IEC 60076-12:2008 | IEC Webstore’. Accessed: Sep. 20, 2021. [Online]. Available: https://webstore.iec.ch/publication/592

[117] ‘GridKey device’, https://networks.online/. Accessed: Sep. 05, 2022. [Online]. Available: https://networks.online/heat/dsos-and-data/

[118] ‘SEL-3555 Real-Time Automation Controller (RTAC)’, selinc.com. Accessed: Sep. 05, 2022. [Online]. Available: https://selinc.com/products/3555/

[119] R. Venkateswaran, ‘Virtual private networks’, *IEEE Potentials*, vol. 20, no. 1, pp. 11–15, Feb. 2001, doi: 10.1109/45.913204.

[120] M. G. Say, ‘Transformers: Testing’, in *The Performance and Design of Alternating Current Machines*, Sir Isaac Pitman & Sons Ltd, 1955.

[121] G. L. Zeng and M. Zeng, ‘Kirchhoff’s Voltage Law (KVL)’, in *Electric Circuits: A Concise, Conceptual Tutorial*, G. L. Zeng and M. Zeng, Eds., Cham: Springer International Publishing, 2021, pp. 23–29. doi: 10.1007/978-3-030-60515-5_4.

[122] ‘JSON’. Accessed: Jan. 07, 2020. [Online]. Available: https://www.json.org/json-en.html

[123] K. Dawood, G. Komurgoz, and F. Isik, ‘Modeling of Distribution Transformer for Analysis of Core Losses of Different Core Materials Using FEM’, in *2019 8th International Conference on Modeling Simulation and Applied Optimization (ICMSAO)*, Apr. 2019, pp. 1–5. doi: 10.1109/ICMSAO.2019.8880392.

[124] S. B. Sadati, A. Tahani, B. Darvishi, M. Dargahi, and H. yousefi, ‘Comparison of distribution transformer losses and capacity under linear and harmonic loads’, in *2008 IEEE 2nd International Power and Energy Conference*, Dec. 2008, pp. 1265–1269. doi: 10.1109/PECON.2008.4762661.

[125] R. Nourollahi, P. Salyani, K. Zare, B. Mohammadi-Ivatloo, and Z. Abdul-Malek, ‘Peak-Load Management of Distribution Network Using Conservation Voltage Reduction and Dynamic Thermal Rating’, *Sustainability*, vol. 14, no. 18, Art. no. 18, Jan. 2022, doi: 10.3390/su141811569.

[126] W. Kong, K. Ma, L. Fang, R. Wei, and F. Li, ‘Cost-Benefit Analysis of Phase Balancing Solution for Data-Scarce LV Networks by Cluster-Wise Gaussian Process Regression’, *IEEE Transactions on Power Systems*, vol. 35, no. 4, pp. 3170–3180, Jul. 2020, doi: 10.1109/TPWRS.2020.2966601.

[127] T. Kober, H.-W. Schiffer, M. Densing, and E. Panos, ‘Global energy perspectives to 2060 – WEC’s World Energy Scenarios 2019’, *Energy Strategy Reviews*, vol. 31, p. 100523, Sep. 2020, doi: 10.1016/j.esr.2020.100523.

[128] Elexon, ‘Electricity user load profiles by profile class - UKERC Energy Data Centre’. Accessed: Sep. 09, 2019. [Online]. Available: https://ukerc.rl.ac.uk/cgi-bin/era001.pl?GoButton=EResult&STerm=elexon&SScope=&GoAct=&AFull=5&EWCompID=42&AllFilters=&RandKey=&TotHead=5%20results%20for%20%E2%80%9Celexon%E2%80%9D%20**

[129] A. Navarro-Espinosa and L. Ochoa, *Dissemination Document ‘Low Voltage Networks Models and Low Carbon Technology Profiles’*. 2015.

[130] J. Andrade, L. F. Ochoa, and W. Freitas, ‘Regional-scale allocation of fast charging stations: travel times and distribution system reinforcements’, *IET Generation, Transmission & Distribution*, vol. 14, no. 19, pp. 4225–4233, 2020, doi: 10.1049/iet-gtd.2019.1786.

[131] L. Zhang, Y. Tang, T. Zhou, C. Tang, H. Liang, and J. Zhang, ‘Research on flexible smart home appliance load participating in demand side response based on power direct control technology’, *Energy Reports*, vol. 8, pp. 424–434, Jul. 2022, doi: 10.1016/j.egyr.2022.01.219.

[132] T. Aljohani and O. Mohammed, ‘Modeling the Impact of the Vehicle-to-Grid Services on the Hourly Operation of the Power Distribution Grid’, *Designs*, vol. 2, no. 4, Art. no. 4, Dec. 2018, doi: 10.3390/designs2040055.

[133] ‘Regenerative Grid Simulator’, Cinergia. Accessed: Apr. 18, 2022. [Online]. Available: https://www.cinergia.coop/family/regenerative-grid-simulator/

[134] ‘Review of Net Zero’, GOV.UK. Accessed: Feb. 23, 2023. [Online]. Available: https://www.gov.uk/government/publications/review-of-net-zero

[135] Southern Electric Power Distribution plc, ‘Low Energy Automated Networks (LEAN) - Low Carbon Networks Fund Full Submission Pro-forma’, SSET207/01, Jan. 2015. Accessed: Sep. 09, 2019. [Online]. Available: https://www.ssepd.co.uk/WorkArea/DownloadAsset.aspx?id=5247

[136] E. Balogun, E. Buechler, S. Bhela, S. Onori, and R. Rajagopal, ‘EV-EcoSim: A Grid-Aware Co-Simulation Platform for the Design and Optimization of Electric Vehicle Charging Infrastructure’, *IEEE Trans. Smart Grid*, pp. 1–1, 2023, doi: 10.1109/TSG.2023.3339374.

[137] ‘Load Data’, in *Electricity Distribution Network Design, 2nd Edition (IEE Power) by Lakervi, E. (1905) Paperback*, pp. 209–221.

[138] L. Calearo, M. Marinelli, and C. Ziras, ‘A review of data sources for electric vehicle integration studies’, *Renewable and Sustainable Energy Reviews*, vol. 151, p. 111518, Nov. 2021, doi: 10.1016/j.rser.2021.111518.

[139] Y. Amara-Ouali, Y. Goude, P. Massart, J.-M. Poggi, and H. Yan, ‘A Review of Electric Vehicle Load Open Data and Models’, *Energies*, vol. 14, no. 8, Art. no. 8, Jan. 2021, doi: 10.3390/en14082233.

[140] ‘FES documents Archive | National Grid ESO’. Accessed: Jun. 05, 2022. [Online]. Available: https://www.nationalgrideso.com/future-energy/future-energy-scenarios/fes-documents-archive

[141] C. Crozier, T. Morstyn, and M. McCulloch, ‘The opportunity for smart charging to mitigate the impact of electric vehicles on transmission and distribution systems’, *Applied Energy*, vol. 268, p. 114973, Jun. 2020, doi: 10.1016/j.apenergy.2020.114973.

[142] S. A. Bozorgavari, J. Aghaei, S. Pirouzi, A. Nikoobakht, H. Farahmand, and M. Korpås, ‘Robust planning of distributed battery energy storage systems in flexible smart distribution networks: A comprehensive study’, *Renewable and Sustainable Energy Reviews*, vol. 123, p. 109739, May 2020, doi: 10.1016/j.rser.2020.109739.

[143] A. Ehsan and Q. Yang, ‘Active Distribution System Reinforcement Planning With EV Charging Stations—Part I: Uncertainty Modeling and Problem Formulation’, *IEEE Transactions on Sustainable Energy*, vol. 11, no. 2, pp. 970–978, Apr. 2020, doi: 10.1109/TSTE.2019.2915338.

[144] O. Alabi, K. Turner, G. Figus, A. Katris, and C. Calvillo, ‘Can spending to upgrade electricity networks to support electric vehicles (EVs) roll-outs unlock value in the wider economy?’, *Energy Policy*, vol. 138, p. 111117, Mar. 2020, doi: 10.1016/j.enpol.2019.111117.

10 Appendices

10.1 Bench Top Scale Model of a Reconfigurable Distribution Substation

10.1.1 Scale Model Transformer Datasheet

Index: 0	Baureihe: / Type: STS Art.-Nr.: / Art.-No.: STS 100/23/24	Datenblatt Technical Specifications	BLOCK Transformatoren-Elektronik GmbH D - 27283 Verden/Aller

Typ Type	: 1~ Steuer- und Sicherheitstransformator 1~ Voltage control and safety isolating transformer
Kernform Core type	: EI 84/43
Bemessungsspannung, Eingang Designated input voltage	: 219V / 230V / 241V
Bemessungsstrom, Eingang Designated input current	: 0,54A / 0,52A / 0,50Aac
Bemessungsspannung, Ausgang Designated output voltage	: 24V
Bemessungsstrom, Ausgang Designated output current	: 4,17Aac
Vorzusehende Absicherung, Ausgang Recommended output fuse	: 4,0AT
Einschaltdauer Duty cycle	: 100%
Bemessungsleistung (bei Leistungsfaktor 1) Designated output power (power factor 1)	: 100VA
Bemessungsleistung (bei Leistungsfaktor 0,5) Designated output power (power factor 0.5)	: 225VA
Verlustleistung Power loss	: ca. 15W (η~86,6%) approx.
Schaltgruppe Connection mode	: Ii0
Betriebsfrequenz Designated frequency	: 50-60Hz
Schutzklasse Safety class	: vorbereitet für Geräte der Schutzklasse I prepared for class I equipment
Schutzart Protection index	: IP00
Kühlungsart Type of cooling	: AN
Isolierstoffklasse Insulation class	: B (UL class 105)
Max. Umgebungstemperatur Ambient temperature	: 40°C
Vorschriften Standards	: EN 61558 Teil 1 mit Teil 2-2 und Teil 2-6 EN 61558 part 1 with part 2-2 and part 2-6
Prüfzeichen Approvals	: VDE 0570 Typ ST/S; Type EI84/43/A File E 103521
Prüfspannung HV-Test voltage	: Primär-Sekundär / Primary-Secondary 3,7 kV; Sekundär-Kern / Secondary-Core 1,3 kV Primär-Kern / Primary-Core 2,6 kV
Anschluß (Eingang) Terminal (Input)	: Schraubklemme 4mm² Screw terminal
Anschluß (Ausgang) Terminal (Output)	: Schraubklemme 4mm² Screw terminal
Anschluß (PE) Terminal (PE)	: Flachsteckanschluss 6,3x0,8mm Plug type terminal
Bemerkungen Notes	: Die angegebenen technischen Daten sind typisch. Material- und fertigungsbedingt können Abweichungen auftreten. Technical specifications are typical, they can vary due to material and production tolerances.

Seite 1/2
Page 1/2

0 Date:	Name:	Date:	Checked:	Amendment:
Date: 11.09.14	Date: 23.9.14	Schutzvermerk nach ISO 16016 beachten		Änderungen vorbehalten
Name: Schlee	Checked: [illegible]	Observe protection clause to ISO 16016		Subject to change

Figure 103 – Manufacturer's datasheet for transformers used in Bench Top Scale Model experiments.

10.1.2 Model Source Code Listings

Below are the OpenDSS model source code listings as used for the Digital Twin model.

```
clear

Set DefaultBaseFrequency=50

new circuit.circuit1 baseKV=0.230 bus1=mainSource pu=1.0 frequency=50 phases=1 !! parameters here

set voltagebases = [0.4, 0.04] !line voltages


!##################### LEFT BRANCH ################################
new line.line1 bus1=mainSource bus2=Switch1Input phases=1 length=1 units=m
new line.switch1 bus1=Switch1Input bus2=Switch1Output phases=1 length=1 units=m switch=true
new line.line2 bus1=Switch1Output bus2=transformer1_hv phases=1 length=1 units=m


New transformer.T1 phases=1 windings=2 buses=[transformer1_hv transformer1_lv]
~ kvs=[0.230 0.026] kvas=[0.1 0.1]
~ %Noloadloss=5.887
~ XHL=0.733
~ %Rs = [3.736, 3.713]
~ %imag=52.515


new line.line3 bus1=transformer1_lv bus2=Switch2Input phases=1 length=1 units=m
new line.switch2 bus1=Switch2Input bus2=Switch2Output phases=1 length=1 units=m switch=true
new line.line4 bus1=Switch2Output bus2=load_bus phases=1 length=1 units=m
!###############################################################



!##################### RIGHT BRANCH ################################
new line.line5 bus1=mainSource bus2=Switch3Input phases=1 length=1 units=m
new line.switch3 bus1=Switch3Input bus2=Switch3Output phases=1 length=1 units=m switch=true
new line.line6 bus1=Switch3Output bus2=transformer2_hv phases=1 length=1 units=m
```

```
New transformer.T2 phases=1 windings=2 buses=[transformer2_hv transformer2_lv]
~ kvs=[0.230 0.026] kvas=[0.1 0.1]
~ %Noloadloss=5.115
~ XHL=0.737
~ %Rs = [3.632 3.609]
~ %imag=44.923


new line.line7 bus1=transformer2_lv bus2=Switch4Input phases=1 length=1 units=m
new line.switch4 bus1=Switch4Input bus2=Switch4Output phases=1 length=1 units=m switch=true
new line.line8 bus1=Switch4Output bus2=load_bus phases=1 length=1 units=m
!####################################################################



!##################### LOADS ##################################
new load.load1 bus1=load_bus phases=1 kv=0.024 kw=0.2 pf=1.0 model=1
~ Vminpu=0.8 Vmaxpu=1.2
!##############################################################


solve mode=snap
```

10.1.3 OCT + SCT Raw Measurement Data from Bench Power Analyser

10.1.3.1 DUT Transformer 1

10.1.3.1.1 OCT

Below are the instrument configuration and parameterisation open circuit test results for transformer 1 used in the bench top scale model.

File Format,N4thv1

Instrument,type,PPA5520

,serial number,853

,firmware version,2.185

,calibration,28_MAY_2013_0924_NW

Record,file name,PPA_R002.TXT

,name,TX1+OCT

,datestamp (ddmmyyyy),01012008

,timestamp,0025

power analyzer,mode,power analyzer

,VAr sign,negative lagging

,power factor sign,negative leading

,selected harmonic,3

,difference THD,disabled

,input compensation,disabled

power analyzer,frequency reference,voltage

,torque + speed,disabled

acquisition control,wiring,single phase 1

,speed,fast

,smoothing,normal

,smoothing response,auto reset

,frequency reference,voltage

,phase angle reference,voltage

,frequency filter,off

,low frequency,off

data start real time

Phase sequence: Phase 1 only

Data sequence: true W, true VA, true PF, V rms, A rms, fundamental W, fundamental VA, fundamental pf, fundamental V, fundamental A

5.0402E+00, 4.5246E+01, 1.1140E-01, 2.3979E+01, 1.8869E+00, 5.0400E+00, 4.5036E+01, 1.1191E-01, 2.3979E+01, 1.8781E+00

10.1.3.1.2 SCT

Below are the short circuit test results for transformer 1 used in the bench top scale model.

Data sequence: true W, true VA, true PF, V rms, A rms, fundamental W, fundamental VA, fundamental pf, fundamental V, fundamental A

1.0921E+01, 1.0974E+01, 9.9520E-01, 2.0878E+01, 5.2559E-01, 1.0921E+01, 1.0973E+01, 9.9521E-01, 2.0878E+01, 5.2558E-01

10.1.3.2 DUT Transformer 2

10.1.3.2.1 OCT

Below are the open circuit test results for transformer 2 used in the bench top scale model.

Data sequence: true W, true VA, true PF, V rms, A rms, fundamental W, fundamental VA, fundamental pf, fundamental V, fundamental A

4.3774E+00, 3.8689E+01, 1.1314E-01, 2.3994E+01, 1.6124E+00, 4.3782E+00, 3.8512E+01, 1.1369E-01, 2.3994E+01, 1.6051E+00

10.1.3.2.2 SCT

Below are the short circuit test results for transformer 2 used in the bench top scale model.

Data sequence: true W, true VA, true PF, V rms, A rms, fundamental W, fundamental VA, fundamental pf, fundamental V, fundamental A

1.0393E+01, 1.0445E+01, 9.9495E-01, 2.0089E+01, 5.1994E-01, 1.0392E+01, 1.0445E+01, 9.9496E-01, 2.0089E+01, 5.1993E-01

10.1.4 Manual Validation Raw Data from Bench Power Analyser

10.1.4.1 Substation Under No-Load Condition

Below are the static measured results for the bench top scale model under no-load condition.

Data sequence: true W, true VA, true PF, V rms, A rms, fundamental W, fundamental VA, fundamental pf, fundamental V, fundamental A

5.6550E+00, 5.5900E+01, 1.0116E-01, 2.3001E+02, 2.4303E-01, 5.6558E+00, 5.5561E+01, 1.0179E-01, 2.3001E+02, 2.4156E-01, 0.0000E-01, 0.0000E-01, 0.0000E-01, 2.5920E+01, 0.0000E-01, 0.0000E-01, 0.0000E-01, 0.0000E-01, 2.5919E+01, 0.0000E-01

10.1.4.2 Substation Under Full-Load Condition

Below are the static measured results for the bench top scale model under full-load condition.

Data sequence: true W, true VA, true PF, V rms, A rms, fundamental W, fundamental VA, fundamental pf, fundamental V, fundamental A

1.1460E+02, 1.2557E+02, 9.1268E-01, 2.3005E+02, 5.4583E-01, 1.1460E+02, 1.2544E+02, 9.1358E-01, 2.3005E+02, 5.4528E-01, 1.0004E+02, 1.0006E+02, 9.9987E-01, 2.3806E+01, 4.2030E+00, 1.0004E+02, 1.0005E+02, 9.9995E-01, 2.3805E+01, 4.2028E+00

10.1.5 Model Validation Raw Data

10.1.5.1 Instantaneous Measurements from Digital Twin Software Application User Interface

10.1.5.1.1 DUT 2 no-load

```
Instruments
        controller:     {'tx_1': '0', 'tx_2': '1'}
        source          {'V': '230.0', 'f': '50.0', 'I': '0.1943', 'P': '-6.4985', 'pf': '-0.1454'}
        tx1 primary:    {'V': '0.0', 'I': '0.0', 'W': '0.0', 'VAr': '0.0', 'VA': '0.0'}
        tx2 primary:    {'V': '229.95', 'I': '0.1951', 'W': '6.4941', 'VAr': '44.3813', 'VA': '44.8539'}
        substation:     {'Input_W': '6.4985', 'Output_W': '0.0', 'Efficiency_%': '0.0'}
        load            {'Bank': '0', 'Wave': '0', 'Load_on': '0', 'I': '0.0', 'V': '25.8002'}
```

Figure 104 - Instantaneous Measurements from Digital Twin Software Application User Interface for no-load condition on transformer 2.

10.1.5.1.2 DUT 2 full-load

```
Instruments
        controller:     {'tx_1': '0', 'tx_2': '1'}
        source          {'V': '230.0', 'f': '50.0', 'I': '0.5445', 'P': '-117.6558', 'pf': '-0.9396'}
        tx1 primary:    {'V': '0.0', 'I': '0.0', 'W': '0.0', 'VAr': '0.0', 'VA': '0.0'}
        tx2 primary:    {'V': '229.8949', 'I': '0.5447', 'W': '117.6211', 'VAr': '42.9703', 'VA': '125.2244'}
        substation:     {'Input_W': '117.6558', 'Output_W': '99.8372', 'Efficiency_%': '84.855'}
        load            {'Bank': '0', 'Wave': '0', 'Load_on': '1', 'I': '4.3088', 'V': '23.1704'}
```

Figure 105 - Instantaneous Measurements from Digital Twin Software Application User Interface for full-load condition on transformer 2.

10.1.5.2 Instantaneous Measurements from Bench Instrument Front Panels

10.1.5.3 Bench Top Scale Model

10.1.5.3.1 DUT 2 no-load

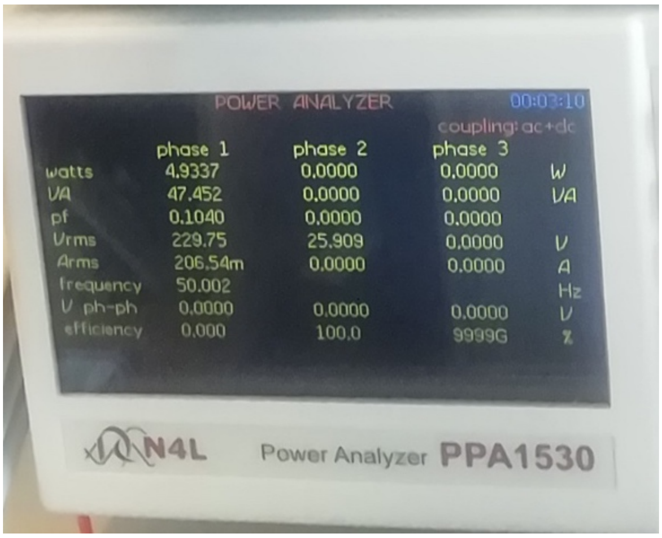

Figure 106 - Instantaneous Measurements from Bench Instrument Front Panel at no-load condition.

10.1.5.3.2 DUT 2 full-load

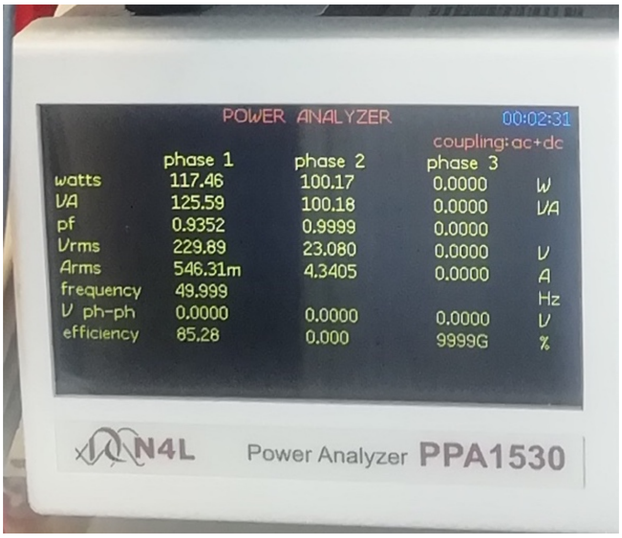

Figure 107 - Instantaneous Measurements from Bench Instrument Front Panel at full-load condition.

10.1.6 Day with highest average load in Net Zero year

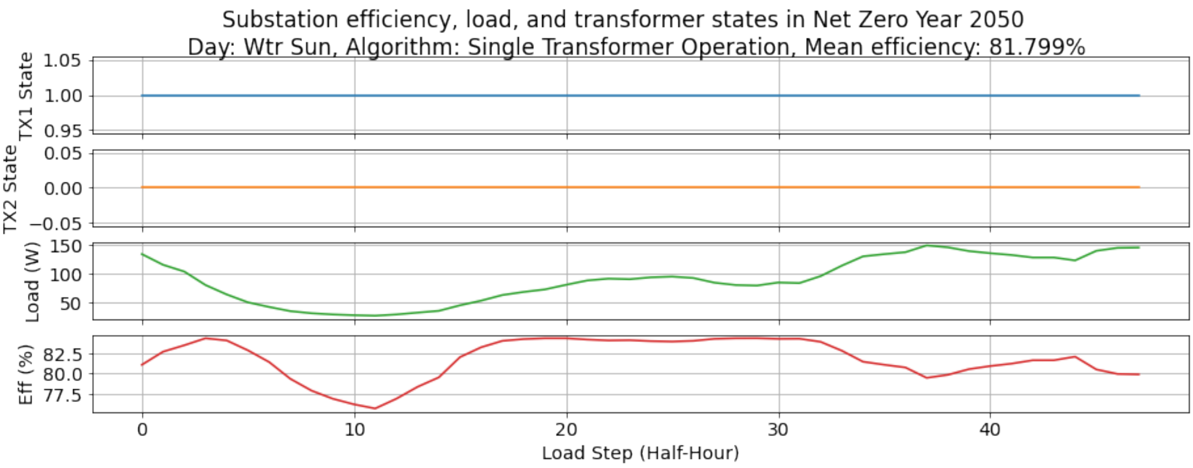

Figure 108 - DT experiment time series results for a Winter Sunday in Net Zero Year with single transformer operation.

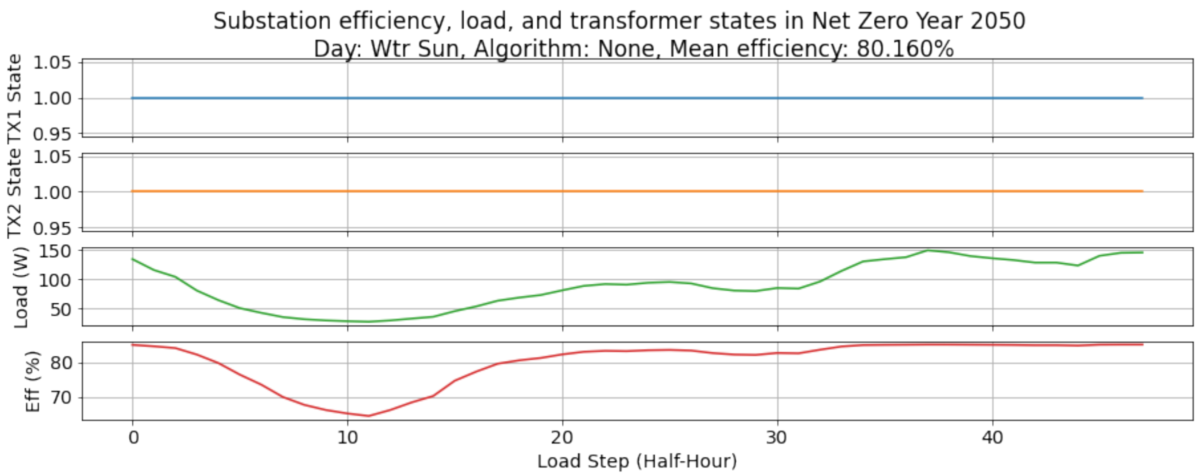

Figure 109 - DT experiment time series results for a Winter Sunday in Net Zero Year with no algorithm.

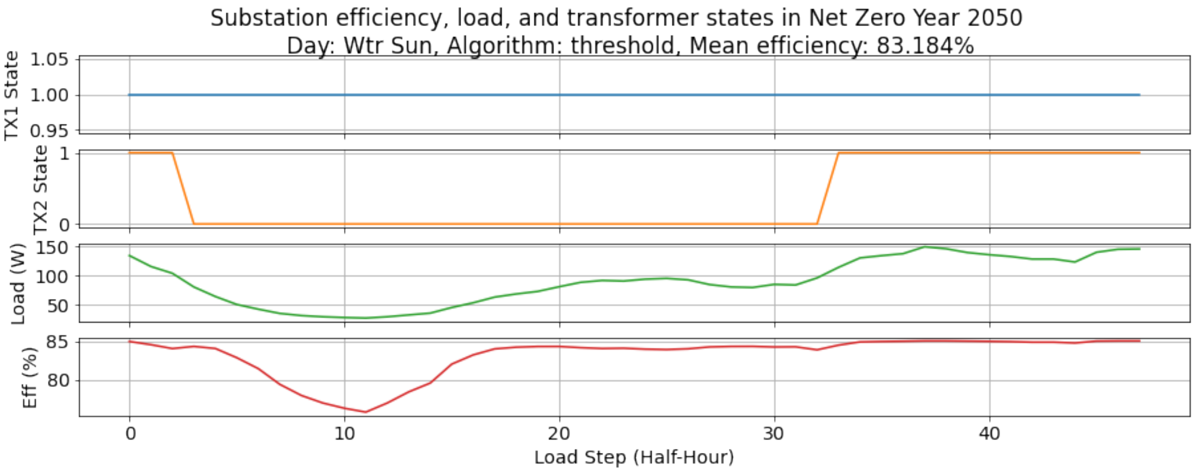

Figure 110 - DT experiment time series results for a Winter Sunday in Net Zero Year with threshold algorithm.

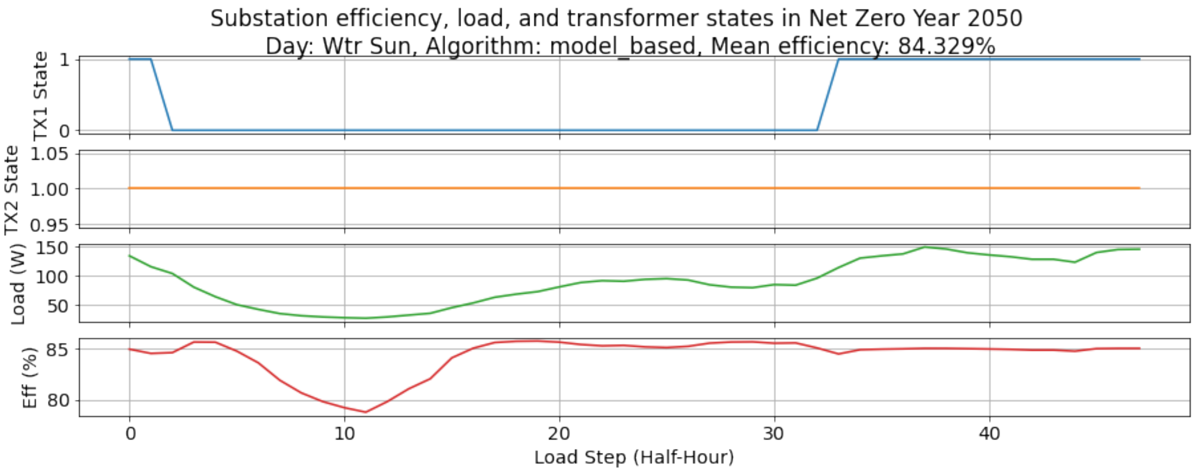

Figure 111 - DT experiment time series results for a Winter Sunday in Net Zero Year with model-based algorithm.

10.1.7 Min, Mean, and Max Combined Load over all Season-Days

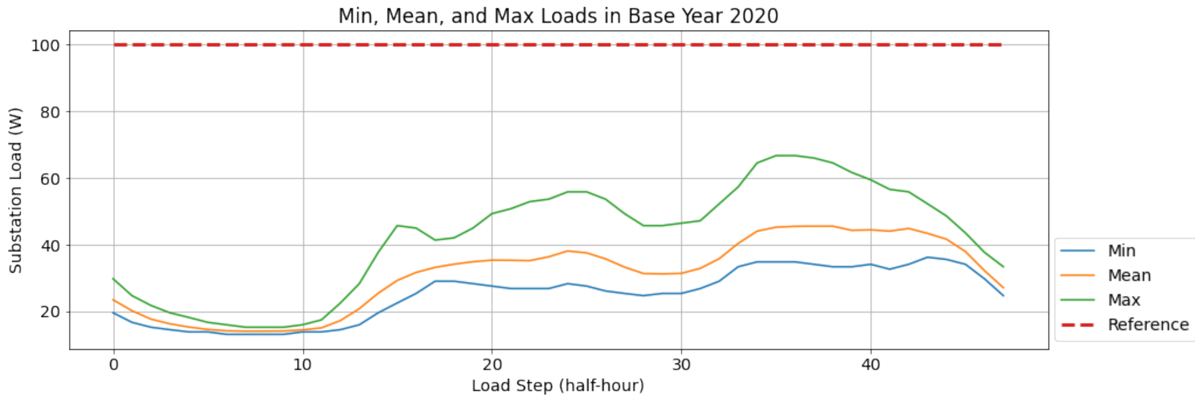

Figure 112 - Min, Mean, and Max Combined Load in Base Year.

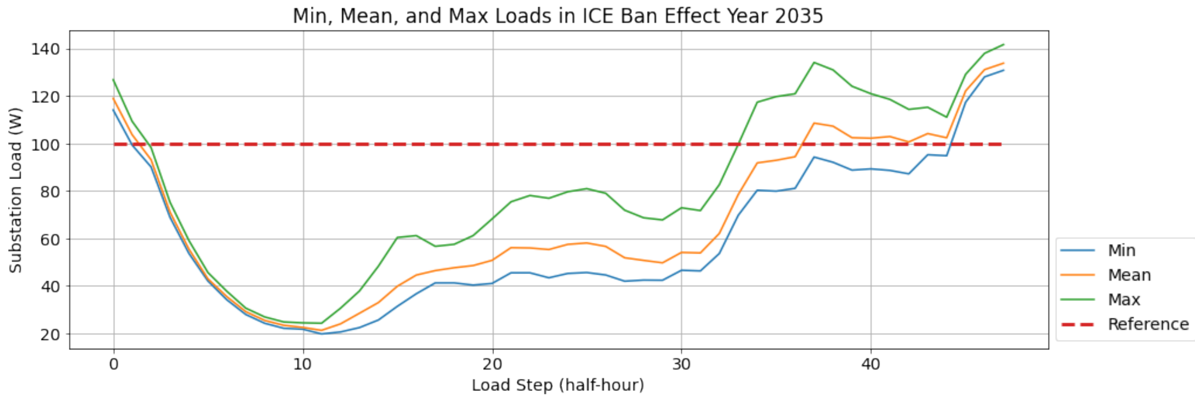

Figure 113 - Min, Mean, and Max Combined Load in ICE Ban Effect Year.

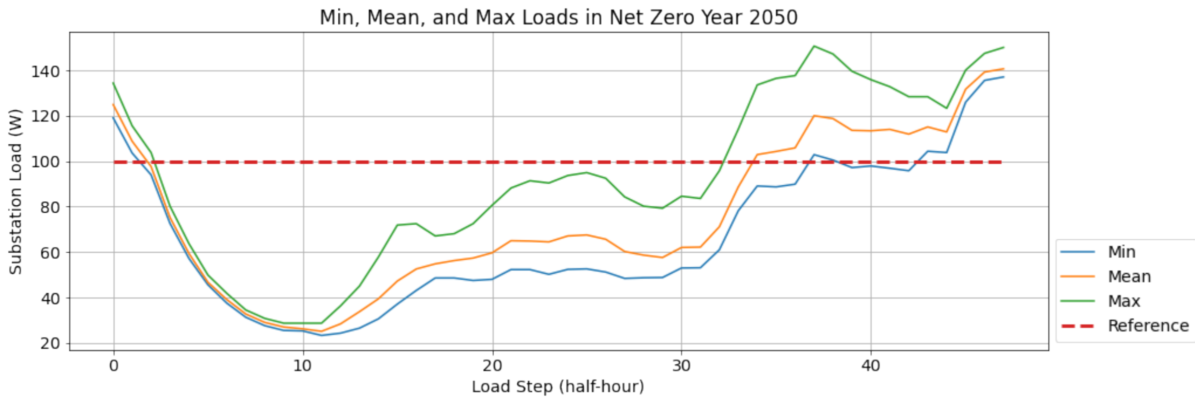

Figure 114 - Min, Mean, and Max Combined Load in Net Zero Year.

10.1.8 Box Plots of Loads for each Season-Day

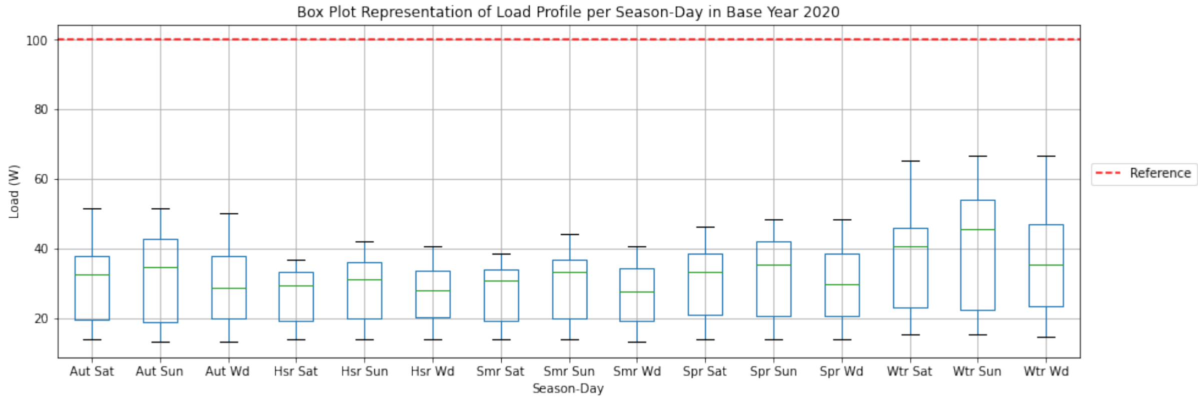

Figure 115 – Load profile box plots showing minimum, maximum, median, first and third quartiles for base year, against a reference of rated substation load before reinforcement.

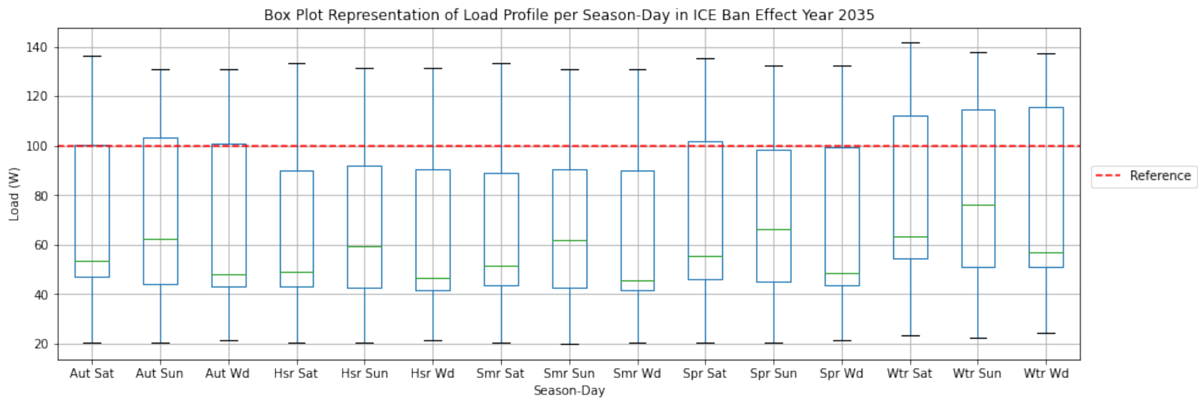

Figure 116 - Load profile box plots showing minimum, maximum, median, first and third quartiles for ICE ban effect year, against a reference of rated substation load before reinforcement.

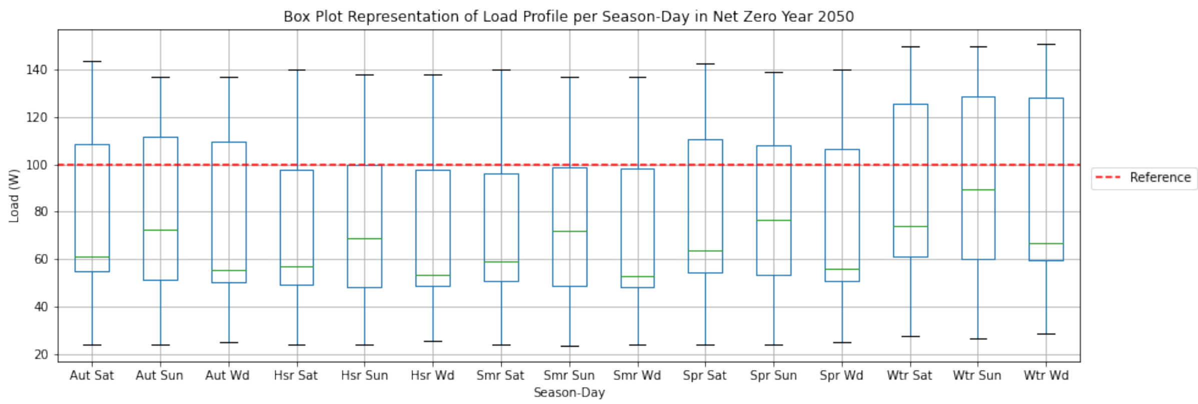

Figure 117 - Load profile box plots showing minimum, maximum, median, first and third quartiles for net zero year, against a reference of rated substation load before reinforcement.

10.2 Mean Substation Efficiencies per Scenario Year

10.2.1 Base Year 2020

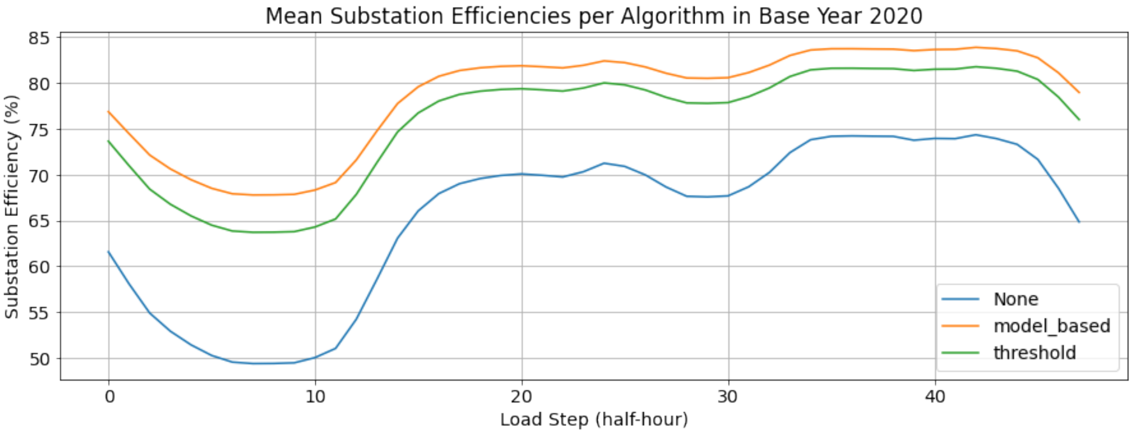

Figure 118 – Digital Twin results of mean efficiencies over all season-days in base year.

10.2.2 ICE Ban Effect Year 2035

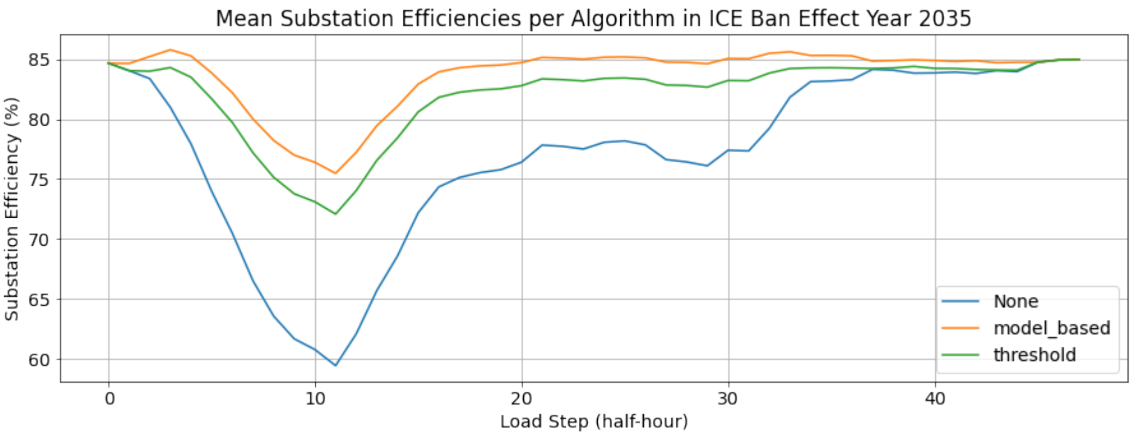

Figure 119 - Digital Twin results of mean efficiencies over all season-days in ICE ban effect year.

10.2.3 Net Zero Year 2050

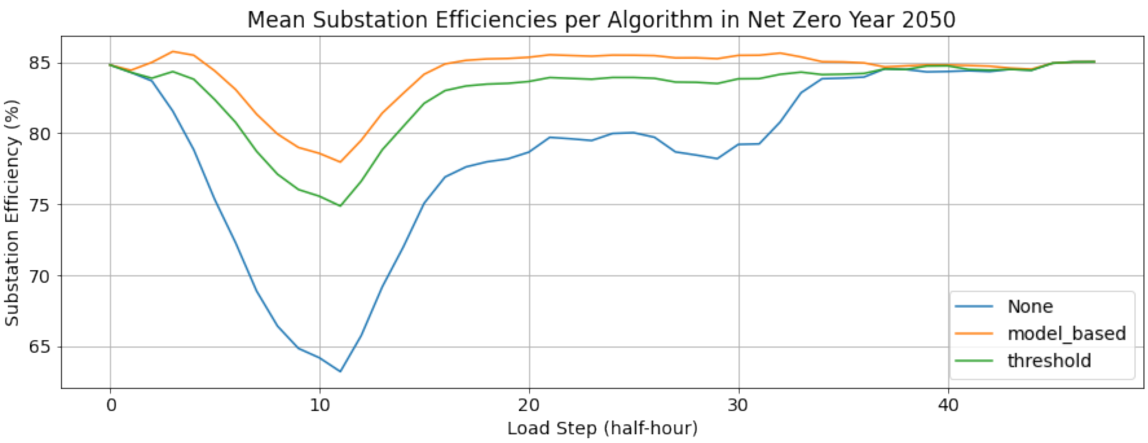

Figure 120 - Digital Twin results of mean efficiencies over all season-days in Net Zero year.

10.3 Efficiency min, mean, and max per season-day and algorithm

10.3.1 Base Year

	Efficiency (%)								
	min			mean			max		
algorithm	None	model_based	threshold	None	model_based	threshold	None	model_based	threshold
scenario_day									
Aut Sat	49.016	67.486	63.389	65.301563	78.616625	75.746479	76.872	84.942	83.062
Aut Sun	47.666	66.335	62.164	65.891542	78.835208	76.024042	76.874	84.942	83.062
Aut Wd	47.665	66.335	62.164	64.577021	78.146896	75.219208	76.436	84.796	82.875
Hsr Sat	49.016	67.486	63.389	63.256750	77.595896	74.540021	71.290	82.595	80.190
Hsr Sun	49.016	67.485	63.389	64.427104	78.215729	75.263396	73.605	83.675	81.488
Hsr Wd	49.016	67.486	63.389	63.144208	77.485042	74.423104	73.015	83.410	81.168
Smr Sat	49.016	67.486	63.389	63.738188	77.824958	74.814896	72.011	82.948	80.608
Smr Sun	49.016	67.486	63.389	64.600146	78.243437	75.312250	74.473	84.046	81.939
Smr Wd	47.665	66.335	62.164	62.962375	77.305042	74.235417	73.014	83.410	81.168
Spr Sat	49.016	67.486	63.389	65.635271	78.872896	76.025937	75.268	84.366	82.334
Spr Sun	49.016	67.486	63.389	66.232312	79.125812	76.336083	75.979	84.634	82.669
Spr Wd	49.016	67.486	63.389	64.603271	78.253354	75.321104	75.980	84.634	82.669
Wtr Sat	51.403	69.452	65.498	68.957792	80.561604	78.003708	80.022	85.698	84.124
Wtr Sun	51.403	69.452	65.498	69.748438	80.812792	78.331958	80.283	85.727	84.178
Wtr Wd	50.182	68.457	64.428	68.335938	80.183458	77.573125	80.284	85.727	84.178

Figure 121 - Digital Twin results of efficiencies for all season-days in base year.

10.3.2 ICE Ban Effect Year

	Efficiency (%)								
	min			mean			max		
algorithm	None	model_based	threshold	None	model_based	threshold	None	model_based	threshold
scenario_day									
Aut Sat	58.745	74.988	71.540	76.963354	83.594125	81.978854	84.989	85.770	84.986
Aut Sun	58.745	74.988	71.540	77.168146	83.496083	81.938833	84.919	85.770	84.917
Aut Wd	59.769	75.700	72.329	76.775083	83.543937	81.935333	84.919	85.757	84.917
Hsr Sat	58.745	74.988	71.540	76.219458	83.533104	81.719625	84.958	85.770	84.955
Hsr Sun	58.745	74.988	71.540	76.715896	83.605521	81.846000	84.932	85.772	84.930
Hsr Wd	59.769	75.700	72.329	76.188688	83.503937	81.712667	84.932	85.765	84.930
Smr Sat	58.745	74.988	71.540	76.479979	83.600833	81.810917	84.958	85.770	84.955
Smr Sun	57.764	74.293	70.771	76.819729	83.591875	81.842042	84.919	85.772	84.917
Smr Wd	58.745	74.988	71.540	76.169458	83.479729	81.655812	84.919	85.757	84.917
Spr Sat	58.745	74.988	71.540	77.131062	83.671042	82.037729	84.978	85.772	84.977
Spr Sun	58.745	74.988	71.540	77.428083	83.665604	82.098833	84.944	85.772	85.020
Spr Wd	59.769	75.700	72.329	76.798500	83.616000	81.975667	84.948	85.765	84.943
Wtr Sat	61.662	76.975	73.753	78.553021	84.063292	82.732563	85.031	85.762	85.028
Wtr Sun	60.740	76.361	73.065	78.802458	83.923667	82.624417	85.005	85.772	85.004
Wtr Wd	62.538	77.548	74.395	78.421292	84.104396	82.750208	84.997	85.772	84.995

Figure 122 - Digital Twin results of efficiencies for all season-days in ICE ban effect year.

10.3.3 Net Zero Year

	Efficiency (%)								
	min			mean			max		
algorithm	None	model_based	threshold	None	model_based	threshold	None	model_based	threshold
scenario_day									
Aut Sat	62.487	77.515	74.358	78.563375	84.166438	82.778667	85.039	85.754	85.037
Aut Sun	62.487	77.515	74.358	78.725542	84.045958	82.689083	84.996	85.772	84.994
Aut Wd	63.397	78.098	75.015	78.385458	84.170375	82.786229	84.996	85.772	84.994
Hsr Sat	62.487	77.515	74.358	77.903479	84.107938	82.557625	85.022	85.754	85.020
Hsr Sun	62.487	77.515	74.358	78.347562	84.102458	82.611021	85.005	85.772	85.003
Hsr Wd	63.485	78.154	75.079	77.871021	84.076792	82.570625	85.005	85.761	85.012
Smr Sat	62.487	77.515	74.358	78.135813	84.135813	82.651875	85.022	85.761	85.080
Smr Sun	61.526	76.886	73.653	78.429521	84.060250	82.606792	84.995	85.771	84.994
Smr Wd	62.487	77.515	74.358	77.841667	84.043604	82.519937	84.995	85.772	84.994
Spr Sat	62.487	77.515	74.358	78.725604	84.189083	82.830042	85.038	85.772	85.032
Spr Sun	62.487	77.515	74.358	78.974625	84.131687	82.778333	85.014	85.770	85.012
Spr Wd	63.397	78.098	75.015	78.418542	84.188292	82.786625	85.023	85.761	85.017
Wtr Sat	65.315	79.287	76.363	79.981625	84.550104	83.376271	85.054	85.772	85.046
Wtr Sun	64.426	78.744	75.745	80.159688	84.328625	83.184083	85.047	85.772	85.046
Wtr Wd	66.007	79.702	76.836	79.854208	84.613708	83.421479	85.046	85.772	85.044

Figure 123 - Digital Twin results of efficiencies for all season-days in Net Zero year.

10.4 Single transformer operation efficiency min, mean, max per season-day

10.4.1 Base Year

		Load (W)			Efficiency (%)		
		min	mean	max	min	mean	max
scenario_year	scenario_day						
BY	Aut Sat	13.8080	30.684423	51.4953	63.388	75.746479	83.064
	Aut Sun	13.0745	32.265733	51.4945	62.164	76.024292	83.065
	Aut Wd	13.0742	29.897948	50.0254	62.164	75.219042	82.880
	Hsr Sat	13.8082	26.705625	36.9528	63.388	74.540188	80.194
	Hsr Sun	13.8082	28.756881	42.0240	63.388	75.263479	81.488
	Hsr Wd	13.8080	26.782338	40.6235	63.388	74.422854	81.169
	Smr Sat	13.8080	27.598098	38.4202	63.388	74.814563	80.611
	Smr Sun	13.8080	29.336138	44.2256	63.388	75.312667	81.940
	Smr Wd	13.0742	26.798994	40.6228	62.164	74.235125	81.169
	Spr Sat	13.8080	30.844333	46.4263	63.388	76.025729	82.334
	Spr Sun	13.8080	32.310490	48.5609	63.388	76.335792	82.674
	Spr Wd	13.8080	29.414558	48.5605	63.388	75.320500	82.670
	Wtr Sat	15.2088	37.910937	65.2315	65.497	78.003458	84.131
	Wtr Sun	15.2088	40.646906	66.7035	65.497	78.332167	84.180
	Wtr Wd	14.4751	37.131712	66.7053	64.427	77.572333	84.182

Figure 124 – Digital Twin results of single transformer operation efficiency min, mean, and max per season-day in base year.

10.4.2 ICE Ban Effect Year

		Load (W)			Efficiency (%)		
		min	mean	max	min	mean	max
scenario_year	scenario_day						
IB	Aut Sat	20.5895	67.003971	136.2639	71.538	81.556792	84.339
	Aut Sun	20.5886	68.980475	130.8439	71.538	81.502104	84.333
	Aut Wd	21.5057	66.021475	130.8439	72.329	81.520750	84.340
	Hsr Sat	20.5902	62.032377	133.5128	71.537	81.474125	84.320
	Hsr Sun	20.5902	64.594988	131.6715	71.537	81.594813	84.309
	Hsr Wd	21.5065	62.127646	131.6715	72.328	81.449729	84.327
	Smr Sat	20.5895	63.147196	133.5043	71.538	81.561396	84.288
	Smr Sun	19.7565	65.319133	130.8410	70.769	81.595062	84.309
	Smr Wd	20.5895	62.148673	130.8410	71.538	81.428646	84.340
	Spr Sat	20.5902	67.203844	135.3441	71.537	81.668667	84.341
	Spr Sun	20.5902	69.035681	132.5940	71.537	81.705979	84.325
	Spr Wd	21.5057	65.416921	132.5889	72.329	81.598917	84.342
	Wtr Sat	23.3405	76.034694	141.6810	73.751	81.903479	84.334
	Wtr Sun	22.4235	79.453781	138.0938	73.064	81.750167	84.339
	Wtr Wd	24.2565	75.060283	137.1775	74.395	81.904438	84.340

Figure 125 - Digital Twin results of single transformer operation efficiency min, mean, and max per season-day in ICE ban effect year.

10.4.3 Net Zero Year

		Load (W)			Efficiency (%)		
		min	mean	max	min	mean	max
scenario_year	scenario_day						
NZ	Aut Sat	24.2030	74.664019	143.4982	74.356	82.053000	84.325
	Aut Sun	24.2019	77.034115	137.0053	74.356	81.938083	84.333
	Aut Wd	25.2036	73.485206	137.0053	75.013	82.040042	84.307
	Hsr Sat	24.2042	68.698687	140.2063	74.354	82.139104	84.339
	Hsr Sun	24.2042	71.773271	138.0005	74.354	82.174063	84.338
	Hsr Wd	25.3031	68.812990	138.0005	75.076	82.108771	84.318
	Smr Sat	24.2030	70.036185	140.1994	74.356	82.183229	84.332
	Smr Sun	23.2039	72.642023	137.0048	73.649	82.146292	84.344
	Smr Wd	24.2030	68.838277	137.0048	74.356	82.080708	84.307
	Spr Sat	24.2042	74.902944	142.4046	74.354	82.158146	84.329
	Spr Sun	24.2042	77.101187	139.1051	74.354	82.129688	84.340
	Spr Wd	25.2036	72.760063	139.8014	75.013	82.138479	84.318
	Wtr Sat	27.5035	85.498148	150.0066	76.361	82.064979	84.338
	Wtr Sun	26.4033	89.600454	149.5044	75.743	81.798938	84.324
	Wtr Wd	28.4026	84.329052	150.6033	76.835	82.085104	84.329

Figure 126 - Digital Twin results of single transformer operation efficiency min, mean, and max per season-day in Net Zero year.